CHEMICAL AND PHYSICAL PROPERTIES OF AMAZONIAN AEROSOL PARTICLES

Dissertation zur Erlangung des Grades/
Dissertation présentée pour l'obtention du diplôme de

„Doktor der Naturwissenschaften" / „Doctorat en Sciences"

am Fachbereich Chemie der Johannes Gutenberg-Universität in Mainz/
à l'université de Paris VII – Denis Diderot, U. F. R. de Chimie
Spécialité: Chimie de la pollution atmosphérique et physique de l'environnement

Vorgelegt von/
Présentée par

Pascal Guyon

Geb. in / né à: Amberieu-en-Bugey, France

Mainz / Paris 2002

Tag der mündlichen Prüfung: 17 Dezember 2002

CHEMICAL AND PHYSICAL PROPERTIES OF AMAZONIAN AEROSOL PARTICLES

par

Pascal Guyon

Thèse présentée en cotutelle à:

Université de Paris VII – Denis Diderot

UFR de Chimie

Spécialité: Chimie de la pollution atmosphérique et physique de l'environnement

et

Johannes Gutenberg-Universität Mainz

Fachbereich Chemie

Pour l'obtention du diplôme de:

Doctorat en Sciences / Doktor der Naturwissenschaften

Soutenance le 17 décembre 2002

RÉSUMÉ COURT POUR BIBLIOTHÈQUE PARIS VII:

Cette thèse a pour objectif principal de déterminer les propriétés chimiques et physiques des particules d'aérosols du bassin amazonien dans des conditions naturellement non polluées et lors des périodes de brûlis, dans le but d'accroître les connaissances actuelles sur les sources et puits de ces aérosols dans cette région, ainsi que sur leur potentiel effets radiatif et climatique. Les mesures ont été effectuées dans le cadre d'une coopération européenne au projet LBA-EUSTACH.

Les données incluent des mesures de concentration en nombre des particules, de leur distribution en taille, de leurs propriétés optiques, ainsi que de leur composition élémentaire et carbonée. La plus grande partie des aérosols était constituée de trois composants principaux durant les deux saison (aérosols biologiques naturels, pyrogèniques, et poussière minérale). Ces trois composants, incluant petites et grosses particules, participaient à l'extinction de la lumière solaire.

Dans l'ensemble, les paramètres mesurés témoignent d'une augmentation d'un facteur dix entre la saison humide et la saison sèche, due à l'injection massive dans l'atmosphère de particules submicroniques d'origine pyrogénique pendant la saison sèche. Parallèlement, l'albédo de diffusion simple baissait de 0,97 à 0,91. Le développement d'une nouvelle méthode basée sur la théorie de Mie a permis de calculer l'indice de réfraction des particules d'aérosols pour les deux saisons. Les calculs ont produit un indice de réfraction équivalent de $1,42 - 0,006i$ pour la saison humide et de $1,41 - 0,013i$ pour la saison sèche. Cette méthode a aussi permis de corriger la distribution en taille mesurée par un compteur optique de particules. D'autres paramètres ayant une importance du point de vue climatique ont pu être calculés à partir de calculs de Mie. Il est probable que ces changements aient un impact au niveau régional mais aussi global dû à l'altération du rayonnement solaire et aux changements des propriétés des nuages.

ADRESSE DU LABORATOIRE:

Max Planck Institute for Chemistry
P.O.B. 3060
D-55020 Mainz, Germany

Université de Paris VII and Universität Mainz

ABSTRACT

Chemical and Physical Properties of Amazonian Aerosol Particles

This dissertation focuses on the determination of the chemical and physical properties of aerosol particles over the Amazon basin under background and biomass burning conditions, in order to increase current knowledge of aerosol sources and sinks in this region, and the potential radiative impact of these particles.

The measurements were made during two campaigns in 1999 as part of the European contribution to the Large-Scale Biosphere-Atmosphere Experiment in Amazonia (LBA-EUSTACH) on a meteorological tower situated within a primary Amazonian rainforest.

The data set includes measurements of aerosol particle number concentrations, size distributions, optical properties, as well as the elemental and carbonaceous content of the sampled aerosol. The results clearly illustrate the dramatic effects that extensive seasonal biomass burning activities are having on the composition and properties of aerosols over Amazonia. The average breathable particulate mass concentrations (diameters < 10 μm) were ca. 6 and 40 μg m^{-3} for the wet and the dry seasons, respectively. Three components were found to comprise the bulk of the total aerosol loading: the wet season aerosols consisted mainly of a natural biogenic component, whereas pyrogenic aerosols dominated the dry season aerosol mass. The third component identified was soil dust, which is believed to be internally mixed with the biomass-burning aerosol during the dry season. All three components, in both fine and coarse particles, contributed significantly to light extinction, suggesting that, in addition to biomass burning particles, biogenic and soil dust aerosols should be taken into account when modeling the physical and optical properties of aerosols in the Amazon.

Overall, the measured parameters showed a roughly ten-fold increase in moving from the wet to the dry season, which could be attributed to a massive injection of submicron smoke particles in the atmosphere during the dry season. Correspondingly, the single-scattering albedo decreased from ca. 0.97 to 0.91. The refractive index of the aerosol particles was calculated for the two seasonal periods using a new iterative method based on Mie theory (for a wavelength of incident light = 545 nm, and ambient relative humidity < 80%), yielding averaged values of $1.42 - 0.006i$ and $1.41 - 0.013i$ for the wet and dry seasons, respectively. This method also allows correcting the size distribution obtained from an optical particle counter. Other climatically relevant parameters were further derived from the Mie calculations, yielding asymmetry parameters of 0.63 ± 0.02 and 0.70 ± 0.03, and backscatter ratios of 0.12 ± 0.01 and 0.08 ± 0.01 for background and biomass burning aerosols, respectively. The potential exists for these changes to impact on regional and global climate through changes to the extinction of solar radiation as well as the alteration of cloud properties.

Université de Paris VII und Universität Mainz

ZUSAMMENFASSUNG

Chemische und physikalische Eigenschaften von Aerosolpartikeln im Amazonasgebiet

Die vorliegende Dissertation befasst sich mit der Bestimmung der chemischen und physikalischen Eigenschaften von Aerosolpartikeln im Amazonasbecken, die während Zeiten mit Biomasseverbrennung und bei Hintergrundbedingungen bestimmt wurden. Die Arbeit diente der Erweiterung des gegenwärtigen Kenntnisstandes über Quellen und Senken von Partikeln in dieser Region und der potentiellen Strahlungseinflüsse der Partikel.

Die Messungen wurden während zwei Kampagnen im Rahmen des europäischen Beitrags zum Large-Scale Biosphere-Atmosphere Experiment in Amazonien (LBA-EUSTACH) auf einem meteorologischen Turm im Primärregenwald des Amazonasgebiets durchgeführt.

Die Daten umfassen Messungen der Anzahlkonzentrationen, Größenverteilungen, optischen Eigenschaften sowie Elementzusammensetzungen und Kohlenstoffgehalte der gesammelten Aerosole. Die Ergebnisse zeigen eindrucksvoll den großen Einfluß großräumiger saisonaler Biomasseverbrennung auf die Zusammensetzung und Eigenschaften von Aerosolen über Amazonien. Die gemittelte Massenkonzentration der lungengängigen Teilchen (Durchmesser < 10 µm) entsprach 6 µg m^{-3} während der Regenzeit und 40 µg m^{-3} während der Trockenzeit.

Die Zusammensetzung des Aerosols wies auf folgende drei Quellen hin: während der Regenzeit setzte sich das Aerosol hauptsächlich aus natürlichen biogenen Bestandteilen zusammen, wohingegen in der Trockenzeit pyrogenes Aerosol dominierte. Mineralstaub tritt während der Trockenzeit vermutlich intern gemischt mit dem Aerosol aus Biomasseverbrennung auf. Partikel, sowohl des feinen als auch groben

Größenbereichs, aller drei Komponenten trugen signifikant zur Extinktion des Sonnenlichts bei. Dies legt nahe, dass außer den Partikeln der Biomasse-verbrennungen auch biogene Aerosolpartikel und Mineralstaub bei der Modellierung physikalischer und optischer Eigenschaften von Aerosolen in Amazonien berücksichtigt werden müssen.

Insgesamt ergab sich eine Steigerung der Meßwerte um ca. das Zehnfache während der Trockenzeit im Vergleich zur Regenzeit, was auf eine massive Einbringung von Rauchpartikeln im Submikrometerbereich in die Atmosphäre während der Trockenzeit zurückzuführen ist. Dementsprechend sank die Einzelstreualbedo von ca. 0,97 auf 0,91. Der Brechungsindex der Aerosolpartikel wurde mit einer neuen iterative Methoden, basierend auf der Mie-Theorie berechnet (bei einer Wellenlänge des einfallenden Lichts von 545 nm und einer relativen Luftfeuchte von < 80 %). Es ergaben sich durchschnittliche Werte von $1,42 - 0,006i$ für die Regenzeit und $1,41 - 0,013i$ für die Trockenperiode. Diese Methode ermöglicht zudem die Korrektur von Größenverteilungen, die mit optischen Partikelzählern erhalten wurden. Weitere klimatisch relevante Parameter, die mit den Mie-Berechnungen abgeleitet werden konnten, ergaben für Hintergrundaerosole und für Aerosole aus Biomasseverbrennung folgende Werte: Asymmetrieparameter von $0,63 \pm 0,02$ bzw. $0,70 \pm 0,03$ und Rückstreuungsverhältnisse von $0,12 \pm 0,01$ bzw. $0,08 \pm 0,01$. Diese Veränderungen haben das Potential, das regionale und globale Klima über die Variierung der Extinktion der Sonneneinstrahlung als auch der Wolkeneigenschaften zu beeinflussen.

RÉSUMÉ

Propriétés Chimiques et Physiques des Particules d'Aérosols du Bassin Amazonien

Cette thèse a pour objectif principal de déterminer les propriétés chimiques et physiques des particules d'aérosols du bassin amazonien dans des conditions naturellement non polluées et lors des périodes de brûlis, dans le but d'accroître les connaissances actuelles sur les sources et puits de ces aérosols dans cette région, ainsi que sur leur potentiel effets radiatif et climatique.

Les mesures ont été effectuées le long d'une tour météorologique située dans une forêt tropicale humide d'Amazonie au cours de deux campagnes de mesures qui se sont déroulées au cours de l'année 1999 dans le cadre d'une coopération européenne au projet LBA-EUSTACH (Large-Scale Biosphere-Atmosphere Experiment in Amazonia).

Les données incluent des mesures de concentration en nombre des particules, de leur distribution en taille, de leurs propriétés optiques, ainsi que de leur composition élémentaire et carbonée. Les résultats illustrent clairement l'ampleur des effets qu'ont les feux de biomasse (lesquels sont utilisés de manière saisonnière à grande échelle en Amazonie) sur la composition et les diverses propriétés physiques des aérosols. La concentration massique moyenne de la fraction respirable des aérosols (diamètres < 10 μm) était de 6 μg m^{-3} pour la saison humide, passant à 40 μg m^{-3} pendant la saison sèche. La plus grande partie des aérosols était constituée de trois composants principaux: les aérosols de la saison humide étaient composés principalement d'aérosols biologiques naturels, alors que les aérosols pyrogèniques dominaient la concentration massique en aérosols lors de la saison sèche. Le troisième composant a été identifié comme étant de la poussière minérale, et était apparemment en mélange interne avec les particules pyrogèniques durant la saison sèche. Ces trois composants, incluant aussi bien les petites que les grosses particules, participaient à l'extinction de la lumière solaire, indiquant que,

en plus des particules pyrogèniques, les particules biologiques et les poussières minérales devraient être incluses dans les modèles simulant les propriétés physiques et optiques des aérosols amazoniens.

Dans l'ensemble, les paramètres mesurés témoignent d'une augmentation d'un facteur dix entre la saison humide et la saison sèche, due à l'injection massive dans l'atmosphère de particules submicroniques pendant la saison sèche. Parallèlement, l'albédo de diffusion simple baissait de 0.97 à 0.91. Le développement d'une nouvelle méthode basée sur la théorie de Mie a permis de calculer l'indice de réfraction des particules d'aérosols pour les deux saisons. Les calculs ont produit un indice de réfraction équivalent de $1,42 - 0,006i$ pour la saison humide et de $1,41 - 0,013i$ pour la saison sèche. Cette méthode a aussi permis de corriger la distribution en taille mesurée par un compteur optique de particules. D'autres paramètres ayant une importance du point de vue climatique ont pu être calculés à partir de calculs de Mie: ces calculs ont produit un paramètre d'asymétrie de 0.63 ± 0.02 pour la saison humide et 0.70 ± 0.03 pour la saison sèche, et une fraction de diffusion vers l'arrière de respectivement 0.12 ± 0.01 et 0.08 ± 0.01 pour les deux saisons. Il est probable que ces changements aient un impact au niveau régional mais aussi global dû à l'altération du rayonnement solaire et aux changements des propriétés des nuages.

TABLE OF CONTENTS

iv

LIST OF FIGURES

LIST OF TABLES

CHAPTER I.

GENERAL INTRODUCTION

Foreword

The Amazon basin is the world's largest rain forested area and, from a global perspective, is probably the single largest continuous emitter of biogenic gases and particles from plants (Harriss et al., 1990; Andreae and Crutzen, 1997). It is also a region subject to intense deforestation, mostly through the use of fire (Gash et al., 1996a). Biomass burning has been estimated to be the second largest source of anthropogenic aerosols (IPCC, 2001). About 80% of this burning activity takes place in the tropics (Hao and Liu, 1994), one third of this in South America alone. Because of the intense convective activity associated with the International Tropical Convergence Zone (ITCZ) and the Hadley Circulation, natural and pyrogenic emissions of gases and aerosols in the tropics can be rapidly uplifted to high altitudes and become subject to long-range transport (Pickering et al., 1996; Andreae et al., 2001; Staudt et al., 2001). In the case of burning emissions, the strong thermal updrafts produced during large fires may also contribute to the transport of gases and particles to distant areas. Thus, understanding the sources, strengths and properties of emissions from the Amazon Basin is important not only from local and regional points of view, but also from a global standpoint, because the potential exists for the associated effects on climate, atmospheric chemistry and health to be felt on all these scales. For all of the above reasons, the Amazon basin has very much been one of the locations of choice for intensive field studies over the past decade.

Aerosol particles are of a special climatic interest because they act as cloud condensation nuclei (CCN)—the "seeds" required for the formation of cloud droplets—and because they scatter and absorb solar radiation, affecting the radiation budget. Aerosol particles are now generally assumed to have an overall cooling effect on the Earth system, estimated to be of the same order of magnitude (but opposite sign) as the well-

known positive forcing of greenhouse gases (Andreae and Crutzen, 1997). However, aerosol optical properties and their spatial distribution are largely inhomogeneous, and this estimate is still subject to large uncertainty (Figure I-1) (IPCC, 2001). The magnitude of climate forcing due to aerosol at any given location is highly dependent on the sources of the aerosol particles and their optical and physical properties. Forcing may range from net heating to net cooling depending on these properties, as well as on the albedo of the underlying surface layer.
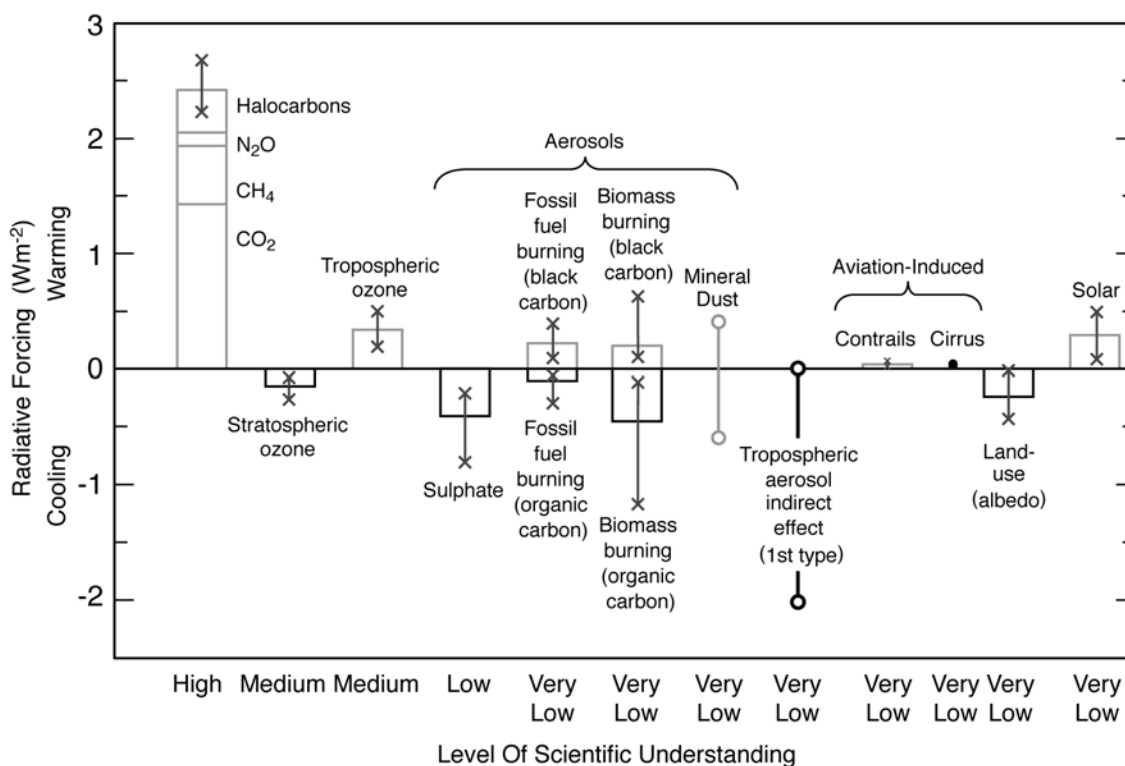
Figure I-1 Global, annual-mean radiative forcing due to a number of mechanisms for the period from pre-industrial (1750) to present (late 1990's; about 2000).
The height of each rectangular bar denotes a central estimate value, while its absence denotes that no best estimate is possible at this stage. The vertical lines about the rectangular bars with "x" delimiters indicate an estimate of the uncertainty range, for the most part guided by the spread in the published values of the forcing. A vertical line without a rectangular bar and with "o" delimiters denotes a forcing for which no central estimate can be given owing to large uncertainties. A "level of scientific understanding" index ranging from high to very low is accorded to each forcing mechanism. Note that the "second" type of aerosol indirect effect, although conceptually important, is not reported in this figure, as there exists very little confidence in the simulated quantitative estimates. Also, the forcing associated with stratospheric aerosols from volcanic eruptions is highly variable over the period and is not considered in this plot (adapted from Ramaswamy et al. (2001)).

The current study was carried out during the recent LBA-EUSTACH 1 and 2 campaigns (LBA = Large-Scale Atmosphere-Biosphere Experiment in Amazonia; EUSTACH = European Studies of Trace Gases and Atmospheric Chemistry) (Andreae et al., 2002), which formed part of the LBA project, a major international initiative designed to investigate the Amazon rainforest ecosystem, its links to the atmosphere and climate, as well as the significant impacts of human activities in the region. The ongoing LBA project aims to contribute towards answering two key questions: 1) How does Amazonia currently function as a regional entity? 2) How will changes in land use and climate affect the biological, chemical and physical functions of Amazonia, including the sustainability of development in the region and the influence of Amazonia on global climate? The EUSTACH project was a European contribution to the LBA project, which sought to assess the global effects of changes occurring in Amazonia related to human activities on the carbon balance, the concentrations of greenhouse gases and aerosol particles, and on the oxidizing power of the atmosphere.

This Ph.D. work focused on the physical and chemical characterization of Amazonian aerosols during both background and biomass burning conditions, and to derive their sources and their parameters relevant for direct climate forcing.

I.1. Sources of aerosols

Aerosol particles are "multi-dimensional" in nature. This means that they cannot be characterized by their concentration only, but have to be characterized by a range of properties. Amongst these properties, those which are most important from the perspective of their role in atmospheric processes are their number concentration, size, mass, chemical composition, and aerodynamic and optical properties. Of particular importance are the size and chemical composition of the particles, because these determine in large part the optical and climatic effects of the aerosol, as well as potential adverse health effects.

Figure I-2 presents a summary of the four main aerosol size modes, as well as their major sources and sinks. Figure I-2 also introduces the concept of "fine" and "coarse"

aerosols (terms used throughout this work), i.e. particles smaller and larger than ca. 2 μm, respectively. It is noted here that unless otherwise specified, the term "particle diameter" is used throughout this text to mean the aerodynamic diameter of the particle—which is defined as the diameter of a sphere with a density equal to that of water, having the same terminal velocity as the particle of consideration—and not, for instance, the geometric diameter. This is because most instruments used in this work measure specific aerosol properties in term of their aerodynamic diameter, and because it is most commonly used diameter type in the aerosol community.

Amongst the four main particle modes, this work focuses mainly on accumulation range particles (Figure I-2) and coarse particles (diameter = 2–10 μm). This is because these two classes of particles (particularly the accumulation mode) are of major importance with respect to aerosol optical (and radiative) effects and cloud processes. Coarse particles usually arise from mechanical processes such as wind abrasion, and are therefore often referred to as "primary particles". Typical coarse mode particles include soil dust/crustal particles, sea salt, fly ash, and biological particles such as spores, pollen grains, animal and plant debris, etc. Their chemical composition usually reflects their source. They have typically "short" lifetimes of minutes to days, and are mainly removed from the atmosphere by sedimentation or washout. Therefore, coarse particles are typically found close to their source. However, coarse particles have also been reported to travel long distances. Saharan desert dust particles, for example, have been measured in the Amazon basin (see e.g., Artaxo and Hansson (1995) and Formenti et al. (2001)). During long-range transport, particles may be subject to changes in their size distribution and composition via processes such as condensational growth and mixing with other particles, which may in turn lead to changes in the properties such as their light extinction efficiency. Certain aerosol parameters may vary by up to several orders of magnitude during a single day due to such transformation processes.

Amongst coarse particles, mineral dust grains are of special interest because of their potentially large contribution to global radiative forcing; however, the sign (positive for warming, and negative for cooling) of this forcing remains uncertain (Figure I-1), and highly linked to the surface albedo. Soil dust particles are usually generated and uplifted

into the atmosphere by winds in dry regions where vegetative cover is sparse (e.g., deserts), in areas subject to land-use (e.g., deforestation, cultivation), and from dust roads.
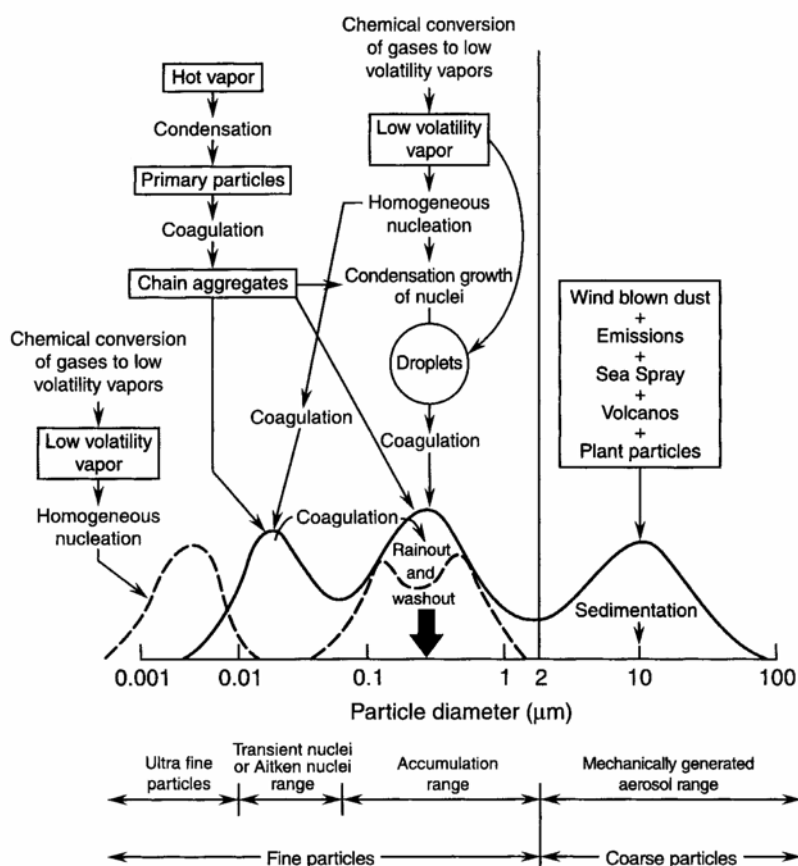
Figure I-2 Schematic of an aerosol size distribution showing four modes, their sources and sinks.
The ultrafine particle mode and the two peaks sometimes observed in the accumulation mode are indicated by the dashed lines (adapted from Finlayson-Pitts and Pitts (2000)).

In contrast to coarse particles, accumulation mode particles, which have diameters ranging from ca. 0.1 to 1–2 μm, typically arise from condensation of low volatility vapors (e.g., following combustion) and via coagulation of smaller particles with themselves or with other accumulation mode particles. They are, therefore, often described as "secondary particles". However, combustion processes, such as biomass burning or burning of fossil fuel, also contribute to massive injection of primary submicron particles in the atmosphere. Considering their sources, accumulation-size particles usually contain a large fraction of organic compounds, and inorganic elements characteristic of their

source(s) (see CHAPTER IV). Owing to their small size, they have typical lifetimes of days to weeks. They are removed from the atmosphere mainly by incorporation into cloud droplets and subsequent rainout, or by washout, as they are too small for rapid gravitational sedimentation. They may also be carried to surfaces by eddy diffusion and advection, and undergo dry deposition. Their removal is, therefore, dependent not only on their physical properties (size distribution), but also largely on their chemical composition, particularly their hygroscopicity. In this respect, the state of mixing of the particles is also of importance. An aerosol population is considered to be "externally mixed" when particles of different sources coexist but are discrete from one another. Particles are "internally mixed" when components of various sources are present in the same particle. Ideally, in an internal mixture the chemical composition of individual particles is identical to that of the bulk. One can differentiate between homogeneously and heterogeneously internally-mixed particles; the former consists of particles in which the constituents are well-mixed within each particle (e.g., a particle formed through evaporation of cloud droplets containing soluble salts), whereas the latter comprises particles in which the constituents are not physically mixed within the particles (e.g., a dust particle with an organic coating). These different states of mixing influence the hygroscopicity of the particles, and therefore the efficiency with which they are removed from the atmosphere by different processes. The state of mixing of a particle also largely influences its optical properties, as discussed below.

I.2. Radiative forcing of aerosol particles

Climate forcing is defined as the change imposed by certain forcing agents (e.g., "greenhouse gases", aerosol particles) on the energy balance of the Earth (in units of W m^{-2}) that alters global temperature (for a recent review, see Haywood and Boucher (2000) and IPCC (2001)). However, this definition is only useful under the assumption that there exists a general relationship between global mean forcing and the global mean equilibrium surface temperature response that is similar for all the different types of forcing. Aerosols can interact both directly with solar radiation and terrestrially re-emitted infrared radiation, and indirectly alter the planetary albedo by modifying the properties of

clouds. The first of these mechanisms is known as the "direct radiative forcing effect" of particles (Charlson et al., 1992), whereas the latter is referred as the "indirect radiative forcing effect" of particles (Twomey, 1991). The most important parameters that influence the magnitude of these effects are the particles' size distribution, complex refractive index (i.e., chemical composition and state of mixing), solubility, and change in size with relative humidity.

In this work, discussion of the possible climatically relevant impact of aerosols focuses almost exclusively on the direct effect. However, a short introduction to both effects is provided here for the purpose of completeness.

I.2.1. The direct radiative forcing of tropospheric aerosols

A simple expression that can be used to estimate the globally- and annually-averaged top-of-atmosphere forcing (ΔF) caused by an aerosol layer has been given by Chylek and Wong (1995) and Haywood and Shine (1995):

$$\Delta F = -\frac{1}{2} F_0 T^2 (1 - A_c)(\omega_0 \beta (1 - R_s)^2 - 2(1 - \omega_0) R_s) \tau \qquad \text{(I-1)}$$

where F_0 is the solar constant ($F_0 = 1360$ W m^{-2}, the associated factor of 1/2 reflecting the fact that any point on the globe is illuminated by sunlight only one-half of the time over the course of a year), T is the transmissivity of the atmosphere above the aerosol layer, A_c is the fractional cloud cover, ω_0 is the single scattering albedo (see Section III.3.5), β is the aerosol hemispheric upscattering fraction (the fraction of incident light redirected back to space; see Section V.4.5), R_s is the surface albedo, and τ is the aerosol layer optical thickness (see Section III.3.6). Other investigators have implemented this simple model with, for example, the parameterization of the solar zenith angle (Russell et al., 1997), or parameterization of aerosol hygroscopic growth upon change in relative humidity (e.g.: Boucher and Anderson (1995), Seinfeld and Pandis (1998)).

The single scattering albedo, ω_0, is one of the most critical parameters in determining the sign and magnitude of the forcing (see Section III.3.5). ω_0 is defined as the ratio of the aerosol scattering over the sum of scattering and absorption. The key

7

parameters that govern the scattering and absorption of light by a particle are the wavelength of the incident light, the complex refractive index of the particle (which describes the particle's optical properties relative to its surrounding medium; see CHAPTER V), and the size of the particle. As mentioned earlier, aerosols in the accumulation mode are the most important in terms of radiative forcing because they are the most efficient at scattering and absorbing solar radiation, and they have the longest atmospheric lifetime (Horvath, 1998). Another parameter that can be of importance when computing aerosol forcing is the shape of the particles, which may vary significantly from one type of particle to another (Mishchenko et al., 1997; Pilinis and Li, 1998).

Scattering

The (elastic) scattering of light is defined as the redistribution of the incident light in non-parallel directions, at the same wavelength as the incident beam. Bearing in mind that the wavelengths of light that reach the Earth's surface range between 290 and 750 nm, scattering of light by accumulation mode particles (with diameters of the same order as the wavelength of the incident light) falls predominantly into the region of Mie scattering (the smallest particles lead to Rayleigh scattering, where the same amount of energy is re-emitted in all directions). Mie scattering is more pronounced in the forward direction; however, a certain fraction of light ("upscattered") is always reflected back into space (i.e. does not reach the earth surface) and, therefore, aerosol scattering produces a negative forcing (cooling effect). At greater solar zenith angles, a larger fraction of the forward scattered light does not reach the Earth, contributing to portion of light that is upscattered (one should be aware of the distinction between forward and backward scattering, which refer to the particle, and upward and downward scattering, which are used in reference to the Earth's surface).

Light scattering by particles can be due to a large variety of aerosol types, amongst which carbonaceous and sulfate-containing particles of natural and anthropogenic origins are usually considered to be the most efficient.

The scattering of light by aerosol particles can both be directly measured (e.g., using an integrating nephelometer; see Sections II.2.4 and III.3.3), or calculated from Mie theory for a given wavelength of incident light if the particle composition, state of mixing (i.e., the refractive index), and size are known (and assuming the particle to be spherical in shape; see CHAPTER V).

Absorption

Absorption consists of a conversion of incident light into thermal energy. Therefore, absorption of light by airborne particles produces a warming (positive forcing) of the aerosol and the surrounding air parcel. This leads to a decrease in the amount of light reaching the Earth's surface, and might therefore be anticipated to lead to a cooling effect at the surface. However, absorbing aerosols are typically emitted from anthropogenic sources (mainly via combustion processes) and are usually concentrated in the lower troposphere, producing an overall warming of the Earth system (Andreae, 2001; Jacobson, 2001). Absorbing aerosols may also reduce heat convection, and contribute to cloud re-evaporation (Ackerman et al., 2000). When located above the ocean, a layer of absorbing aerosols may also reduce evaporation and perturb the whole hydrological cycle (Ramanathan et al., 2001).

With the exception of dust aerosols, the absorption of light due to aerosol particles is thought to be mainly due to elemental (graphitic) carbon. However, recent studies have suggested that biomass burning may release large amounts of polymeric organic compounds (Mukai and Ambe, 1986; Zappoli et al., 1999; Mayol-Bracero et al., 2002), which may also contribute significantly to absorption, as it is discussed later.

Similarly to scattering, absorption by aerosol particles can be both directly measured (see Sections II.2.5 and III.3.4, for a comprehensive review of the measurement techniques, refer to (Horvath, 1993) or estimated via theoretical calculations (see CHAPTER V).

I.2.2. The indirect radiative forcing of aerosols

Because aerosol particles can serve as CCN, a change in aerosol chemical composition and number concentration can alter the microphysics, radiative properties and lifetime of clouds. The indirect effect of aerosols can be split into the so-called first and second indirect effects.

The first indirect effect is a direct consequence of an increase in CCN number concentration. Considering a given liquid water content for a given air parcel, an increase in CCN number (due to, for example, pollution, burning, etc.) leads to an increased amount of smaller droplets, since the available water has to be shared between a greater number of droplet nuclei (Twomey, 1991). As mentioned above, smaller aerosols (in this case, droplets) scatter more in the backward direction than larger aerosols, and, seen from space, these clouds appear "brighter". For this reason, this effect is also called the cloud albedo effect. It results in a net cooling effect (Figure I-1).

The second indirect effect arises as a consequence of the first one. In order to produce rain, cloud droplets need to overcome a threshold radius of ca. 14 μm. An increased CCN concentration could prevent droplets from reaching this radius, thereby resulting in rainfall suppression, increased cloud lifetime (Albrecht, 1989), and, therefore, increased fractional cloud cover. For this reason, this effect is also called the cloud lifetime effect. An increased cloud cover could result in both a warming effect via trapping of terrestrial infrared radiation (especially at night), and a cooling effect due to a larger reflection of incoming light. Model calculations suggest an overall cooling effect (Haywood and Boucher, 2000).

Although it is recognized that the second indirect effect could be a major agent of climate change (Haywood and Boucher, 2000; IPCC, 2001), the mechanism and impacts of this effect are still poorly understood (no estimate is given in Figure I-1).

I.3. Outline of the thesis

The major objective of the work reported in this dissertation was to increase our understanding of the possible effect of large-scale forest biomass burning in the tropics, by studying in detail the chemical and physical properties of the aerosol particles emitted during such burning in the Amazon basin. Because understanding the changes imposed by these pyrogenic particles requires a knowledge of the "natural state", i.e. the composition, properties and effects of background (naturally-emitted) particles, both type of aerosols were studied in this work. The study mainly involved measurements of aerosols over an undisturbed primary tropical forest in Rondônia, Brazil, during two intensive field studies, namely the LBA-EUSTACH 1 and 2 campaigns, which occurred between April and November 1999.

CHAPTER II contains a detailed description of the measurement sites, the measurement techniques, and the sampling procedures used.

CHAPTER III describes the results of measurements of particle number concentration, particle number, volume, and mass/size distributions, scattering and absorption properties of aerosols, and the optical thickness of the aerosol layer under the pristine background conditions typical of the wet season, as well as during the biomass-burning-influenced dry season. These physical properties are discussed and compared for both seasons. From this, more complex parameters such as particle density and single scattering albedo are derived and discussed, comparing them to state-of-art measurements from other field studies. The sign of the forcing due to pyrogenic aerosols is estimated, and it is suggested that the changes in atmospheric aerosol resulting from biomass burning may have dramatic effects on the radiation balance, as well as cloud formation and rain-out processes (and thus the whole water cycle), in the Amazon basin.

CHAPTER IV presents the results of measurements of the elemental composition of the aerosol particles characteristic for background and biomass burning conditions, as well as their organic and elemental carbon content. In order to provide better understanding of the interacting processes occurring between the Amazonian forest and the atmosphere, the height profiles of some chosen tracer elements (derived from the data

obtained from three different sampling heights) are discussed in detail. The plausible sources for the various trace elements are also discussed in this chapter. Following this, the optical effect of aerosols characteristic of the wet and dry seasons are quantified in terms of mass scattering (α_s) and mass absorption efficiencies (α_a), which describe the efficiency of a given class of aerosol to scatter and absorb incoming radiation, respectively. Finally, the contribution of biomass burning and natural sources to the total aerosol mass are derived using a multivariate regression technique, from which an apportionment of the scattering and absorption properties of the total aerosol is estimated in terms of the major contributing aerosol sources.

CHAPTER V presents a new method developed to determine the refractive index of the sampled aerosols—one of the least-well characterized aerosol parameters. This method also allows for correction of the size distribution obtained from an optical particle counter. The model is based on Mie calculations applied to in situ measured scattering and absorption coefficients, and number size distributions. In order to verify the validity of the model, the output data are examined on four levels: 1) the sensitivity of the model to each parameter is assessed, 2) the calculated refractive indices are compared to those obtained from a chemical balance approach, 3) the corrected size distributions are compared to those obtained using a cascade impactor, and 4) the refractive index data are compared to those found in the literature for both wet and dry season types of aerosols. Finally, other climatically-relevant aerosol parameters, such as the backscattered fraction and the asymmetry parameter, are presented.

CHAPTER II.

SAMPLING LOCATION AND METHODOLOGY OF MEASUREMENTS

II.1. Sampling locations

Aerosols were sampled over two field campaigns at a pasture site (Fazenda Nossa Senhora Aparecida (FNS), located at 10° 45' 44" S, 61° 21' 27" W, 315 m above sea level) and on a 54 m meteorological tower situated in a primary rainforest with a mean canopy height of about 32 m (Reserva Biologica Jarú (RBJ), 10° 04' 55" S, 61° 55' 48" W, 110 m above sea level). Both sites are located in the state of Rondônia, Brazil, and separated by a distance of ca. 80 km (Figure II-1). The location of these sites was chosen to be representative for pasture and forest locations of this region of Amazonia (Gash et al., 1996b). The first campaign (LBA-EUSTACH 1) occurred in April–May 1999 and covered the end of the "wet season" period and the transition period toward the biomass burning influenced "dry season". The second campaign (LBA-EUSTACH 2) was conducted in September–October 1999 throughout the end of the "dry season" and the transition period toward the "wet season" again. LBA-EUSTACH 2 was largely dominated by biomass burning conditions, whereas LBA-EUSTACH 1 was more characteristic for background, pristine conditions.

The RBJ (Figure II-2) site was situated within the bounds of the rainforest ecological reserve, some 400 m eastwards of the "Rio Machado", which sets the limits of the reserve (Figure II-1). New farming is observable west of the tower site. Since 1998 some landless people started to settle within the natural reserve some 2 km south of the RBJ tower, extending up to ca. 100 km east from this point. Occasionally, some biomass burning plumes coming from these areas reached the tower site during the dry season. Deforestation started in the area of Ji-Paraná some 25 years ago, after the Cuiabá-Porto

Velho highway was constructed in 1968, from which settlers started clearing the forest, creating the "fishbone" pattern observable in Figure II-1.
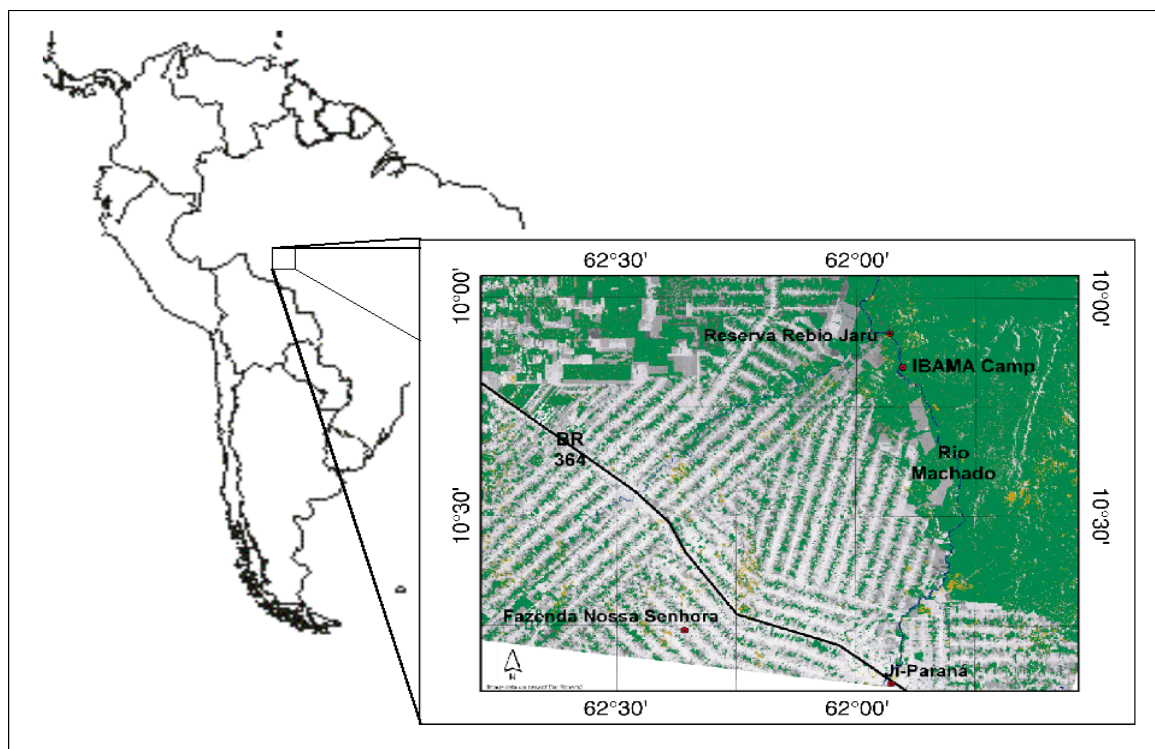
Figure II-1 Location of the sampling sites within South America.
The satellite picture shows the location of the tower in the Reserva Biológica Jaru (RBJ), the base camp (IBAMA camp), the Fazenda Nossa Senhora (FNS) pasture site, the river Rio Machado, and the main town Ji-Parana. BR 364 indicates the Cuiabá-Porto Velho highway. The light color represents the deforested areas (adapted from Andreae et al. (2002)).

Continuous power supply at the RBJ site was assured by two 30-kW diesel generators working alternatively. The generators were positioned on a raft on the Rio Machado (ca. 400 m away from the tower), with the exhausts directed just above the water level in order to minimize particulate emissions into the atmosphere. During the wet season, the RBJ site was only accessible by boat via the Rio Machado (ca. 4–6 hours from Ji-Paraná), whereas land transportation could be used during the dry season.

At the FNS site (Figure II-3), aerosol samplers were mounted on a 5-m heigh scaffold. The power supply was directly available from power lines, but the site was located ca. 500 m from a road (with low traffic) and some charcoal producers were situated a few kilometers from the site, which may have caused some local anthropogenic interference in the measurements during the wet season especially.

Figure II-2 View of the RBJ meteorological tower looking South from a second tower.

Figure II-3 Aerial view of the FNS pasture site.
Instruments were set up on a 5-m heigh scaffold inside the fenced area and also inside the huts. The area was first deforested by fire in 1977.

Table II-1 presents a summary of the aerosol measurements performed on the RBJ tower during LBA-EUSTACH 1 and 2. The major part of this dissertation relates to the data collected at this site. Data collected at the FNS site are mainly discussed in CHAPTER IV. For a more complete description of the measurement locations and overall sampling conditions, refer to (Andreae et al., 2002).

Table II-1 Summary of the measurements made during the LBA EUSTACH 1 and 2 campaigns in 1999 at the RBJ meteorological tower, Rondônia, Brazil[1]

Instrument	Type of measurement	Height (m)	Measuring period (LBA-EUSTACH 1)	Measuring period (LBA-EUSTACH 2)
CPC	Number concentration	53	23 Apr–21 May	14 Sep–29 Oct
PCASP	Number size distribution	53	6 May–21 May	7 Sep–26 Oct
Nephelometer	Scattering coefficient	49	8 Apr–21 May	20 Sep–1 Nov
PSAP	Absorption coefficient	52	8 Apr–12 Apr	8 Sep–9 Oct
			22 Apr–21 May	21 Oct–1 Nov
Aethalometer	Absorption coefficient	50 and	—	17 Sep–1 Nov
		3	—	25 Sep–1 Nov
MFR radiometer	Aerosol optical depth	ground	7 Apr–21 May	6 Sep–31 Oct
SFU[3]	Nuclepore filter sampling	48, 22, and 3	7 Apr–21 May (28)[4]	6 Sep–31 Oct (81)[4]
SFU[3]	Nuclepore filter sampling	FNS	28 Jan–22 May (76)	13 Sep–25 Oct (80)
HVDS	Quartz filter sampling	47	17 Apr–21 May (11)	3 Sep–31 Oct (28)
MOUDI	Mass size distribution	47	6 Apr–20 May (8)	04 Sep–31 Oct (35)

[1] Values in brackets are the number of samples collected during time frame indicated.
[2] —: no measurements.
[3] Sampling segregated into day and nighttime.
[4] Maximum numbers of filters sets collected at one of the measurement heights.

II.2. Real-time aerosol monitors

II.2.1. Relative humidity

Water is one of the major components of atmospheric aerosols, however its concentration and effects are usually unknown. These effects have already been partly integrated into modeling studies (see, e.g., Boucher and Anderson, 1995), and are usually calculated by combining hygroscopic growth factors with dry aerosol measurements. In

the present work it was decided to characterize the aerosol properties only under near ambient conditions of humidity; however, several methods used to dry the aerosols were tested within the frame of this work, and are briefly described here.

A critical issue to address when attempting to measure dry aerosol is the need to prevent losses of particles, and aerosol constituents other than water. A common method is to attach a diffusion dryer to the inlet of the measurement instrument. In this case, the discontinuity between the aerosol inlet (typically 1/4 inch in diameter (ca. 6.5 mm)) and the dryer (typically 1/2 inch in diameter (ca. 13 mm)) may be a source for turbulent flow and particle losses. As outlined in Section II.2.2, the use of a diffusion dryer on a condensation particle counter (CPC) inlet led to total particle losses of ca 19% (it is not clear which particle size fraction was affected most). Drying is usually not very efficient using a diffusion dryer, so that the tube needs to be relatively long, and the silica gel exchanged regularly (a procedure not always possible in the field). A common alternative is to heat the aerosol inlet; however, this may lead to significant losses of volatile/semi-volatile compounds such as organics or nitrates, which might be of importance when accounting for the optical properties of the particles.

During the course of the current work, the suitability of a Nafion dryer (Perma Pure Inc., Toms River, NJ, USA) for the drying of sampled aerosol was tested. This dryer is now being used in field studies, which seek to compare the dry and ambient aerosol in the Amazon basin. Nafion dryers are permeable membrane tubes that were primarily designed for drying and humidifying gas streams. Inside the dryer, water diffuses through the membrane, driven by the humidity gradient between the inside and the outside of the tubing. Nafion is a modified type of Teflon containing hydrophilic sulfonic acid groups. The Nafion is highly selective to water, but is known to produce losses of polar organic components (e.g., dimethylsulfoxide, alcohols, aldehydes, ketones, organic acids) and ammonia from the gas phase. The drying capacity of the Nafion dryer is compatible with field measurements in the tropics. A single Nafion tube (ca. 61 cm long, 7 mm diameter) produced a RH < ca. 40% for a sampling flow of 1.5 L min^{-1} at an ambient temperature of ca. 30 °C, and RH close to 100%. The results of a test comparing its performance with a stainless tube of the same length and diameter demonstrated that the Nafion tube was

responsible for only about a 1% reduction in scattering measured by a nephelometer (an example of the test is shown in Figure II-4). However, because Nafion consists principally of Teflon, electrostatic losses of the smallest particles, which do not contribute significantly to scattering, could be expected. Such a test could be extended to a full range of instruments; however, preliminary results at least suggest that Nafion dryers are a very viable means of aerosol sampling under controlled RH, when low flows are needed.
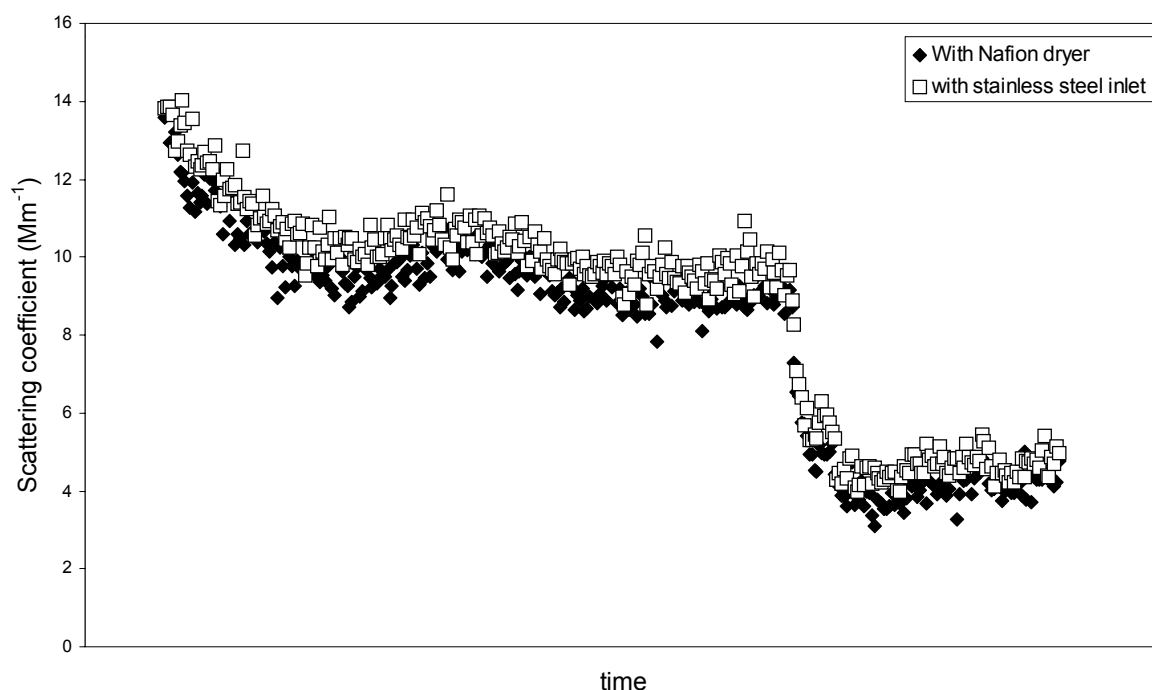
Figure II-4 Test of a Nafion dryer for particle losses, as indicated by a reduction in scattering coefficient measured by a nephelometer.
Each measurement represent a 2-min average scattering coefficient obtained from two inter-calibrated nephelometers sampling the same air, one mounted with a Nafion dryer at the inlet, the other with a stainless steel tube. The Nafion dryer was used in the non-drying mode (i.e., RH inside the Nafion equals that outside the Nafion membrane).

II.2.2. Particle concentrations

Aerosol particle concentrations in the diameter size range 0.01–3-μm diameter were measured at the RBJ site with a condensation particle counter (CPC 3010 or 3762, TSI, USA). Within a CPC, particles are grown into larger droplets several micrometers in diameter by condensation using a supersaturated vapor of butanol. The particles are then

directed through a detection chamber fitted with a laser-diode light source, where they scatter light. The scattered light pulses are then detected by a photodiode and counted as electrical pulses. The instruments used in this work can count individual particles up to a concentration of ca. 10,000 particles cm^{-3}.

The instruments were mounted on the meteorological tower at a height of 53 m above ground level, and were fitted with a diffusion drier installed in front of the inlet, because direct sampling of the extremely humid ambient air would have led to condensation of water within the instrument. The diffusion dryer consisted of a cylindrical metal mesh (length 0.59 m, diameter ca. 13 mm) surrounded by a plastic tube filled with silica-gel. The losses due to the inlet tubing and the diffusion drier were determined to be ca. 19%, for which the measurements were corrected. In addition, the raw data were adjusted for coincidence losses by applying an algorithm recommended by the manufacturer. The sample air flow was determined using a bubble flow meter (Gilibrator-2, Gilian, USA). On a few occasions (< 0.3% of total measurement time) during the LBA-EUSTACH 2 campaign (always at night), the CPC instrument was saturated when smoke plumes passed over the site.

II.2.3. Size distributions

Continuous particle number/size distributions were measured using a passive cavity aerosol spectrometer probe, the PCASP-100x (PCASP, DMT, USA, now owned by Particle Metrics, Longmont, USA), with a one-minute time resolution. The PCASP measured particle size distribution from 0.1 to 3 μm in 18 channels, derived from the light scattering properties of the particles at a wavelength of 633 nm between angles of 35° and 135°. The instrument was calibrated by the manufacturer, using polystyrene latex particles of known size. The refractive index of latex beads (1.59 − 0i) is different from that of atmospheric particles, resulting in a size distribution that is "latex equivalent". The refractive index of ambient aerosol particles may be subject to large intra- and interday variations, as a function of aerosol sources, age, and relative humidity (RH) (see CHAPTER V). Refractive indices were obtained using Mie scattering theory in combination with a new iterative process described in CHAPTER V, which utilizes the

raw PCASP-measured size distributions and independently measured scattering and absorption data as inputs. Accordingly, the PCASP size distributions were corrected utilizing the obtained refractive index (see CHAPTER V).

Successful operation of the PCASP requires that the particles pass through the radiation beam in the internal chamber of the instrument one at a time, so that the scattering efficiency can be measured for each individual particle. High particle concentrations ($>$10,000 cm^{-3}) may lead to particle coincidence, and therefore counting and sizing errors (Reid, 1998). Such conditions were only encountered occasionally during LBA-EUSTACH 2 (when individual young biomass burning plumes traversed the measurement site), and the data collected during these periods was excluded from further analysis. Reid (1998) also estimated the uncertainty in particle number concentration measured from the PCASP to be less than 10%. Because the error in particle number concentration can, for the most part, be attributed to the particle coincidence effect, the PCASP was considered to measure the concentration with a 10% accuracy at high particle concentration (Reid, 1998), as encountered during the LBA-EUSTACH 2 campaign, and with a 5% accuracy during the wet season campaign, when particle number concentration was about one order of magnitude lower. (Median total number concentrations measured by a condensation particle counter (CPC models 3010 and 3762, TSI, USA) were 400 cm^{-3} for the wet season and 4000 cm^{-3} for the biomass-burning-influenced campaign.)

In order not to significantly alter the properties of the sampled ambient aerosols, the de-icing heater that is situated at the inlet of the PCASP instrument was not used, and the sheath flow was not dried with silica gel. Collins et al. (2000) estimated the total internal temperature increase of the instrument to be about 3.5 ± 2 °C, which reduces the relative humidity (RH) inside the instrument and, consequently, the size of the sampled aerosols due to evaporative loss of water. Measurement of the RH inside the instrument is not possible with the current instrument design, and so it is not possible to determine the exact magnitude of this effect. Nevertheless, according to psychrometric charts the temperature increase inside the PCASP would be expected to lead to a decrease in RH of about 10–15%, under the conditions of RH and temperature encountered.

II.2.4. Scattering coefficients

Light-scattering measurements were made with a single-wavelength (λ = 545 nm) nephelometer (model M903, Radiance Research, Seattle, USA). Aerosols were sampled continuously and the data averaged and collected on a one-minute time resolution. No attempt was made to dry the particles prior to sampling. Nevertheless, the internal heat produced by the instrument itself may have partially dried out the sampled particles. On average, the RH inside the instrument was 15% (±6%) lower than ambient RH, comparable to that inside the PCASP.

The Radiance Research nephelometer measures light scattering between 8.9° and 170° angles, so that the scattering coefficients retrieved from the instrument are truncated for the very forward and backward scattering angles, and are lower than the effective total scattering from the sampled particle population (Figure II-5). Anderson et al. (1996) proposed a method for correcting scattering measurements obtained from a three wavelength TSI 3563 nephelometer (an instrument with similar characteristics to the Radiance Research nephelometer), based on the Ångström exponent derived from the scattering values obtained at 450 and 700 nm. They found that this instrument underestimates the total scattering coefficients by up to 10% for submicrometer particles, and 20–50% for supermicrometer particles. This correction procedure could not be employed for the Radiance Research nephelometer, since it measures at only a single wavelength. Nevertheless, a correction factor could be estimated from measured size distribution data and Mie scattering theory and found comparable truncation characteristics to that of the TSI instrument (see Section III.3.3). The errors associated with the scattering values presented herein are therefore considered to be due only to measurement error of the instrument itself (ca. 5%).
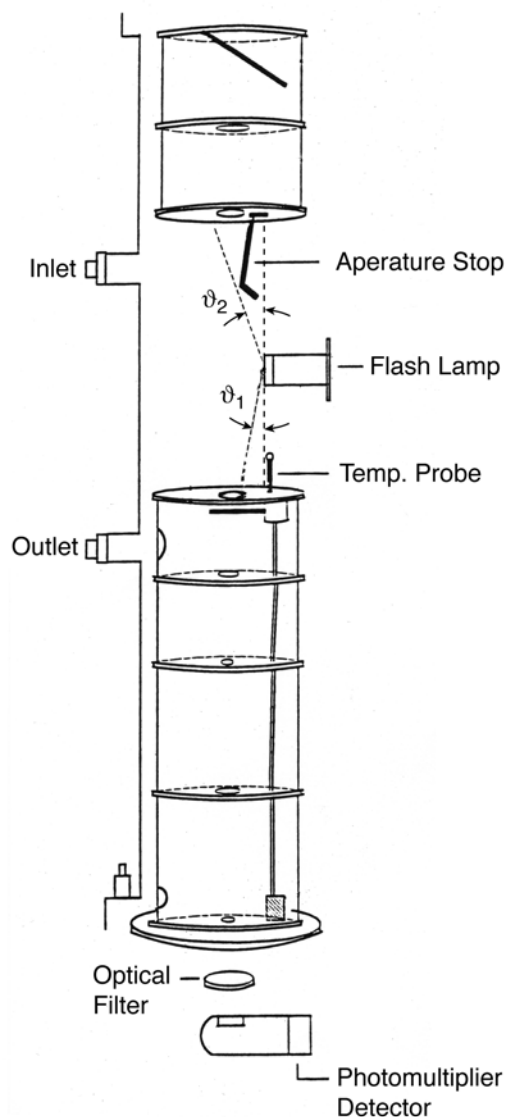
Figure II-5 Sectional view of the Radiance Research nephelometer.
The drawing shows the optical design of the instrument. θ_1 and θ_2 represent the forward and backward truncation angles, respectively.

II.2.5. Absorption coefficients

Continuous absorption measurements were made using a particle soot absorption photometer (PSAP, Radiance Research, Seattle, USA), which was positioned at 52 m above the ground on the RBJ meteorological tower. The PSAP operates on the principle of an integrating plate, measuring the transmittance of light with a center wavelength of 565 nm through a glass fiber filter onto which the sampled aerosols are deposited. Values

were collected every 5 minutes during the LBA-EUSTACH 1 campaign, whilst a sampling time of one minute was used during LBA-EUSTACH 2 because of the much higher aerosol loading resulting from local biomass burning. Absorption coefficients, σ_a, were retrieved according to Reid et al. (1998b) and Bond et al. (1999).

Care was taken to monitor the accuracy of the air flow through the PSAP using a Gilibrator bubble flow meter, and to correct the absorption coefficients measured by the PSAP for the deposit spot area. In the present case, the measured spot area was 1.795×10^{-5} m^2 (diameter of 4.78 mm), compared to the value of 1.783×10^{-5} m^2 (diameter of 4.765 mm) quoted in the PSAP manual, and the area of 2.043×10^{-5} m^2 (diameter of 5.1 mm) actually assumed by the PSAP internal calibration. Bond et al. (1999) and Anderson et al. (1999) suggest correcting the actual deposit area of the PSAP instrument as compared to the assumed one by multiplying the PSAP output by the following F_{spot} factor:

$$F_{spot} = \left(\frac{D_{meas}}{D_{calib}} \right)^2,$$

(II-1)

where D_{meas} is the diameter of the spot measured for the instrument, and D_{calib} is the diameter assumed by the instrument ($D_{calib} = 5.1$ mm).

The rest of the Bond calibration was then applied to the PSAP data corrected for the actual flow and deposit spot area (σ_{am}), according to:

$$\sigma_a = \left(\sigma_{am} - C_{a,scat} \sigma_{s,trunc} \right) C_{a,cal}$$

(II-2)

where σ_a is the corrected absorption coefficient, $C_{a,scat}$ the correction factor for the PSAP response to scattering ($C_{a,scat} = 0.02 \pm 0.01$), $\sigma_{s,trunc}$ the corresponding measured scattering coefficient (without correction for the angular truncation), and $C_{a,cal}$ the adjusted PSAP response to absorption ($C_{a,cal} = 0.820$).

Precision uncertainty, $\sigma_{a,prec}$, for the PSAP instrument is also given by Bond et al. (1999) as

$$\delta \sigma_{a,prec}^2 = \delta \sigma_{a,noise}^2 + F_{drift}^2 \sigma_a^2$$

(II-3)

where F_{drift} (with a value of 0.06) is the drift slope uncertainty obtained from the agreement of three PSAPs between each other (Anderson et al., 1999), and $\sigma_{\text{a,noise}}$ is the instrument noise. In the present case the 95% confidence interval for instrument noise, obtained from filtered air measurements, was found to be 0.008 Mm^{-1} for hourly time resolution, much smaller than the value of 0.11 Mm^{-1} obtained by Anderson et al. (1999) for the same time resolution (0.18 Mm^{-1} for a 24-min time resolution).

During the dry season, absorption was also measured at the RBJ site using two Magee Scientific Co. aethalometers, positioned at 3 and 50 m above the ground on the meteorological tower. The aethalometer, like the PSAP, operates using the principle of an integrating plate, and measures transmittance through a glass fiber filter at a wavelength of 880 nm. The aethalometers were operated with a 5–min time resolution. Data were corrected for the non-linearity of the measured values with filter loading (Reid et al., 1998b), and the internal calibration absorption efficiency of 19 $\text{m}^2\ \text{g}^{-1}$ was used to convert the concentration output of the instruments ($\mu\text{g m}^{-3}$) into absorption coefficients (Mm^{-1}).

The absorption coefficients obtained at the pasture site were also measured using an aethalometer (Artaxo et al., 2002), which was operated in an identical fashion to that described above for the forest instruments.

II.2.6. Aerosol optical depth

Aerosol optical depth (AOD, τ) under cloud-free atmospheric conditions was measured during both measurement campaigns using a Yankee multifilter rotating shadowband radiometer (MFR) (MFRSR-7, Yankee Environmental Systems, Turner Falls, USA) (Harrison et al., 1994). In the present study, five wavelengths were used (415, 500, 615, 671, and 867 nm). First, the Langley technique was applied on morning and afternoon data of air masses, m, ranging between 2 and 6, in order to acquire an estimate of the solar constant from the intercept of the regression line of the measured irradiance on the air masses (Harrison and Michalsky, 1994). A set of clear days was chosen from each period to obtain the value of the solar constant for each wavelength and then the Beer-Lambert-Bouguer law was applied to derive instantaneous measurements of the total

optical depth (one-minute time resolution). The AODs for the five wavelengths were then obtained by subtracting the contribution of Rayleigh scattering and ozone absorption from the total optical depth. A more detailed description of the instrumentation, methodology, and quality control can be found in Formenti et al. (2000) and references therein.

II.3. Filter sampling and chemical analysis

II.3.1. Elemental Analysis

Aerosol particles were collected for elemental analysis on 47 mm Nuclepore filters (8.0 and 0.4 µm pore size polycarbonate filters, available from Merck Eurolab) using Stacked Filter Units (SFUs) (Maenhaut et al., 1994). Nuclepore filters were stored in sterile Petri-slides. The SFUs located at the pasture site were positioned ca. 3 m above ground level on a scaffold. The SFUs situated in the forest were positioned at three different heights on the measurement tower, namely 48 m (ca. 16 m above maximum canopy height), 22 m (within the canopy), and 3 m above ground level. The SFUs, which were fitted with a PM10 inlet, were operated according to Parker and Buzzard (1977) at a flow rate of typically 16 L min^{-1} (controlled by a rotameter and a volume meter), with two filters in series being used to collect the "coarse" ($2.0 < D_p < 10$ µm; with D_p the aerodynamic diameter) and "fine" ($D_p < 2.0$ µm) size fractions. Day and nighttime samples were differentiated, with typical sampling times of 36 h during LBA-EUSTACH 1, and 4–12 h during LBA-EUSTACH 2. The sampling time had to be decreased drastically during the second campaign due to the high aerosol concentration resulting from biomass burning. Despite this reduction in sampling time, significant flow reductions that had to be accounted for in the calculations were still sometimes experienced, or even clogging of some filters, which had to be discarded.

Elemental concentrations were obtained by Particle-induced X-ray emission analysis (PIXE) for both coarse and fine SFU aerosol fractions (Johansson and Campbell, 1988). With this technique, concentrations of up to 19 elements could be determined (Mg, Al, Si, P, S, Cl, K, Ca, Ti, Cr, Mn, Fe, Ni, Cu, Zn, Br, Sr, Zr, and Pb). Detection limits were typically 5 ng m^{-3} for elements in the range $13 < Z < 22$, and 0.4 ng m^{-3} for elements

with $Z > 23$. Precision of the elemental concentration was typically better than 10%, and up to 20% for elements with concentrations close to the detection limit. Mass concentrations were obtained by gravimetric analysis. SFU filters were weighed before and after sampling using a Mettler M3 electronic balance with $1-\mu g$ sensitivity, and an accuracy of $\pm$ 5 μg. So-called "black carbon equivalent" (BC_e) concentrations were obtained for the fine fraction of the SFU filters by a light reflectance technique (Andreae, 1983). BC_e is defined as the concentration of soot carbon that gives the same absorption response in the instrument as the absorbing substances contained in the sample. There is much uncertainty in the measurement of "true" black carbon by the light reflectance technique; therefore, BC_e should only be considered as an estimate of the absorbing matter.

II.3.2. Carbonaceous content

Aerosol particles were collected for carbon analysis on quartz fiber filters (cat. No. 2500 QAO, available from Pallflex Corp.) using a High Volume Dichotomous Sampler (HVDS). Quartz filters were prepared and stored following a standard procedure (Salmon et al., 1998), in order to keep blank measurements of organic carbon and elemental carbon low. Quartz fiber filters were pre-fired at 600°C overnight in pre-baked aluminum foils, and were kept stored in these aluminum pockets until sampling. Filters were manipulated only with clean, solvent-rinsed tweezers. After sampling, filters were stored in pre-baked glass jars at −18°C or colder until analysis.

The HVDS (Solomon et al., 1983), which split the aerosol into two size fractions (particles of D_p larger and smaller than ca. 2.5 μm), was positioned 48 m above ground level on the measurement tower at the forest site. A total flow rate of 330 L min^{-1} was used, with sampling times ranging between 48–72 h for the LBA-EUSTACH 1 campaign, and 24–48 h for LBA-EUSTACH 2.

Because the HVDS used in this work was borrowed from California Institute of Technology, Pasadena, California, the instrument was prepared and calibrated according to Salmon et al. (1998), using critical orifices and pressure gauges to control the flow.

Figure II-6 presents a sectional view of the HVDS, and the configuration of the complete system for flow rate control. The large gas meter is only needed for calibrating the instrument. A characteristic of the HVDS is that the instrument is a "virtual impactor". To achieve a particle cutoff diameter of ca. 2.5 μm, about one tenth of the total sampled flow is passed through the coarse particle filter; therefore, about one tenth of the fine particles are entrained with the coarse particle flow and are collected on the coarse particle filter (ideally, in a virtual impactor, no flow should be allowed though the coarse mode filter). Mass concentrations were corrected for this artifact according to Dzubay et al. (1978). However, it is noted here that, due to the overwhelming amount of fine particle sampled during the dry season, coarse particle concentrations were sometimes found to be negative after applying the Dzubay correction, and coarse particle analyses of the HDVS samples were discarded.
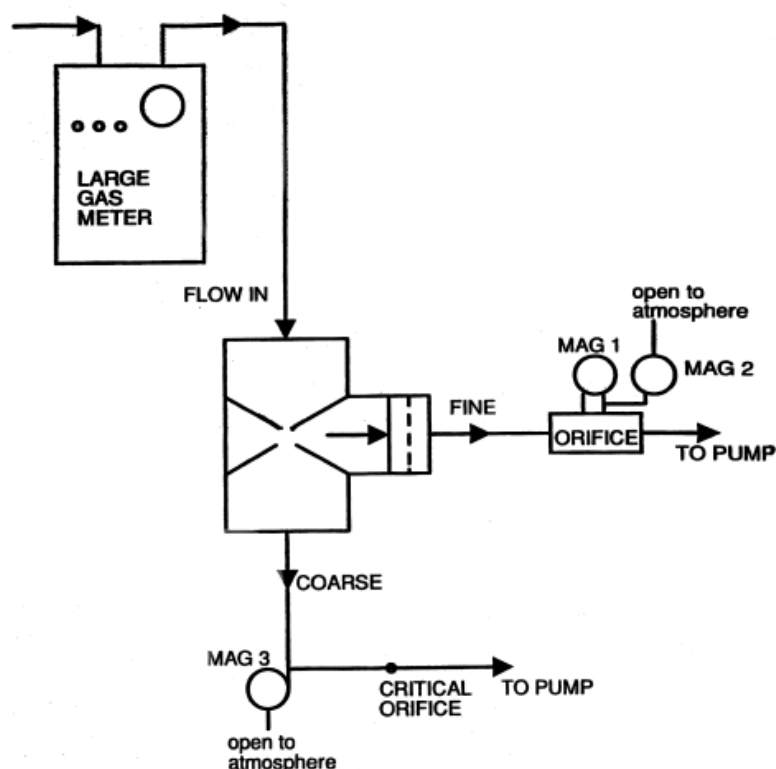
Figure II-6 Sectional view of the complete HVDS system.
MAG 1–3 are the differential pressure gauges used to control the flow. In the field, the instrument was used upside down with a rain hat fitted to the inlet to prevent rain from entering the instrument.

Organic carbon (OC), apparent elemental carbon (EC_a), and total carbon (TC; TC = OC + EC_a) analyses were performed on the HVDS quartz filter aerosol samples using a thermo-optical transmission (TOT) technique (Birch and Cary, 1996). Briefly, in the TOT analysis a portion (typically one rectangular 1-cm^2 punch of the filter for the dry season samples, and two punches for the wet season samples) of the filter deposit area (61.51 cm^2 in this case) is analyzed. In the first step, the sample is heated up to a temperature of about 820°C in a pure helium atmosphere. The evolved organic and carbonate carbon is oxidized to CO_2 over a MnO_2 catalyst maintained at 900°C, reduced to CH_4 in an Ni/firebrick methanator maintained at 450°C, and quantified as CH_4 by a flame ionization detector. In the second step, the temperature is ramped in a mixed oxygen-helium atmosphere, and the pyrolitically generated EC (resulting from the "charring" of some OC) as well as EC_a are oxidized and analyzed. The limit of detection of the TOT technique is about 0.23 μg of carbon (Birch and Cary, 1996).

Elemental carbon is usually assumed to be the only light absorbing matter in aerosols (with the exception of metal oxides, normally present in negligible quantities). As mentioned above, OC and EC_a obtained from TOT measurements are defined in terms of the thermal refractory property of the carbon, with a correction applied based on the optical transmission measurement. The presence of refractory high-molecular-weight organic matter—now known to be produced during biomass burning—can complicate the apportionment of TC between the EC_a and OC components, and may lead to large error in the quantification of the light absorbing matter, as discussed in more detail in section IV.3.2. The TOT technique corrects for the artifact EC_a formed by charring during pyrolysis of the organic compounds by defining EC_a as only the carbon that evolves after the light transmittance through the sample has reached the original transmittance (an optical feature allows continuous monitoring of the filter transmittance). Therefore, the OC quantity obtained from the TOT analysis is, by definition, non-light-absorbing. Nevertheless, uncertainties in the discrimination between EC_a and OC may arise from the fact that some organic compounds may also be light-absorbing.

It has also been found that the relative amounts of OC and EC_a, as provided by the TOT technique, can depend on the temperature program used for certain sample types (Yu

et al., 2002; W. Maenhaut, unpublished results) and that the technique may provide too low EC_a/OC for heavily loaded filter samples (Kubátová et al., 1999).

II.3.3. Mass/size distribution

The mass/size distribution of the aerosols was also measured with a microorifice uniform deposit impactor (MOUDI, model 110, MSP corporation, Minneapolis, USA). The MOUDI cascade impactor was operated in the nonrotating mode at a sampling flow rate of 30 L min^{-1}, using 47-mm diameter (25 μm thick) aluminum substrates for sample collection. The airflow was controlled by a valve and monitored by a pressure gauge measuring the pressure difference between atmospheric pressure and stage number 7 of the MOUDI. Aluminum substrates were pre-fired at 600°C overnight, and stored in Petri dishes covered with a baked aluminum lining. After sampling, substrates were stored in a freezer at −18°C or colder until analysis.

Aerosols of aerodynamic diameter between 18 and 0.051 μm were collected in 10 fractions with calibrated D_{50} aerodynamic cutoffs of 18, 9.9, 6.2, 3.1, 1.8, 1.0, 0.578, 0.346, 0.200, 0.093, and 0.051 μm (calibration done by the manufacturer based on nozzle pressure drop). The sampling time was typically 72 hours during LBA-EUSTACH 1, and varied between 24 and 48 hours during LBA-EUSTACH 2. No pre-drying of the incoming air was performed prior to sampling. The aerosols likely had a high water content due to the high humidity conditions encountered during both campaigns. Thus, sampling errors arising from re-entrainment ("particle bounce") were probably minimal due to the high "sticking efficiency" of such particles (Marple et al., 1991). Mass concentrations were obtained by gravimetric analysis. Substrates were weighed before and after sampling, with a Mettler microbalance (1 μg sensitivity), after having been left equilibrating under controlled conditions of RH (50%) and temperature (20 °C) for at least 24 hours. The accuracy of the measurements is ca. ±3 μg for aluminum foils and ±5 μg for Nuclepore filters.

The MOUDI mass/size distributions were inverted following the work of Roberts et al. (2002), which is an adaptation of the Twomey nonlinear iterative algorithm

described by Winklmayr et al. (1990). Collection efficiencies $E(D)$ for the MOUDI which was used in this study were obtained by calculating the steepness factor s associated with each MOUDI stage from the collection efficiencies reported by Marple et al. (1991), using

$$E(D\ ) = \left[1 + \left(\frac{D_{50}}{D}\right)^{2s}\right]^{-1} \tag{II-4}$$

with D the particle diameter, and D_{50} the 50% cutoff diameter, and fitting the $E(D)$ s-shaped function to the D_{50} characteristic for the instrument used here. This procedure allowed us to retrieve continuous size distributions, which contain more information than the histogram obtained from directly plotting the mass concentration measured for each MOUDI stage.

CHAPTER III.

PHYSICAL PROPERTIES AND CONCENTRATION OF AEROSOL PARTICLES OVER THE AMAZON TROPICAL FOREST

Abstract

The size distribution, scattering and absorption properties of Amazonian aerosols and the optical thickness of the aerosol layer under the pristine background conditions typical of the wet season, as well as during the biomass-burning-influenced dry season are investigated in this chapter. The measurements were made during two campaigns in 1999 as part of the European contribution to the Large-Scale Biosphere-Atmosphere Experiment in Amazonia (LBA-EUSTACH). In moving from the wet to the dry season, median particle numbers were observed to increase from values comparable to those of the remote marine boundary layer (~400 cm^{-3}) to values more commonly associated with urban smog (~4000 cm^{-3}), due to a massive injection of submicron smoke particles. Scattering and absorption coefficients, measured at 550 nm, showed a concomitant increase from average values of 6.8 and 0.4 Mm^{-1} to values of 91 and 10 Mm^{-1}, respectively, corresponding to an estimated decrease in single-scattering albedo from ca. 0.97 to 0.91. Aerosol optical depths at 500 nm increased from 0.05 to 0.8. The roughly ten-fold increase in many of the measured parameters attests to the dramatic effect that extensive seasonal biomass burning (deforestation, pasture cleaning) is having on the composition and properties of aerosols over Amazonia. The potential exists for these changes to impact on regional and global climate through changes to the extinction of solar radiation as well as the alteration of cloud properties.

III.1. Introduction

Solar radiation is modified when passing through the atmosphere by two main processes: light scattering and light absorption. Light scattering is a redistribution of the incident light in nonparallel directions, whilst light absorption consists of a conversion of the incident light into thermal energy. The attenuation of light by these processes has important climatic consequences (Andreae and Crutzen, 1997; IPCC, 2001).

Trace gases like CO_2, H_2O, NO_2 and CH_4 efficiently absorb radiation in the infrared range, trapping the radiation emitted from the earth, causing the well-known "greenhouse effect". In contrast, aerosol particles are thought to have an overall cooling effect, estimated to be of the same order of magnitude as the positive forcing of greenhouse gases (IPCC, 2001). However, these estimates are still subject to wide uncertainties, mainly due to the fact that aerosol climate forcing depends on the optical properties and spatial distribution of the aerosols, both of which vary greatly according to the sources, location, and age of the aerosols. Aerosol particles both absorb and scatter light, with the efficiency of the processes being highly dependent on their size distribution, chemical composition and the wavelength of the incident radiation. Scattering efficiency is predominantly a function of particle size, morphology, and chemical composition, and is mainly due to aerosol particles in the accumulation range (0.1–1 μm). The light absorption by aerosols covers the whole spectrum, and is largely due to near-graphitic carbon (also called elemental, or black carbon), whose unique known source are combustion processes.

Of the various major aerosol particle types, those emitted during biomass burning are amongst the most optically active (Reid and Hobbs, 1998) due to the fact that they are predominantly in the form of submicrometer, accumulation-mode particles, and also contain a high content of light-absorbing components. This, coupled with the fact that biomass burning has been estimated to be the second largest source of anthropogenic aerosols (IPCC, 2001), has led to extensive investigation of smoke aerosols (both laboratory and field based), with a primary aim being to determine their contribution to Earth's radiation balance. Despite these efforts, however, the radiative forcing due to aerosol particles is still subject to large uncertainties (at least a factor of two), and the

confidence level of global estimates is considered as 'low' (Andreae and Crutzen, 1997; Shine and Forster, 1999; IPCC, 2001).

Biomass burning activities are most concentrated in the tropical areas of Africa, Indonesia and South America (Andreae, 1991), where fire is routinely used for both deforestation and seasonal burning of secondary forests and pastures. Of these regions, the Amazon basin has perhaps been the focus of most international attention, due to the fact that it contains the world's largest tropical rainforest and continues to experience one of the highest rates of deforestation in the world. Measurement campaigns like the Smoke, Cloud, Aerosol and Radiation-Brazil (SCAR-B) experiment (Kaufman et al., 1998) and the dry and wet season Amazon Boundary Layer Experiments (ABLE 2A and 2B) (Harriss et al., 1988; Harriss et al., 1990), have sought specifically to improve our understanding of the environmental and climatic effects of biomass burning and background aerosols in this region. As a result, it is now clear that smoke aerosols emitted there have a very strong local impact on incoming radiation (Ross et al., 1998). Moreover, recent studies have shown that the smoke produced in the tropics may be subject to high altitude uplift and long-range transport due to the intense convective activity (Andreae, 1991; Pickering et al., 1996; Andreae et al., 2001; Staudt et al., 2001). The potential, therefore, exists for the extensive biomass burning in the Amazon basin to have a global influence (Andreae et al., 2002). Ongoing studies of the sources, properties and processes involving aerosols are therefore critical for this region.

This chapter focuses on a comparison of the physical properties of aerosols (number concentration, size distribution, scattering and absorption coefficients, single-scattering albedo, and aerosol optical depth) representative for background conditions (LBA-EUSTACH 1) with those for fresh and aged smoke from anthropogenic biomass burning (LBA-EUSTACH 2). This study contributes towards a more thorough understanding of the regional and global climatic effects of widespread biomass burning in Amazonia and other tropical regions.

III.2. Sampling location and methodology of measurements

Sampling location

Aerosols were sampled during two field campaigns on a 54 m tower situated in a primary rainforest (Reserva Biologica Jarú, Rondônia, Brazil, 10° 04' 55" S, 61° 55' 48" W, 110 m above sea level), in April–May 1999 (LBA-EUSTACH 1) and September–October 1999 (LBA-EUSTACH 2). The LBA-EUSTACH 1 campaign covered the end of the wet season period and the transition period toward the biomass-burning-influenced dry season. LBA-EUSTACH 2 was conducted throughout the end of the dry season and the transition period toward the wet season again. For a more complete description of the site and overall sampling conditions, refer to Section II.1 and Andreae et al. (2002).

Size distributions

Continuous particle number/size distributions were measured using PCASP, with a one-minute time resolution (Section II.2.3). PCASP size distributions corrected for an average refractive index calculated for three periods of interest are presented in this chapter. The three periods were designated as follows: (1) LBA-EUSTACH 1, before the transition period (representative for background, wet season conditions), (2) LBA-EUSTACH 1, during the transition period toward the biomass-burning-influenced, dry season period, and (3) LBA-EUSTACH 2, largely dominated by biomass burning conditions. The average refractive indices associated with each period were 1.42 (±0.04) − 0.006 (±0.003)i, 1.46 (±0.06) − 0.016 (±0.003)i, and 1.41 (±0.05) − 0.013 (±0.005)i, respectively. Refractive indices were obtained using Mie scattering theory in combination with a new iterative process, which utilizes the raw PCASP-measured size distributions and independently measured scattering and absorption data as inputs (CHAPTER V). To facilitate comparison of the size distributions observed during the different periods studied, the distributions were normalized by the concentration of the size bin of the PCASP showing the largest value in the accumulation mode (0.1–1 μm).

Mass/size distributions were obtained from a MOUDI impactor (see Section II.3.3).

Uni- and bimodal number, volume, and mass/size distribution were parameterized by a lognormal equation:

$$\frac{dQ}{d\,log\,D} = \sum_{i=1}^{2} \frac{Q_i}{\sqrt{2\pi}\sigma_i} exp\left[-\frac{\left(ln\,D - ln\,D_{Q,i}\right)^2}{2\sigma_i^{\,2}} \right] \qquad \text{(III-1)}$$

where Q expresses the number, volume or mass quantity, $D_{Q,i}$ is the median particle diameter of the mode i for the quantity Q, and σ_i is the standard deviation.

Further instrumentation

Aerosol particle number concentrations, light scattering, light absorption, and optical depth measurements used in the subsequent sections of this chapter were performed conform to what is described in Section II.2.

III.3. Results and discussion

III.3.1. Aerosol particle concentration

During both the LBA-EUSTACH 1 and the LBA-EUSTACH 2 campaigns, two CPC instruments were used to acquire total aerosol particle concentration data for particles in the size range of 0.01–3.0 μm diameter (Figure III-1).

The low concentrations (median of ca. 400 cm^{-3}) measured at the beginning of the first campaign (April) compare to those found for marine air, which typically exhibits particle concentrations of 100–300 cm^{-3} (Fitzgerald, 1991; Finlayson-Pitts and Pitts, 2000; Raes et al., 2000). Given that the removal of fine mode aerosols from the troposphere is usually largely due to the incorporation of the aerosols into cloud droplets, followed by precipitation, as well as to scavenging below clouds during rain (Finlayson-Pitts and Pitts, 2000), these remarkably low concentrations are undoubtedly associated with the large amount of precipitation observed during the month of April (Andreae et al.,

2002), as well as with the weak sources of aerosol particles in the Amazon basin during the non-burning season. Similar concentrations were observed by (Roberts et al., 2001) and (Zhou et al., 2002) in the Amazonian site of Balbina, north of Manaus, in 1998 (average particle concentrations of 460 ± 320 cm^{-3}), suggesting that conditions encountered in the unpolluted Amazon basin resemble more those observed from marine environments in contrast to what is typically reported for continental environments.

Precipitation decreased during the month of May, and particle concentrations consequently increased (median of ca. 600 cm^{-3}, Figure III-1), indicating a transition from the wet season toward the dry season (Andreae et al., 2002). This increase in particle concentration also coincided with the onset of fire activity in the states neighboring Rondônia. Table III-1 shows a summary of daily fire activity (normalized per 100,000 km^2) detected by the NOAA-12 satellite, for the days the satellite was exactly over the region of interest.
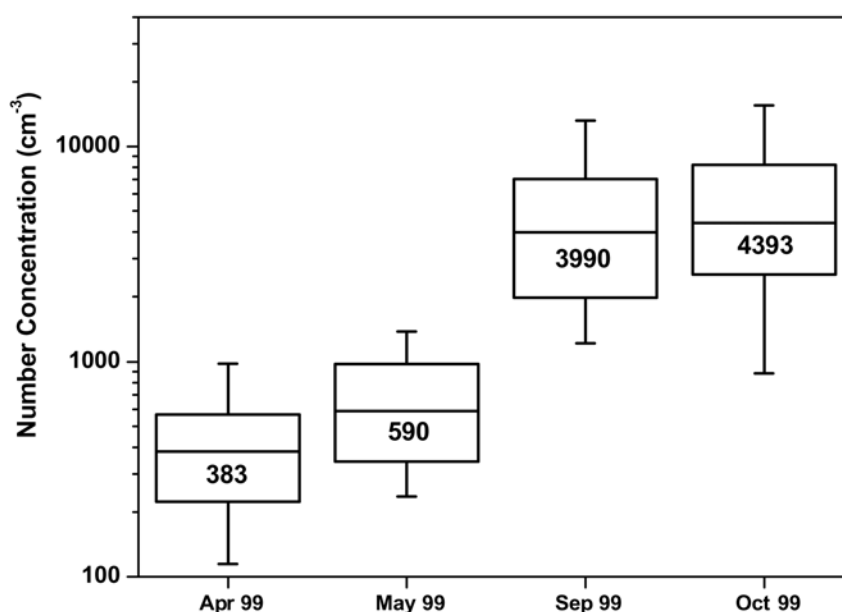
Figure III-1 Aerosol particle number concentration.
Distribution of aerosol particle concentrations (diameter >10 nm) during the wet-to-dry season transition (LBA-EUSTACH 1, Apr–May) and the dry-to-wet season transition (LBA-EUSTACH 2, Sep–Oct). The horizontal bars and the corresponding values inside the boxes represent the median concentrations, while the box defines the first and third quartiles, and the vertical bars the 5th and 95th percentiles.

It is noteworthy that there were actually no fire pixels detected in the state of Rondônia, where the measurements took place, and virtually none north of the tower, over the two months covering the LBA-EUSTACH 1 campaign. However, five-day back trajectories calculated for a starting altitude of 500 m (above ground level) using the NOAA/Air Resources Laboratory HYbrid Single-Particle Lagrangian Integrated Trajectory (HYSPLIT-4) model (Draxler and Hess, 1998) clearly show that air masses passing over the sampling site during this period were all coming from those areas that contributed to most of the fire activity in the region, namely Mato Grosso (MT), Mato Grosso do Sul (MS), and Goias (GO) states (Table III-1). According to the back trajectories (Figure III-2), these biomass-burning-influenced air masses required some 2–3 days to reach the sampling site. In light of this, the beginning of the LBA-EUSTACH 1 campaign (08 April–12 May 1999) was considered to be representative for background Amazonian conditions, whilst the second part of the campaign (13–21 May 1999) was influenced by aged smoke from biomass burning.
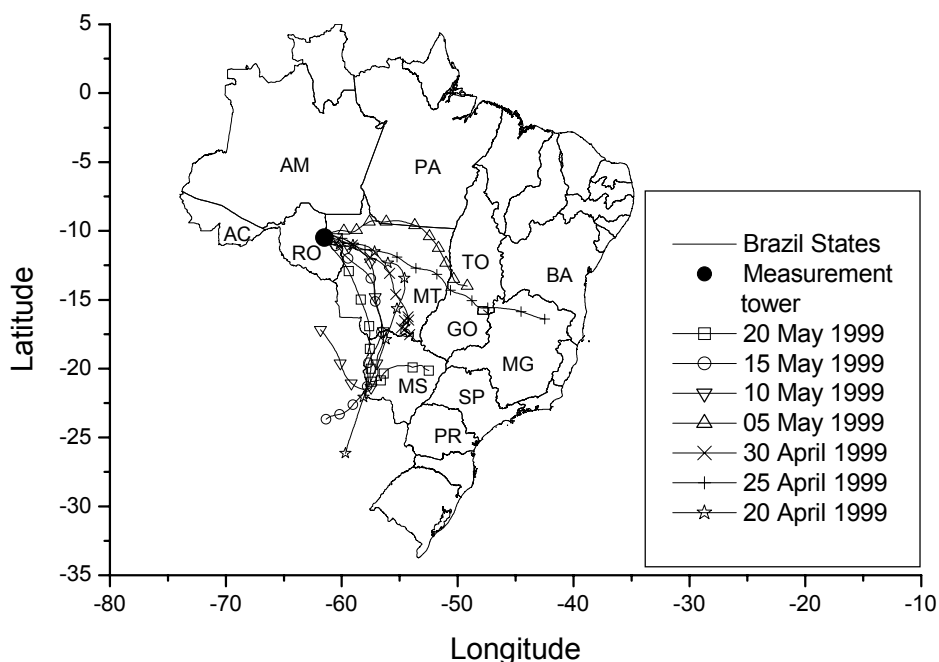
Figure III-2 Representative five-day (HYSPLIT-4) back trajectories calculated for the LBA-EUSTACH 1 campaign.
The starting point was the measurement tower (10°05' S, 61°56' W), for an altitude of 500 m above ground level. The symbols are spaced at 12-hour intervals along the trajectories.

Table III-1 Daily fire activity detected by the AVHRR-NOAA-12 satellite over the Amazon basin during LBA-EUSTACH 1 and 2.
The data presented are the total number of fire pixels per 100,000 km^2 detected over the Brazilian states showing significant biomass burning activity. The data for Brazil's neighboring countries are not normalized over the area of the country because the NOAA-12 satellite was scanning only a fraction of these countries at the time considered. The numbers given for these countries are the total numbers of fire pixels detected at that time. (available from CPTEC at http://www.cptec.inpe.br/products/queimadas/)

Brazilian state or Neighbor country	LBA-EUSTACH 1						LBA-EUSTACH 2					
	1 May	4 May	5 May	10 May	14 May	19 May	22 Sep	26 Sep	30 Sep	5 Oct	10 Oct	23 Oct
Goias (GO)	1	—	—	—	2	2	7	9	7	5	11	4
Mato Grosso (MT)	1	—	1	2	6	7	34	24	43	82	52	7
Mato Grosso do Sul (MS)	3	16	3	1	4	4	16	78	35	28	33	14
Paraná (PA)	—	—	—	—	—	—	15	3	2	4	88	20
Pará (PR)	—	0.3	—	0.4	0.1	1	8	4	2	2	1	1
Rondônia (RO)	—	—	—	—	—	—	44	37	5	158	44	8
São Paulo (SP)	6	2	3	18	16	15	17	29	14	11	25	8
Tocantins (TO)	—	—	—	—	—	1	0	7	2	3	13	1
Argentina	3	5	2	6	3	2	77	46	811	53	58	5
Bolivia	—	12	5	—	—	5	38	84	269	339	189	52
Venezuela	65	47	56	54	36	17	7	6	3	1	—	2
Paraguay	10	2	—	6	16	5	100	344	102	56	299	143

The burning season in Rondônia reached its peak during the month of September, when the LBA-EUSTACH 2 campaign started. This was a month later than for its neighboring state to the East, MT, where the most intense biomass burning activity for the year 1999 occurred in Brazil (Table III-1, http://www.cptec.inpe.br/products/queimadas/). This burning activity had a dramatic effect on the measured aerosol particle concentrations. The total amount of particles increased by an order of magnitude compared to the LBA-EUSTACH 1 campaign, with the median number concentration exceeding 4000 cm^{-3}. This is clear evidence of the strong impact that human activities are having on the atmospheric conditions over the Amazon region.

The measured aerosol concentrations in Rondônia decreased significantly in the last week of October (median of ca. 1700 cm^{-3}, compared to an overall median of ca. 4400 cm^{-3}). During this week, rainfall frequency increased, signaling the transition towards the next wet season (Andreae et al., 2002).

III.3.2. Number, volume, and mass size distributions

The mean normalized number size distributions ($\Delta N/\Delta \log_{10}(D)$) measured by the PCASP for pristine background conditions (period preceding 12 May), background conditions affected by aged biomass smoke (period 12–21 May), as well as for regional biomass burning haze (LBA-EUSTACH 2 campaign), are presented in Figures III-3a–c. In each case, the accumulation mode (particles of $D < 1$ μm) of the size distribution could be fitted by a lognormal equation ($r^2 > 0.86$), yielding the geometric mean diameter and geometric standard deviation parameters summarized in the first column of Table III-2.

The overall shape of the normalized number distributions did not vary significantly from the beginning (Figure III-3a) to the end of the LBA-EUSTACH 1 (Figure III-3b) campaign, although absolute concentrations increased significantly (Section III.3.1). Both median number distributions show a similar bimodal profile with maxima at ca. 0.17 and 3–4 μm for the accumulation and coarse modes, respectively. The standard deviations for the two distributions are also quite similar, with a slightly broader distribution in the second period (especially for particles with diameters of ca. 0.2–0.3

μm). The coarse mode could not be successfully fitted to a lognormal curve because of its relatively low abundance and because of interference by a smaller intermediate mode at ca. 0.8–1.5 μm. For the whole of the LBA-EUSTACH 1 campaign, the relative concentration ratios for the size bins within the accumulation mode varied from the median values by less than a factor of 1.5 for 75% of the time, whereas they varied by up to a factor of ca. 3 for the coarse and intermediate modes. This higher variability for the larger particle sizes could be due to the poorer counting statistics in this range (Le Canut et al., 1996).

Compared to the distributions observed for the LBA-EUSTACH 1 campaign, the dry-season number/size distribution (Figure III-3c) shows a broader accumulation mode and a greater abundance of accumulation mode particles relative to coarse mode particles. This is due to the fact that biomass burning contributes mostly to the release of accumulation mode particles into the atmosphere. This mode, which shows a number median diameter centered at ca. 0.19 μm, is similar in shape to that measured by Reid et al. (1998a) for local haze in Cuiabá (using a PCASP instrument and assuming a particle refractive index value of $1.50 - 0.02i$). The accumulation mode seems to be composed of two sub-modes—a dominating mode at ca. 0.15 μm (comparable to the other distributions), and a second one at ca. 0.3 μm. Similar to the observations made in this study, Reid et al. (1998a) and Le Canut et al. (1996) also found two modes with maxima at ca. 0.1–0.18 μm and ca. 0.2–0.3 μm in the number size distribution of "background aged biomass-burning smoke". The second mode within the accumulation mode could be attributed to condensational growth and/or coagulation as the particles aged. Radke et al. (1995) observed growth of forest fire particles from the emitted Aitken mode ($D < 0.2$ μm) to accumulation mode sizes ($D = 0.2$–2 μm) within the first few hours after emission. Assuming, in the present case, a mixture of aged and younger smoke particles would be consistent with the observations made on site of concentrated regional haze disturbed occasionally by more local younger plumes. However, these two modes are typically observed from PCASP data as, for example, Reid and Hobbs, (1998) did not observe such a pattern in their differential mobility particle sizer data, and it cannot be excluded that this could not be a product of some artifact in the PCASP data.
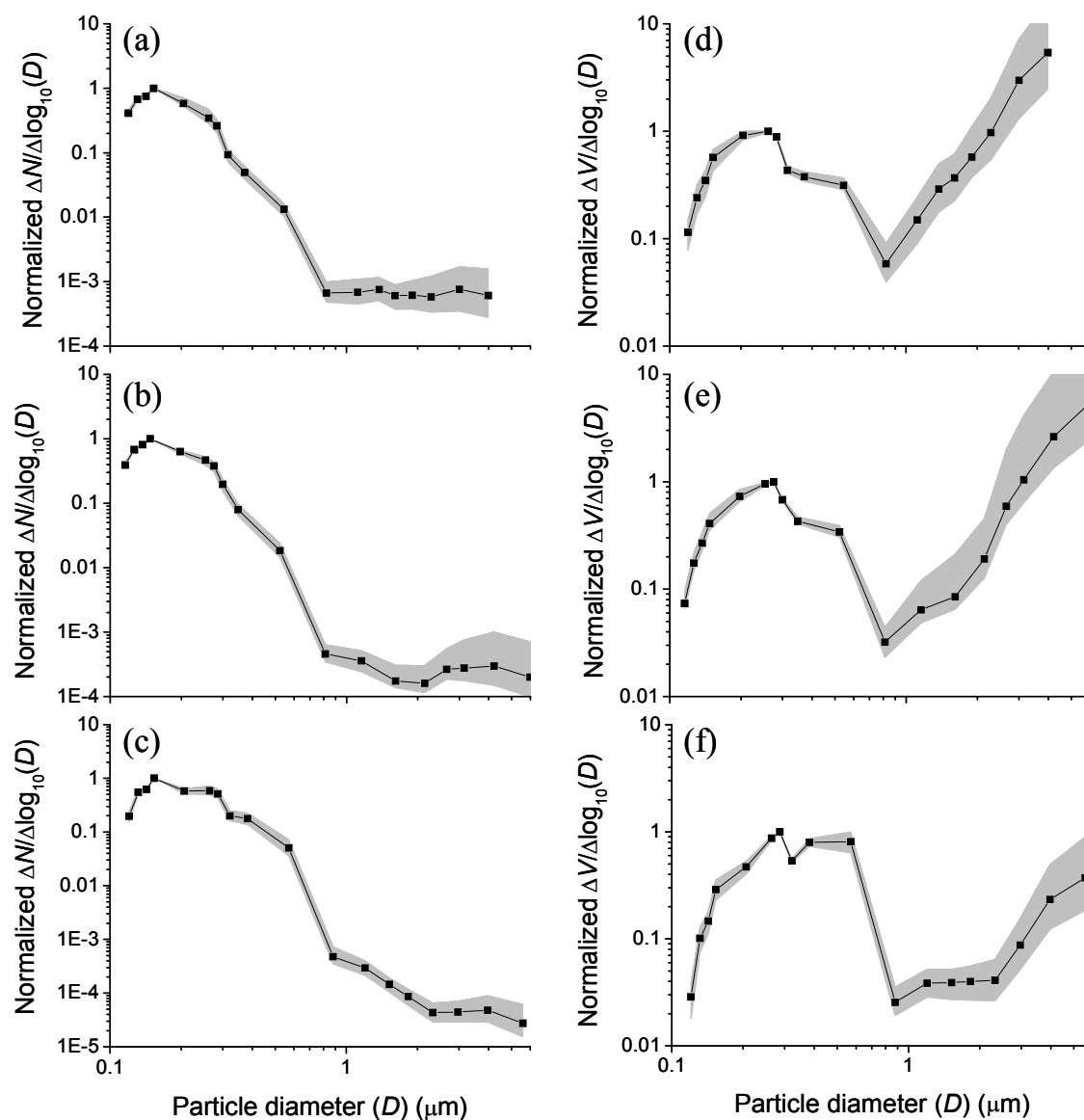
Figure III-3 Normalized number and volume/size distribution
Normalized number/size distribution for (a) background aerosols, (b) background aerosols altered by an aged biomass smoke, (c) and regional biomass burning haze measured over the Amazonian rain forest in Brazil during the LBA-EUSTACH campaigns. In each case, the solid line represents the median size distribution obtained over the considered period. The gray zone is the area between the first and the third quartile size distribution for each period. Figures d–f show the same as a–c but for normalized volume/size distributions.

It can be seen from Figures III-3a–c that the number size distributions obtained from the PCASP instrument are truncated for particles smaller than 0.1 μm, and that this lower cutoff diameter occurs near the maxima observed for the accumulation modes. A consequence of this is that during the LBA-EUSTACH 2 campaign, the PCASP could only account for ca. 60% of the total number of particles detected by the CPC. The unaccounted-for fraction consists predominantly of particles of the Aitken mode emitted during the pyrogenic process. Although very numerous, these fine particles contribute little to the total aerosol mass and volume, and are characterized by poor optical efficiencies.

The normalized volume distributions ($\Delta V / \Delta \log_{10}(D)$) for the three periods defined above are shown in Figures III-3d–f. It can be seen that the PCASP accounts for most of the accumulation mode volume, but truncates the coarse mode. All three distributions appear to have a bimodal accumulation mode, which could be due to an artifact of the instrument, as described above. However, examination of the raw data showed that the correction is not a primary source of error, but emphasizes the irregularities already existing in the distribution. Therefore, and despite the resulting poor fit (r^2 of 0.87 for the dry season data, but fitting poorly the central size bins at $D = 0.2$–0.6 μm), it was decided to apply a unique lognormal equation to the accumulation mode of these curves, which has probably a more physical meaning. It is noted here that it cannot be excluded that the accumulation mode might actually be bimodal in nature for the dry season distribution; however, the two peaks are too sharp in shape, and overlap too much to be successfully fitted individually by lognormal equations.

The parameters describing the best fit of lognormal equations to the volume distributions are summarized in the second column of Table III-2. The standard errors associated with the lognormal parameterization of the coarse mode are large because of the upper truncation of this mode. The correction for the refractive index applied to the PCASP data might overestimate the sizes of the particles in the coarse mode, because a unique refractive index is assumed over the whole size distribution, and the absorption in this mode might be overestimated (CHAPTER V). The volume mean diameter for the accumulation mode increases with increasing amounts of haze aerosols, from ca. 0.23 μm

during the wet season to ca. 0.36 μm for the smoke haze period. Reid et al. (1998a) reported values in the range 0.25–0.30 (± 0.02) μm for regional haze using the same instrument (see above). The same authors also reported a mean volume diameter of 0.28–0.35 (± 0.05) μm, obtained using a differential mobility particle sizer. Dubovik et al. (2002) reported an AOD-dependent mean volume radius of $0.14 + 0.013 \times AOD$ (at 440 nm), and a geometric standard deviation of 0.40 ± 0.04 for aerosols emitted by biomass burning in the Amazon. Applying a centered AOD of ca. 0.9 at 440 nm (Section III.3.6) to this equation would yield a mean volume diameter of ca. 0.30 μm. The latter values, derived from ground-base radiometer measurements, are slightly lower than those found in the current study, but confirm the observed trend of increasing accumulation mode mean volume diameter with increasing burning activity.

Typical mass size distributions (obtained as described in Section II.3.3) for the three periods are shown in Figure III-4, and the lognormal fit parameters associated with each distribution are summarized in the third column of Table III-2. The discrepancy in geometric standard deviation observed between the number, volume, and mass/size distributions of each period is an indication of the overall uncertainty associated with these distributions, as the standard deviation of a distribution should remain the same for all distribution types (Seinfeld and Pandis, 1998; Hinds, 1999; Finlayson-Pitts and Pitts, 2000). In most cases, the lognormal fit of the regional haze coarse mode (5–6 Oct. 1999) was difficult, if not impossible to apply, due to the overlap of this mode with the large accumulation mode. However, the profile of the coarse mode during this period was generally similar to that found under background conditions, although slightly higher concentrations were observed. As was the case for the PCASP data, a second peak is noticeable within the regional haze accumulation mode at $D \sim 0.55$ μm. However, this peak is less pronounced in the MOUDI compared to the PCASP data, and the MOUDI distribution is narrower than the PCASP volume distribution, which could be due to overcorrection of the PCASP data or in inverting the MOUDI data. A peak in fine particles could also be observed at 0.05–0.07 μm.

It is noted here that on some occasions, MOUDI samples were obtained with the dominant fraction collected one stage lower than usual (stage 8, of aerodynamic cutoff

D_{50} = 0.200 μm, instead of stage 7, D_{50} = 0.346 μm). One of these samples (2–3 Oct 1999) was identified as a young biomass-burning plume (Section V.4.5), and the lognormal fit yielded mean diameters (standard deviations) of 0.31 ± 0.01 (0.50 ± 0.05) and 3.15 ± 0.16 (0.46 ± 0.01) μm for the fine and coarse mode, respectively. Characteristically, this sample did not exhibit a second peak within the accumulation mode at larger diameter, suggesting that the presence of this peak in the regional haze samples could be attributed to condensational growth.
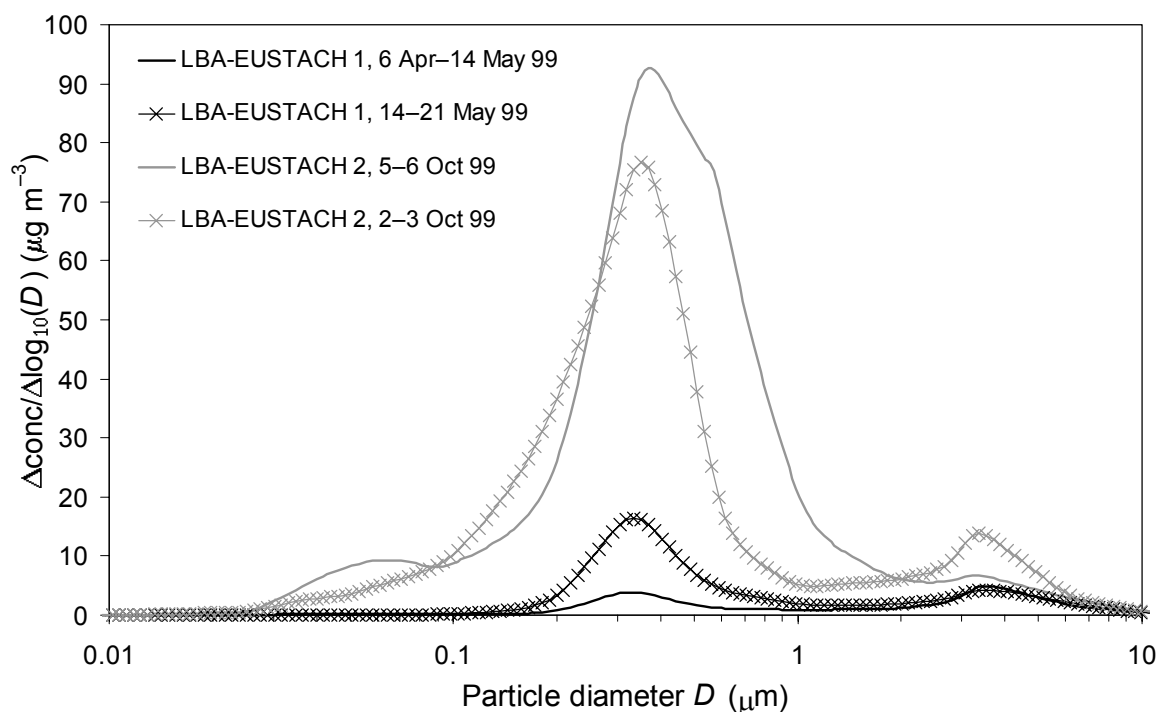
Figure III-4 Typical MOUDI mass size distributions
For background aerosol (black line, 6 Apr–14 May 1999), background aerosol under increasing influence of biomass burning (dotted line, 14–21 May 1999), concentrated biomass burning aerosol (gray line, 5–6 Oct. 1999), and young biomass burning plume (linked black crosses, 2–3 Oct. 1999) measured in the Amazon basin during the LBA-EUSTACH campaigns. The background size distribution is an average distribution from six three-day MOUDI samples, whilst the biomass burning-influenced background distribution is an average of two three-day samples.

Table III-2 Particle size parameters (mean ± standard error for the lognormal fitting equation) for Amazonian aerosols observed during the LBA-EUSTACH 1 and 2 campaigns.

	Particle number distribution		Particle volume distribution		Particle mass distribution	
	Mean diameter (μm)	Standard deviation	Mean diameter (μm)	Standard deviation	Mean diameter (μm)	Standard deviation
6-12 May 1999[1]	0.17 ± 0.003	0.30 ± 0.03	0.23 ± 0.008 6.86 ± 2.04	0.33 ± 0.04 0.55 ± 0.10	0.35 ± 0.01 3.77 ± 0.04	0.36 ± 0.01 0.41 ± 0.01
13-21 May 1999[2]	0.17 ± 0.004	0.34 ± 003	0.24 ± 0.008 9.39 ± 1.68	0.37 ± 0.03 0.55 ± 0.07	0.34 ± 0.01 2.78 ± 0.10	0.32 ± 0.01 0.87 ± 0.04
Sep-Oct 1999[3]	0.19 ± 0.007	0.36 ± 0.05	0.36 ± 0.03 6.65 ± 10.1	0.52 ± 0.06 0.49 ± 0.8	0.41 ± 0.02	0.46 ± 0.01

[1] MOUDI samples taken from 6 Apr to 14 May 1999, [2] from 14 to 21 May 1999, and [3] on 5–6 Oct 1999.

Figure III-5 shows a scatter plot of the MOUDI mass concentrations measured during the LBA-EUSTACH 2 campaign against the corresponding integrated volume concentrations, for particles with diameters of 0.1–1 μm. Plotted are both volume concentrations derived directly from the "raw" PCASP size distributions, as well as the ones derived after adjustment of the PCASP size bins for the refractive index of the sampled aerosol. For this adjustment procedure the average refractive index value of 1.41 − 0.013i calculated in CHAPTER V for biomass burning aerosols during this campaign was used. The regression analysis (with intercept forced to zero—the intercept being meaningless in the present case, and insignificantly changing the r^2 of the regression) yielded an accumulation mode particle density of 1.38 g cm^{-3} (standard error of 0.03, r^2 = 0.95) using the uncorrected PCASP data, and 0.65 g cm^{-3} (standard error of 0.01, r^2 = 0.94) using the refractive index-adjusted PCASP data. The higher estimate is probably an overestimation of the average density, as the PCASP size bins were not corrected for the refractive index, and the particle volume increases with the third power of this correction. On the other hand, the lower value could be an underestimation of the particle density because the PCASP was measuring ambient aerosols, whilst the MOUDI substrates were left equilibrating under controlled conditions of RH (50 %) and temperature (20 °C) for at least 24 hours prior to weighing, and volatile and semi-volatile constituents of the aerosol (including water) may have evaporated. These compounds may also have evaporated during daytime sampling, when the MOUDI was exposed to larger temperatures. However, it cannot be excluded that the correction for the refractive index applied to the PCASP overcorrects the data, resulting in an underestimation of the particle density.

Reid and Hobbs (1998) reported an average density for smoke particles ($D < 4$ μm) in Brazil of 1.35 ± 0.15 g cm^{-3}, with a technique similar to ours. However, their analysis comprised data for particles in the size range of 1–4 μm, and could therefore also include, for example, dust particles (uplifted by convection during a fire) whose specific density is larger than the biomass burning aerosols of interest here. Martins et al. (1998a) reported density values ranging between 1.00 and 1.21 g cm^{-3} for different types and ages of biomass burning aerosols in Brazil, without stipulating how they obtained these values. A value of ca. 1.5 g cm^{-3} was found from a mass closure analysis of the LBA-EUSTACH

2 aerosol data ($D < 2$ μm) (Section V.4.2). It is also noted, however, that this value might be an overestimation because voids and/or the water content of the aerosols were not taken into account, which would have lowered the density. These calculations are also based on specific densities for organics and black carbon estimated from literature values, which cover a broad range. A typical value often reported in the literature for the density of biomass burning aerosol particles is 1.0 g cm^{-3} (Radke et al., 1991), derived from the work of Stith et al. (1981). The latter authors determined the density of particles emitted from three prescribed burns of conifer slash by regressing a set of volume size distributions (obtained from an optical inversion technique) against mass size distributions. They retrieved values of 0.75, 0.94, and 1.34 g cm^{-3} for the three separate fires, and noted that these values were positively correlated with the fuel moisture content. Too little information on the density of this type of aerosol is available to date, resulting in large uncertainties in aerosol model calculations.
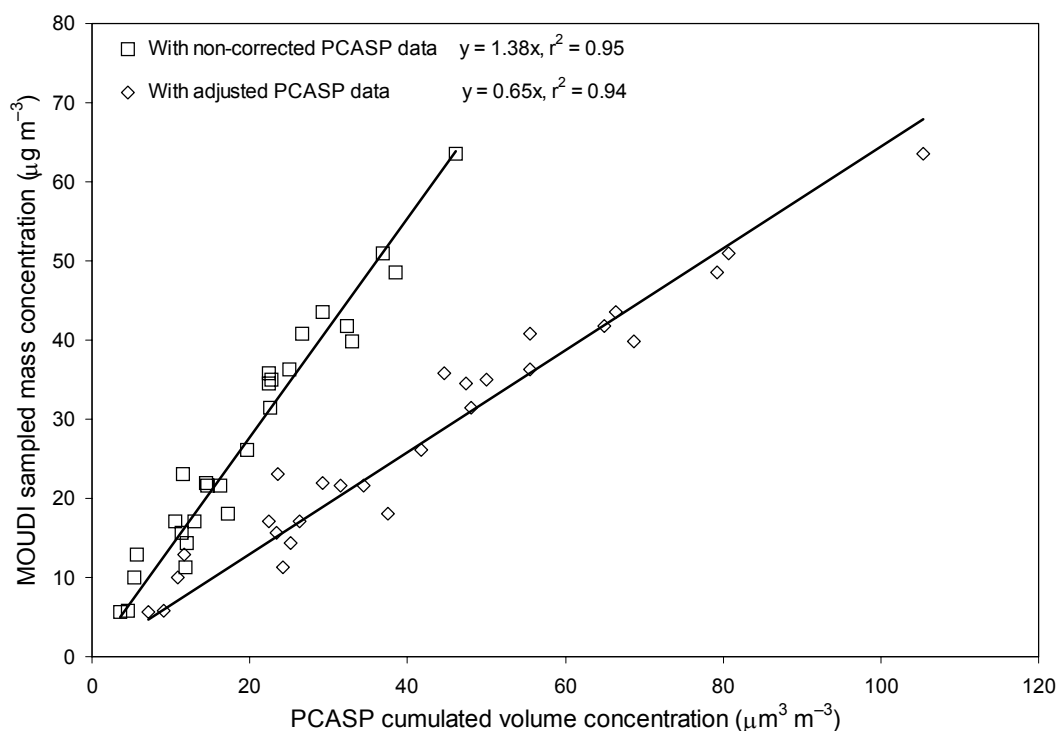
Figure III-5 Density of biomass burning accumulation mode particles.
Scatter plot of integrated volume concentrations obtained from a PCASP instrument against the MOUDI mass concentrations within a size range of 0.1–1 μm for the LBA-EUSTACH 2 campaign. The open squares were obtained using the volume concentrations derived directly from the "raw" PCASP size distributions, the open diamonds using the volume concentrations derived after adjustment of the PCASP size bins for the refractive index of the sampled aerosol (1.41 – 0.013i).

The regression of the only five MOUDI samples collected in parallel to the PCASP during the LBA-EUSTACH 1 campaign yielded a density of 3.23 g cm^{-3} (standard error of 0.08, $r^2 = 0.99$) using the uncorrected PCASP data, and 1.89 g cm^{-3} (standard error of 0.10, $r^2 = 0.99$) using the refractive index-adjusted PCASP data, for background aerosols of diameter 0.2–1 μm, over the Amazon basin. The higher values compared to the LBA-EUSTACH 2 campaign reflect the presence of particles such as dust grains, which form a proportionately greater fraction of the wet season aerosol (Artaxo et al., 1990; Echalar et al., 1998), and which have an aerosol density much larger than that of biomass burning particles.

III.3.3. Scattering coefficients

Scattering coefficients were measured at a wavelength of 545 nm during both campaigns, using a Radiance Research integrating nephelometer. This nephelometer measures the scattering coefficients of an aerosol population between the scattering angles of 8.9° and 170°, i.e., the very forward and backward scattering are not measured. Since Anderson et al. (1996) have shown that neglecting this truncation may lead to errors in scattering coefficients of up to 10% for submicron particles, and between 20 to 50% for the supermicron mode, it was considered it pertinent to determine an appropriate correction factor in order to calculate more accurate estimates of the total aerosol scattering coefficients. Fortunately, such a correction factor could be retrieved as a "by-product" of an iterative procedure that was recently developed for estimating the refractive index of atmospheric aerosols (CHAPTER V). In this procedure, hourly averages of scattering coefficients, absorption coefficients and PCASP number size distributions from both measurement campaigns were used concomitantly in combination with a standard Mie scattering model so that absorption and scattering coefficients could be recalculated from the size distribution of the PCASP. The angular truncation of the nephelometer was taken into account in the Mie program, and the corrected scattering coefficient (σ_s), as well as the truncated scattering coefficients ($\sigma_{s,trunc}$) (identical to the one measured by the nephelometer), were retrieved. From these, a correction factor, F_{trunc}

(= $\sigma_s / \sigma_{s,trunc}$), could be extracted and applied to the whole data set, as explained in detail below.

Figures III-6a and 6b present daily averages of the scattering coefficients measured by the nephelometer when ambient RH was below 92%, as well as when it was below 80%, together with the scattering coefficients corrected for truncation for the LBA-EUSTACH 1 and 2 campaigns, respectively. Scattering coefficients (σ_s) recorded at RH > 92% were removed from the data set because an ambient RH of 92% (equivalent to ca. 78% inside the instrument) was found to be the threshold value above which most scattering coefficient data showed an erratic response to increasing RH, at least for the LBA-EUSTACH 1 campaign. The presence of dense smoke plumes crossing the measurement site over almost the whole LBA-EUSTACH 2 campaign caused large variations in the measurements and made it more difficult to determine an upper RH limit for this season. Nevertheless, the aerosols exhibited reasonable properties up to an ambient RH greater than 92%, and this value was therefore also chosen as the upper limit for this campaign. Because of the consistently very high RH observed at night during both campaigns (typically between 90 and 100%), nighttime data are not presented.

Generally, it was observed that scattering coefficients increased with increasing RH, beginning at values of ambient RH as low as 60%, suggesting that the aerosols (especially during the first campaign) were taking up water even at low RH. Overall, the scattering coefficients measured at RH < 80% were only ca. 3% lower than those measured at RH < 92% for both the LBA-EUSTACH 1 and 2 campaigns.

Daily averages of the corrected scattering coefficients measured during the first campaign at RH < 92% were found to range from 0.9 ± 0.7 to 30.6 ± 5.1 Mm^{-1} (Figure III-6a). The σ_s values increased sharply around 12 May 1999, attributable to the increasing influence of biomass burning aerosols, together with the reduced precipitation rate toward the end of this campaign (see Section III.3.1). The increase coincided with increased particle numbers measured by the CPC, with an overall correlation of $r^2 = 0.82$ between the truncation-corrected scattering coefficient and total particle concentration for the LBA-EUSTACH 1 campaign.
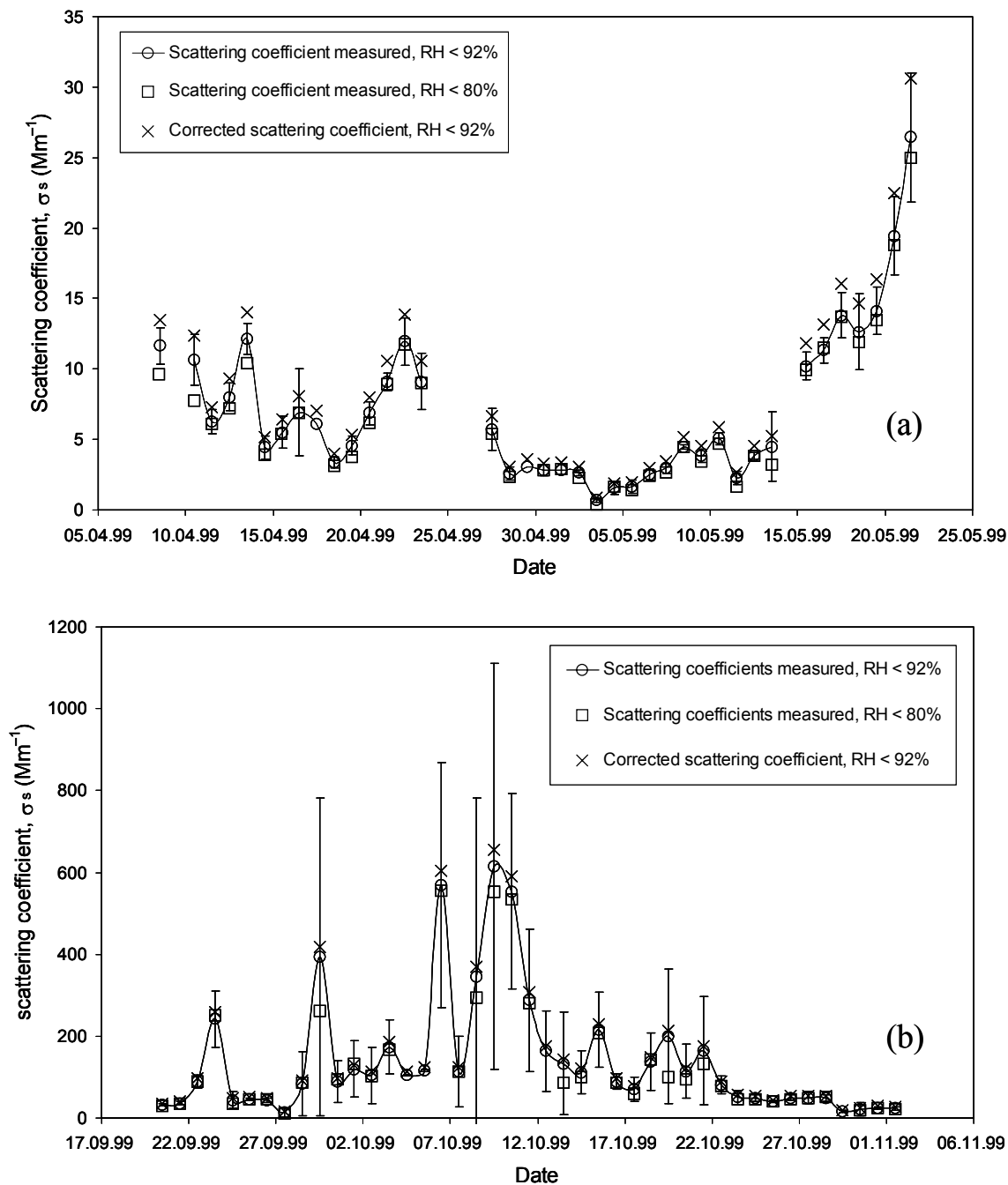
Figure III-6 Scattering coefficients of aerosol particles for the LBA-EUSTACH 1 and 2 campaigns.
Daily averages of the scattering coefficients measured by a Radiance Research nephelometer ($\sigma_{s,trunc}$), and of the scattering coefficients corrected for the truncation angles (σ_s), during the LBA-EUSTACH 1 (a) and LBA-EUSTACH 2 (b) campaigns. Values of σ_s recorded at RH lower than 92% (crosses), $\sigma_{s,trunc}$ measured at RH lower than 80% (open squares) and 92% (open circles) are presented. The bars represent the standard deviation of the measurements.

The average value of σ_s for the period 8 Apr–12 May, which was considered to be representative for pristine background conditions, was 6.8 ± 4.3 Mm^{-1} (for ambient RH < 92%). This is slightly lower than that measured by Formenti et al. (2001) (mean background ambient σ_s of 10 ± 1 Mm^{-1}) for the Amazonian site of Balbina, north of Manaus, in 1998. This difference is probably due to the fact that the current study was performed at a more remote location. The values obtained in this study are also about half those measured for clean marine boundary layer during the ACE-2 experiment (Collins et al., 2000).

In contrast to LBA-EUSTACH 1, the LBA-EUSTACH 2 campaign showed highly variable light scattering values (indicated in Figure III-6b by the large standard deviation associated with the measurements), due to the frequent passage of biomass burning plumes over the measurement site. Daily averages of daytime values were found to vary between 16 and 654 Mm^{-1}, with an overall median value (first; third quartile) of 91 Mm^{-1} (51; 201). These values fall within the lower range of scattering coefficients measured by Reid and Hobbs (1998) for younger plumes, in the direct vicinity of the fires. The data show a general increase in σ_s values around 9 October, followed by a decrease that coincided with an observable decline in fire activity (Table II-1). The lowest values were mostly recorded after 23 October, which was a period characterized by increased rainfall. The scattering coefficient data followed a similar temporal trend to the CPC data, with an overall correlation of $r^2 = 0.53$ between the hourly-averaged scattering coefficient (truncation corrected) and total particle concentration for the LBA-EUSTACH 2 campaign.

Figure III-7 presents a scatter plot of the corrected scattering coefficients, as obtained from the iteration calculation, against the truncated scattering coefficients for both LBA-EUSTACH 1 and 2 (for hourly averaged data measured at an ambient RH lower than 80%). Linear regression yielded fitting equations of $\sigma_s = 1.16\, \sigma_{s,trunc} + 0.05$ ($r^2 = 1.00$, $n = 64$) and $\sigma_s = 1.06\, \sigma_{s,trunc} + 2.03$ ($r^2 = 1.00$, $n = 170$) (scattering coefficients in Mm^{-1}) for LBA-EUSTACH 1 and 2, respectively (with n the total number of data points considered for each season). This indicates that, within the range of $\sigma_{s,trunc}$ observed for each season, not correcting for truncation leads to an error of ca. 16% for the LBA-

EUSTACH 1 campaign, and ca. 6% for LBA-EUSTACH 2. It is noted here that inclusion of data collected between 80% and 92% RH did not produce a significant change in the regression parameters obtained.
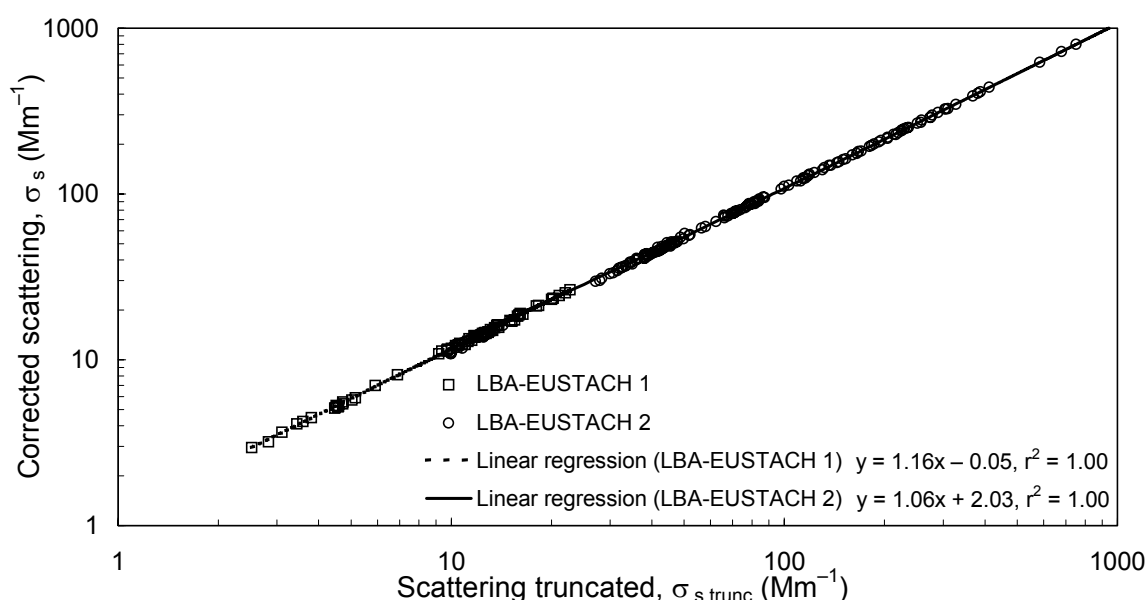
Figure III-7 Scatter plot of the truncation factor, F_{trunc}, defined as the ratio of σ_s over $\sigma_{s,trunc}$ for both LBA-EUSTACH 1 and 2 campaigns.
The least-square linear fit of the LBA-EUSTACH 1 (dotted line) and LBA-EUSTACH 2 (solid line) data are presented.

A sensitivity study for the truncation factor, F_{trunc}, was performed using the individual uncertainties associated with the measurements from the various instruments (see Section V.3.3 for a detailed description of the sensitivity test). The slope (F_{trunc}) was found to be virtually insensitive to changes in any of the individual parameters. It can be concluded that F_{trunc} is constant over the whole range of scattering coefficients and particle number concentrations observed during both seasons, and is therefore only dependent on particle type and size. The method proposed here for calculating the truncated part of the scattering coefficient obtained from an integrating nephelometer, therefore, appears very robust. Nevertheless, it should be noted that the lowest values measured during the second measurement campaign ($\sigma_{s,trunc}$ < ca. 30 Mm^{-1}) do not lie on the linear fit obtained for this season, but tend to be closer to the one for the LBA-

EUSTACH 1 data. The two equations found for the truncation factor agree well with those found by Anderson et al. (1996), if it is considered that the LBA-EUSTACH 2 campaign was largely dominated by submicron smoke particles, whereas the LBA-EUSTACH 1 campaign included a large contribution of supermicrometer particles (Section III.3.2).

III.3.4. Absorption coefficients

Daily averages of measured ($\sigma_{a,meas}$) and Bond-corrected absorption coefficients (σ_a) for the LBA-EUSTACH 1 and 2 campaigns are presented in Figure III-8a and Figure III-8b, respectively. Because the Bond correction of the PSAP data requires the use of simultaneously measured scattering coefficients, the corrected σ_a were computed for RH < 92% only, in order to not overcorrect for the instrument response to scattering (see Section III.3.3). The missing σ_a values, comparing to $\sigma_{a,meas}$, are due to either the absence of scattering data or to extensive periods of RH > 92%, in which cases the Bond correction could not be applied to the PSAP data. Overall, absorption coefficients showed a similar temporal variation to the other aerosol properties that were measured. Daily averages of the values recorded during the first part of the LBA-EUSTACH 1 campaign were below 1.4 ± 0.8 Mm^{-1} (average of 0.4 ± 0.5 Mm^{-1} for the period 08 April–12 May 1999), increasing to a value of 5.6 ± 0.5 Mm^{-1} (on 21 May 1999) when aged biomass burning smoke began reaching the site.

The background values obtained in this study are lower than the ones reported by Artaxo et al. (2002) for the same campaign. An aethalometer situated at a pasture site 80 km away from the forest site measured 0.19 ± 0.22 μg m^{-3} of absorbing material on average, corresponding to a σ_a value of 1.9 ± 2.2 Mm^{-1}, assuming an absorption cross section of 10 m^2 g^{-1}. However, their measurements were more influenced by local anthropogenic pollution. This is supported by higher particle concentrations measured with a CPC at the pasture site (890 ± 920 cm^{-3}) compared to the tower site (median of ca. 400 cm^{-3}), indicating that the conditions encountered at the tower site during the LBA-EUSTACH 1 campaign were closer to pristine background conditions.
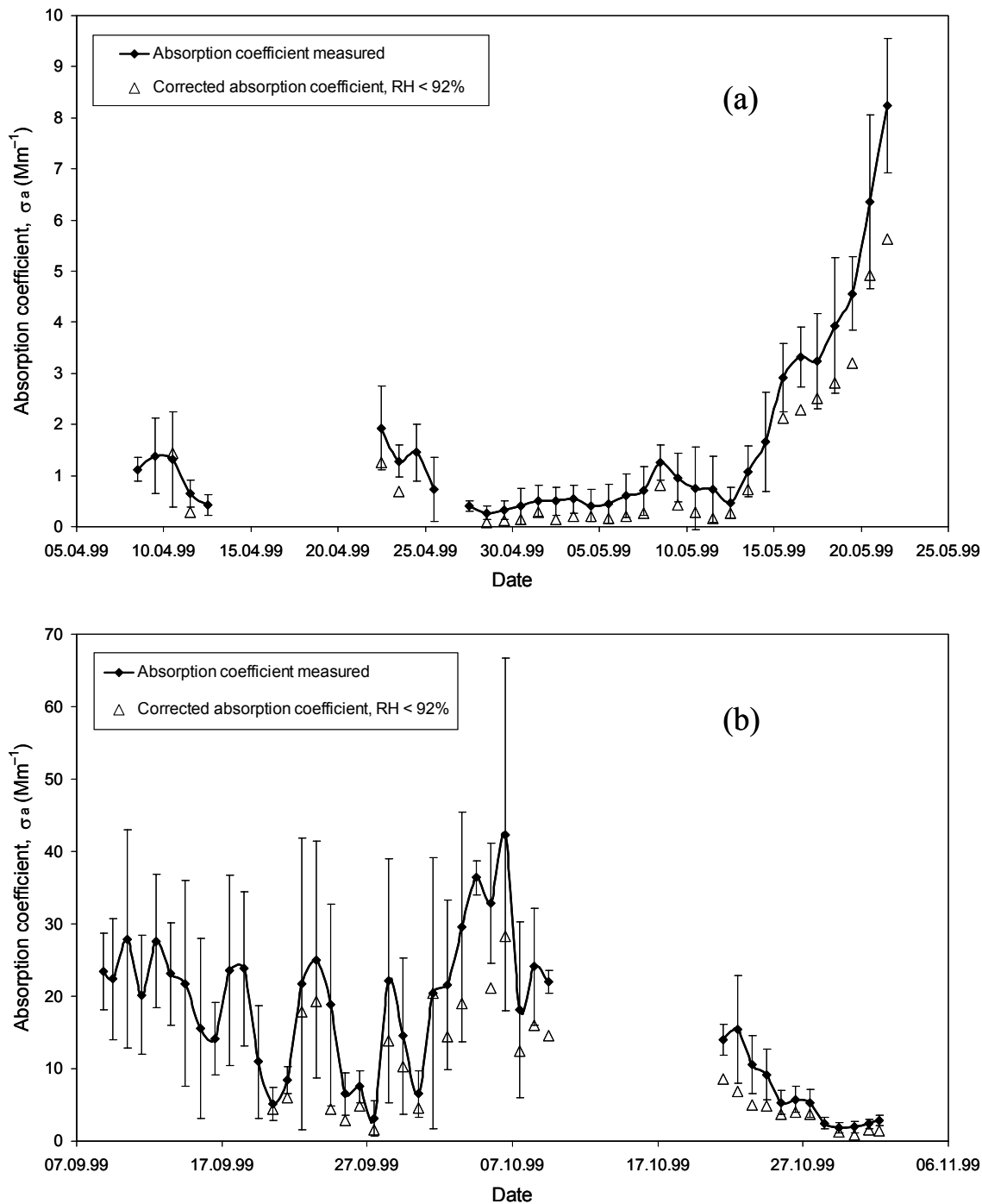
Figure III-8 Absorption coefficients of aerosol particles for the LBA-EUSTACH 1 and 2 campaigns. Daily averages of the absorption coefficients measured by a Radiance Research PSAP (σa) during the LBA-EUSTACH 1 (a) and LBA-EUSTACH 2 (b) campaigns. The vertical bars represent the standard deviation of the measurements.

During LBA-EUSTACH 2, absorption coefficients fluctuated, as all other aerosol characteristics did, depending on local meteorology and biomass burning activity. A large day-to-day variation is noticeable from Figure III-8b, as well as a large within-day variation, indicated by the large measurement standard deviations. An overall median (first; third quartile) σ_a value of ca. 5.4 Mm^{-1} (3.3; 13.0) was observed, peaking at ca. 40–60 Mm^{-1} for short periods of time on the 22 Sep, 3 Oct, and 6 Oct, 1999.

III.3.5. Single-scattering albedos

By combining measurements of scattering coefficients corrected for the truncation (σ_s), and absorption coefficients (σ_a), an estimate of the single-scattering albedo, ω_0, for a wavelength of 550 nm could be obtained according to:

$$\omega_0 = \frac{\sigma_s}{\sigma_s + \sigma_a} \qquad\qquad (\text{III-2})$$

Figure III-9 presents a frequency plot of the single-scattering albedo measured over both field campaigns when ambient RH was below 80%, relative to the maximum frequency value for each campaign. The errors associated with the single-scattering albedo measurements were obtained by error propagation, using an error of 5% for the nephelometer (Section II.2.4) and 20% for the PSAP (the largest possible absolute error associated with this instrument) (Bond et al., 1999). Because the error in σ_a is larger than that in σ_s, the error in ω_0 increases with decreasing values of ω_0. Absolute errors ranged from ± 0.01, for the beginning of the first campaign, to ± 0.03 towards the end of this campaign. Errors in ω_0 for the LBA-EUSTACH 2 campaign ranged between these two values. Note should be taken that correcting the PSAP data according to Bond et al. (1999) created ca. 3% of artifact negative σ_a values at RH < 80% during LBA-EUSTACH 1, and, therefore corresponding ω_0 values larger than unity. This was already observed by Anderson et al. (1999), and could be an indication that the Bond correction may overcorrect the PSAP data in some cases. However, this pattern was not observed during the LBA-EUSTACH 2 campaign, when absorption coefficients were larger overall.
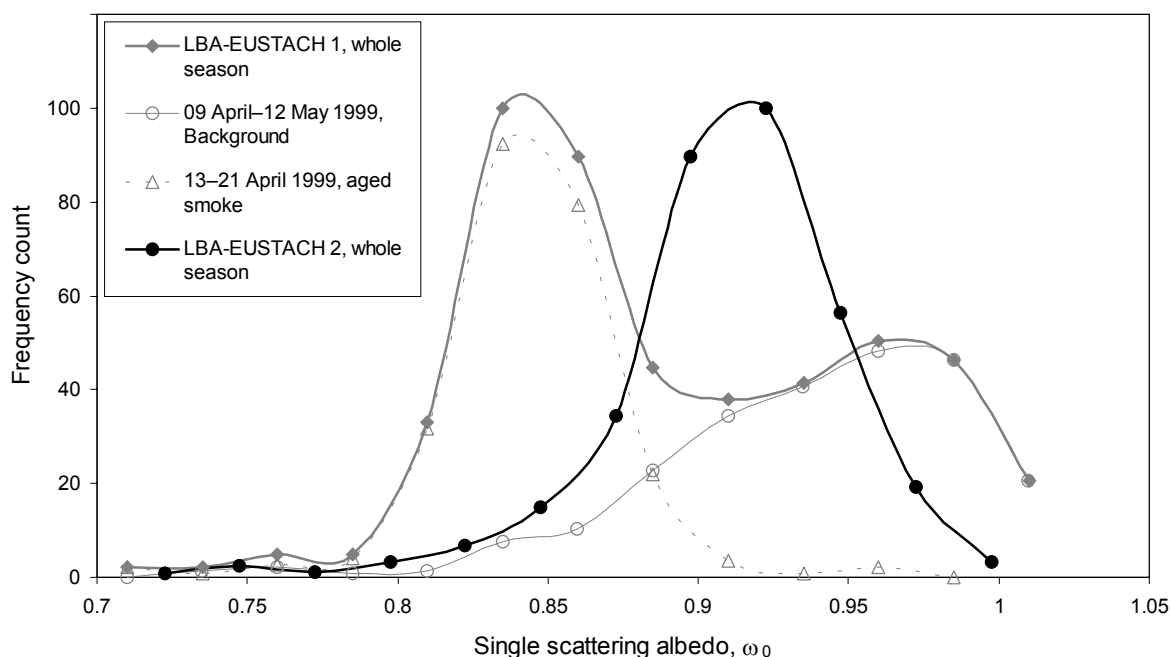
Figure III-9 Single-scattering albedo of Amazonian aerosol particles.
Frequency plot of the single-scattering albedo, ω_0, calculated for the LBA-EUSTACH 1 (gray lines and symbols) and LBA-EUSTACH 2 (black line and symbols) campaigns. The *y*-axis scale is normalized over the highest frequency bin for each campaign to 100. The symbols represent the center of the different frequency bins. The LBA-EUSTACH 1 data set has been separated into two parts: 9 April–12 May 1999 (open circles and light gray line) and 13–21 April 1999 (open triangles and light gray dashed line). Note that the few values larger than 1 observed during the wet season are due to an artifact when correcting the absorption data according to Bond et al. (1999) (see text).

It is clear from Figure III-9 that the LBA-EUSTACH 1 campaign showed two distinct frequency maxima. The first period of the campaign (9 April–12 May 1999), characteristic of pristine background conditions, showed a maximum at $\omega_0 = 0.97$. For a comparison, Carrico et al. (2000) found ω_0 values centered around 0.95 ± 0.04 at 550 nm for clean marine air, at comparable ambient RH and using a similar instrumentation to ours. However, the whole campaign period exhibited a median ω_0 value (first; third quartile) of only 0.95 (0.90; 0.98) due to some biomass burning-influenced episodes occurring throughout the campaign. The single-scattering albedo dropped dramatically from 13 May 1999 onwards, when aged biomass smoke reached the site, to values centered at $\omega_0 = 0.84$ (0.83; 0.86). It is important to note that for Figure III-9 the apparent higher frequency of low ω_0 values (observed predominantly during the second part of the LBA-ESTACH 1 campaign) is an artifact arising from the large fraction of the

background ω_0 values that had to be discarded from the analysis because of the high ambient RH at which they were measured.

Ackerman et al. (2000) found in a model study of similar absorbing aerosols (ω_0 = 0.88 at 500 nm) that a modest number concentration increase, comparable to the one observed here, may result in a dramatic alteration of radiative forcing through cloud evaporation. Thus, even the modest increase in particle number concentration observed between 13-21 May 1999, resulting from diluted plumes arriving from fire sources some 2–3 days away from the sampling site (Figure III-1), may potentially have a significant bearing on climatic and water cycle processes occurring within the region.

It is interesting to note that for the biomass burning haze period (LBA-EUSTACH 2), the median single-scattering albedo (ω_0 = 0.91 (0.90; 0.93)) was found to be higher than that observed at the end of the first campaign. This could be attributable to the formation of a shell around a soot core for aged smoke plume particles, which would have enhanced the absorption properties of the aerosols sampled during the second part of the LBA-EUSTACH 1 campaign relative to those sampled during LBA-EUSTACH 2 (Hallett et al., 1989; Horvath, 1993; Martins et al., 1998a).

The aerosol community has recently become aware of a possible systematic discrepancy between values of ω_0 measured in situ and those retrieved from remote sensing data. For example, in situ measurements performed by Reid et al. (1998a) during SCAR-B yielded average ω_0 values of 0.79 for young plumes and regional haze, and 0.83–0.86 for aged haze (at 550 nm). Somewhat controversially, Remer et al. (1998) argued that such low values could not be reconciled with sky radiance data obtained during the same experiment, and gave a ω_0 estimate of 0.90 at 550 nm. Other sky radiance measurements of biomass burning haze during SCAR-B yielded ω_0 values ranging from approximately 0.82 to 0.94 (Eck et al., 1998). More recently, Dubovik et al. (2002) used sky radiance data to estimate ω_0 values of ca. 0.94 ± 0.02 at 440 nm and 0.93 ± 0.02 at 670 nm for biomass burning aerosols found over the Amazonian rainforest, and ca. 0.90 for smoke aerosol produced by the burning of Brazilian cerrado. Remote sensing techniques based on upward radiance, usually involving satellite sensors, show typically

even higher ω_0 values. Kaufman et al. (1990), for instance, reported an average ω_0 value of 0.98 for forest fire aerosol in Rondônia between mid-visible (630 nm) and near-infrared (840 nm) wavelengths. Using a similar method, Ferrare et al. (1990) reported an average ω_0 value of 0.96 (ranging from 0.90 to 1.0) for forest fire in western Canada. More recently, Li et al. (2000) used in situ-measured ω_0 values (e.g., $\omega_0 = 0.881$ for forest fire) from the SCAR-B experiment to retrieve aerosol optical depth from satellite data. Wong and Li (2002), however, argued that the aerosol properties (single-scattering albedo and asymmetry parameter) reported from various field experiments cannot be used to retrieve comparable aerosol optical depth. They found that in order to use a ω_0 of ca. 0.87 for forest fire aerosols in their model, the asymmetry parameter would have to be substantially decreased to values < 0.4 at 650 nm (a typical value is 0.57 at this wavelength). The in situ ω_0 measurements presented here for biomass burning haze are higher than those reported by Reid et al. (1998a), but are still in the lower range of most of those derived from remote sensing measurements. Certainly the correction of the nephelometer data toward larger values, together with the Bond correction of the PSAP absorption coefficients, contributed toward reducing this discrepancy. Nevertheless, the disparity in ω_0 estimates obtained from remote sensing and in situ methods remains unexplained and requires further investigation, especially given that the derivation of accurate aerosol radiative forcing estimates is dependent upon this parameter.

Although an estimate of the aerosol layer radiative forcing is far beyond the scope of this study, the sign of the top-of-atmosphere forcing can be estimated. The boundary between cooling and heating can be given relative to a critical single-scattering albedo, ω_{crit}, as a function of the surface albedo, R_s, and the upscatter fraction, β (Seinfeld and Pandis, 1998):

$$\omega_{crit} = \frac{2R_s}{2R_s + \beta(1-R_s)^2} \qquad \text{(III-3)}$$

where values of $\omega_0 > \omega_{crit}$ lead to a net cooling.

Ross et al. (1998) reported R_s values of 0.05 for tropical forest, and 0.06 for the reflectance of the ocean, at wavelengths between 500 and 700 nm. Estimates of β were

derived from Mie scattering calculations, for a solar zenith angle $\theta_0 = 0°$ (i.e., the backscattered fraction) (Section V.4.5). Average β values of 0.12 ± 0.01, 0.10 ± 0.01, and 0.08 ± 0.01 were found for the first and second periods of the LBA-EUSTACH 1 campaign, and LBA-EUSTACH 2, respectively. Consequently, in the present case the value of ω_{crit} would be 0.46–0.61 over tropical forest and 0.51–0.66 over the ocean, leading to a net cooling by the aerosols for both environments. It is noted here that at increasing solar zenith angle, β would increase, decreasing further ω_{crit}. Therefore, even when biomass burning dominates the aerosol loading and ω_0 decreases, the sign of the forcing remains negative, although its amplitude may vary. This effect is certainly due to the very low R_s values characteristic for evergreen forests and oceans. Applying a typical global mean R_s of about 0.15 would lead to an almost negligible effect for the aged haze at the end of the first campaign, and a net cooling for the regional biomass burning haze (at a solar zenith angle of 0°). Biomass burning aerosol over cerrado, with an R_s value of ca. 0.11, would lead to similar effects.

III.3.6. Aerosol optical depth

Daily AOD (at 500 nm—unless otherwise stipulated, this wavelength will be henceforth used as reference) and Ångström exponents (estimated from AOD values obtained at 868 and 416 nm) derived from the 1-minute time resolution MFR measurements are presented for both field campaigns in Figure III-10. The number of data points retrieved was mainly restricted by the large number of cloudy days observed during both field campaigns. For the same reason, some of the averages presented were obtained for shorter periods than over the whole day (excluding values at high air masses, $m > 6$).

AOD showed very little diurnal variability, especially during the LBA-EUSTACH 1 campaign, so that even a few hours of measurements can be an acceptable estimate of the daily average. However, morning values were generally higher than the daily average, as were the scattering coefficients, which may be attributed to the high relative humidity observed in the mornings.
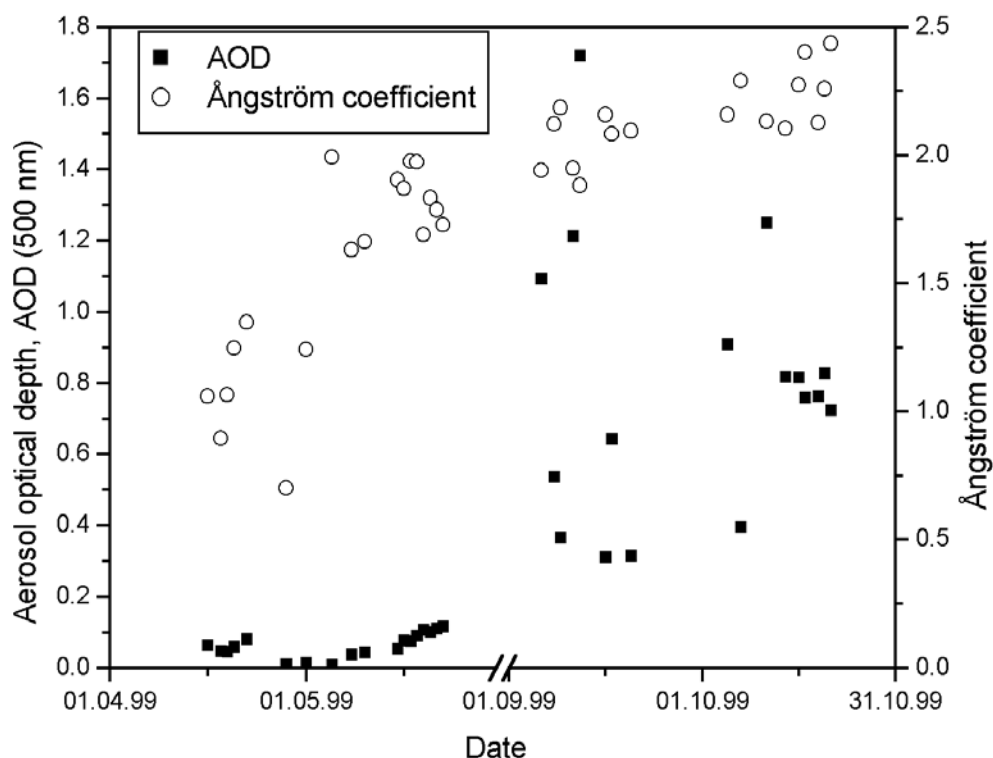
Figure III-10 Aerosol optical depth and Ångström exponent of aerosol particles during the LBA-EUSTACH 1 and 2 campaigns.
Daily averages of the aerosol optical depth (AOD) observed at 500 nm (black squares), and the Ångström exponents (open circles) estimated from AOD values obtained at 868 and 416 nm, with the MFR instrument. Data obtained for both the LBA-EUSTACH 1 and 2 campaigns are presented.

The same overall temporal trend was observed in AOD values as for the other aerosol data measured during the LBA-EUSTACH 1 campaign. Background AOD values (period preceding 12 May 1999) were centered at 0.048 (first and third quartile of 0.040 and 0.056, respectively), which is only about twice the estimated detection limit for the instrument (Formenti et al., 2000). These values are in the lower range (0.038–1.41) of values given by Horvath (1998) for clean continental conditions at 500 nm, and again, about half those measured by Formenti et al. (2001) in Balbina during non-dusty days. AOD then progressively increased, reaching a value of 0.12 on 22 May.

The biomass burning season (LBA-EUSTACH 2) was characterized by large day-to-day fluctuations in AOD, ranging from 0.1 to 2.0, with a median value (first; third

quartile) of 0.79 (0.53; 1.02). These values are in the range of what has been measured at the pasture site during the same period by the AERONET sunphotometer network (Artaxo et al., 2002) (average of 0.91, standard deviation of 0.56, and maximum of 3.3, at 500 nm). This highlights the regional influence of biomass burning, since the results appear to show that the atmosphere above the remote forest site was influenced by biomass burning aerosols to about the same extent as that over the pasture site. Other authors, such as Dubovik et al. (2002), also reported AOD values (at 440 nm) ranging from 0.1–3.0 (0.74 on average) for biomass burning-influenced periods in 1993 and 1994 over the Brazilian Amazonian forest, and in 1998 and 1999 over the Bolivian Amazonian forest. The range of AODs obtained for this season is of the same magnitude as those reported by Horvath (1998) for polluted urban environments at 500 nm (0.4–4.36). The large range of values reported in these data sets, however, indicates the danger associated with using a single average AOD value to represent biomass burning haze in order to retrieve aerosol radiative forcing estimates.

AOD values at 550 nm were interpolated using the Ångström exponents obtained from the values for the neighboring wavelengths (500 and 616 nm), and were regressed against the corresponding extinction coefficients obtained at ambient RH < 92% (the sum of the absorption and scattering coefficients at 550 nm). The slope of the fitting equation provides an estimate of the height of the optically-active aerosol layer if it is assumed that the aerosols are well-mixed within the layer. Regression of the 10 minute-averaged values yielded a layer height of ca. 4.5 km for the period preceding 12 May (r^2 = 0.93, 51 observations). This is much higher than the value of 1 km reported by Jacob and Wofsy (1988) and Fisch et al. (2002) for the convective boundary layer (CBL) height at this site, or the value of ca. 2.0 km for the planetary boundary layer (PBL) given by Jacob and Wofsy (1990) for late-morning hours in the Amazon basin during the wet season. These authors found the PBL to be well mixed with the underlying sublayers, but fairly decoupled from the layer above. This indicates that the aerosols measured in situ on the tower during this period were probably not characteristic of the whole column, and that there was a significant contribution by free tropospheric aerosols to the (very low) AOD during this period.

Regression of the data for the 12–21 May period suggested a much shallower optically-active aerosol layer, ca. 1.1 km in depth (r^2 = 0.44, 154 observations). As already noted in the section discussing the single-scattering albedo values for this period, this reflects how biomass burning aerosol particles, even in relatively low amounts, can dominate the overall aerosol optical properties of the whole column when mixed in with background aerosol in remote areas.

The overriding influence of the smoke aerosol is also seen in the Ångström exponent data retrieved for the LBA-EUSTACH 1 campaign (Figure III-10). Ångström exponents showed a dramatic increase from the beginning to the end of the first campaign, and then to the dry season campaign: values increased from below unity to over 2 (Figure III-10). Ångström exponent values of ca. 2 are typical for small smoke particles, whereas values tending toward zero are representative of large particles (e.g., dust) (Dubovik et al., 2002). This attests to the growing contribution of fine particles to the optically-active aerosol loading with increasing biomass burning activity, whereas background aerosols seem to be characterized by a prevailing coarse mode. The increase in Ångström exponents is particularly noticeable between the beginning and the end of the LBA-EUSTACH 1 campaign, indicating a radical change in the make-up of the optically-active aerosol layer. This is consistent with the shift from a prominent biogenic coarse-mode aerosol prevailing over the unpolluted Amazon to conditions dominated by biomass smoke during the dry season (Artaxo et al., 2002).

III.4. Conclusion

In this chapter, the main physical characteristics of Amazonian aerosols and their abundance were described for both the wet and dry seasons, as well as during the transition periods between the seasons. It is clearly evident from the data set that anthropogenic biomass burning activities have a dramatic impact on the total aerosol loading, even above a remote site located within a primary rainforest reserve. Scattering and absorption by even relatively modest amounts of smoke aerosol overwhelms the effects of the background aerosol, which is present at very low concentrations during the wet season under unpolluted conditions. The potential certainly exists for these changes to

alter the radiation balance, as well as cloud formation and rain-out processes, and thus the whole hydrological cycle in the Amazon basin. However, whilst the data attest to the significant difference between biomass burning and background atmospheric conditions, the actual climatic impacts of burning activities remain uncertain. For instance, the values of ω_0 for forest fires cover a wide range and could lead to a prediction of a considerable warming or cooling effect by biomass burning aerosol, depending on which values are chosen. Thus, it is considered vital that intensive research efforts continue to be directed toward more accurate measurements of absorption and single-scattering albedo. Such studies are critical not only for the Amazon region, but also from a global perspective, due to the fact that the large-scale atmospheric circulation in the tropics may mean that the products of burning activities can be carried to higher latitudes, where their climatic effects may also be significant (Andreae, 1991; Pickering et al., 1996; Andreae and Merlet, 2001; Andreae et al., 2001).

CHAPTER IV.

COMPOSITION, SOURCE APPORTIONMENT, AND OPTICAL PROPERTIES OF AEROSOL PARTICLES OVER THE AMAZON TROPICAL FOREST

Abstract

As part of the European contribution to the Large-Scale Biosphere-Atmosphere Experiment in Amazonia (LBA-EUSTACH), size-fractionated aerosol samples were collected at a primary rainforest and at a pasture site in the Brazilian Amazon basin during two field campaigns in April–May and September–October 1999. These two periods encompassed parts of the wet and dry seasons, respectively. Daytime-nighttime segregated sampling was carried out at three different heights (above, within and below canopy level) on a 54 m meteorological tower at the forest site in order to better characterize the aerosol sources. The samples were analyzed for up to 19 trace elements by particle-induced X-ray emission analysis PIXE, and for carbonaceous components by thermal-optical analysis. Equivalent black carbon (BC_e) and gravimetric analyses were also performed. The average inhalable particulate mass concentrations were 2 and 33 μg m^{-3} for the wet and the dry seasons, respectively. The elements related to biomass burning and soil dust generally exhibited highest concentrations above the canopy and during daytime, whilst forest-derived aerosol was more concentrated underneath the canopy and during nighttime. These variations can be largely attributed to daytime convective mixing and the formation of a shallow nocturnal boundary layer. Mass scattering (α_s) and mass absorption efficiency (α_a) data indicate that scattering was dominated by fine aerosol, whilst fine and coarse aerosol both contributed significantly to absorption during both seasons. The data suggest that non-elemental carbon components were responsible for a substantial fraction of the absorption. Absolute principal component analysis revealed

that the wet and dry season aerosols contained the same three main components, but that these were present in different (absolute and relative) amounts: the wet season aerosol consisted mainly of a natural biogenic component, whereas pyrogenic aerosols dominated the dry season aerosol mass. The third component identified was soil dust, which is believed to be internally mixed with the biomass-burning aerosol during the dry season. All three components contributed significantly to light extinction, suggesting that, in addition to biomass burning particles, biogenic and soil dust aerosols should be taken into account when modeling the physical and optical properties of aerosols in the Amazon.

IV.1. Introduction

The composition and sources of Amazonian aerosols have been studied with increasing interest over the last decade. Natural Amazonian forest aerosols have been described previously (Artaxo et al., 1990; Artaxo et al., 1994; Artaxo and Hansson, 1995; Echalar et al., 1998). These are the dominant aerosols found during the "wet season" months (November-April), when anthropogenic burning activities are suppressed by high rainfall. They usually consist mainly of biogenic and dust particles. Biogenic emissions from forests include large ($D > 2$ μm) primary particles released by biological processes and wind abrasion, and submicron particles originating from the gas-to-particle conversion of biogenic trace gases emitted by plants or microorganisms. Such particles are characteristically composed of organic material and trace elements such as Na, Mg, P, S, K, Zn, and Rb (Artaxo et al., 1990; Artaxo et al., 1994). Higher plants also contain the elements N, Ca, and Fe as macronutrients, and Mn, B, Cu, Mo, Cl, Co, Si, Se, and Ni as micronutrients, which are constituents of biogenic particles. However, these elements are often present at very low concentrations, or are released in larger amounts by other sources, making their apportionment difficult. Dust particles are produced under the action of the wind, and typically contain Al, Si, Ca, Ti, Mn, and Fe. Particles of other origins have also been reported in the Amazon basin during the wet season, with sources including biomass burning, urban pollution, and gold mining (Echalar et al., 1998), but these are usually confined to a local scale. Formenti et al. (2001) found dust particles of Saharan origin at a remote site in the Amazon basin (see also Swap et al. (1996)).

Characteristics and source apportionment of Amazonian pyrogenic aerosols, dominant during the "dry season", have also been reported previously (see e.g., Andreae et al. (1988), Ward et al. (1992), Maenhaut et al. (1996), Artaxo et al. (1998), Echalar et al. (1998), and Maenhaut et al. (2002)). Pyrogenic aerosols contain the same trace elements as biogenic particles, but also include a black carbon component due to combustion (see e.g., Maenhaut et al. (1996)) and are primarily confined to the accumulation mode.

This chapter focuses on the source apportionment of optically active aerosols in the Amazon basin for both the wet and dry seasons. The chapter begins by presenting and

discussing the elemental composition of the aerosols of the wet and dry seasons, measured at three different heights on a meteorological tower situated in a primary rainforest. Next, mass scattering (α_s) and mass absorption efficiency (α_a) data, calculated for both the coarse (10 μm > D_p > 2 μm) and fine (D_p < 2 μm) fractions of the natural background aerosol characteristic of the wet season, as well as the pyrogenic aerosol emitted during the dry season are presented. Finally, the results of a source identification and quantitative apportionment study of the wet and dry season aerosols are presented, which includes an apportionment of the scattering and absorption properties of the total aerosol in terms of the major contributing aerosol sources.

IV.2. Sampling location and experimental method

Sampling location

Aerosol particiocles were sampled over two field campaigns at a pasture site (Fazenda Nossa Senhora Aparecida, FNS, located at 10° 45' 44" S, 61° 21' 27" W, 315 m above sea level) and on a 54 m tower situated in a primary rainforest with a mean canopy height of about 32 m (Reserva Biologica Jarú, RBJ, 10° 04' 55" S, 61° 55' 48" W, 110 m above sea level). Both sites are located in the state of Rondônia, Brazil, and separated by a distance of ca. 80 km. The first campaign (LBA-EUSTACH 1) occurred in April–May 1999 and covered the end of the "wet season" period and the transition period toward the biomass-burning-influenced "dry season". The second campaign (LBA-EUSTACH 2) was conducted in September–October 1999 throughout the end of the "dry season" and the transition period toward the "wet season" again. For a more complete description of the measurement locations, meteorological, and overall sampling conditions, refer to Andreae et al. (2002), and Silva Dias et al. (2002).

Filter sampling and chemical analysis

Aerosol particles were collected on Nuclepore filters using Stacked Filter Units (SFUs) for elemental, gravimetric and a light reflectance ("black carbon equivalent" (BC_e)) analyses (Section II.3.1), and on quartz fiber filters using a High Volume

Dichotomous Sampler (HVDS) for characterization of aerosols carbonaceous content (Section II.3.2).

Real-time aerosol monitoring

Light-scattering measurements were performed at the Jarú tower site using a single-wavelength (λ = 545 nm) Radiance Research nephelometer (see Section II.2.4). Absorption coefficient measurements were performed using a Radiance Research particle soot absorption photometer (PSAP), which was positioned at 52 m above the ground, and, during the dry season, using two additional Magee Scientific Co. aethalometers positioned at 3 and 50 m above the ground, on the meteorological tower. The absorption coefficients obtained at the pasture site were also measured using an aethalometer (see section II.2.5).

The retrieval of the absorption coefficients (σ_a) and associated uncertainties for the PSAP instrument are described in section II.2.5. σ_a values were retrieved according to Bond et al. (1999), and uncertainties were computed following the work of Anderson et al. (1999). Because the Bond correction of the PSAP data requires the use of light scattering data, as obtained from a nephelometer, corrected PSAP data could only be obtained when ambient RH was < 92%, and when the nephelometer was functioning simultaneously. Therefore, in this chapter, ca. 30% of the dry season Bond-corrected absorption coefficient values (σ_a) obtained from the PSAP were estimated from the linear regression of the available σ_a data on the uncorrected absorption coefficient data ($\sigma_{a,raw}$), for periods with ambient RH < 92% when the nephelometer data were not available. The linear equation used in these cases was σ_a = uncorrected $\sigma_{a,raw}$ X 0.61 − 0.03 Mm^{-1} (obtained from the regression of 3170 10–min averaged measurements, r^2 = 0.98), and was mainly used for estimating σ_a values from the beginning of the second campaign (9– 19 September 1999), when the nephelometer was not yet available. It is noted here that this equation accounts for all three corrections that have to be applied to the PSAP data— the deposit area, the over-response to scattering, and the adjusted calibration response (Bond et al., 1999). However, once integrated over the sampling time of the corresponding filter sample, the estimated σ_a values had little influence on the overall analysis.

Absolute principal component analysis

Aerosol sources were computed using the multivariate statistical technique, known as absolute principal component analysis (APCA) (Thurston and Spengler, 1985; Keiding et al., 1986). APCA does not require *a priori* knowledge about the number and types of particulate sources. The sources are first identified using principal component analysis (PCA), which involves constructing a model of trace element concentration variability (in the present study only variables that were below the detection limit less than 5% of the time were allowed in the model). During the analysis, a set of inter-correlated variables is transformed into a set of independent variables by finding the eigenvalues and eigenvectors (factors/components) of the correlation matrix. The most prominent eigenvectors are retained and subjected to VARIMAX rotation, to yield a "component-loading" matrix that represents the correlations between the elements and each component. In APCA, absolute principal component scores (APCS) are also obtained, which indicate the importance of the identified components in individual samples. Mass/elemental component apportionments are then obtained from the regressions of the measured mass/elemental concentrations on the calculated APCS (Artaxo et al., 1988; Artaxo et al., 1990; Maenhaut et al., 1996; Artaxo et al., 1998; Echalar et al., 1998). The stability of this analytical procedure depends on the number of degrees of freedom in the analysis (i.e., the number of samples) (Ito et al., 1986). It has been suggested that at least 30 are required to obtain statistically-robust results (Henry, 1991). This issue will be returned to later in more detail.

In the present study, the use of the APCA technique is extended to regress aerosol absorption and scattering (integrated over the sampling time of the corresponding SFU sample) on the previously calculated APCS. This technique allowed us to identify the major sources of optically-active aerosol over the Amazon basin under background and biomass burning conditions, and to quantify for the first time their relative contributions to the total aerosol scattering and absorption.

IV.3. Results and discussion

IV.3.1. Elemental composition of Amazonian aerosols

IV.3.1.1. Wet season

Table IV-1 presents the average particulate mass (PM), black carbon (BC_e), and trace element concentrations for fine and coarse fraction aerosols measured during the wet season for the three different sampling heights on the RBJ meteorological tower. When assumed to be in the state of their most common oxides (Mason and Moore, 1982), the sum of the trace elements averaged ca. 24% and 15% of the fine (FPM) and coarse particulate masses (CPM), respectively. The rest of the aerosol mass is composed predominantly of elemental carbon, organic matter, nitrates and elements lighter than Mg. BC_e was only measured in the fine aerosol fraction and represented ca. 13% of FPM. However, it is suggested in Section V.4.2 that the BC_e value obtained for this season may be an overestimate of the "true" value. The PM concentrations observed for wet season background conditions are lower than those reported by Echalar et al. (1998) for wet season data collected between 1992 and 1995 at the Amazonian site of Alta Floresta (5.5 ± 3.5 and 16.4 ± 9.4 μg m^{-3} for the fine and coarse fractions, respectively). However, the values compare well with those reported by Formenti et al. (2001) for background conditions at the Amazonian site of Balbina (1.6 and 5.8 μg m^{-3} for the FPM and CPM, respectively), and by Artaxo et al. (1990) for two Amazonian sites located near Manaus (2.1 ± 0.7 and 6.1 ± 1.8 μg m^{-3} for FPM and CPM, respectively). The observed elemental concentrations are also mostly within the range of the values reported by Artaxo et al. (1990), with the exception of the soil dust elements (typically Al, Si, Ti, Mn, and Fe), which were present in slightly lower concentrations in the present study. This indicates that the present data for the wet season aerosol are representative of background aerosols measured in the Amazon.

Table IV-1 Wet season mean atmospheric concentrations[1] and standard deviations (s.d.) of fine and coarse particulate mass, equivalent black carbon, and trace elements for aerosol samples collected on three levels of the Jarú meteorological tower (upper, canopy, and ground level) in Rondônia, Brazil (8 April–21 May 1999).
n is the number of samples from a set of 28 in which the element was measured above its detection limit.

	Wet season																	
	Above-canopy level						Canopy level						Below-canopy level					
	Fine fraction			Coarse fraction			Fine fraction			Coarse fraction			Fine fraction			Coarse fraction		
	Mean	s.d.	n	Mean	s.d.	n	Mean	s.d.	n	Mean	s.d.	n	Mean	s.d.	n	Mean	s.d.	n
Mass	2.21	1.39	(28)	3.77	1.32	(28)	2.09	1.31	(26)	4.91	2.46	(26)	2.2	1.36	(28)	6.57	2.97	(28)
TC	896.7	504.6	(11)	—	—	—	—	—	—	—	—	—	—	—	—	—	—	—
EC$_a$	76.6	59.3	(11)	—	—	—	—	—	—	—	—	—	—	—	—	—	—	—
BC$_e$	276.9	137	(28)	—	—	—	292	137.5	(26)	—	—	—	277.6	142.9	(28)	—	—	—
Mg	—	—	—	29	23.2	(23)	—	—	—	27	13.9	(20)	—	—	—	—	—	—
Al	34.5	30.9	(24)	52.5	50.8	(24)	39.4	31.5	(18)	46	44.6	(20)	32.7	25.5	(13)	33.4	34	(22)
Si	42.5	37.9	(28)	52	59.8	(25)	39.9	33.7	(26)	42.4	52	(24)	31.3	29.9	(28)	58.7	51.8	(16)
P	5.6	1.9	(28)	23.4	9.3	(28)	5.5	1.8	(26)	32.7	18.5	(26)	3.5	1.2	(28)	45.9	31.9	(28)
S	87.7	87.2	(28)	23.5	14.8	(28)	85.4	86.7	(26)	27.5	14.9	(26)	90	95.5	(28)	33.5	17	(28)
Cl	6.1	7.9	(11)	8.9	5.4	(28)	3.6	1.8	(8)	11.1	5.5	(26)	—	—	—	7.8	4.6	(21)
K	26.8	26.5	(28)	48.2	14.9	(28)	24.7	26	(26)	64.7	28.3	(26)	27.1	28	(28)	107.6	58.2	(28)

Table IV-1 (continued)

	Fine fraction			Coarse fraction			Fine fraction			Coarse fraction			Fine fraction			Coarse fraction		
	Mean	s.d.	n	Mean	s.d.	n	Mean	s.d.	n	Mean	s.d.	n	Mean	s.d.	n	Mean	s.d.	n
Ca	8.4	6.1	(28)	12.2	7.5	(26)	6.7	5.6	(26)	11.1	5.6	(26)	3.2	2.2	(20)	9.1	4.5	(28)
Ti	3.8	4.1	(14)	6.5	7.3	(14)	4	3.7	(11)	5.5	6.6	(12)	2.9	2.8	(15)	4.5	5.24	(18)
Cr	—	—	—	2.5	1.5	(8)	—	—	—	4.3	2.3	(7)	—	—	—	2	1.39	(5)
Mn	0.56	0.36	(28)	0.87	0.57	(28)	0.55	0.36	(25)	0.86	0.45	(26)	0.63	0.24	(8)	0.72	0.49	(28)
Fe	21.6	29.7	(26)	34.2	46.8	(26)	21.3	27.9	(21)	29.9	41.3	(23)	21.4	26.8	(28)	26.3	34.6	(28)
Ni	0.33	—	(1)	—	—	—	0.21	0.05	(2)	—	—	—	—	—	—	0.23	0.03	(2)
Cu	0.42	0.44	(27)	0.32	0.2	(28)	0.15	0.12	(15)	0.23	0.08	(23)	0.37	0.39	(8)	1.68	—	(1)
Zn	0.68	0.72	(23)	0.72	0.39	(28)	0.67	0.8	(20)	1.25	1	(25)	1.35	1.13	(8)	1.08	0.44	(20)
Br	1.05	—	(1)	—	—	—	1.32	—	(1)	—	—	—	0.85	0.32	(4)	—	—	—
Sr	0.16	0.07	(10)	0.26	0.13	(9)	0.13	0.06	(7)	0.3	0.25	(9)	—	—	—	—	—	—
Zr	0.18	0.08	(6)	0.77	0.78	(4)	0.42	0.21	(5)	0.27	0.02	(2)	2	—	(1)	1.23	0.73	(3)
Pb	0.84	0.92	(18)	0.46	0.17	(3)	1.02	1.04	(15)	0.54	0.34	(3)	—	—	—	—	—	—

[1] Mass concentrations are in $\mu g\ m^{-3}$; total carbon (TC), apparent elemental carbon (EC_a), and equivalent black carbon (BC_e) and trace elements concentrations are in $ng\ m^{-3}$.

In order to help establish the origin of the various elements, mean crustal enrichment factors (EFs) were calculated using the average crustal rock data from Mason and Moore (1982), and taking Al as the reference element. EFs were defined as follows:

$$\mathrm{EF}(X) = \frac{[\mathrm{C}(X)/\mathrm{C}(\mathrm{Al})]_{\mathrm{aerosol}}}{[\mathrm{C}(X)/\mathrm{C}(\mathrm{Al})]_{\mathrm{crustalrock}}} \qquad (\text{IV-1})$$

where C(X) and C(Al) are the concentration of element X and Al for the aerosol or in average crustal rock. An EF value close to unity indicates that the concentration of the element in the aerosol is consistent with what would be expected from soil dust dispersal, suggesting soil dust as the probable source. It should be cautioned, however, that soil composition is variable, so that elemental EFs calculated using the crustal average can sometimes deviate significantly from unity even though the elements may truly be of soil origin.

Figures IV-1a and 1b present the EFs calculated for the fine and coarse aerosol fractions, respectively. EFs were calculated separately for the three different sampling heights. The data confirm that the elements Ti, Mn, Fe, and Sr can be mainly attributed to soil dust in both the fine and coarse aerosol fractions. The consistent depletion of the other elements typically associated with mineral dust, Mg, Si, and Ca, could be attributed to a different soil composition in this region compared to the mean global crustal composition. Artaxo et al. (1990) also reported depletion of Ca and K at a site situated near Manaus. Depletion of Si is commonly found in atmospheric aerosols and is attributed to crust-to-air fractionation (Rahn, 1976).

In the present study, K was enriched by a factor of ca. 2 in the fine aerosol at all levels, and 3–10 from above to below canopy in the coarse aerosol. This indicates that coarse aerosol K mainly originates from biogenic sources. In fact, the contribution of this source may be even greater than suggested by the EF values if Amazonian soil dust is slightly depleted in K, as has been suggested by Artaxo et al. (1990). Coarse fraction P, S, Cl and Zn showed large EFs that followed the same spatial pattern as K, with the largest enrichments observed below the canopy, and are therefore also likely of biogenic origin. Cu is usually also considered as a biogenic component, although the spatial and temporal variation of this element can sometimes be very distinct from those of other biogenic

elements (P. Artaxo, unpublished data). Little is known about the sources of Cr, but the high coarse EFs that were observed suggest a non-crustal origin. However, Cr has typically high blank values in Nuclepore polycarbonate filters. Pb is generally used as a tracer for anthropogenic activities. Pb-containing particles have also been reported to be generated by higher plants under the action of biological process and wind abrasion (Beauford et al., 1977).

An initial comparison of the average FPM and elemental concentrations for the three sampling levels suggested that there was generally little vertical gradient in the fine fraction aerosol concentrations and, hence, that either the various sources and sinks roughly balanced each other, or that the fine particles were well-mixed throughout and beyond the canopy. However, a closer examination of the time series of the profiles for the measured elements revealed a more complex structure. In order to be able to better compare the individual profiles obtained over the whole campaign between each other, the concentrations of all the elements measured on simultaneously-sampled filters (i.e., above, within and below canopy level) were normalized over the concentration of the element measured on the filter collected at the above-canopy level, to yield "enrichment ratios":

$$E_r = \frac{C(X)_j}{C(X)_t} - 1 \qquad \qquad \text{(IV-2)}$$

where $C(X)_t$ is the concentration of the element X at the above-canopy level, and $C(X)_j$ is the concentration of the element X at the jth tower level, for the fine fraction. E_r values at the above-canopy level are always equal to zero, as a reference. An $E_r > 0$ means an enrichment in the element relative to its above-canopy concentration, while an $E_r < 0$ indicates a depletion in the element relative to the above-canopy value (i.e., either the element is deposited or sinks were larger than sources at this level compared to the above-canopy level). A larger absolute E_r value corresponds to an increased positive/negative enrichment.
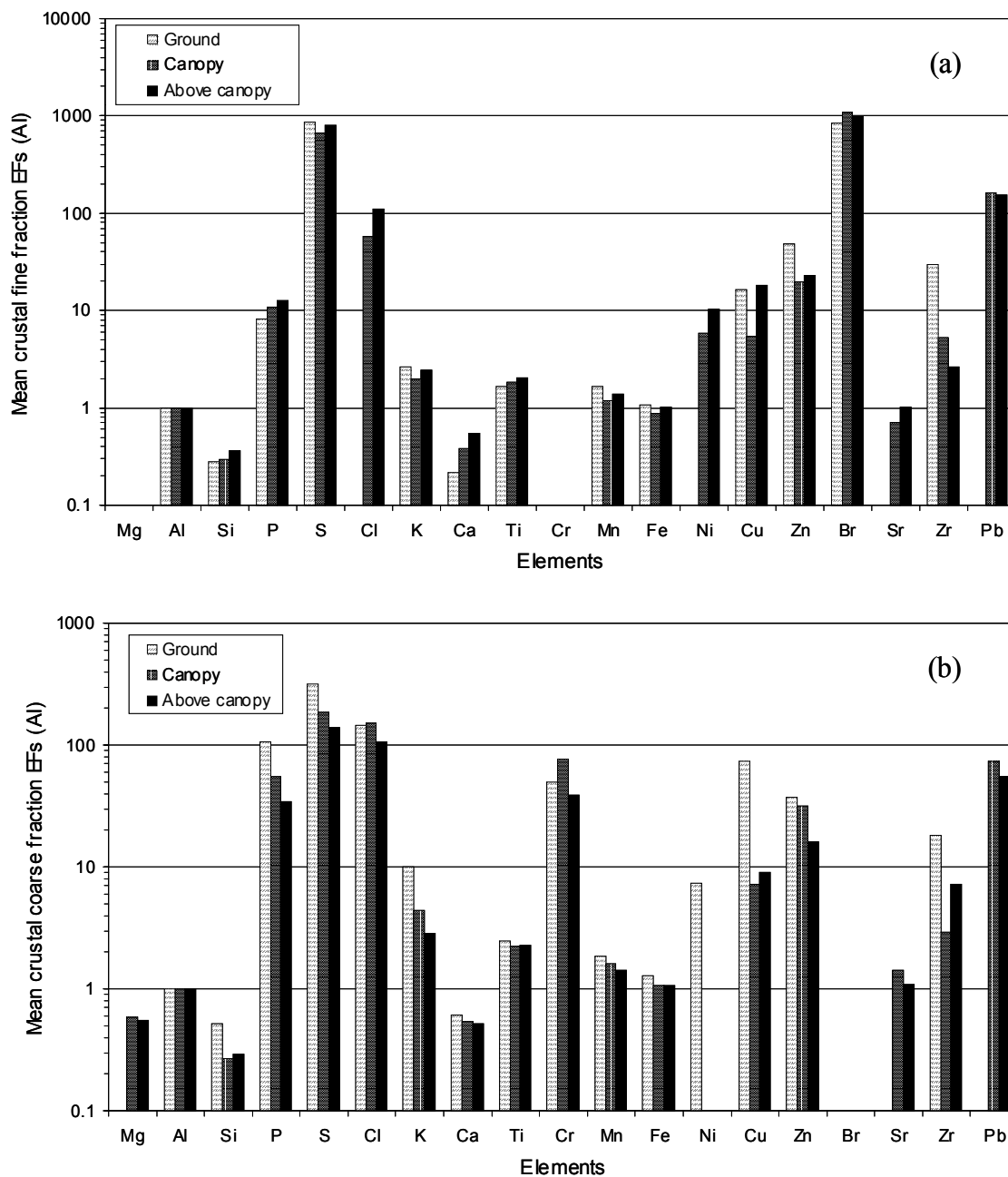
Figure IV-1 Mean crustal enrichment factors for the LBA-EUSTACH 1 aerosol particles.
Mean crustal enrichment factors (EFs) for the fine (a) and coarse (b) aerosol fractions collected at three different heights on the Jarú meteorological tower (top, canopy, and ground level) in Rondônia, Brazil, during the wet season (8 April–21 May 1999). EF values were calculated relative to the average crustal rock composition of Mason and Moore (1982) using Al as the reference element.

Figures IV-2a and 2b show the average day and nighttime E_r values for FPM computed for the three sampling heights on the tower. In addition, E_r values for two elements representative of the biogenic and soil dust aerosol components (P and Al, respectively) are also shown. Most of the other elements characteristic for these components behaved in a similar manner to the chosen elements. With the exception of coarse mass and P concentrations, daytime E_r values indicated a relative depletion within and below the canopy, representing deposition in the forest canopy. The larger elemental concentrations in fine particles above the canopy is consistent with the observations made CHAPTER III that, despite overall very clean conditions, there was some biomass burning influence during the wet season, which could have been a major source for these fine particles above the canopy. For FPM, the largest depletion step was observed in moving from the above-canopy to within-canopy level. Dry deposition of accumulation-size particles tends to depend on micrometeorological conditions, increasing as conditions become more dynamically unstable (Wesely and Hicks, 2000). This is the case above the canopy during daytime. Rummel et al. (2002b) have shown that in a closed-canopy forest system with very dense foliage (integrated one-side leaf area index of ca. 6), above and below-canopy levels are fairly well decoupled during daytime. The stratification of the upper-canopy and the sublayer directly above is unstable, whereas the lower canopy and below-canopy levels are generally very stable (Rummel et al., 2002b). Therefore, a large fraction of the fine aerosol coming from aloft is expected to deposit within the upper-canopy.

P and Al tended to have more negative E_r values at ground level (up to ca. 60% lower for P), which is inconsistent with the fact that turbulence was low under the canopy during daytime. Fine biogenic and soil dust particles are not expected to be produced in significant amounts below the canopy. The downward transport of these fine aerosols, therefore, depends on the sporadic occurrence of large-scale eddies (Rummel et al., 2002b), with the fine particles then depositing in the lower-canopy, tree stems, and/or palm-rich understory (Andreae et al., 2002). However, the observed differences between P and Al and FPM remain unexplained, which may suggest that another kind of fine particles was produced below the canopy.

The nighttime E_r values for fine particles showed a completely different behavior. Figure IV-2b shows that there was a tendency for FPM concentrations to decrease with increasing height. The variability in the P and Al data was large at night, but P tended to show the largest concentration at canopy level, while Al was most depleted at this level.
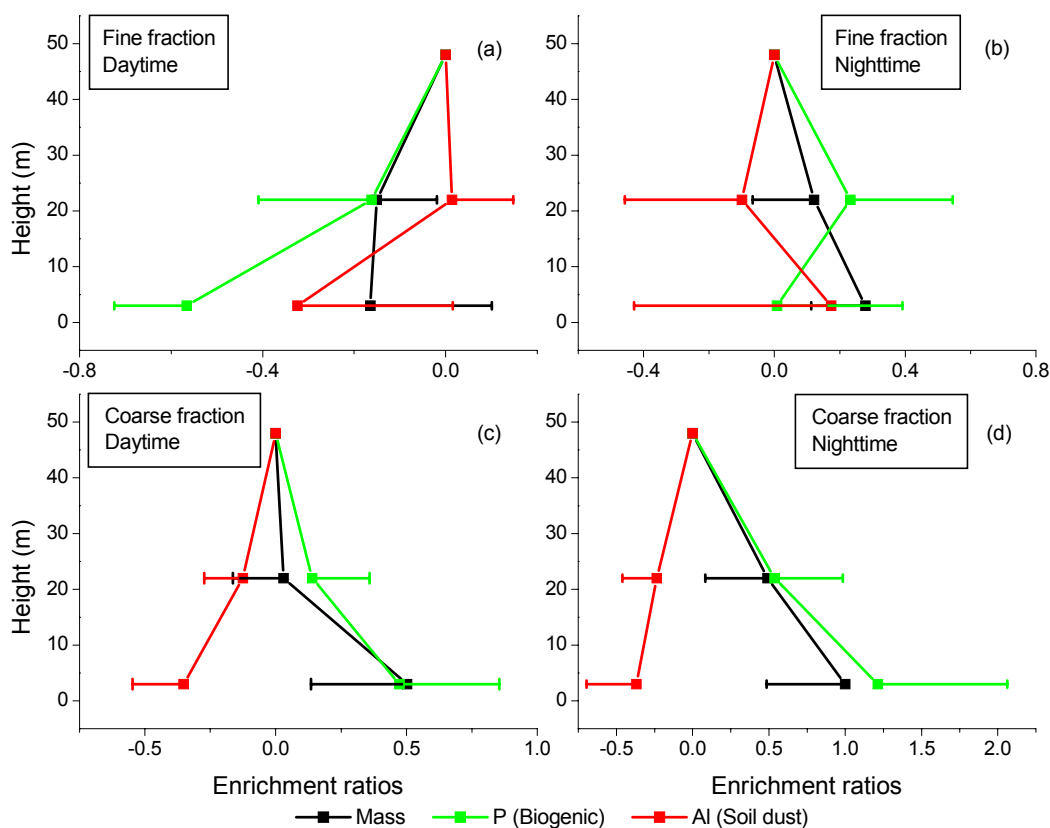
Figure IV-2 Enrichment ratios for the LBA-EUSTACH 1 aerosol particles.
Wet season enrichment ratios (E_r) calculated for FPM (black lines), and P (green lines) and Al (red lines) concentrations in the fine aerosol fraction during day (a) and nighttime (b), in Rondônia, Brazil (8 April–21 May 1999). The corresponding E_r for the coarse aerosol fraction measured during day (c) and nighttime (d) are also shown. The squares represent the average of the E_r values calculated from each individual set of concentration measurements (above, within and below canopy), and the error bars the associated standard deviation.

Coarse fraction E_r values, defined as above for the three heights, showed two distinct sets of vertical gradients for both daytime and nighttime, as can be observed in Figures IV-2c and 2d, respectively. CPM, together with P (and other elements typically related to biogenic emissions) showed a clear increase in concentrations from above to

below the canopy, indicating that these aerosols are mainly produced under the canopy. Artaxo et al. (2002) already reported that this pattern was enhanced at night (cf. Figures IV-2c and 2d), drawing attention to the potential importance of this source of P, which is the limiting nutrient in the Amazonian forest, and generally the second most frequently limiting macronutrient for plant growth after N (Schachtman et al., 1998). At night, very stable meteorological conditions accompanied the formation of a shallow nocturnal boundary layer and a cessation of convective activity. However, the lower part of the canopy was often decoupled from the layer above, and a temperature inversion inside the canopy produced an increase in turbulent motion below the canopy (Rummel et al., 2002a; Rummel et al., 2002b). It is likely that this turbulence enhanced the uplift and dispersal of biogenic litter, which is abundant on the tropical forest floor. There is also the possibility that this nighttime increase in biogenic material was enhanced through the active release of certain types of particles (e.g., some species of fungal spores) at night (Degroot, 1968). The depletion at canopy level indicates that there was a sink for these particles within the canopy; however, because the above-canopy concentration of P is not zero, this suggests that deposition velocity of these coarse particles was low, or that the canopy was also a source for these particles. These could have been produced by wind abrasion of the canopy vegetation. This source would have been more prominent during daytime, with the large particles tending to sediment at night when wind was low above the canopy. In accord with this, the largest difference in biogenic and CPM E_r values between the canopy and above-canopy levels was observed at night.

Coarse fraction Al (and other soil dust elements) showed a clear decrease in concentrations from above to below the canopy (increasingly negative E_r values). This is consistent with the fact that the forest floor is not a substantial source for dust particles (Artaxo et al., 1990), and suggests that soil dust was deposited into the forest from air masses advected above the canopy to the site.

To further characterize daytime-nighttime variability, ratios of nighttime-to-daytime elemental concentrations were computed. Figures IV-3a and 3b present the average ratios obtained for the three sampling heights for the fine and the coarse aerosol fractions, respectively. Fine particles showed consistently higher concentrations of almost

all elements during daytime (ratios below unity). Convective downward mixing of air from aloft is significantly enhanced during daylight hours, so this observation appears to indicate that the source of much of the fine aerosol was long-range transported material, or organic material produced photochemically above the forest. The only element significantly enriched at night in the fine fraction was P, which showed a gradient from below to above the canopy, with the largest enrichments being observed below the canopy. The same gradient was observed for S and K, confirming their source to also be biogenic aerosol. These findings are consistent with the earlier observations of Artaxo et al. (1990) and Artaxo et al. (2002). Comparing these ratios to the E_r values (Figures IV-2a and 2b) suggests that there were probably two different sources for fine biogenic aerosols during this season. The largest concentrations of P observed above the canopy during daytime suggest long-range transport of what could be attributed to biomass burning (CHAPTER III), whereas the large increase of nighttime P concentrations at ground level suggests that there was a source for these aerosols at this level. However, P (but also Ca and Mn) is usually not enriched in pyrogenic aerosols of the fine fraction. This is in contrast to elements such as S, K, Zn, Rb, and the halogen elements Cl, Br, and I, which are also present in plants, but become substantially enriched in the fine pyrogenic aerosol (Kleeman et al., 1999; Maenhaut et al., 2002). Therefore the source for the element P in the fine fraction above the canopy is still not well understood.

Coarse aerosol night-to-day elemental ratios fell into three distinct classes. The main biogenic-related elements (P, S, Cl, and K), together with CPM, displayed large enrichments in concentration at night, with a maximum observed either at canopy level or below the canopy. This is consistent with what was observed above Figures IV-2c and 2d). However, Cu and Zn, which are also usually considered to be of biogenic origin, showed the opposite profile. The mechanisms controlling the emission of these elements within the Amazonian rain forest are yet not fully understood (Artaxo and Hansson, 1995; Artaxo et al., 2001). All dust-related elements (i.e.: Mg, Al, Si, Ti, Mn, Fe, Sr, with the exception of Ca which is also present in plants as a macronutrient) showed very little differences comparing night to day ratios, and no significant profile pattern could be observed in these ratios for the three heights (indicating that night and day concentrations of coarse soil dust particles were about constant for each of the three heights). This is

somewhat puzzling as soil dust arises mainly from wind abrasion, road traffic or mining in dryer areas, which all occur predominantly during the daytime. However, deposition velocities of coarse particles are highly variable, and the influence of stable atmospheric conditions on deposition behavior is still not fully understood (Wesely and Hicks, 2000).
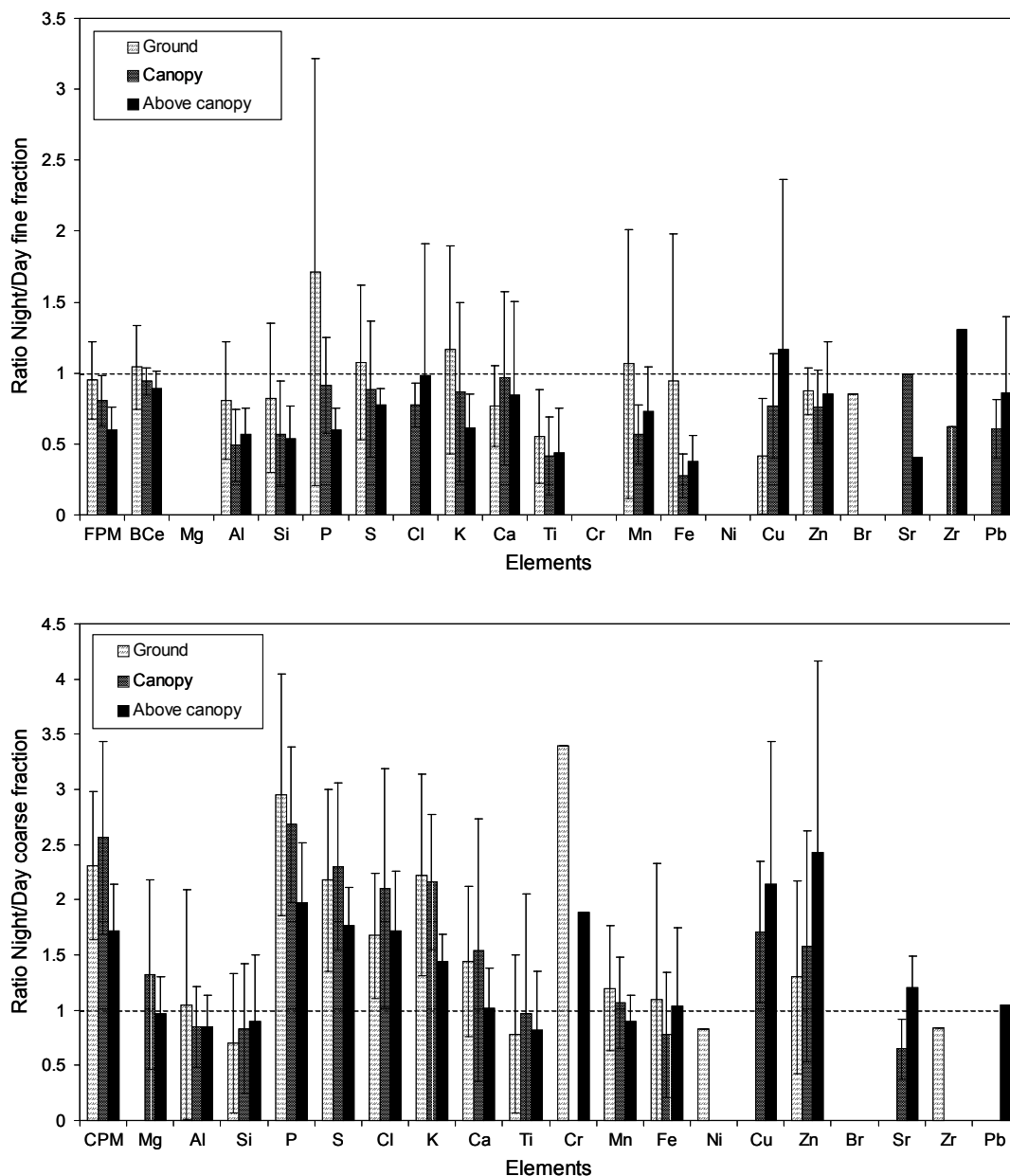
Figure IV-3 Nighttime-to-daytime ratios for the LBA-EUSTACH 1 aerosol particles.
Nighttime-to-daytime ratios of mass, equivalent black carbon (BC_e), and elemental concentrations for the fine (a) and coarse (b) aerosol fractions collected at three different heights on the Jarú meteorological tower (top, canopy, and ground level) in Rondônia, Brazil, during the wet season (8 April–21 May 1999).

IV.3.1.2. Dry season

Average PM, BC, and trace element concentrations for the fine and coarse aerosol measured during the dry season at the three different levels of the meteorological tower are presented in Table IV-2. When assumed to be present in the form of their most common oxide, the listed trace elements could account for approximately the same fraction of CPM as during the wet season. For FPM, however, this fraction decreased by a factor of about two compared to the wet season, which could be attributed to the large amounts of submicron organic particles emitted during biomass burning.

The concentrations that were observed for most elements lay in between those reported by Echalar et al. (1998) for dry season data collected in Alta Floresta during August 1992–March 1995 (FPM = 47 ± 41 µg m^{-3}), and those collected in Cuiabá for the period July 1990–August 1995 (FPM = 17 ± 41 µg m^{-3}). Overall, trace element concentration increased by a factor of ca. 2–6 from the wet to the dry season for most elements in the fine fraction (FPM increased by a factor ca. 15), but, withstanding a few exceptions, by only ca. 1–4 for the coarse aerosol (CPM increased by a factor of ca. 2 above the canopy level, but only ca. 1.2 below the canopy). The largest differences observed between the two seasons were for the fine aerosol elements generally associated with biogenic material in the wet season, along with BC_e (BC_e, P, S, K, Zn and Br increased by factors of ca. 5–19). All of these elements are expected to be emitted during the burning of plant material. Soil dust-related elements increased to a lesser extent (by a factor of ca. 3 at the most). This increase is probably attributable to the thermal uplifting of dust particles that occurs during large fires.

Table IV-2 Dry season mean atmospheric concentrations[1] and standard deviations (s.d.) of fine and coarse fraction particulate mass, equivalent black carbon, and trace elements for samples collected on three levels of the Jarú meteorological tower (upper, canopy, and ground level) in Rondônia, Brazil (6 September–31 October 1999).

n is the number of samples from a set of 81 in which the element was measured above its detection limit.

Dry season

	Above-canopy level						Canopy level						Below-canopy level					
	Fine fraction			Coarse fraction			Fine fraction			Coarse fraction			Fine fraction			Coarse fraction		
	Mean	s.d.	n	Mean	s.d.	n	Mean	s.d.	n	Mean	s.d.	n	Mean	s.d.	n	Mean	s.d.	n
Mass	33.5	21.8	(79)	6.6	3	(79)	33.0	21.6	(80)	7.8	3.9	(80)	27.9	19.6	(81)	7.6	4.3	(81)
TC	17.1	8.8	(28)	—	—	—	—	—	—	—	—	—	—	—	—	—	—	—
EC_a	0.74	0.34	(28)	—	—	—	—	—	—	—	—	—	—	—	—	—	—	—
BC_e	1.82	1.3	(79)	—	—	—	1.81	1.35	(80)	—	—	—	1.69	1.3	(81)	—	—	—
Al	91	63.7	(72)	80	50	(26)	75.8	41.3	(20)	82.9	50.1	(18)	53.7	25.4	(17)	53.1	38.8	(23)
Si	118.8	97.1	(80)	95	133.8	(62)	111.4	110.3	(56)	87.8	163.5	(53)	80.8	63.5	(67)	65.7	68.6	(74)
P	26.7	11.7	(81)	47.7	23	(81)	30.7	12.5	(81)	55.4	28.2	(79)	18.5	7.6	(81)	51.2	28.4	(79)
S	532.7	288.8	(81)	59.8	26.6	(81)	538.2	273.6	(81)	64.2	28.8	(79)	510.9	263.1	(81)	56.8	27.2	(79)
Cl	20.4	11.5	(19)	10.1	5.1	(20)	23.5	6.6	(10)	16.13	16.5	(17)	15.4	7.1	(31)	16	15.7	(26)

Table IV-2 (continued)

	Fine fraction			Coarse fraction			Fine fraction			Coarse fraction			Fine fraction			Coarse fraction		
	Mean	s.d.	n	Mean	s.d.	n	Mean	s.d.	n	Mean	s.d.	n	Mean	s.d.	n	Mean	s.d.	n
K	506.2	355.3	(81)	93.1	56.2	(79)	488.2	342	(81)	102	59.7	(78)	435.8	316.1	(81)	109.8	81.7	(79)
Ca	25.1	26.2	(75)	52.3	74.8	(76)	24.8	20.8	(54)	56.3	86.2	(73)	16.2	16.1	(53)	38.5	45.7	(74)
Ti	6	4.4	(50)	8	5.3	(42)	6.4	4.2	(43)	7	4.3	(36)	9.8	7.8	(21)	4.2	3.3	(12)
Cr	10.3	6.2	(15)	15.4	17.1	(31)	8.9	5.7	(10)	20.9	24.8	(36)	5.6	2.2	(10)	14.8	8.7	(20)
Mn	1.87	1.4	(79)	4.5	5.5	(79)	2	1.6	(81)	4.2	4.2	(79)	2.3	1.4	(70)	3.1	2.6	(57)
Fe	28.6	28	(81)	48	47.5	(77)	24.9	25.8	(76)	35.9	40.6	(78)	22.2	20.4	(74)	31.1	26.7	(77)
Cu	1.66	1.57	(67)	3.9	6.1	(24)	—	—		3.8	2.6	(11)	1.73	1.25	(39)	2.35	1.33	(23)
Zn	4.3	3.5	(81)	4.3	4.8	(7)	5	3.2	(10)	3.1	1.6	(7)	5.4	3.4	(43)	3.1	1.6	(17)
Br	10.2	6.4	(43)	25.1	15.6	(5)	10.9	7	(41)	21.4	14.3	(9)	—	—		—	—	—

[1] Mass, TC, EC_a, and BC_e concentrations are in µg m^{-3}; trace elements concentrations are in ng m^{-3}.

The height-resolved concentration data (Table IV-2) indicate that almost all the measured fine and coarse aerosol components exhibited either highest concentrations above the canopy and lowest below, or little significant variation between the different levels. However, the variability in elemental concentrations was large during the dry season, as indicated by the standard deviations associated with the average concentrations (Table IV-2). To help understand the profiles measured during this season, enrichment ratios were computed in the same fashion as described in Section IV.3.1.1 for the wet season period. The results are presented Figures IV-4a–d. Here, the soil-dust tracer Fe was used instead of Al, because of the large amount of data below the detection limit for the latter element, particularly at night. This could be due to the fact that Al is a low Z element, with substantial X-ray absorption. For example, the detection limit for Fe in PIXE is about 5 times higher than for Al. Also, the detection of Al with the PIXE technique suffers from interferences from Bromine, that is a contaminant in Nuclepore filters, and the detection limit for Al may vary from one Nuclepore batch to the other, depending on the amount of Bromine in Nuclepore Filters.

In the case of the fine aerosol (Figures IV-4a and 4b), for which biomass burning was the dominant source during the dry season, E_r values showed little overall difference between the three sampling heights. This indicates that these particles were introduced into the forest from aloft and either deposited slowly or were well-mixed within the forest. It is interesting that, despite the large standard deviation associated with the measurements, FPM, P and Fe displayed quite similar nighttime profiles as for the wet season. The behavior of P was perhaps the most varied, with the largest enrichment observed at canopy height, and a depletion occurring between canopy and ground level.

For the coarse fraction, the observed daytime vertical profile contrasts with that observed during the wet season and appears to indicate that the deposition of coarse fire-associated particles (ash and dust) from aloft largely counterbalances the positive above-to-below canopy concentration gradient observed for the natural background forest aerosol. Daytime E_r values for coarse fraction Fe covered a broad range (large standard deviations), due to the large variability in fire activity and fire proximity during this season. For the nighttime period, E_r profiles for coarse aerosol elements compare well

with those measured during the wet season. At ground level, the concentrations for coarse fraction P and K are comparable to those measured during the wet season (Table IV-2), suggesting that most of the coarse biogenic material measured at this height during the dry season was also emitted directly from plants. However, the large enrichment in coarse aerosol P at canopy level during the dry season suggests that significant amounts of large biogenic particles of biomass-burning origin came from aloft and were being deposited within the forest canopy.
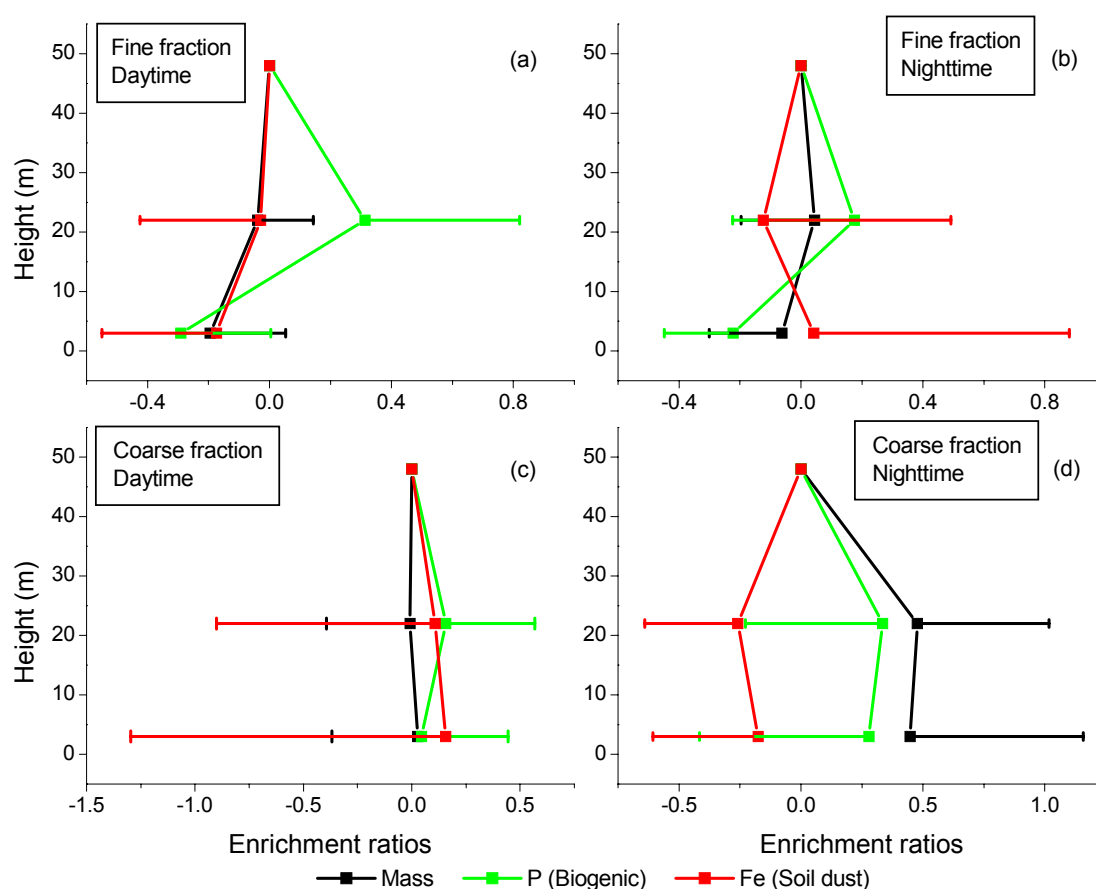
Figure IV-4 Enrichment ratios for the LBA-EUSTACH 2 aerosol particles.
Dry season enrichment ratios (E_r) calculated for FPM (black lines), and P (green lines) and Fe (red lines) concentrations in the fine aerosol fraction during day (a) and nighttime (b), in Rondônia, Brazil (6 September–31 October 1999). The corresponding E_r for the coarse aerosol fraction measured during day (c) and nighttime (d) are also shown. The squares represent the average of the E_r values calculated from each individual set of concentration measurements (above, within and below canopy), and the error bars the associated standard deviation.

Figures IV-5a and 5b present the dry season EFs computed (as in Section IV.3.1.1) for the three sampling heights on the meteorological tower for the fine and coarse aerosol fraction, respectively. The fine fraction EFs are comparable to those observed during the wet season, except that biogenic-related elements (mainly P, S, K, Zn, and Br) showed even larger enrichments compared to the average crustal composition, confirming the contribution of smoke to the atmospheric loading of these elements. Soil dust-related elements also showed a trend similar to the one observed in the wet season data, with the exception of Fe, which displayed a slight depletion, and Mn, a slight enrichment. In the wet season, the majority of the airborne soil dust probably did not originate in the direct vicinity of the measurement site, but from more distant, dryer regions. During the dry season, however, soil dust uplifted from the local fires would have contributed substantially to the total dust loading. Hence, seasonal differences in the composition of the dust component of the aerosol are not unexpected.

With the exception of Ca, and to a larger extent Mn, which both showed an enrichment in the dry season data, the coarse element EFs for the dry season were very similar to those observed during the wet season, with no obvious additional enhancement of EF values that could be attributed to biomass burning. This confirms that natural sources of coarse fraction particles cannot be neglected during the dry season, and probably even remain the dominant source of coarse biogenic material during this period. Ca and Mn are constituents of higher plants, and are usually found in the coarse aerosol fraction and are considered to be biogenic elements. However, they have already been reported to be also associated with biomass burning in some cases (Artaxo et al., 1998; Echalar et al., 1998).
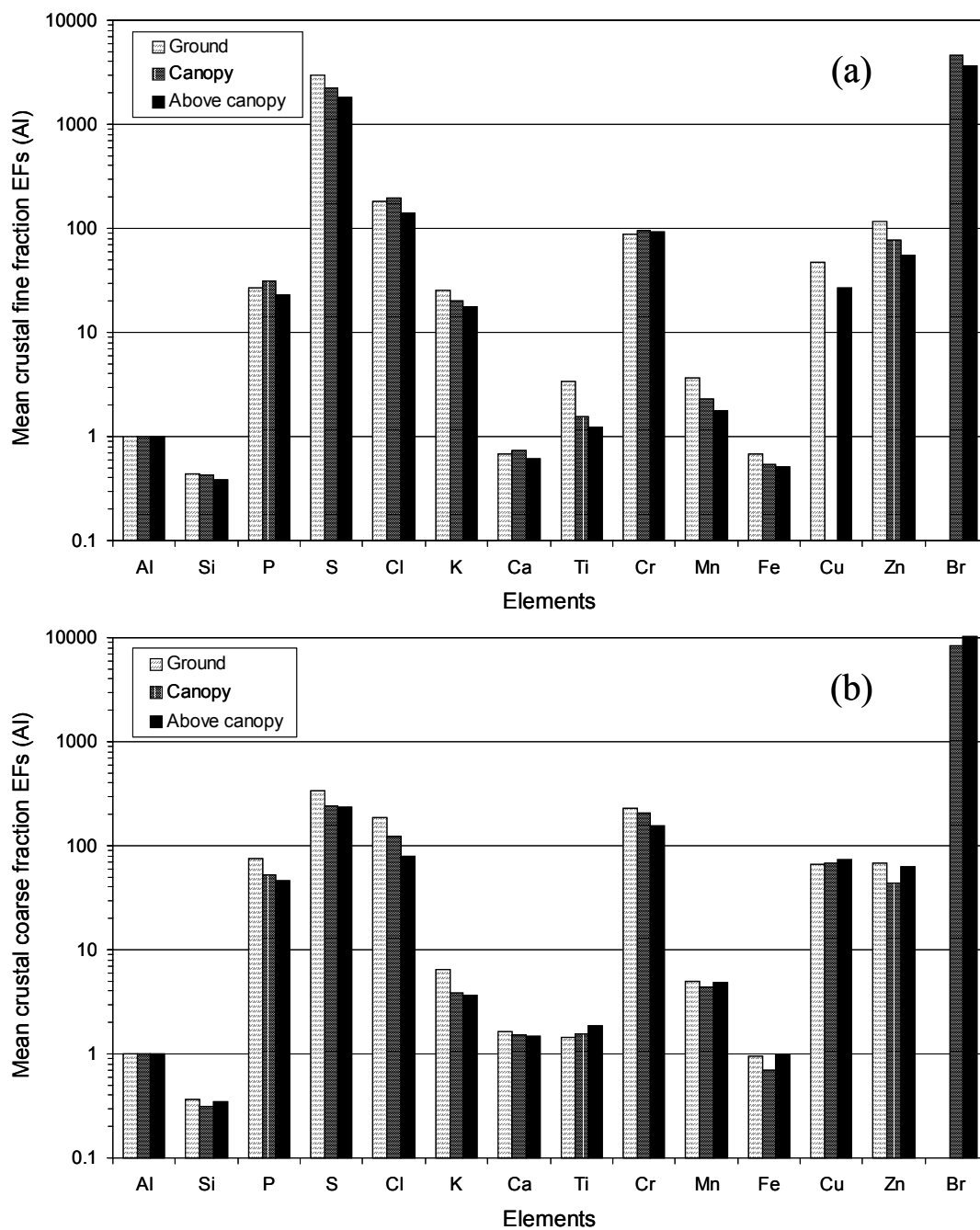
Figure IV-5 Mean crustal enrichment factors for the LBA-EUSTACH 2 aerosol particles.
Mean crustal enrichment factors (EFs) for the fine (a) and coarse (b) aerosol fractions collected at three different heights on the Jarú meteorological tower (top, canopy, and ground level) in Rondônia, Brazil, during the dry season (6 September–31 October 1999). EF values were calculated relative to the average crustal rock composition of Mason and Moore (1982) using Al as the reference element.

Night-to-day ratios of elemental concentrations for all three-measurement heights are presented in Figures IV-6a and 6b for the fine and coarse aerosol fraction, respectively. Fine aerosol ratios showed no significant differences in concentrations between night and daytime for almost all elements, and all heights. This suggests that the fine aerosol was present as a well-mixed, regional haze. This is not surprising, given that fine pyrogenic aerosols have a lifetime of ca. 10 days (neglecting wet deposition due to rainfall), and the intense convective mixing within the Amazon basin. Although fresh smoke plumes were sometimes observed during daytime, it could also be that the formation of a shallow nocturnal boundary layer served to compensate for any day-night variation that might have been expected to result from these.

For the coarse fraction, soil dust-related elements displayed little or no day-night variation within the canopy or at ground level, but seemed to be slightly enriched at night above the canopy. As mentioned in Section IV.3.1.1 for the wet season data, this effect is still not well understood, but could be a consequence of the formation of a shallow nocturnal boundary layer. Biogenic-related elements (P, S, Cl, K, and Br), along with CPM, were enriched at night by a factor of ca. 2 compared to daytime concentrations. The highest night-to-day ratios were observed at the canopy or below-canopy level, and the lowest consistently above the canopy. This vertical profile is essentially the same as was observed during the wet season, and supports the contention that coarse biogenic particles produced within the forest account for a major fraction of CPM even in the dry season.
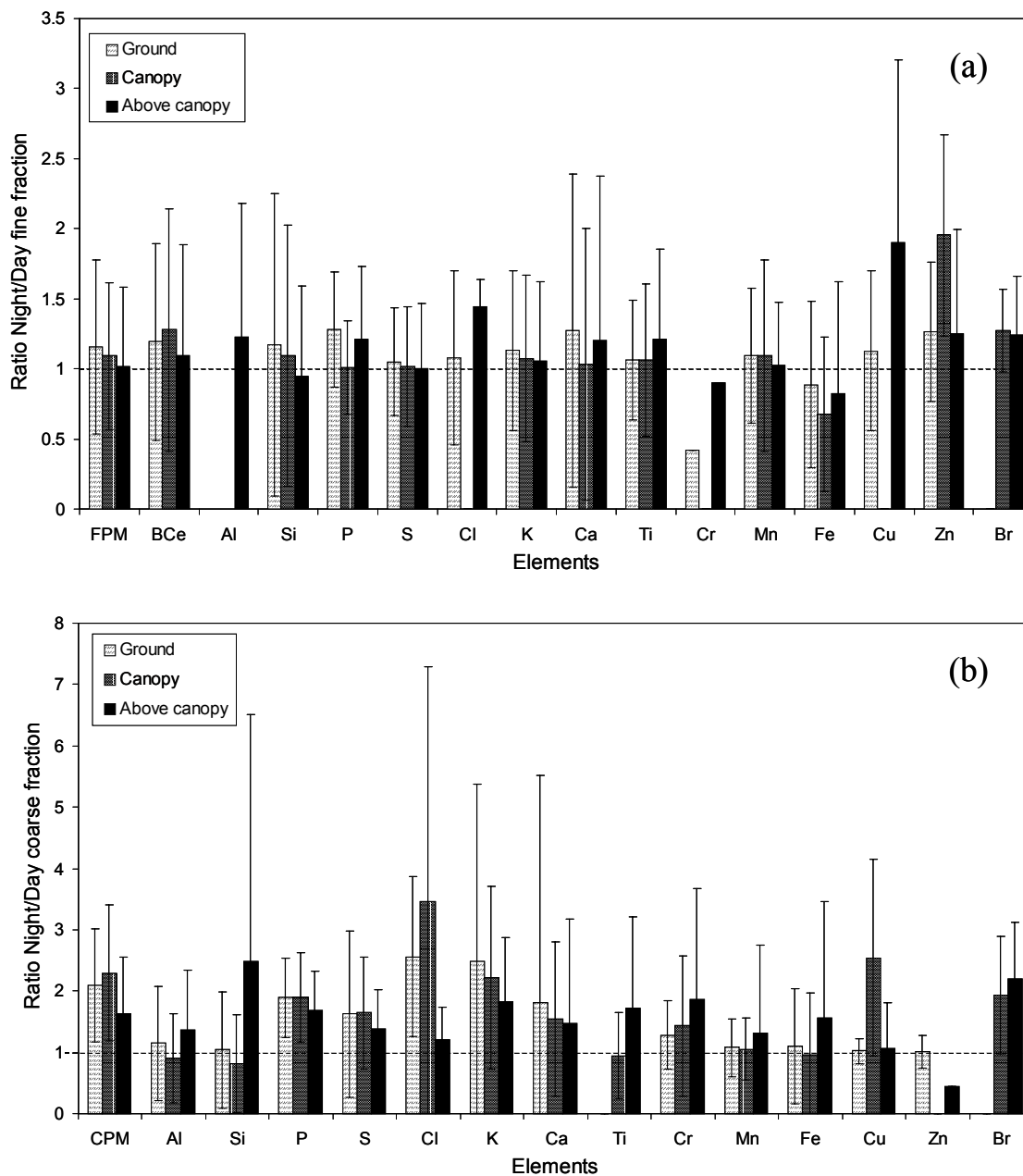
Figure IV-6 Nighttime-to-daytime ratios for the LBA-EUSTACH 1 aerosol particles.
Nighttime-to-daytime ratios of mass, equivalent black carbon (BC$_e$), and elemental concentrations for the fine (a) and coarse (b) aerosol fractions collected at three different heights on the Jarú meteorological tower (top, canopy, and ground level) in Rondônia, Brazil, during the dry season (6 September–31 October 1999).

IV.3.2. Carbonaceous content of Amazonian aerosols

TC, OC, and EC_a analyses were performed on 11 quartz fiber filters for the wet season and 28 for the dry season. Figures IV-7a and 7b show scatter plots of EC_a versus TC for the fine aerosol (D_p < ca. 2.5 μm) sampled during the LBA-EUSTACH 1 and 2 campaigns, respectively. The reasonably good correlations between EC_a and TC for both seasons might suggest that fine carbonaceous aerosols probably had a pyrogenic source throughout the year. This is not surprising for the dry season as this period was heavily influenced by smoke emitted from biomass burning. For the wet season, although a large fraction of the fine aerosol fraction is expected to be of biogenic origin (e.g., Echalar et al. (1998)), it is shown in CHAPTER III that this period was also influenced by biomass burning, especially toward the end of the LBA-EUSTACH 1 campaign (13–21 May 1999). It is also important to underline that fire is still widely used in Brazil throughout the year for domestic purposes and charcoal production, and in various factories (e.g., brick making) (Andreae, 1991; Liousse et al., 1996; Echalar et al., 1998; Artaxo et al., 2002). An alternative explanation for the correlation of EC_a and TC during the wet season might be that biogenic sources also release thermally refractory OC, which shows up as EC_a in the TOT analysis.

The average EC_a/TC mass ratios values obtained for the LBA-EUSTACH 1 and 2 campaigns are summarized in Table IV-3, together with some other relevant values taken from literature. The values obtained here (0.08 ± 0.03 and 0.05 ± 0.01 for LBA-EUSTACH 1 and 2, respectively) are in the lower range of what has usually been reported for aerosols collected under similar conditions. It should be stressed, however, that these ratios may vary depending on the type of combustion, fuel, age of the particles, etc. In addition, the definition of elemental (or black) carbon is operational and method-dependent. On the simplest level, elemental (or black) carbon measurements fall into two classes—optical, in which light absorption is used to measure "black carbon equivalent" (BC_e), and thermal, in which "apparent elemental carbon" (EC_a) is distinguished on the basis of its highly refractory nature. The first group of methods derives BC_e concentrations via conversion of the measured absorption using a user-defined mass absorption factor. The second are based on the assumption that elemental carbon can be

differentiated from organic carbon by the temperature at which it evolves. A comprehensive description of the different methods used to derive EC_a can be found in Schmid et al. (2001). These authors describe an intercomparison of EC_a, OC, and TC measurements made on aerosol samples collected in an urban environment. Most techniques showed good agreement for the determination of TC, but very large discrepancies concerning EC_a. The method used in the present study was concluded to be one of the more suitable ones for the determination of EC_a. However, it is important to note that whereas EC_a and OC in urban aerosols are quite distinct chemical fractions, biomass-burning samples also include other refractory and light absorbing carbonaceous material apart from pure soot (e.g., polyaromatic hydrocarbons (Finlayson-Pitts and Pitts, 2000), and polymeric organic compounds (Mukai and Ambe, 1986; Zappoli et al., 1999; Mayol-Bracero et al., 2002)), which might complicate the analysis. Moreover, biomass-burning samples often contain large amounts of K and Na, which have been shown to catalytically influence the temperature at which EC_a evolves (Novakov and Corrigan, 1996; Martins et al., 1998a). Therefore, despite the fact that one can be confident in the analytical method used in this study and that the values of EC_a presented herein are the best estimate that could be made at this stage, care should be taken in drawing conclusions from the data. There is an urgent need for international definitions and standards for BC_e and EC_a.

Given that elemental carbon is produced mainly under high temperature flaming conditions with an oxygen deficiency (Kuhlbusch and Crutzen, 1996), the relatively low EC_a/TC ratios that were observed for samples suggest that smoldering combustion contributed significantly to the total aerosol loading. This is consistent with the visual observation of forest fires in Rondônia. Forest fires typically exhibit a longer smoldering phase as compared to, for example, savanna fires. Using an optical transmission and a TOT method, O. L. Mayol-Bracero (unpublished data) found EC_a/TC ratios comparable to ours for the pasture location, during the LBA-EUSTACH 2 campaign (EC_a/TC = 0.05 ± 0.01 determined on 8 samples using the TOT method and 0.07 ± 0.01 determined on 9 samples using the optical transmission method). Interestingly, using a linear temperature thermal combustion method known as evolved gas analysis, Mayol-Bracero et al. (2002)

found that a significant fraction of the EC_a material (on average ca. 50%) seemed to be highly refractory organic material soluble in water.
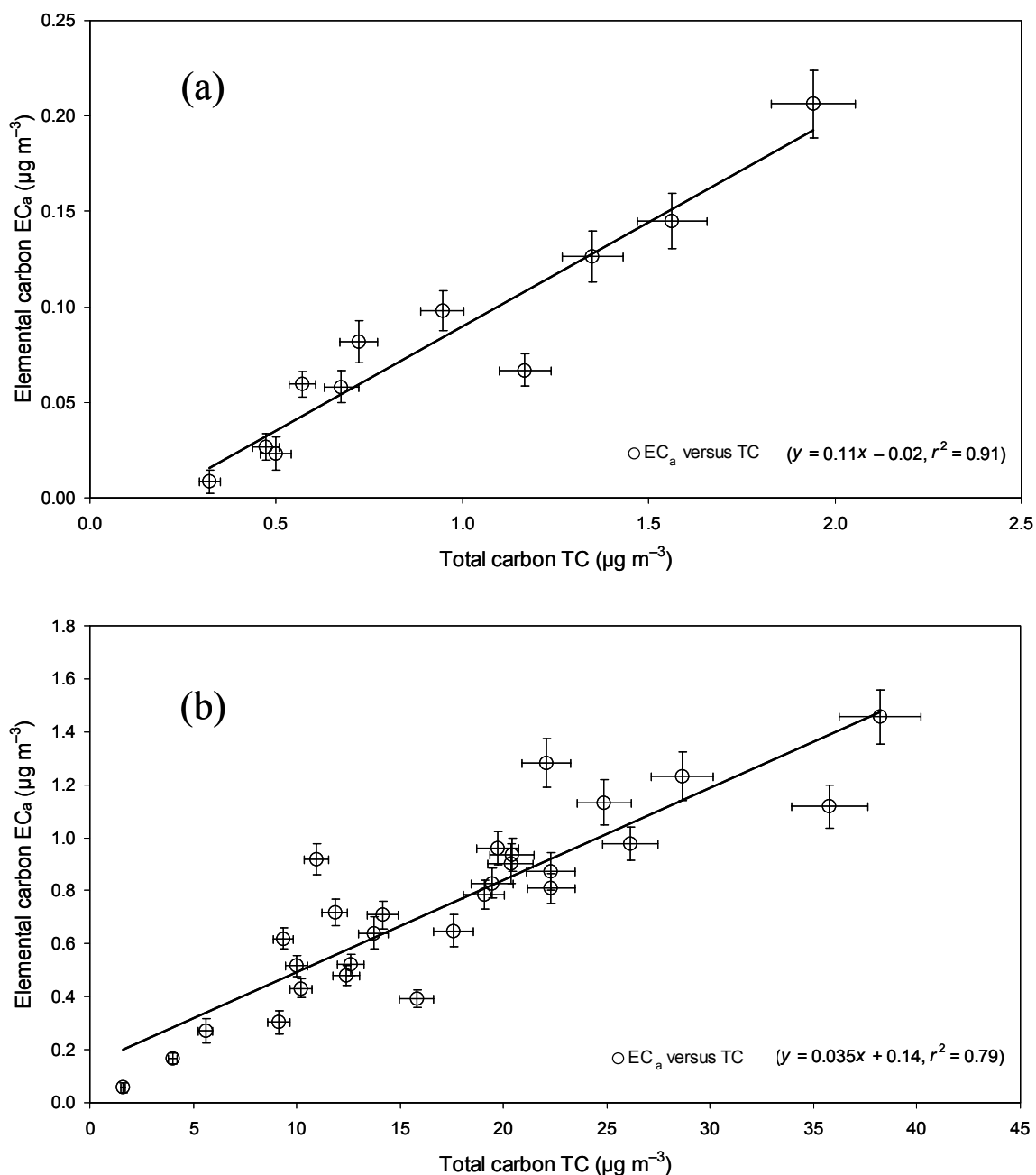
Figure IV-7 Elemental and total carbon concentrations for the LBA-EUSTACH 1 and 2 campaigns.
Scatter plot of EC_a against TC concentrations measured for fine aerosol (D_p < ca. 2.5 μm) collected during the wet (a) and dry seasons (b) near the top of the Jarú meteorological tower in Rondônia, Brazil. TC and EC_a analyses were performed on 11 fine quartz fiber filters for the wet season (8 April–21 May 1999) and 28 for the dry season (6 September–31 October 1999).

Table IV-3 Ratios of the apparent elemental carbon (EC$_a$) to total carbon (TC) for biomass burning aerosols of various origin.
Values represent the average of the EC$_a$/TC mass ratios ± associated standard deviation of the measurements.

Location	Measurement method	Size cut (μm)	EC$_a$/TC	Reference
Brazil, wet season	Thermo-optical transmission	< ca. 2.5	0.08 ± 0.03	This study
Brazil, dry season, forest fire	Thermo-optical transmission	< ca. 2.5	0.05 ± 0.01	This Study
Brazil, dry season, forest/pasture fire	Thermal combustion	< ca. 2.5	0.07 ± 0.01	O. L. Mayol-Bracero (unpublished data)
	Thermo-optical transmission	< ca. 2.5	0.05 ± 0.01	
Brazil, dry season, cerrado, grass, and forest fires	Two-step thermal analysis	< 4	ca. 0.13 (flaming) ca. 0.08 (smoldering)	Ferek et al. (1998)
Ivory Coast, savanna burning	Two-step thermal analysis		0.03–0.2	Cachier et al. (1995)
Southern Africa, savanna burning	Two-step thermal analysis		0.1–0.3	Andreae et al. (1998)

IV.3.3. Mass scattering and absorption efficiencies

In order to quantify the optical effect of the Amazonian aerosols characteristic of the wet and dry seasons, mass scattering (α_s) and mass absorption efficiencies (α_a) of these aerosols were computed at a wavelength of ca. 550 nm. Mass scattering/absorption efficiencies are defined as the ratio of the scattering or absorption coefficient to the aerosol mass concentration, in units of $m^2\ g^{-1}$, and specify how effectively the aerosol components interact with light. To determine these values, we used multivariate regression of in situ-measured aerosol scattering (σ_s) and absorption coefficients (σ_a) on the mass concentrations (measured for the SFU samples), according to the following model:

$$\sigma_{s/a,\lambda} = k + \alpha_{s/a,\lambda,CPM}[CPM] + \alpha_{s/a,\lambda,FPM}[FPM] \qquad \text{(IV-3)}$$

where $\sigma_{s/a,\lambda}$ is the aerosol scattering or absorption (Mm^{-1}) at wavelength λ of incident light, k is a constant representing contributions to scattering not related to either coarse or fine aerosol fractions, $\alpha_{s/a,\lambda,CPM}$ and $\alpha_{s/a,\lambda,FPM}$ are the mass-scattering or absorption coefficients for the coarse and fine particulate mass at wavelength λ, and [CPM] and [FPM] are the coarse and fine particulate mass concentrations. For the purpose of the regression analysis, these values were averaged over the sampling time of the corresponding filters (see Section IV.2). Time series of σ_s and σ_a for both field experiments have been presented and discussed in Sections III.3.3 and III.3.4, respectively.

The values of α_s and α_a computed for the FPM and CPM fractions for the two measurement campaigns are summarized in Table IV-4. Overall, good multiple linear fits were obtained between the optical and SFU mass measurement data. Because of the small number of SFU samples collected during the LBA-EUSTACH 1, the first part of the campaign, characteristic of more pristine conditions, could not be differentiated from the end the campaign, which was disturbed by aged biomass burning plumes (CHAPTER III). Therefore, the optical efficiency parameters obtained from the LBA-EUSTACH 1 data certainly show the influence of the latter period, and cannot strictly be considered representative of clean background conditions, but only as an approximation.

Table IV-4 Mass scattering (α_s) and absorption efficiencies (α_a) of background and biomass burning aerosols in the Amazon basin (mean values ± standard error of the fit).
n is the number of data points used in the regression analysis.

Parameter	LBA-EUSTACH 1			LBA-EUSTACH 2		
	α_{550nm}	r^2	*n*	α_{550nm}	r^2	*n*
$\alpha_{s,FPM}$	3.2 ± 0.6	0.93	13	5.9 ± 0.3	0.84	62
$\alpha_{s,CPM}$[1]	NS	—	—	NS	—	—
$\alpha_{a,FPM}$	0.57 ± 0.06	0.87	22	0.31 ± 0.03	0.84	49
$\alpha_{a,CPM}$	0.22 ± 0.07	0.87	22	0.43 ± 0.19	0.84	49
$\alpha_{a,BCe}$	6.7 ± 0.5	0.91	22	5.8 ± 0.4	0.80	49
$\alpha_{a,ECa}$	20.1 ± 1.9	0.94	10	13.6 ± 1.9	0.83	12

[1] NS: Not significant; —: no value or not computed

One of the major conclusions that can be drawn from the results is that the CPM of both background and pyrogenic aerosols did not contribute significantly to total scattering but played a substantial role in aerosol light absorption. During the LBA-EUSTACH 1 campaign, the coarse particle fraction ($D_p > 2$ μm) comprised ca. 50–80% of the total aerosol mass (Section IV.3.1.1), and is, therefore, estimated to have been responsible for ca. 30–60% of the absorption during the wet season (assuming $\alpha_{a,FPM}$ and $\alpha_{a,CPM}$ values of 0.57 and 0.22 m^2 g^{-1}, respectively). However, it is most surprising that the wet season coarse fraction aerosol was not found to contribute to the scattering from the analysis. The intercept k of the regression was small (−1.0 ± 1.5 Mm^{-1}), which excludes the eventuality that the coarse fraction may have contributed to a constant background scattering. Therefore, at this stage of the analysis, this behavior of the coarse fraction remains unexplained. It is noted here that assuming a conservative mass scattering efficiency of 0.2 m^2 g^{-1} for CPM would have led to a contribution of this mode to the total scattering ranging between 6 and 20%.

During the biomass-burning season, the relative mass contribution of the coarse aerosol was much lower (median of 18% of the total mass, first and third quartile of 13 and 26% respectively) (Artaxo et al., 2002). Nevertheless, the relatively large $\alpha_{a,CPM}$ value

of 0.43 $m^2 g^{-1}$ estimated for this season suggests that CPM would have still accounted for ca. 20–40% of the CPM to the total absorption for the biomass burning season. Despite the large standard error associated with the dry season $\alpha_{a,CPM}$ value, it was found to be significant in the analysis to a $p_{value} = 0.02$. Whilst it may appear surprisingly large, especially since elemental carbon emitted during combustion usually concentrates in the fine particle mode (typically particles of $D < 1$ μm), it should be recalled that large particles are also emitted during wild fires, including dust, ash, and plant debris (above the canopy, CPM increased by a factor of ca. 2 from the wet to the dry season; see Section IV.3.1.1). This contribution of coarse mode particles is currently being underestimated, if not completely ignored, in modeling studies of aerosol optical properties, probably due to a lack of information in this field. The results of the current study, however, indicate that this is an issue that should be investigated further.

Assuming fine mode EC_a to be the only aerosol component contributing to light absorption, average $\alpha_{a,ECa}$ values of ca. 20 and 14 $m^2 g^{-1}$ were obtained for the LBA-EUSTACH 1 and 2 campaigns, respectively. These values are larger than those typically reported for soot. A typical value given in the literature is ca. 7–12 $m^2 g^{-1}$ for submicrometer soot particles, at 550 nm (Horvath, 1993; Horvath, 1998; Penner et al., 1998). Modeling studies, however, indicate that α_a may vary from 7–30 $m^2 g^{-1}$, depending on the incident wavelength and on the mixing stage of the particle (for example, the presence of a non-absorbing coating) (Martins et al., 1998a). Liousse et al. (1995) showed that α_a can increase with smoke age from 15–25 $m^2 g^{-1}$. Viewed from this perspective, the values presented herein—especially those for the first campaign—appear to suggest that the aerosols were aged and probably included a non-absorbing coating. This is consistent with the satellite observations and backward trajectory calculations reported in Section III.3.1 for the LBA-EUSTACH 1 campaign, which indicate that smoke-bearing air masses reaching the measurement site toward the end of the LBA-EUSTACH 1 campaign derived from fires some 2–3 days earlier, allowing ample time for the formation of an aerosol coating.

Additional evidence for absorption characteristics different from typical soot carbon can be seen in the $\alpha_{a,BCe}$ values of ca. 6–7 $m^2 g^{-1}$ that were calculated for biomass

burning and background aerosol, assuming BC_e to be the only aerosol component contributing to light absorption. This is due to the fact that BC_e values are consistently higher than EC_a concentrations in the EUSTACH samples. BC_e is defined as the amount of black carbon standard that gives the same absorption as the total amount of absorbing material in the fine fraction of the sampled aerosol. If BC_e is larger than the chemically determined EC_a, this may either be due to the absorption efficiency of the black carbon in the sample being higher than that of the standard BC, or to the presence of absorbing substances that are not measured as EC_a in the TOT analysis. Thus, it cannot be excluded that the high $\alpha_{a,ECa}$ values that were obtained result from the presence of compounds other than EC_a that contribute to the absorption (see Section IV.3.2). If this interpretation is accepted, the results would suggest that EC_a contributes to only about half the absorption observed in the fine mode during the burning season, and a third for background conditions.

The high correlation between EC_a and σ_a (Table IV-4) suggest that the other absorbing compounds might be (directly or indirectly) of the same origin as EC_a, i.e. pyrogenic. As mentioned earlier, soil dust is uplifted into the atmosphere during fires due to convective updrafts. It could also be that low-molecular-weight polar organic compounds emitted during combustion condense and polymerize in the aerosol-phase, to form light absorbing "humic-like substances". Extending the latter hypothesis, it could also be that EC_a, when produced from biomass burning, does not exist exclusively in the form of purely elemental carbon, but is a range of highly polymerized carbon structures in varying states of oxidation (depending e.g. on the fire efficiency, etc.). Accounting for the oxygen and hydrogen in the EC_a would increase the mass concentration of this fraction, and decrease the value of $\alpha_{a,ECa}$.

Overall, the average $\alpha_{s,FPM}$ value almost doubled from the first to the second LBA-EUSTACH campaign (with the first campaign being influenced by aged biomass-burning plumes and the second one exhibiting biomass burning haze conditions), whereas $\alpha_{a,FPM}$ decreased by approximately half. These changes resulted in a lower single-scattering albedo ($\omega_0 \sim 0.84$) for the first campaign (background conditions) compared to that of the second (ω_0 of ca. 0.91) (Section III.3.5).

In order to further investigate the origin of the light absorbing and scattering material, factor analysis was performed to retrieve the aerosol sources and the in situ measured aerosol optical properties were regressed against the obtained absolute factor scores, as detailed in the following sections.

IV.3.4. Aerosol source identification and apportionment

IV.3.4.1. Wet season, the sources of the LBA-EUSTACH 1 aerosols

The left-hand side of Table IV-5 shows a summary of the PCA results obtained for the wet season aerosol sampled above the canopy at the tower site in Rondônia. In this analysis, fine and coarse aerosol data were combined together, in order to facilitate further correlation of the identified sources with aerosol optical properties. The series of values reported for each element (or variable) correspond to the "component loadings" of the element in the different components. Only component loadings larger than 3 times their associated standard deviation are statistically significant (Heidam, 1982). In the present study standard deviations were typically lower than 0.1, so that component loadings larger than ca. 0.3 can be considered as being statistically significant.

It is evident from Table IV-5 that most of the variance in the element mass concentrations was explained by a four-component model (as indicated by the communality values approaching a value of 1), in which all four components have eigenvalues larger than unity. Prior to performing the PCA analysis the Kaiser-Meyer-Olkin measure-of-sampling-adequacy test was computed. The test yielded a value of 0.71, indicating that the variance in the data may be explained by underlying factors, and that factor analysis was appropriate. However, it should be noted that these results were obtained using data derived from the analysis of only 28 SFU samples, and, as noted earlier in Section IV.2, 30 degrees of freedom is generally considered to be the minimum required to achieve statistically-robust results.

During LBA-EUSTACH 1, aerosol samples (76) were also collected at a pasture site situated only ca. 80 km from the RBJ site, and analyzed in an identical fashion to the samples collected for the present study (Artaxo et al., 2002). Therefore, a separate PCA

was performed using this data set in order to check the robustness of the results for the forest site data analysis. The results, also reported in Table IV-5, indicate that the aerosols measured at the forest and pasture sites had the same origin—the first and second components for each site show high correlations with the same elements, and the fourth component of the forest data set (probably of minor importance) is similar to the third for the pasture site. These three components were responsible for about the same percentage of the variance at both sites. The main difference found between the two data sets was the identification of a third component for the forest site aerosol, mainly dominated by Cu in both the fine and coarse fractions. Copper is often identified as a single component in the analysis of Amazonian aerosol data and is suspected to be of biogenic origin. A Cu-containing component was not identified for the pasture site simply because this element was not measured frequently enough at this site to be included in the APCA model. Therefore, despite the fact that the pasture site was suspected to be more influenced by anthropogenic activities, and showed slightly higher concentrations of dust particles (see CHAPTER III and Artaxo et al. (2002)), the results of the component analysis for the pasture site support those obtained for the forest site PCA.

The four components extracted from the PCA analyses explain ca. 86% of the total sample variance. As the combined uncertainties associated with sampling and analysis are estimated to have been about 10%, the two models satisfactorily explain all the variability associated with the data sets. The communalities of FPM and CPM are larger than 0.87, indicating that most of the variability in each of these two mass concentrations could be explained.

Table IV-5 VARIMAX-rotated principal component analysis loading matrices for the fine and coarse aerosol fractions collected at the Rondônian forest and pasture sites during the 1999 wet season.

Var.[1]	Wet season								
	Forest site					Pasture site			
	Comp. 1	Comp. 2	Comp. 3	Comp. 4	Comm.	Comp. 1	Comp. 2	Comp. 3	Comm.
FPM	0.94	−0.06	0.01	−0.17	0.91	0.87	−0.17	−0.05	0.78
CPM	0.27	0.88	−0.08	0.1	0.87	0.39	0.86	0.02	0.89
BCe	0.93	0.18	−0.02	−0.18	0.93	0.86	0.23	−0.10	0.8
Sif	0.91	−0.20	0.05	0.11	0.88	0.6	−0.40	0.54	0.82
Pf	0.57	−0.47	0.47	0.08	0.76	0.18	−0.27	0.68	0.57
Sf	0.92	0.24	−0.02	−0.21	0.95	0.93	−0.13	−0.05	0.89
Kf	0.93	0.15	0	−0.22	0.94	0.94	−0.10	−0.07	0.91
Caf	—	—	—	—	—	0.42	−0.38	0.57	0.64
Mnf	0.89	−0.21	−0.06	0.06	0.83	0.83	−0.39	0.13	0.85
Fef	0.94	−0.07	−0.00	−0.17	0.91	0.86	−0.37	−0.06	0.88
Cuf	−0.00	−0.24	0.86	−0.09	0.81	—	—	—	—
Znf	—	—	—	—	—	0.93	−0.06	−0.17	0.9

Table IV-5 (continued)

Var.[1]	Comp. 1	Comp. 2	Comp. 3	Comp. 4	Comm.	Comp. 1	Comp. 2	Comp. 3	Comm.
Sic	—	—	—	—	—	0.9	-0.13	-0.16	0.85
Pc	-0.41	0.84	0.01	0.21	0.92	-0.04	0.95	0.13	0.92
Sc	0.45	0.74	-0.07	0.03	0.76	0.62	0.762	-0.03	0.92
Clc	-0.37	0.29	-0.09	0.77	0.83	-0.02	0.75	0.52	0.83
Kc	0.01	0.84	-0.04	0.44	0.89	0.23	0.94	0.05	0.93
Cac	0.78	0.13	-0.08	0.53	0.92	0.62	0.26	0.48	0.68
Mnc	0.88	0.05	-0.07	0.19	0.82	0.92	-0.06	-0.19	0.88
Fec	0.94	0.19	-0.06	-0.16	0.95	0.94	-0.05	-0.27	0.86
Cuc	-0.23	0.51	0.72	-0.12	0.83	—	—	—	—
Znc	0.08	0.81	0.02	-0.12	0.68	0.54	0.76	-0.11	0.87
λ^2	9.2	4.5	1.6	1.2		9.9	5	1.8	
% variance	48.5	23.4	8.2	6.1		49.6	25.1	9.1	

[1] "Var." is the variable included in the model, with the subscripts "f" and "c" denoting the fine and coarse fraction, respectively. "Comp." is the extracted principal component, and "Comm." the communality associated with each variable in the model.

[2] λ is the eigenvalue associated with the principal component.

The four components were identified as follows. The first component was responsible for ca. 49% of the variance in the data. It is likely associated with biomass burning and contains elements of the fine fraction typically considered to be of biogenic origin and enriched in pyrogenic aerosols (S, K, and Zn), as well as BC_e from combustion (Artaxo et al., 1988; Maenhaut et al., 1996; Echalar et al., 1998). However, this component also correlated well with some soil dust-associated elements (the fine fraction elements Si, Mn, and Fe, and Ca, Mn, and Fe of the coarse fraction), which may have been due to uplift of significant quantities of dust during fires. It is worth noting also, however, that backward trajectory analyses carried out Section III.3.1 showed that the biomass burning sources were some 2–3 days away from the sampling sites during the wet season. The correlation between biomass burning and dust-associated elements may, therefore, also have been due to mixing of independently-emitted smoke and dust aerosol during long-range transport, essentially forming one indivisible component (Artaxo and Hansson, 1995). As noted earlier (Section IV.3.1.1), both biomass-burning aerosol and soil dust cannot originate from the Amazonian rain forest during the wet season, and the sources of these aerosols were most likely the dryer neighboring regions. This component, which was further associated with a mixed soil dust/biomass burning aerosol, also displayed high correlation with FPM, whereas all the other components showed low correlation of with this mass fraction.

The second component could be readily identified as coarse fraction biogenic aerosol (high P, S, K, Cu, and Zn loadings), and was responsible for ca. 23% of the variance in the data, and for most of the variance in the CPM values. This component is also slightly anti-correlated with fine fraction P, in the same manner that the first component is with coarse fraction P. The third and fourth components displayed very low correlation values with PM, and are therefore of minor importance for the aerosol mass burden. The third component showed high loadings with coarse and fine fraction Cu, and, to a lesser extent, fine fraction P, and is probably associated with biogenic material. The fourth component was mainly loaded with the elements Cl, K, and Ca of the coarse fraction. In order to facilitate the identification of this latter component, cluster analysis were also performed. Cluster analysis is a method that can be used to group variables

based on their distance in the elemental space, relying on different statistics than PCA. The cluster analysis was performed using Ward's method, and the results are presented Figure IV-8 in the form of a dendrogram. Clusters were identified when the distance between themselves was larger than 5. As for the PCA, three main clusters could be identified. Cluster 1 corresponds to component 1 of the PCA. It is again evident that pyrogenic aerosol and soil dust were mixed; Fe, in particular, could not be dissociated from the biomass-burning cluster. The second cluster is composed of fine fraction P and Cu, and corresponds to component 3 of the PCA, suggesting a natural source for fine biogenic particles, independent from biomass burning. Coarse fraction Cu is now grouped with the bulk of the coarse fraction biogenic material, which also includes coarse fraction Cl. This suggests that the latter element was probably of biogenic origin, and not associated with sea salt aerosol, as might have been assumed initially.
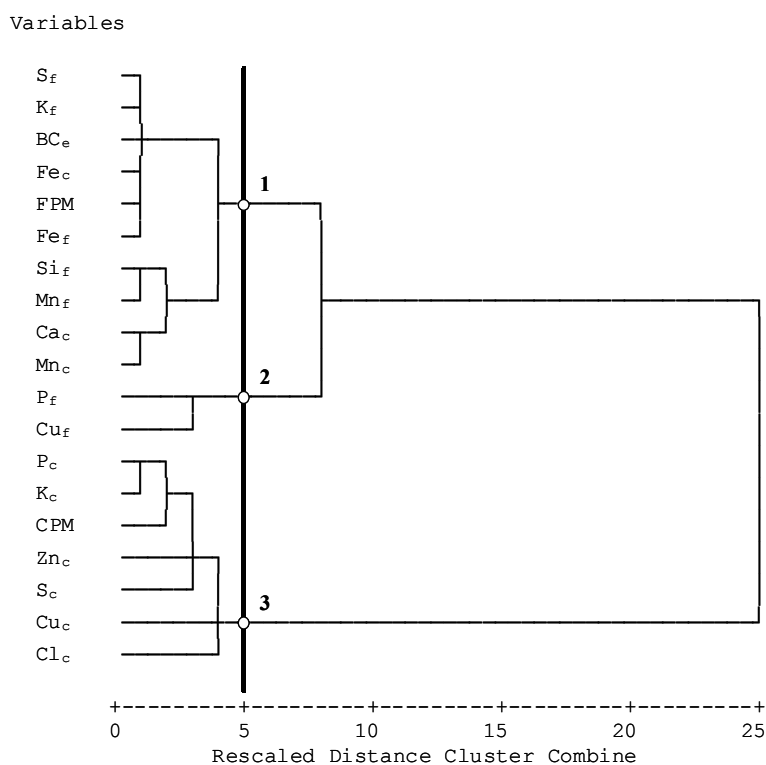
Figure IV-8 Dendogram representing the cluster analysis (from the standpoint of elemental composition) of the wet season aerosols measured near the top of the Jarú meteorological tower, Rondônia, Brazil (8 April–21 May 1999).
Cluster analysis was performed using Ward's linkage method, and the main clusters were identified when the distance between themselves was larger than 5 (black vertical line).

It is somewhat unfortunate that soil dust (present in the coarse and fine fraction) and biomass burning particles (most abundant in the fine fraction) formed one inseparable component, as it seemed reasonable to suspect that these two aerosol types were the most important in terms of light extinction, and one of the main focus of this study was to apportion the optical effects of the total aerosol between the various contributing sources (see below). Performing separate PCA/APCA analyses for the fine and coarse aerosol fractions could have apparently separated the two aerosol types. However, this separation would not have allowed us to perform further multivariate regressions of the sources on the aerosol optical properties because of the co-variability of these two components. Therefore, it was chosen to continue the analysis with fine and coarse fraction data merged together. Care should be taken when conducting APCA analysis with the coarse and fine aerosol fractions separated and regressing them on an "independent dataset" (e.g., absorption or scattering coefficients). Although more information (components) can be obtained when analyzing coarse and fine aerosol fractions separately, the apparent "better solution" may mask some co-variability in the data between the fractions, and lead to errors in the quantification of the sources identified by APCA for the independent dataset of interest.

The average mass source apportionment for the total aerosol, as estimated from the APCA results was obtained from multivariate regression of the measured PM on the absolute component scores. The r^2 value for the regression (28 samples) was 0.99. As expected from their low correlation with FPM and CPM in the PCA analysis, components 3 and 4 did not significantly correlate with PM, and each contributed to only ca. $4 \pm 4\%$ of the total PM for the wet season aerosols. Therefore, the wet season aerosols were mainly constituted of soil dust/biomass burning and biogenic material, which contributed to ca. 42 and 50% of the PM, respectively (Figure IV-9a). The main aerosol component during the wet season was therefore biogenic material (e.g., pollen grains, bacteria, spores, plant debris, etc.), confirming the results of previous studies in the region. Artaxo et al. (1990) already reported that only two components could explain ca 90% of the variance in their data for fine and coarse fraction Amazonian aerosols of the wet season at a forest site near Manaus. These two components were soil dust (in the present case mixed with some

biomass burning) and natural biogenic aerosols, the latter accounting for 55–95% of the PM.

In contrast to Artaxo et al.'s (1990) findings from Manaus, it was found that in Rondônia biomass burning may have contributed substantially to the PM, highlighting the dramatic influence that anthropogenic activities have on total aerosol loading in the Amazon basin, even during the wet season. Maenhaut et al. (2002) also found a biomass burning contribution to the wet season aerosols at the Amazonian site of Alta Floresta (16% of the FPM concentrations on average), whereas Echalar et al. (1998) did not identify a pyrogenic component for that season at the same site, and attributed 65% of the FPM concentrations to biogenic aerosols.

As a further step, an apportionment of the aerosol light absorption between the various sources identified above for the total aerosol loading is attempted by performing multivariate regression of absorption on the APCS, which is a technique based on a linear least square fitting. Light absorption data, which were obtained from a PSAP for the tower site, were available and integrated for 22 of the 28 samples. Multivariate regressions were also performed using the BC_e data obtained for 28 samples of the fine fraction. The r^2 of the regressions were 0.98 for both cases. It can be seen from the results, shown in Figure IV-9b for the regression using the BC_e data, that only the soil dust/biomass burning and the biogenic aerosol components contributed to the absorption. This was confirmed by the results obtained from the regression using the PSAP data, which differed from those presented in Figure IV-9b by 6% only, with the soil dust/biomass burning component contributing 72 % of the absorption, and the biogenic component the remaining 28%). As expected, the soil dust/biomass-burning component contributed more to the absorption than the biogenic component did (in opposite relation to their mass concentration), indicating a larger absorption efficiency for this component. However, biogenic aerosols were found to contribute significantly to the absorption (ca. 30%) during this season.

The apportionment of the identified sources to the scattering coefficients was performed for 13 samples. The results indicated that only the soil dust/biomass burning component contributed significantly to the scattering, confirming the results obtained in

Section IV.3.3 that particles of the coarse fraction did not scatter significantly during this season.
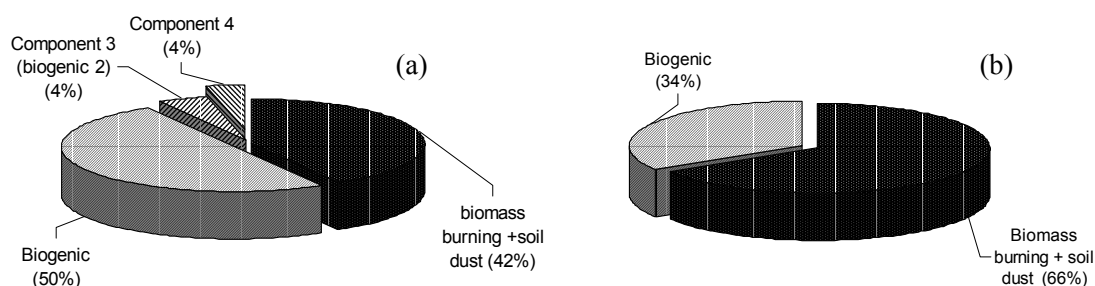
Figure IV-9 Jarú tower wet season source apportionment of the total aerosol mass and light absorption.
Relative source apportionment of the total aerosol mass (a) and the light absorption as measured using a reflectance photometer technique (BC_e) (b), for the wet season aerosol sampled near the top of the Jarú meteorological tower in Rondônia, Brazil, between 8 April and 21 May 1999.

The same analyses as presented above were performed on the results obtained from 76 samples collected at the pasture site (Artaxo et al., 2002), allowing better statistics than those presented for the forest site data. The two first components presented in Table IV-5 were associated with soil dust/biomass burning and coarse fraction natural biogenic particles, respectively, on the basis of what was discussed above. The third component was less straightforward to identify, and displayed high loadings with: 1) some fine fraction elements typical for biogenic material (P and Cl (the latter, when not attributed to sea-salt)), 2) fine fraction Ca and Mn (and coarse fraction Ca), which can be found in both plant material and soil dust (Artaxo et al., 1994), and 3) the element Si of the fine fraction, usually more typical for soil dust particles, but which can also be emitted from plants (Artaxo and Hansson, 1995). This component is therefore most likely associated with fine fraction biogenic particles, which may have mixed with soil-dust particles as has already been observed in this region (Artaxo et al., 1990; Artaxo and Hansson, 1995).

The APCA analysis of the pasture site data revealed that all three components contributed significantly to the PM. It can be seen from the results, shown in Figure

IV-10a, that, apart from the now significant fine biogenic/soil dust component, the main difference between these data and the RBJ ones is the dramatic decrease of the relative apportionment of the soil dust/biomass burning component. In absolute amounts, the two models applied to the forest and the pasture site data showed comparable amounts of the soil dust/biomass burning component, but a larger biogenic component was found for the pasture site. Although the data obtained at the pasture site encompassed more wet season period (only 6 of the 74 samples were taken during the period after 12 May 1999) than the RBJ data, which were more representative of the transition of the wet season toward the dry season (6 of the 28 samples were taken during the period after 12 May 1999), these results remain surprising because pasture site aerosols were more influenced by anthropogenic activity (Artaxo et al., 2002). This might be due to the low statistical significance of the wet season PCA/APCA results for the RBJ data.
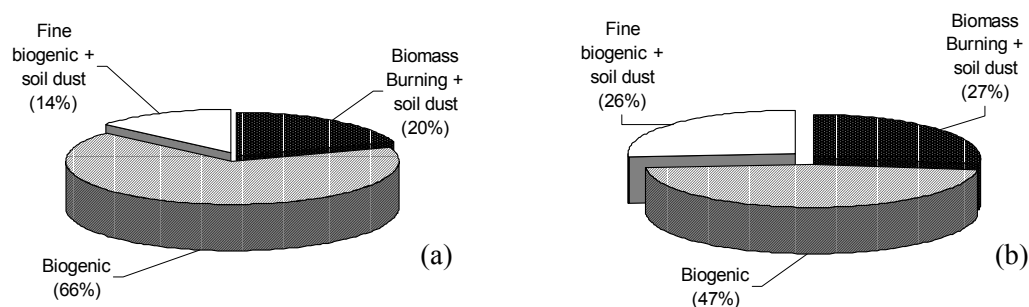
Figure IV-10 FNS pasture site wet season source apportionment of the total aerosol mass and light absorption.
Relative source apportionment of the total aerosol mass (a) and the light absorption as measured using a reflectance photometer technique (BC_e) (b), for the wet season aerosol sampled at the Fazenda Nossa Senhora Aparecida pasture site in Rondônia, Brazil, between 28 January and 22 May 1999.

The regression of the wet season fine mode BC_e on the APCS for the pasture site yielded relative contributions to the absorption of ca. 27, 47, and 26% for soil dust/biomass burning, biogenic, and fine biogenic/soil dust aerosols, respectively (Figure IV-10b). This is suggesting that all three kinds of aerosols contributed significantly to the absorption in the Amazon basin, and that their optical properties might be of importance in aerosol models. These results also show that natural biogenic particles contributed

considerably to absorption during the wet season. It is shown in CHAPTER V that, overall, the imaginary part of the refractive index of the Amazonian particles was low during the wet season in Rondônia, and it is likely that biogenic particles also contributed to absorption. However, the two other components contributed relatively more to the absorption relative to their mass concentration.

IV.3.4.2. Dry season, the sources of the LBA-EUSTACH 2 aerosols

Table IV-6 presents a summary of the PCA results obtained from analysis of compositional data relating to 81 Nuclepore filter samples collected near the top of tower during the dry season campaign (in this case, sufficient data was available for the forest site to yield statistically-robust results). The procedure was identical to the one applied to the wet season data, and fine and coarse aerosol data were combined together in order to facilitate further correlation of the identified sources with aerosol optical properties. The three components extracted from the PCA analysis (with eigenvalues larger than unity) explain ca. 80% of the total sample variance. The lowest of all computed communalities was associated with CPM, indicating that the model does not explain very well the variability of coarse aerosol for this season. When the model was implemented with a fourth component, which an associated eigenvalue of 0.75 only (explaining ca. 5% of the variance in the sample), the communality associated with CPM increased to 0.83. This fourth component was mainly associated with biogenic material (the highest loadings were for coarse fraction Mn, K, and P, and fine fraction Mn and Zn). However, close examination of the time series of the APCA computed-components (Figure IV-11) revealed that the fourth component was mainly due to only a few samples in the data set. In agreement with this, a communality of 0.78 was obtained for CPM when the samples numbered 34 and 64 (the two main ones responsible for the fourth component) were removed from the analysis and the APCA repeated with only the three initial components. Therefore, despite the low communality associated with CPM, it was decided to only include the three components with eigenvalues > 1 in the further analysis (as presented in Table IV-6).

Table IV-6 VARIMAX-rotated principal component analysis loading matrix for the aerosol (fine and coarse combined) collected at the Rondônian forest site during the 1999 dry season.

Var.	Dry season			
	Forest site, fine and coarse aerosol fractions			
	Comp. 1 Biomass burning + soil dust	Comp. 2 Biogenic	Comp. 3 Soil dust	Comm.
FPM	0.85	0.18	0.39	0.91
CPM	0.36	0.68	0.01	0.59
BC_e	0.84	0.15	0.39	0.88
Si_f	0.76	0.29	–0.12	0.68
P_f	0.78	0.45	0.03	0.81
S_f	0.81	–0.14	0.34	0.79
K_f	0.87	0.24	0.32	0.92
Mn_f	0.69	0.42	0.32	0.76
Fe_f	0.52	–0.05	0.64	0.75
Zn_f	0.73	0.42	0.36	0.84
P_c	0.15	0.91	0.04	0.85
S_c	0.21	0.63	0.50	0.69
K_c	0.06	0.84	0.48	0.94
Mn_c	0.27	0.50	0.64	0.73
Fe_c	0.20	0.23	0.89	0.88
λ	8.62	2.04	1.35	
% variance	57.5	13.6	9.0	
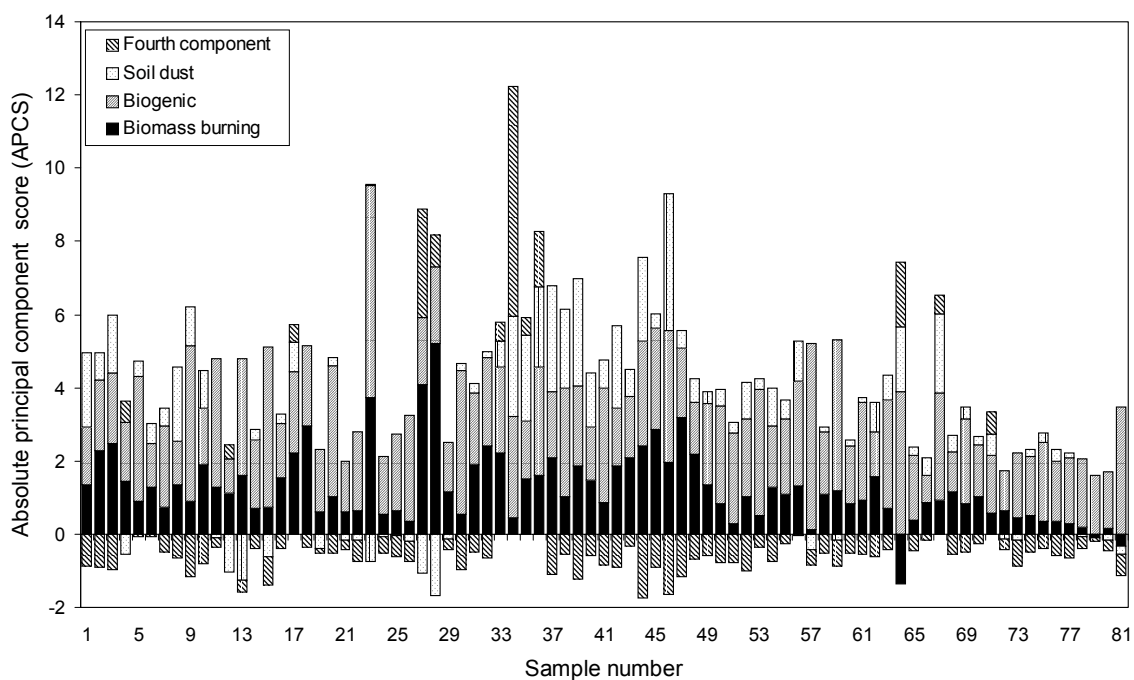
Figure IV-11 Time series of the sources for the LBA-EUSTACH 2 aerosols.
Absolute principal component scores (APCS), as obtained from a four-component APCA model, for each of the aerosol samples collected near the top of the Jarú meteorological tower in Rondônia, Brazil, between 6 September and 31 October 1999.

The three components were identified as follows. The first component, which explains ca. 58% of the variance, showed high loadings for FPM, typical biogenic elements (P, S, K, and Zn) and BC_e in the fine fraction, and to a lesser extent, fine fraction Si, Mn, and Fe. This suggests that this component was associated with biomass burning and some soil dust. It is interesting to note at this point that scanning electron microscopy of a fine aerosol sample from the dry season revealed that a large number of aerosol particles were soil dust/organic agglomerates (i.e., dust particles covered with an organic layer, which probably originated from biomass burning). The dust component of these particles exhibits characteristic sharp angular edges (Figure IV-12), while a "fluffier" component is thought to be composed of organic material derived from biomass burning. The second component was mainly loaded with CPM, and coarse fraction elements associated with biogenic aerosol (P, S, and K).

The third component showed high loadings for fine and coarse fraction Fe—usually considered as a good tracer for soil dust—and with coarse fraction Mn. Figure

111

IV-13 shows a scatter plot of coarse and fine fraction Fe against the other typical tracers elements for soil dust (Al, Si, and Ti) that were present in the samples more than 5% of the time below detection limit, and therefore not included in the PCA analysis. Aside from fine fraction Si (which was shown to correlate with biomass burning), Fe correlated well with all other soil dust markers, especially within—but also between—the fractions. This supports the contention that the third component was associated with soil dust. The fact that fine and coarse fraction soil elements were relatively well correlated indicates that the soil dust particles in both size fractions were probably derived from the same source. This was most likely biomass burning, as suggested by the correlation of the soil dust elements of the fine fraction with the biomass-burning component.
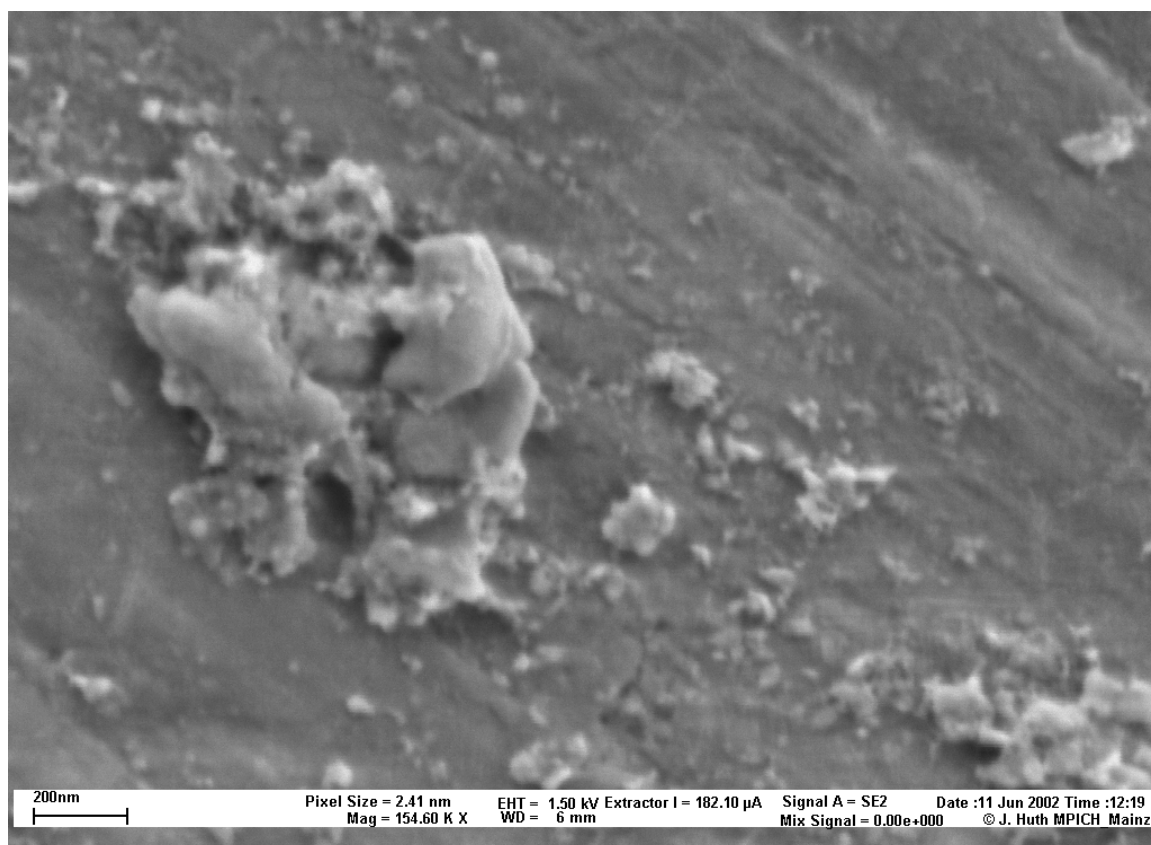
Figure IV-12 Typical scanning electron micrograph of an internally-mixed soil dust/biomass-burning fine aerosol particle from the dry season.
The particle was collected on 5 October 1999 on stage number seven (aerodynamic cutoff $D_{50} = 0.346$ μm) of a MOUDI impactor on an aluminum substrate (for a complete description of the instrument and the sampling procedure, refer to Section II.3.3). The picture was taken using a high-resolution field emission scanning electron microscope (FESEM 1530, Oxford Instruments) with a 1.50 kV electron beam, and a magnification of 154.6 K.
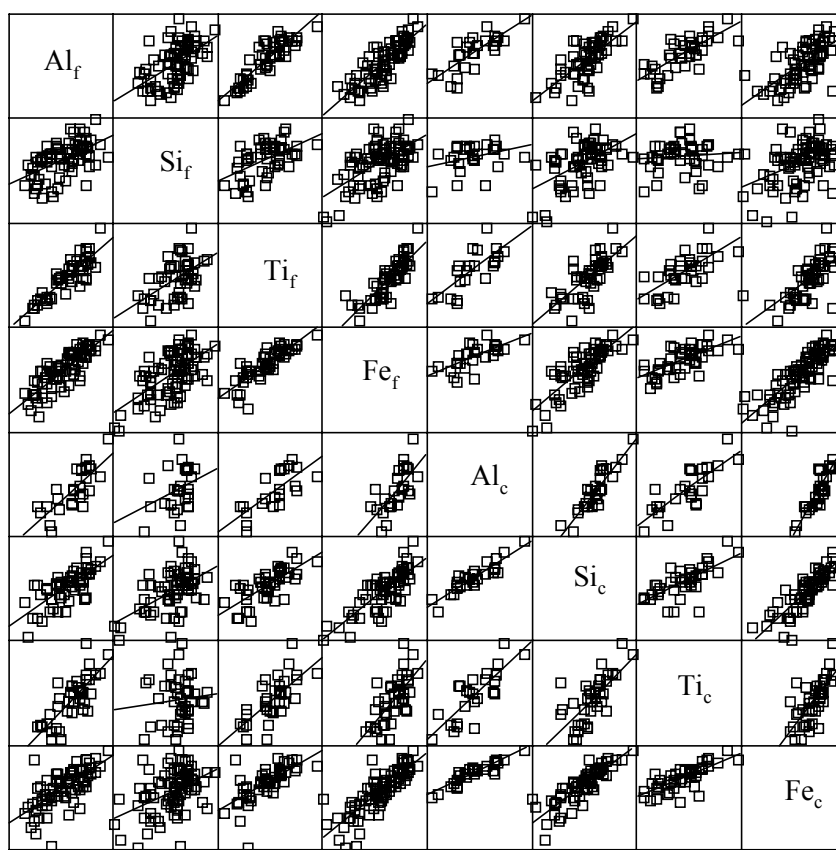
Figure IV-13 Inter-correlation of soil dust tracers for the LBA-EUSTACH 2 campaign.
Scatter plots (log-log coordinate scales) of the concentrations of Al, Si, Ti, and Fe in the fine (f) and coarse
(c) dry season aerosol sampled near the top of the Jarú meteorological tower in Rondônia, Brazil, between 6
September and 31 October 1999.

It is interesting to note in Figure IV-11 the decreasing influence of the biomass-
burning component toward the end of the campaign, which coincided with the transitional
period between the dry season and the impending wet season. In contrast, the biogenic
component remained relatively constant, indicating that it is part of the continuously-
emitted natural background aerosol.

Figure IV-14a presents the average source apportionment for the total dry season
aerosol sampled near the top of the Jarú tower, as estimated from the APCA results. As
expected, biomass burning was found to be the major contributor to aerosol mass (65%),
but biogenic organics and soil dust were also present in non-negligible amounts in the
samples, accounting for 30 and 5% of the total particulate mass, respectively. It could be

that the contribution of the soil dust component was underestimated in the present study, because parts of the soil dust elements of the fine fraction were included in the biomass-burning component. Artaxo et al. (1998) reported that biomass burning, natural biogenic, and soil dust components accounted for 54, 19, and 16%, respectively, of the total aerosol mass during the SCAR-B (Smoke, Clouds, and Radiation-Brazil) experiment, in Aug–Sep 1995. Additionally, they reported a second soil source and a sea-salt NaCl component, each making up to ca. 6% the total particulate mass. It is possible that the soil dust component that could not be differentiated from biomass burning in the analysis corresponds to one of the two soil dust components seen by the latter authors. It was not possible for us to identify a NaCl component, because Na was not measured in the present study, and Cl was not detectable frequently enough to be incorporated in the analysis. However, the RBJ measurement site was situated ca. 2000 km from the coast, and it is likely that NaCl was present in fairly negligible amounts in the samples.

The relative mass apportionment obtained for the biogenic and the pyrogenic components are each ca. 11% larger than the values reported by Artaxo et al. (1998). This may be partially explained by the fact that only ca. 80% of the variance in the data could be explained here, whereas Artaxo et al. (1998) could explain ca. 91% of theirs. Also, the latter authors sampled aboard an airplane, while the samplers used in this study were positioned much closer to the sources for biogenic aerosol, which is composed predominantly of coarse particles and might be expected to have a limited dispersal range.

It may appear astonishing that biogenic aerosol would make up such a high fraction of the aerosol mass during the dry season. Artaxo et al. (1998) already mentioned that the two main sources for biogenic particles are primary biogenic aerosol particles, and gas-to-particle conversion from biogenic volatile organic compounds (VOCs), but conclude that the nature and mechanism of emission of these particles is not fully understood. It has also been mentioned that biomass burning could have additionally contributed to the release of coarse fraction biogenic particles in the atmosphere.
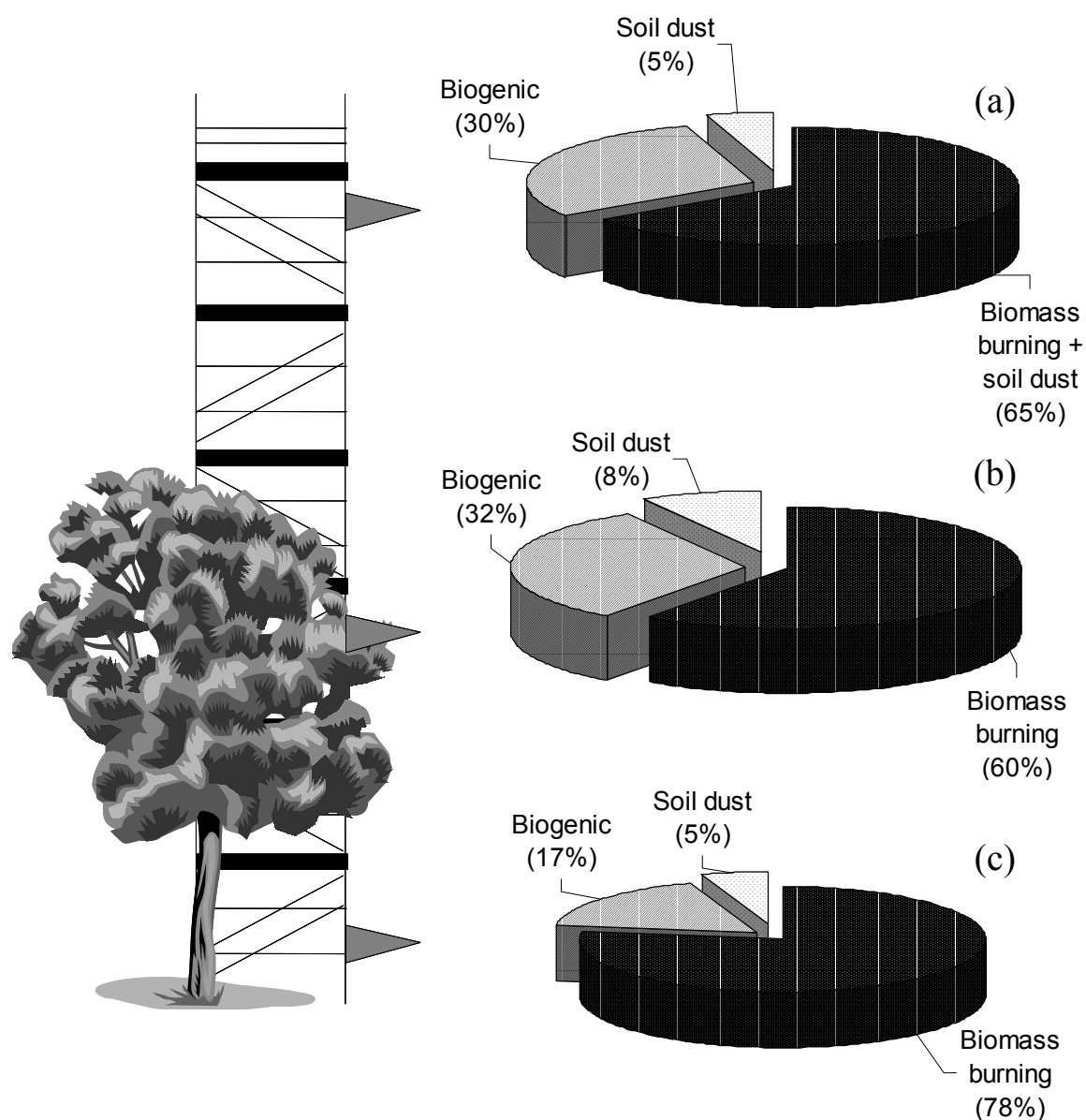
Figure IV-14 Jarú tower dry season mass source apportionment.
Total aerosol mass source apportionment for the dry season aerosol sampled near the top (a), at canopy level (b), and at ground level (c) on the Jarú meteorological tower in Rondônia, Brazil, between 6 September and 31 October 1999. The gray triangles on the side of the tower represent the sampling heights, whereas the tree represents the mean canopy height. The size of the pie charts is proportional to the mean mass concentration measured for each level.

The relative contribution of the sources identified above for the dry season aerosol to the light absorption measured with a PSAP and an aethalometer (both situated near the top of the tower), and to BC_e measured on the filter samples was calculated by multivariate regression of the integrated absorption values on the corresponding APCS. The regressions were performed for 49, 62, and 81 samples, yielding r^2 values of 0.95, 0.84, and 0.96 for the PSAP, aethalometer, and BC_e data, respectively. The results obtained using the BC_e data are shown in Figure IV-15a. The source apportionment of the absorption derived from the PSAP and the aethalometer instruments were very similar despite different sampling dates and number of data points. The biomass burning, the biogenic, and the soil dust components were found to contribute to 58, 31, and 11% of the absorption, respectively, using the PSAP data, and to 66, 27, and 7% of the absorption, respectively, using the aethalometer data. The contribution of the biomass burning/soil dust component is slightly greater according to the regression parameters obtained using the aethalometer data, which could be due to the fact that PSAP data were not available between 9–20 October (corresponding to filters 44–67), a period which included a number of intense biomass burning events (Figure IV-11).

Overall, the results indicate the major contribution of the biomass burning/soil dust component to the light absorption. Dust particles, which contributed up to 11% of the total absorption, are known absorbers (Andreae, 1996; Tegen et al., 1996); however, the surprising result to emerge from the analysis was the relatively large contribution of biogenic aerosols to absorption (ca. 30% according to the analysis performed using the PSAP and aethalometer data, and 17% when using the BC_e data), confirming the findings of the wet season data analysis. An explanation could be that this absorption is due primarily to large biogenic particles, since the source apportionment of BC_e, which was measured in the fine particle fraction only, indicated that a much larger fraction of the absorption in the fine aerosol (ca. 77%) was attributable to pyrogenic particles (neither the PSAP or aethalometer were equipped with an upper cut off diameter inlet, so the absorption measured by these instruments relates to the total aerosol).
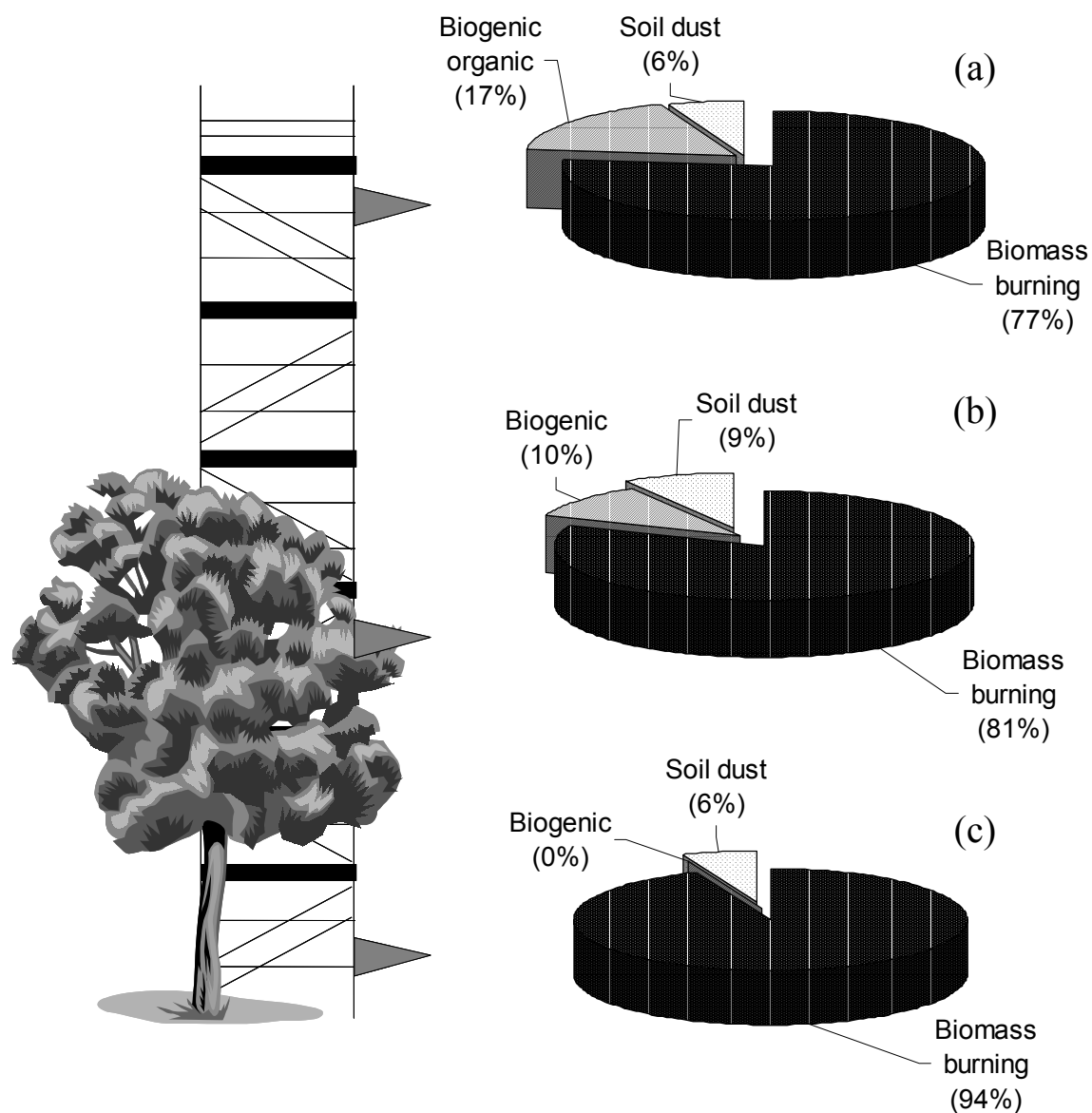
Figure IV-15 Jarú tower dry season light absorption source apportionment.
Relative source apportionment of the light absorption, as measured using a reflectance photometer
technique (BC_e), for the dry season aerosols sampled near the top (a), at canopy level (b), and at ground
level (c) on the Jarú meteorological tower in Rondônia, Brazil, between 6 September and 31 October 1999.
The gray triangles on the side of the tower represent the sampling heights, whereas the tree represents the
mean canopy height. The size of the pie charts is proportional to the mean BC_e concentration measured for
each level.

117

Figure IV-16 shows the relative source apportionment of the light scattering measured with a nephelometer near the top of the forest tower, obtained from the regression of the dry season APCS on the scattering coefficients averaged over the sampling time of the corresponding filter. The regression was calculated on the basis of 62 data points, and yielded an r^2 value of 0.89. The results suggest that biomass burning was the major aerosol source responsible for light scatter (ca. 80%), with soil dust and biogenic aerosol contributing roughly equally to the remaining 20%. It should be noted, however, that the regression analysis was not significant for the biogenic component (p value of 0.18), whereas it was highly significant for the other components, and the apportionment of this compound to scattering might be overestimated here. The results, therefore, indicate that biogenic aerosols contributed less to scattering than to absorption.
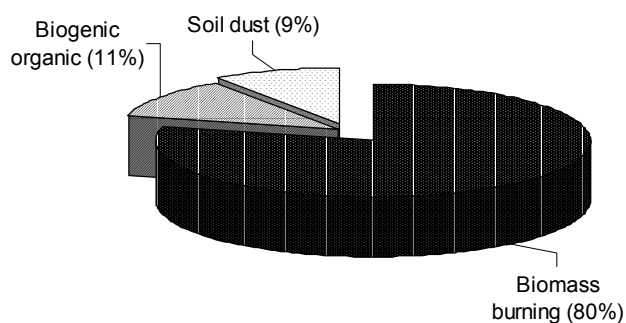
Figure IV-16 Jarú tower dry season light scattering source apportionment.
Relative source apportionment of the light scattering, as measured by a nephelometer, for the dry season aerosol sampled near the top of the Jarú meteorological tower in Rondônia, Brazil, between 6 September and 31 October 1999.

IV.3.4.3. Dry season, the tower profile

In the preceding sections only the APCA analyses of the above-canopy concentrations have been discussed when referring to the forest tower data. In order to further characterize the various aerosol sources, it would be also interesting to perform the analysis on the data obtained for the other sampling heights. Unfortunately, this was not possible for the wet season because too few data were available to obtain meaningful results. For the dry season, 80 and 81 samples were available for the within-canopy and below-canopy levels, respectively; however, even in this case the relatively large amount of "missing" data (due to elemental concentrations lying below detection limit) prevented us from obtaining statistically-robust models of aerosol variability at these levels. Nevertheless, a brief description of the APCA results for these latter data sets is presented here because canopy profile data for Amazon forest aerosols is rare in the literature. It must be cautioned, however, that the conclusions drawn from these results are tentative at this stage.

Three components were extracted from the PCA of the ground level data (Table IV-7), explaining ca. 88% of the data variance. The first component is loaded with the typical biogenic elements (P, S, and K) of the fine fraction, plus BC_e and FPM, and was assigned to pyrogenic aerosol. The second component contains the same elements in the coarse fraction, and CPM, representing biogenic material. The third component is only loaded with coarse fraction Fe, and represents soil dust. Whilst the eigenvalue for this component is only 0.6, it was retained in the model in order to facilitate comparison of the contribution of soil dust aerosol to the total aerosol loading at the three different sampling heights.

Three components were identified for the canopy level (Table IV-7), explaining ca. 86% of the data variance. The first component is loaded with FPM and fine fraction BC_e, S, and K, and can be associated with biomass burning (probably mixed with some soil dust, as indicated by the correlations with Mn and Fe). The second component is mainly loaded with coarse and fine fraction Mn and Fe, which are typically associated with soil dust, and with fine fraction P. Because this component contains both fine and coarse fraction soil dust, the soil dust was likely released into the atmosphere during

biomass burning, explaining the fine fraction P (presumably derived from combustion of biogenic material) that it is apparently mixed with. The third component is highly loaded with coarse fraction biogenic tracers (P, S, and K) and CPM, and is associated with natural biogenic particles. APCA for the canopy level data led to relative mass source apportionment values of 56, 15, and 29% for biomass burning, soil dust/biomass burning, and biogenic particles, respectively. As already noted above, biomass-burning aerosols were often mixed with dust particles during the dry season. However, in this case the presence of fine fraction P in the soil dust component enhanced the apparent contribution of this component to the canopy level, dry season aerosol, whilst decreasing that of the biomass-burning component.

For the ground and above-canopy sampling levels, the APCA had identified a "pure" soil dust component, which was not seen at canopy level. In order to better facilitate comparison of the composition of the aerosols between the various measurement heights, fine fraction P was therefore removed from the canopy-height data and the PCA and APCA were repeated. This procedure was further justified by the fact that this element showed the lowest communality in the analysis, and its variance was therefore the least explained by the model. Communalities and correlations for the new canopy-level model remained virtually unchanged compared to those presented Table IV-7. However, the percentage of variance explained by each component changed significantly, and the new model yielded values of 54, 24, and 10% for biomass burning, biogenic, and soil dust particles, respectively (corresponding to respective eigenvalues of 6.4, 2.9, and 1.1).

Table IV-7 VARIMAX-rotated principal component analysis loading matrix for the aerosol (fine and coarse combined) collected within the canopy and at ground level at the Rondônian forest site during the 1999 dry season.

	Dry season							
	Forest site, canopy level				Forest site, ground level			
Var.	Comp. 1 Biomass burning	Comp. 2 Soil dust	Comp. 3 Biogenic	Comm.	Comp. 1 Biomass burning	Comp. 2 Biogenic	Comp. 3 Soil dust	Comm.
FPM	0.87	0.40	0.16	0.94	0.92	0.04	0.29	0.92
CPM	−0.03	0.08	0.93	0.88	−0.03	0.91	−0.05	0.82
BC_e	0.90	0.43	0.16	0.95	0.93	0.03	0.27	0.95
P_f	0.43	0.72	0.15	0.72	0.81	0.15	−0.01	0.67
S_f	0.91	0.27	0.00	0.89	0.91	−0.13	0.16	0.86
K_f	0.84	0.44	0.20	0.94	0.94	0.07	0.15	0.92
Mn_f	0.40	0.76	0.25	0.79	—	—	—	—
Fe_f	0.28	0.82	−0.09	0.76	—	—	—	—
P_c	0.02	0.06	0.96	0.92	−0.03	0.94	−0.16	0.91
S_c	0.36	0.08	0.82	0.81	0.23	0.87	0.13	0.82
K_c	0.14	0.18	0.94	0.94	−0.02	0.96	−0.03	0.91
Mn_c	0.36	0.74	0.26	0.74	—	—	—	—
Fe_c	0.18	0.90	0.07	0.85	0.46	−0.10	0.86	0.96
λ	7.0	2.9	1.2		4.8	3.4	0.6	
% variance	54.2	22.4	9.1		47.5	34.3	5.7	

Figures IV-14b and 14c show the relative mass source apportionments, obtained from APCA, for the dry season aerosol sampled within the canopy and at ground level, respectively. Comparison of these apportionments with that described earlier for the above-canopy level (Figure IV-14a), suggests that biomass-burning particles were responsible for the bulk of the particulate mass at all measurement heights during the dry season. Overall, the relative composition of the sampled aerosol at the above-canopy and canopy levels were very similar; however, the below-canopy level aerosol featured a larger contribution of pyrogenic aerosol and a smaller contribution of biogenic aerosol. This indicates that the above-canopy and canopy levels were probably fairly well decoupled from the below-canopy level, as stated in Section IV.3.1.1, and that they were subject to different emission/sink processes. In order to help analyze the vertical profile of the three aerosol components identified by APCA, enrichment ratios (E_r) were calculated in a similar fashion to those presented in Sections 3.1.1 and 3.1.2, using the APCS values obtained for each filter sample. However, E_r values showed large variability for all three components, and no significant information could be retrieved from these gradients.

Figures IV-15b and 15c present the relative apportionment of the sources identified above to the fine fraction BC_e measured at canopy and ground levels, respectively. The relative contribution of biomass burning aerosol to the absorption was found to increase from above to below the canopy, indicating efficient downward mixing of the fine aerosol, whilst soil dust particles probably were deposited in the forest. The source apportionment for the light absorption measured at ground level with an aethalometer agreed to within 2% with the results obtained using the BC_e at this level, indicating that biomass-burning aerosol was responsible for 92-94% of absorption at this level, with soil dust accounting for the remaining minor fraction. At ground level, particles of biogenic origin did not contribute to absorption, whereas these particles accounted for ca. 10% of the absorption at the canopy level and 17% at the above-canopy level (ca. 30% when using the PSAP or aethalometer data). Due to the large amount of fine pyrogenic particles present in the atmosphere during this season, it is not surprising that the natural biogenic particles emitted at the ground level (see Section IV.3.1.1) did not contribute significantly to absorption, whereas particles such as fly ash (which may

not have been differentiated from the biogenic component in our analyses for the upper two levels) may well have.

IV.4. Summary and conclusion

The data set presented here indicates that there are large differences in aerosol concentrations and composition between the wet and the dry season in the Amazon basin, mainly due to a large atmospheric input of fine aerosol from biomass burning activities occurring in the dry season. Above the forest canopy, FPM increased by, on average, a factor of 15 from the wet to the dry season. Particles in this fraction were found to be fairly well-mixed throughout the canopy, indicating that biomass burning activities could be leading to a substantial redistribution of nutrients within the Amazon rainforest system. Coarse particle concentrations also increased, from the wet to the dry season, but to a much lower extent. Their concentrations roughly doubled above the canopy, but remained relatively unchanged at ground level. During the wet season, coarse particles of crustal origin were deposited from air masses advected over the forest, whilst coarse particles of biogenic origin were naturally emitted by the forest, showing highest concentrations at ground level and at night. The emission mechanism for the latter particles remains unknown, and one could only speculate about their origin. However, the observed phenomena could serve as a mechanism for redistributing nutrients within the Amazon forest and could, therefore, be of major importance for natural cycles in this ecosystem. This is particularly the case for P, which is known to be a limiting nutrient in the Amazon forest.

Overall, three aerosol types were found to make up the bulk of the total aerosol mass, namely biomass burning smoke, natural biogenic aerosol, and soil dust. Even in the wet season, the contribution of biomass burning smoke (largely aged) to the fine aerosol loading was found to be substantial. All three of the identified components were found to contribute significantly to the optical properties of the aerosol. This suggests that along with biomass burning emissions, biogenic and soil dust particles should be implemented into aerosol models for the Amazon region designed to account for their optical properties

and climatic impacts. The data also reveal that these components cannot be assumed to be completely independent from one another; biomass-burning aerosols, for example, were often found to be internally mixed with soil dust particles in single-particle analysis, and PCA analysis also suggested these particles to be (internally and/or externally) mixed.

The data confirmed that fine particulate matter contributes most significantly to aerosol optical properties; however, coarse particles also exhibited substantial absorption, even in the burning season. Their role in aerosol light extinction might be underestimated (when it is not completely neglected) in many current models of aerosol optical properties.

CHAPTER V.

REFRACTIVE INDEX OF AEROSOL PARTICLES OVER THE AMAZON TROPICAL FOREST

Abstract

Optical properties of aerosol particles were characterized over two intensive field campaigns at a remote primary rain forest site in Rondônia, Brazil, as part of the project European Studies on Trace Gases and Atmospheric Chemistry, a contribution to the Large-Scale Biosphere-Atmosphere Experiment in Amazonia (LBA-EUSTACH). The two field campaigns included measurements of background (wet season), biomass burning (dry season), and transition period conditions. Optical measurements of light scattering together with absorption and data on number/size distributions were used in a new iterative method, in order to retrieve the effective imaginary refractive index of the particles, at a wavelength of 545 nm. For ambient relative humidities lower than 80%, background aerosols exhibited an average refractive index of 1.42 − 0.006i. Biomass burning aerosols displayed a much larger imaginary part, with an average refractive index of 1.41 − 0.013i. Other climatically relevant parameters were derived from Mie calculations, yielding single-scattering albedos of 0.93 ± 0.03 and 0.90 ± 0.03 (at ambient humidity), asymmetry parameters of 0.63 ± 0.02 and 0.70 ± 0.03, and backscatter ratios of 0.12 ± 0.01 and 0.08 ± 0.01 for background and biomass burning aerosols, respectively.

V.1. Introduction

Optical particle counters (OPCs) are frequently used to determine the size distribution of aerosol particle populations (see, for example, Reid et al. (1998a), Collins et al. (2000), and Redemann et al. (2000) for recent publications). OPCs measure the magnitude of light scattering by individual aerosols and then use an internal calibration function to determine their size. The scattering coefficients of a population of aerosols can then be retrieved from the size distribution by performing Mie calculations. Comparisons of scattering coefficients calculated in this way with those measured directly using an integrating nephelometer have been reported previously (see, for example, Stolzenburg et al. (1998), Collins et al. (2000), and Liu and Daum (2000)).

OPCs are usually calibrated using latex particles, which have a refractive index of $m = 1.588 - 0i$. These particles are highly efficient at scattering radiation, as indicated by the large real component of the refractive index, and are completely nonabsorbing (no imaginary component). Ambient particles, by comparison, are usually less efficient scatterers of radiation but display some absorptive properties. Consequently, OPCs generally underestimate the true diameter of ambient aerosols, and the measured size distributions should be corrected for the refractive index of the sampled particles. In most instances, however, this is not a trivial task because it is very difficult to determine the refractive index of ambient aerosol particles that have complex chemical compositions; indeed, the refractive index remains one of the least well-characterized properties of such aerosols.

Aerosol models tend to predict more and more of the details of the aerosol microphysics (size distribution, chemical composition, and state of mixture), from which the aerosol optical properties need to be computed. Such a modeling approach requires new techniques to estimate an aerosol refractive index from observations, which can serve as a test for the models. Because it is not feasible to determine the refractive index of each individual particle within an aerosol population, an "average" or effective refractive index is normally used to represent the whole size distribution. This parameter is most often derived from the volume average of the chemical composition of the aerosols (e.g., Horvath (1998)). Such an approach makes the assumption that the particles are uniformly

internally mixed and, ideally, requires a complete knowledge of the aerosol particle composition (mass closure) (e.g., Pesava et al. (2001) and Ebert et al. (2002)), as well as the refractive indices and densities of all the individual compounds (or classes of compounds) present in the aerosol particles. In practice, however, typically only the two or three compound classes that contribute most significantly to the scattering and absorption of light by the aerosols are considered.

An alternative approach to determining the appropriate index of refraction to derive corrected size distribution data from the raw OPC data is to use an iterative process. On the simplest level, this involves varying the index of refraction until the scattering coefficients that one derives from the corresponding OPC size distributions (using Mie calculations) agree most closely with those measured directly with, for example, an integrating nephelometer. Liu and Daum (2000) estimated that not correcting the OPC (in their case a passive cavity aerosol spectrometer probe, PCASP) size distribution for the particle refractive index prior to calculating the light scattering coefficients, would lead to a nearly 60% error in the estimation of the total scattering coefficient. Usually, the contribution of absorption to the extinction of radiation by the aerosols has been ignored in such iterative calculations. This, however, may be an additional important factor to consider, because an absorbing aerosol will scatter light less effectively than an otherwise identical, nonabsorbing aerosol. The real (scattering) component of the refractive index obtained by only considering the scattering of radiation by aerosols will therefore be overestimated, and the diameters will be underestimated.

In this chapter, a new, more comprehensive approach to the correction of size distribution data measured by OPCs is presented, as well as the retrieval of effective refractive indices for aerosol populations. Additionally, values of the asymmetry parameter (g), the single-scattering albedo (ω_0), and the backscattered fraction (β) ratio were derived using further Mie calculations. The approach is similar to the iterative one described above, but takes into account both the scattering and absorption properties of aerosols, as determined through in situ measurements of the same air mass sampled by an OPC. In the present study, size distribution data collected with a PCASP were used in

combination with scattering and absorption coefficients measured using an integrating nephelometer and a particle soot absorbance photometer (PSAP), respectively.

The overall method is demonstrated using data collected over an undisturbed primary tropical forest in Rondônia, Brazil, during the LBA-EUSTACH campaigns (Andreae et al., 2002). The development of accurate methods for measuring aerosol parameters of climatic relevance is particularly pertinent to the study of aerosols in regions such as this for a variety of reasons (Boucher and Haywood, 2001). First, Brazil contains the world's largest rainforest, which provides a constant release of biogenic aerosols, formed either by direct emission (primary) or through gas-to-particle conversion of gases emitted by vegetation (secondary). In addition, each year a massive injection of smoke aerosols occurs during the dry season due to widespread biomass burning. The intense convective activity associated with the tropics means that these aerosols may be rapidly uplifted to high altitudes, where they can be transported over long distances and have effects on regional and global climate (Andreae et al., 2001).

V.2. Instrumentation and methods

Sampling conditions

Measurements were made near the top of a 54-m high measurement tower during two field campaigns that took place in April–May 1999 (LBA-EUSTACH 1) and September–October 1999 (LBA-EUSTACH 2). The tower was located at 10° 04'55" S, 61° 55'48" W, 110 m above sea level, in the Jarú Biological Reserve—a primary tropical forest situated in the Brazilian state of Rondônia. LBA-EUSTACH 1 encompassed the end of the wet season and the transition toward the biomass-burning-influenced dry season. LBA-EUSTACH 2 was largely dominated by biomass burning conditions. All instruments which data are used in this chapter were placed near the top of the measurement tower to ensure sampling of a regionally representative air mass.

Instrumentation

Number/size distributions were measured with a PCASP instrument, which derived particle size distribution from 0.1 to 3 μm in 18 channels from the light scattering properties of the particles at a wavelength of 633 nm. Aerosol mass/size distributions were obtained using a MOUDI cascade impactor. Scattering coefficients were measured using a single-wavelength Radiance Research integrating nephelometer at a wavelength of 545 nm. Continuous absorption measurements at a center wavelength of 565 nm were made using a Radiance Research PSAP.

Aerosol composition

To characterize the chemical composition of the aerosols, the concentrations of organic carbon (OC), apparent elemental carbon (EC_a), equivalent black carbon (BC_e), 8 ions (Na^+, NH_4^+, K^+, Mg^{2+}, Ca^{2+}, NO_3^-, SO_4^{2-}, Cl^-), and up to 17 elements (Al, Si, P, S, Cl, K, Ca, Ti, Cr, Mn, Fe, Cu, Zn, Br, Sr, Zr, and Pb) in the aerosols were measured on filter samples. One of the major purposes of this was to enable calculation of approximate refractive indices, which could then be compared with the values derived from the iterative approach using the data from the PCASP, PSAP, and nephelometer.

The concentrations of selected ions in the quartz filter samples were determined by ion chromatography. Cations were separated over a Dionex Ion Pak CS12 analytical column and Dionex Ion Pak CG12 guard column. A solution of 20 mM methanesulfonic acid was used as eluent. Anions were separated over a Dionex Ion Pak AS4A-SC analytical column and Dionex Ion Pak AG4A-SC guard column. The eluent was a solution of 1.8 mM Na_2CO_3 and 1.7 mM $NaHCO_3$. In both systems, a Dionex micromembrane suppressor was used and ions were detected by conductivity. For a detailed description of carbonaceous and elemental chemical analysis, see Section II.3.

V.3. Correction of PCASP-derived size distributions and calculation of refractive indices

V.3.1. Description of the model

The method proposed here for calculating the refractive index of atmospheric particles, and for correcting the size distribution data from the PCASP is based on an iterative process, outlined schematically in Figure V-1. A modified size distribution is calculated from the initial size distribution retrieved from the PCASP, using a variable refractive index, $m_{assumed}$. The program used to calculate the new size distribution is essentially the one distributed by the manufacturer, but modified to allow for a wider range and precision of refractive indices. Scattering and absorption coefficients are obtained by performing usual Mie calculations on the modified size distribution, using the same assumed refractive index, $m_{assumed}$, at a wavelength of 545 nm (the wavelength at which the nephelometer operates, and close to that used by the PSAP (565 nm)). The calculated scattering and absorption coefficients ($\sigma_{s,calc}$ and $\sigma_{a,calc}$, respectively) are then compared to the respective measured values (σ_s and σ_a, respectively), and the refractive index, $m_{assumed}$, adjusted until both $\sigma_{s,calc}$ and $\sigma_{a,calc}$ are within 1% of σ_s and σ_a, respectively (2% for the LBA-EUSTACH 1 data set because of the low measured σ_s and σ_a).

PCASP, PSAP, and nephelometer data were averaged hourly for both measurement campaigns, and the model applied to all data points for which data of the three instruments were available. Initially, the real component of the refractive index was allowed to vary between 1.33 (that of water) and 1.59 (that of latex) in incremental steps of 0.01, whilst the imaginary part could range from 0 to $0.05i$, with 0.005 incremental steps. Incremental steps were then set to 0.005 and 0.0025 for the real and the imaginary refractive index values, respectively, when $\sigma_{s,calc}$ and $\sigma_{a,calc}$ approached within 5% of the measured σ_s and σ_a values.
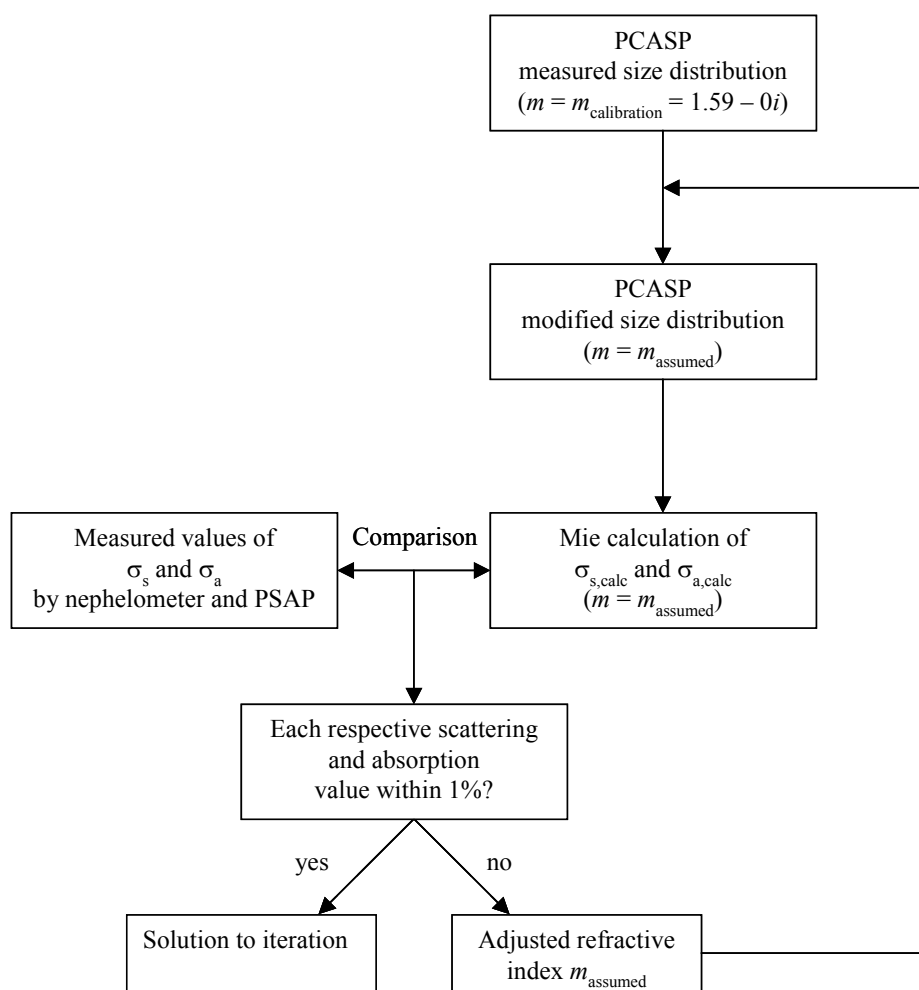
Figure V-1 Calculation of the aerosol refractive index; an iterative approach.
Flow chart of the iteration method used for retrieving the effective refractive index and corrected size distribution of atmospheric aerosols using size distribution (PCASP), absorption (PSAP), and nephelometer scattering data.

An example of a convergent solution obtained with the iteration procedure is given in Figure V-2, for a representative data set from the LBA-EUSTACH 2 campaign (similar convergent behavior was observed for data sets from the first campaign, except that a solution was generally found in fewer steps due to the typically smaller refractive index observed during the wet season). The iteration was initiated with both parts of the refractive index, $m_{assumed}$, set to the minimum values (i.e., the real part $n = 1.33$ and the imaginary part $k = 0$). The imaginary part was then increased until $\sigma_{a,calc}$ matched σ_a within ±5%. An increasing imaginary part has the effect of increasing the corrected

particle sizes, resulting in an increase in the corresponding $\sigma_{s,calc}$ value, along with $\sigma_{a,calc}$. When $\sigma_{a,calc}$ reached σ_a (at $m = 1.33 - 0.008i$ in this example), the calculated scattering coefficient, $\sigma_{s,calc}$, was always found to be greater than the observed one (represented by the dashed line), and the size of the particles was overestimated (due to the low real and high imaginary components of the refractive index). The real part of $m_{assumed}$ was subsequently increased, decreasing the corrected sizes of the particles, together with the values of $\sigma_{s,calc}$ and $\sigma_{a,calc}$. The value of the imaginary part had to be readjusted once more and $\sigma_{a,calc}$ was found to start to oscillate around the observed value (the dotted line), while $\sigma_{s,calc}$ converged towards its solution.
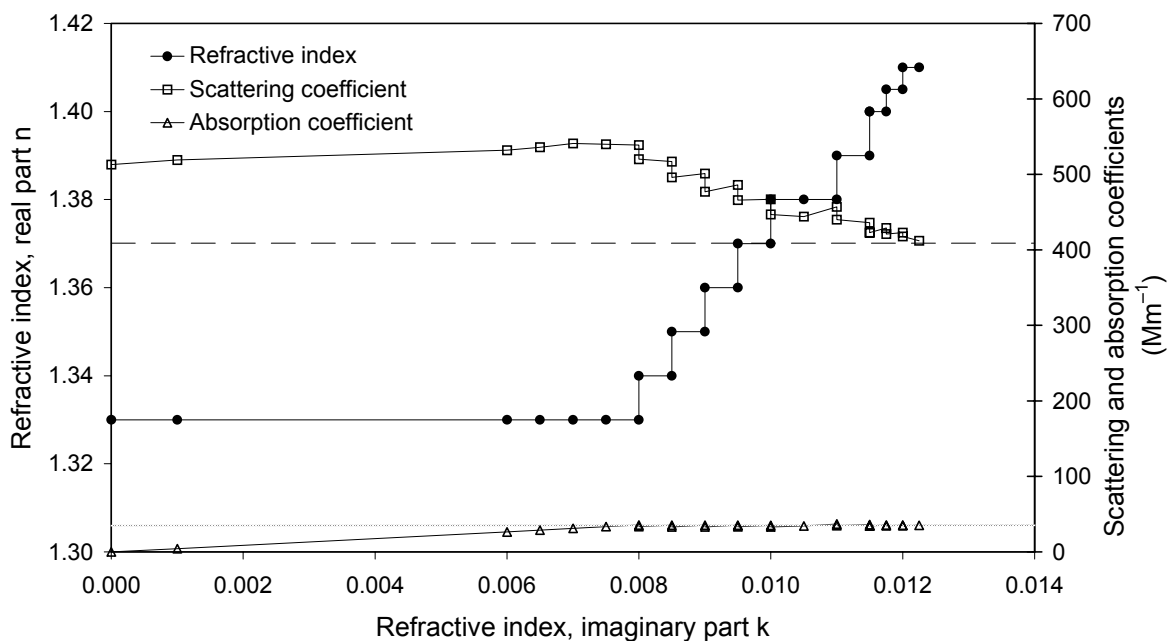
Figure V-2 Example of the iterative calculation procedure for a typical data set from the LBA-EUSTACH 2 campaign (6 October 1999, 1400 local time).
The graph shows the convergence of the calculated scattering (open squares) and absorption (open triangles) coefficients towards the measured scattering (dashed line) and absorption (dotted line) coefficients, together with the calculated complex refractive index, $m = n - ik$ (black dots).

The iterative calculations always converged toward a unique solution within the range of refractive indices open to the model, except in some unusual cases. These were all characterized by a high ambient RH, close to 100% or at least greater than 92%, which mostly occurred at night or in the early morning hours. Under these conditions, the inability to reconcile the data from the three online instruments using the iteration procedure is probably due to the nonlinear scattering responses of the nephelometer and PCASP at high RH. In light of this fact, only measurements made at ambient RH below 80% were considered in the subsequent analyses. Figures V-3a and 3b show the refractive indices calculated by the iteration procedure for all such data sets, for the LBA-EUSTACH 1 and 2 campaigns, respectively. The behavior of the refractive index with increasing RH will be discussed below.

V.3.2. Applicability of the model

A critical assumption made in the Mie calculations computed herein is that the aerosols are spherical in shape and homogeneously internally mixed. Although this represents an approximation of the true state of the sampled aerosols, it is believed to be a reasonable one, and one that does not lead to large errors in the refractive indices derived for Amazonian aerosols. The various reasons for this are discussed in some detail below.

The assumption of spherical homogeneity is most critical for aerosol particles in the accumulation mode (i.e., particles with diameters ranging from ca. 0.1 to 1 μm), since these are known to be the most efficient at scattering and absorbing light. Particles in the accumulation mode usually arise from the coagulation of smaller particles or from the condensation of low volatility vapors. They are also involved in cloud processing and are subject to water uptake and growth at high RH, forming spherical wet aerosols or solution droplets.
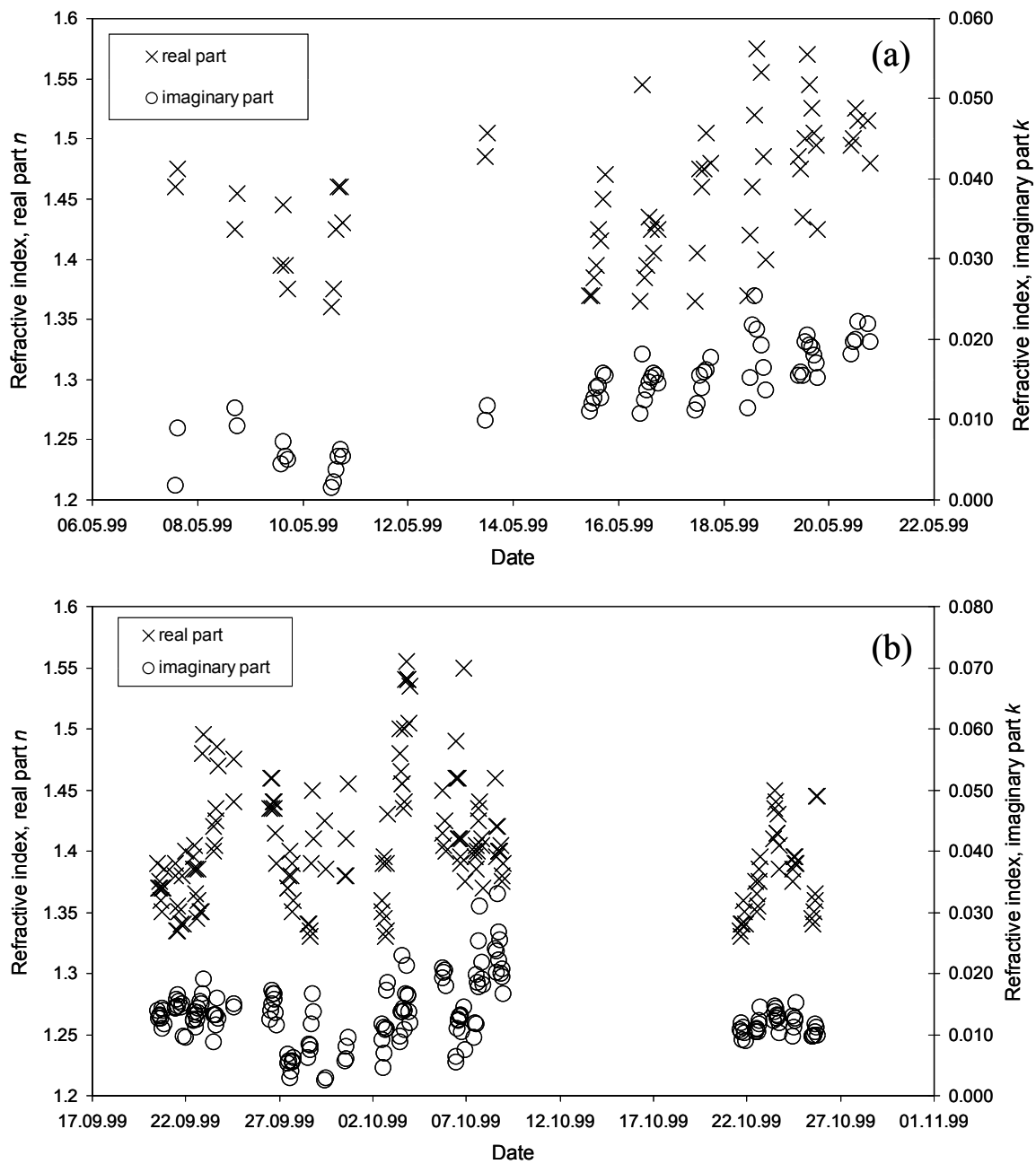
Figure V-3 Refractive indices calculated using the iteration procedure for the LBA-EUSTACH 1 (a) and LBA-EUSTACH 2 (b) campaigns.
Only data measured at a RH <80% are presented.

Although the water content of the aerosols was not measured during LBA-EUSTACH 1 and 2, it is probable that most of the sampled aerosols had been through at least one cycle of cloud or fog formation. In the Amazon, each volume of air cycles through a convective cloud about twice a day (Miller et al., 1985), and an air parcel is likely to be processed through 10 or more non-precipitating cloud cycles (Hoppel et al., 1990). Fog was often observed in the mornings during both seasons. Moreover, it is likely that the aerosols still had a significant water content upon collection, due to the consistently high humidity encountered during both seasons. During LBA-EUSTACH 1, the ambient relative humidity (RH) was greater than 64% for 95% of the time, and in the range 98–100% for 50% of the time. For LBA-EUSTACH 2, the RH was greater than 48% for 95% of the time, and 98–100% for 31% of the time.

All of the above observations lead us to the conclusion that the majority of particles in the accumulation mode had most likely deliquesced prior to sampling and still contained some water when sampled during the LBA-EUSTACH campaigns. Therefore, treating the accumulation mode as spherical, internally mixed particles in the Mie calculations is a reasonable approximation in the present case.

Particles in the Aitken mode (i.e., particles below ca. 0.1 μm in diameter), and particles in the mechanically generated coarse mode (diameter larger than ca. 1 μm) are more likely to be nonspherical. Particles in the Aitken mode do not usually contribute significantly to the optical properties of an aerosol population. Moreover, particles that are much smaller in size than the wavelength considered (545 nm) have a phase function comparable to those of spheres anyway. The presence of a large amount of coarse mode aerosol with non-spherical geometries may lead to some errors in the Mie approximation, but these are likely to be tolerable in most cases.

To assess this potential source of error, mass scattering efficiencies (α_s) and mass absorption efficiencies (α_a) were calculated for both the coarse (10 μm > D > 2 μm) and fine (D < 2 μm) mode aerosol fractions by multivariate regression, using the data obtained with the nephelometer, PSAP, and SFU filters (Section IV.3.3). The results indicate that coarse mode particles did not contribute significantly to the scattering during either field campaign. α_a for the coarse mode was found to be significant during LBA-EUSTACH 2,

but the fine particle mass was largely dominating the total aerosol mass. α_a was approximately a third that of the fine mode during LBA-EUSTACH 1, corresponding to a contribution by the coarse mode of 30–60% to the total absorption measured for this season. In the latter case, the scattering and absorption by the coarse mode particles correlated well with mineral dust elements (i.e., Al, Fe, Mn, and Si), a finding that is particularly noteworthy in light of the modeling studies of Mishchenko et al. (1997). They found that although aerosol shape may have dramatic effects on the scattering phase function (especially for the side and back scattering angles), other optical characteristics (the extinction, scattering and absorption cross sections, single-scattering albedo, asymmetry parameter, and the backscatter fraction) of spherical particles differ by only a few percent from those of modeled particles representative of mineral dust, with the difference decreasing with increasing particle size. Therefore, treating the coarse mode aerosol as spherical in nature is likely to have led to only small overall errors in the analyses.

Focusing on aerosols derived from biomass burning, Martins et al. (1998b) measured the degree of nonsphericity (α_o) of particles in Brazil during the Smoke, Clouds, and Radiation-Brazil (SCAR-B) experiment, using electro-optical light-scattering measurements and scanning electron microscopy. They concluded that smoke particles more than 1 hour old have a value of α_o lower than 13% in all cases, and lower than 4% in 72% of cases, indicating that smoke particles are, for the most part, close to spherical in shape. These results are in agreement with previous measurements of the shape of forest fire smoke aerosols from electron micrographs, which revealed an increasing sphericity in shape with age (Hallett et al., 1989; Westphal and Toon, 1991). Thus, for these particles there is additional strong experimental evidence that Mie calculations can be applied without the introduction of significant errors.

An additional potential source of error in the analyses arises from the fact that the size distribution measured by the PCASP instrument has a lower cutoff diameter at 0.1 μm, so that the tail of the accumulation mode and the whole Aitken mode are not measured, whereas the nephelometer and the PSAP measure the aerosol properties over the whole aerosol population. However, as discussed previously, the contribution of the

Aitken mode to the overall optical properties of the aerosols relative to the accumulation mode is negligible. Hegg et al. (1996) suggested that the truncation in the PCASP retrieved distribution might be responsible for the low scattering coefficients calculated from this size distribution (using Mie calculations), as compared to the measured scattering coefficients. Liu and Daum (2000) estimated the magnitude of this effect and concluded that, in their case, the relative contribution of particles with diameters of 0.05–0.1 μm to the total light scattering coefficient calculated from the truncated size distribution (with the lower cutoff diameter at 0.1 μm) was of the order of only ca. 2%. There is no reason to suspect that the contribution of particles smaller than 0.1 μm to scattering and absorption might be more significant in the present case, and data were restricted solely to consideration of the size distribution as measured by the PCASP instrument.

V.3.3. Sensitivity of the model

In order to estimate the accuracy of the values of the refractive index calculated from the iteration procedure, the different parameters used in the iteration were individually varied by an amount equal to the error estimates for the nephelometer, PSAP, and PCASP instruments (given in Section II.2), whilst the other parameters were kept equal to their original values. These sensitivity tests were applied to ten cases representative of both field campaigns. Figures V-4a and 4b show the sensitivity of the real part of the refractive index to changes in the individual parameters used in the model calculations for the LBA-EUSTACH 1 and 2 campaigns, respectively; Figures V-4c and 4d show the corresponding sensitivity of the imaginary part of the refractive index. Table V-1 presents a summary of the regression of the refractive index obtained by alteration of the individual parameters against the refractive index calculated from the original data. It can be seen that varying the parameters leads to slope factors of 0.78–1.28 and 0.90–1.10 for n and k, respectively. It is noteworthy, however, that the slope is, in all cases, somewhat compensated for by the corresponding shift (intercept) in the regression, so that the overall effect is generally below a few percent in the refractive index range considered here (n = 1.33 to 1.59, k = 0 to 0.025). The precision is typically better than 5% for n and

10% for k for the largest values of n and k within the range of observed refractive indices (the precision decreases with increasing n and k values). This indicates that, given the accuracies of the measurements in the present study, this new procedure is quite a robust method for estimating refractive indices.

Figures V-4a–d and Table V-1 clearly show that the real part of the calculated refractive index is more sensitive to variation of the particle number measured by the PCASP than the imaginary part of the refractive index. An underestimation of the scattering coefficient leads to a greater value of n (smaller particles, but relatively more scattering) and a greater value of k (larger particles, relatively more absorbing), compensating for the effects of an increase in n. It is interesting to note, however, that scattering has a small influence on k overall. In contrast to this, changes in the absorption coefficients impact predominantly on k. The Bond correction of the PSAP data had negligible effects on n, but decreased k by on average 26 and 30 % for the LBA-EUSTACH 1 and 2 campaigns, respectively. When absorption is set to zero, the iteration results in only a slight underestimation of n (less than 4%).
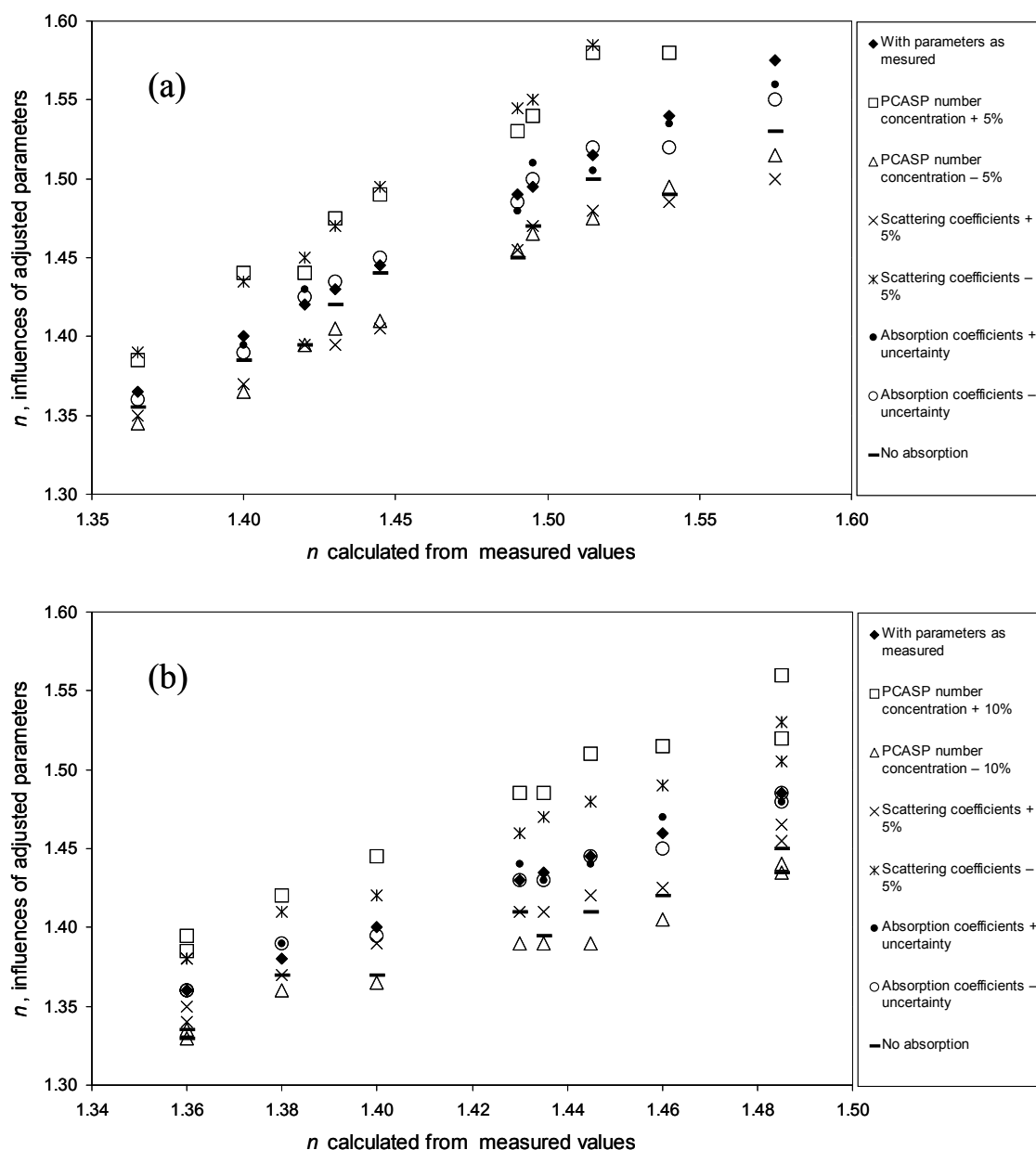
Figure V-4 Sensitivity test for the real part of the refractive index.
Sensitivity of the real part of the refractive index to changes in the individual parameters used in the iteration calculations for the LBA-EUSTACH 1 (a) and the LBA-EUSTACH 2 (b) campaigns. This sensitivity test was applied to ten representative data sets from the LBA-EUSTACH 1 and 2 campaigns, respectively.
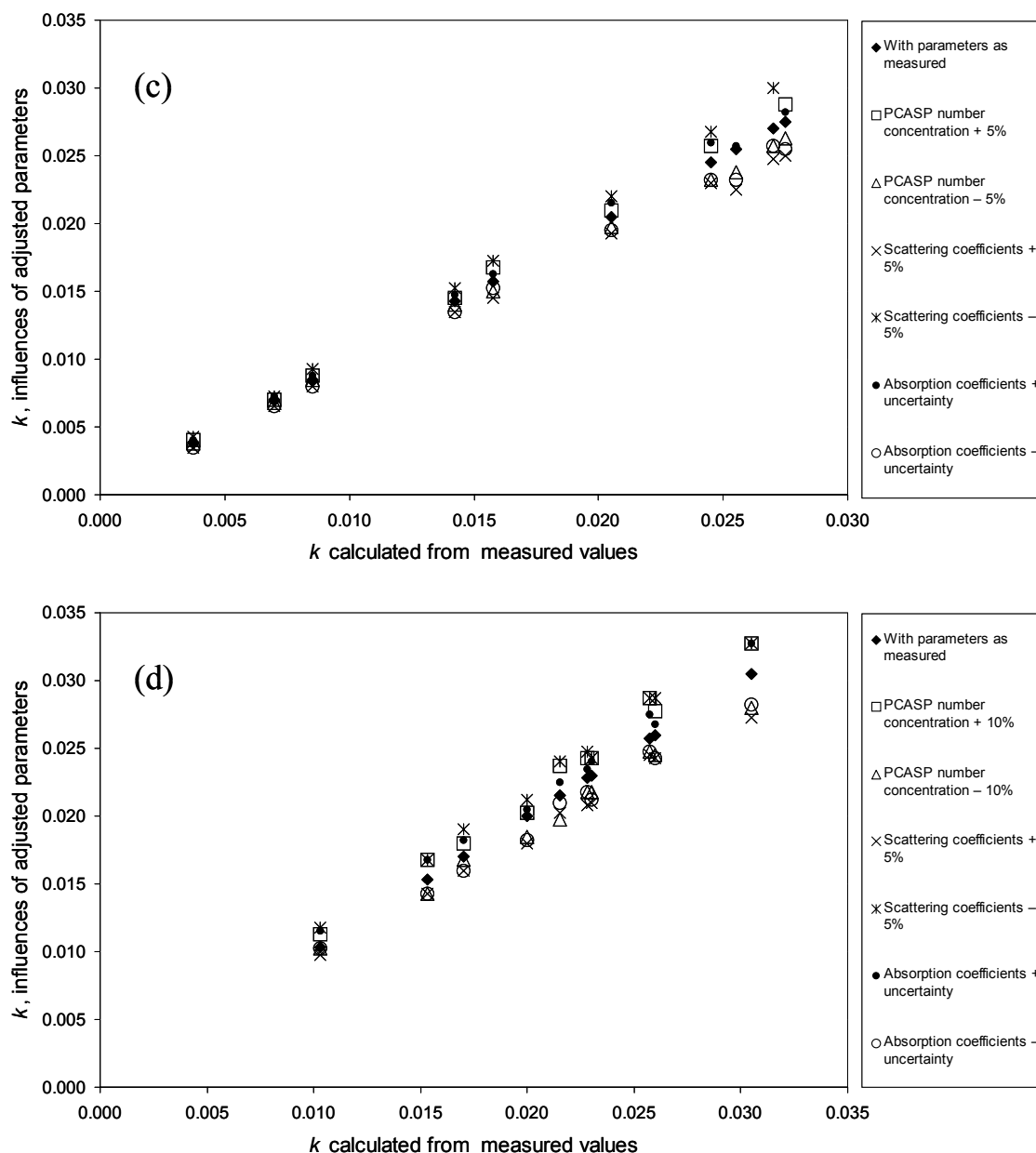
Figure V-4 (continued) Sensitivity test for the imaginary part of the refractive index.
Sensitivity of the real part of the refractive index to changes in the individual parameters used in the iteration calculations for the LBA-EUSTACH 1 (a) and the LBA-EUSTACH 2 (b) campaigns. This sensitivity test was applied to ten representative data sets from the LBA-EUSTACH 1 and 2 campaigns, respectively.

Table V-1 Summary of the regression parameters of the refractive index obtained by the alteration of individual parameters against the refractive index calculated from the original data.
The regression data is derived from ten cases representative of the range of refractive indices observed for each campaign.

Varied parameter	LBA-EUSTACH 1				LBA-EUSTACH 2			
	Refractive index Real part n		Refractive index Imaginary part k		Refractive index Real part n		Refractive index Imaginary part k	
	Fitting equation	r^2	Fitting equation	r^2	Fitting equation	r^2	Fitting equation	r^2
PCASP number concentration + 10%					$y = 1.21x - 0.25$	0.96	$y = 1.08x - 9E{-}05$	0.99
PCASP number concentration − 10%					$y = 0.78x + 0.27$	0.97	$y = 0.90x + 8E{-}04$	0.99
PCASP number concentration + 5%	$y = 1.15x - 0.18$	0.98	$y = 1.05x - 1E{-}04$	1	$y = 1.11x - 0.13$	0.97	$y = 1.03x + 2E{-}04$	0.99
PCASP number concentration − 5%	$y = 0.85x + 0.18$	0.99	$y = 0.94x + 4E{-}04$	1	$y = 0.87x + 0.16$	0.99	$y = 0.94x + 7E{-}04$	1
Scattering coefficients + 5%	$y = 0.79x + 0.27$	0.97	$y = 0.90x + 3E{-}04$	1	$y = 0.87x + 0.17$	0.98	$y = 0.90x + 6E{-}04$	0.99
Scattering coefficients − 5%	$y = 1.28x - 0.36$	0.99	$y = 1.10x - 1E{-}04$	1	$y = 1.10x - 0.11$	0.98	$y = 1.06x + 6E{-}04$	0.99
Absorption coefficients + uncertainty	$y = 0.94x + 0.09$	0.98	$y = 1.02x + 1E{-}04$	1	$y = 0.98x + 0.04$	0.98	$y = 1.03x + 6E{-}04$	0.99
Absorption coefficients − uncertainty	$y = 0.92x + 0.12$	0.97	$y = 0.94x + 1E{-}04$	1	$y = 0.95x + 0.07$	0.99	$y = 0.92x + 6E{-}04$	0.99
No absorption	$y = 0.82x + 0.24$	0.96			$y = 0.84x + 0.20$	0.96		

V.4. Results and discussion

V.4.1. Effective refractive indices derived from the iteration procedure

The refractive indices calculated for LBA-EUSTACH 1 and 2 using the iteration procedure, for ambient RH lower than 80%, are shown in Figures V-3a and 3b, respectively. In the first instance, a single effective refractive index was calculated to represent the whole size distribution measured by the PCASP. Despite the fact that the coarse mode particles (diameter greater than ca. 1 μm) are usually expected to have a refractive index with a lower imaginary part than that of the fine mode particles, this approach is justified by the fact that particles of both modes showed similar absorption properties (Section V.3.2), leading to little influence on the effective refractive index of the aerosol population. This assumption is discussed later in more detail for both wet and dry season data.

A noticeable feature of the LBA-EUSTACH 1 data is the large increase in the imaginary part, and to a lesser extent in the real part, of the refractive index upon entering the transition period toward the burning season. Values of the refractive index for the first part of the LBA-EUSTACH 1 campaign (7–12 May 1999) are centered on $m = 1.42(\pm 0.04) - 0.006(\pm 0.003)i$, reaching $1.46(\pm 0.06) - 0.016(\pm 0.006)i$ at the end of the campaign (13–21 May 1999), a value comparable to that obtained for the biomass burning period (LBA-EUSTACH 2). The observed increase for the imaginary part of the refractive index can be attributed to an increase in the black carbon content of the aerosol, associated with a general buildup in fire activity in Brazil. This increase in fire activity toward the end of the LBA-EUSTACH 1 campaign is clearly evident from fire pixel data measured by the NOAA-12 satellite (available from CPTEC at http://www.cptec.inpe.br/products/queimadas/queimap.html).

It is noteworthy that there were no fire pixels detected in the state of Rondônia, where the measurements took place during LBA-EUSTACH 1. However, back trajectories calculated for this period showed air masses coming from the neighboring states of Mato Grosso, Mato Grosso do Sul, and Goias, which contributed to most of the fire activity in the region. These biomass-burning-influenced air masses required some 2–3 days to reach the sampling site, providing sufficient time for the aerosols to be involved

in cloud processing, and thus justifying the treatment of the aerosols as internally mixed particles in the model calculations for this period (Horvath, 1998). On the basis of these observations, the refractive index calculated for the first part of LBA-EUSTACH 1 is considered as representative of background Amazonian aerosol, and that found for the end of this campaign as typical of aged biomass-burning aerosol.

A daily variation in refractive index was observed that is most likely attributable to changes in ambient RH, although no significant correlation could be established, probably because of the variability of the aerosol sources and composition with time. Overall, the refractive index decreased with increasing RH. At high ambient RH, the real part of the refractive index approached that of water (1.33); however, the imaginary part showed less variation, usually not reaching zero.

The refractive indices obtained for the second campaign (Figure V-3b) showed a larger range of scatter (as did the other aerosol measurements), partly attributable to the variation in RH, but mainly because of the passage of smoke plumes over the measurement site, arising from variable burning activities in closer proximity to the site than during LBA-EUSTACH 1. The refractive indices found for this campaign are most representative of aerosols belonging to haze and younger smoke plumes. It is difficult, in the present case, to distinguish between haze and younger plumes because it was not possible to sample very young plumes in the immediate vicinity of a fire. The closest fires observed were at least one kilometer from the measurement site, but they were not necessarily sampled, depending on wind direction. Therefore, when young plumes passed over the site, they were usually already mixed with the very hazy background air. This is also supported by the fire pixel data from the NOAA-12 satellite during the LBA-EUSTACH 2 campaign, which testifies to the dramatic increase in fire activity in the transition from the wet to the dry season. Rondônia ranks among the top three states contributing to fire activity in Brazil, and it is here where biomass burning activity is most concentrated.

V.4.2. Comparison with refractive indices estimated from the volume-averaged chemical composition

The refractive indices obtained from the iteration model were compared with volume-average estimates calculated from the chemical composition of the aerosols (e.g., Horvath (1998) for three periods of interest. The three periods were designated as follows: (1) LBA-EUSTACH 1, before the transition period (representative of background, wet season conditions), (2) LBA-EUSTACH 1, during the transition period toward the biomass-burning-influenced, dry season period, and (3) LBA-EUSTACH 2, largely dominated by biomass burning conditions.

Aerosol composition was established as described in the methods section. In order to calculate the approximate amount of particulate organic matter (POM) present in the aerosols of diameter smaller than ca. 2–2.5 μm, it was assumed that all elements were present in the aerosol in the state of their most common oxide (Mason and Moore, 1982), and the sum of oxides, ions, and elemental carbon was subtracted from the total mass of aerosol in the fine mode filter samples. From this, an estimate of the OC to POM mass conversion factor was obtained, which is defined as the ratio of estimated POM mass to measured OC mass. These POM/OC ratios are useful in order to estimate the validity of the mass closure calculated here. Results yielded ratios of 1.57 ± 0.30 and 2.13 ± 0.55 for the beginning and end of the LBA-EUSTACH 1 campaign, respectively. For LBA-EUSTACH 2, a ratio of 1.86 ± 0.3 was obtained. The large error assigned to the ratio was mainly attributable to the precision in determining the aerosol mass concentration, the variations in relative concentrations obtained in measuring ambient particles, and to the discrepancy (up to about a factor two) which was observed in the measurement of SO_4^{2-} obtained by the IC and PIXE techniques, with the largest values obtained by IC. This discrepancy is most likely a consequence of the different filter substrates used. While PIXE was performed on Nuclepore filters, the IC analysis was performed on quartz filters, which are known to adsorb compounds like H_2SO_4, HCl, and HNO_3 (Savoie et al., 1987) from the gas phase. It should also be noted that the SFU and HVDS samplers used in the current study have slightly different cutoff diameters for the fine fraction (ca. 2.0 μm and 2.5 μm, respectively), which could also partially explain the differences between the IC

and PIXE results. Furthermore, the quartz filters in the HVDS may also have adsorbed volatile organic compounds (Turpin *et al.*, 2000), so that the OC data are an overestimate of the true particulate OC. Therefore, the POM/OC ratios obtained herein should only be considered as estimates, with the large errors highlighting the difficulties associated with estimating POM concentrations in aerosols and, consequently, the refractive index of the particles from a mass closure approach. It is worth noting, nevertheless, that the mass conversion factors obtained in this study compare fairly well with the values recently reported by Turpin and Lim (2001). These authors argue that the values of 1.2–1.4 commonly assumed for the POM/OC ratio are too low, and have provided updated estimates of about 1.6 ± 0.2 for urban aerosols, 2.1 ± 0.2 for aged nonurban aerosols, and 2.4 ± 0.2 for biomass burning aerosols.

Although a considerable amount of elemental information was available from the PIXE analyses, it was decided to calculate volume-averages involving four classes of compounds only. The four classes of compounds were black carbon (either BC_e or EC_a), hematite (present in non-negligible amounts, especially during LBA-EUSTACH 1), POM, and inorganic nonabsorbing matter (INAM). The latter is defined as the sum of the masses of the inorganic species as defined previously (with the exception of hematite).

Calculations of the volume average of the refractive index were performed using the density and refractive index of each class of compound as prescribed by Horvath (1998) (except when indicated otherwise). According to the literature, the refractive index of soot, at wavelengths close to 550 nm, can vary from 1.3 to 2.5 for the real part and from 0.1 to 1 for the imaginary part (Fuller et al., 1999; Marley et al., 2001). Its density ranges from 625 to 2250 kg m^{-3}, depending on the type of soot considered (Fuller et al., 1999). It was chosen to use the commonly accepted refractive index value of $1.50 - 0.47i$, and a density of 1200 kg m^{-3}. The refractive indices and specific densities of POM and INAM are also subject to much uncertainty. It was decided to use respective values of $1.40 - 0i$ and 1200 kg m^{-3} for POM (Turpin and Lim, 2001) and $1.50 - 0i$ and 1800 kg m^{-3} for the inorganic nonabsorbing matter. For hematite, a refractive index of $3.0 - 0.60i$ and a density of 4500 kg m^{-3} were used, following the work of Sokolik and Toon (1999).

Tables V-2a and 2b summarize the volume average of POM, inorganic matter, hematite, and black carbon from the mass closure described above, as well as the corresponding calculated range of refractive indices, separated into real (n) and imaginary (k) parts, for the three periods described above. For reasons outlined earlier, the refractive indices were calculated using the sulfate concentrations derived from the PIXE measurements. The calculations were performed using either the EC_a content measured on the quartz filters (Table V-2a) or BC_e determined from the Nuclepore filters (Table V-2b). BC_e already takes into account the contribution of hematite to absorption, and this compound was therefore not included in the calculations of Table V-2b. The last two columns of each table show the averaged real and imaginary parts as obtained from the iteration procedure for each period.

Considering first the real parts of the refractive indices, the values obtained from the iteration model are in the range of the volume-average estimates. It should be noted, however, that the latter values do not take into account the water content of the aerosols, whereas values from the iteration procedure were derived from ambient condition measurements (as discussed in Section V.3). Accounting for water (with a refractive index m_{water} of $1.33 - 0i$) in the volume-average calculations is expected to lower these calculated values.

The values of the imaginary part of the refractive indices obtained by the iteration procedure compare well with the volume-average values calculated using the EC_a values of the LBA-EUSTACH 1 campaign; however, it was not possible to reconcile the model results for LBA-EUSTACH 2 with the low average percentage values of EC_a measured for this campaign. The filter samples from LBA-EUSTACH 2 were heavily loaded, and, as noted above, the thermal optical transmission technique may provide too low EC_a/OC ratios for such samples (Kubátová et al., 1999). Indeed, as LBA-EUSTACH 2 was characterized by intensive biomass burning, the percentage of EC_a in the fine aerosol sample is expected to be at least as high as during the other two periods. Alternatively, or additionally, the inability to reconcile the refractive index estimates could also be due to the fact that other absorbing material besides EC_a is produced during the biomass burning process, including polyaromatic hydrocarbons (Finlayson-Pitts and Pitts, 2000) and

polymeric organic compounds (Mukai and Ambe, 1986; Zappoli et al., 1999; Mayol-Bracero et al., 2002). However, as the OC quantity obtained by the TOT technique is by definition non-light-absorbing, the refractive index value of $1.40 - 0i$ that was assumed for POM does not take into account the presence of such light-absorbing organic compounds.

The refractive index imaginary parts obtained using the BC_e values compare poorly with those calculated from the iteration model. It is suspected that the high percentage of BC_e measured for LBA-EUSTACH 1 (about 10% of the volume) represents an overestimate of the true value. This could be attributed to the larger error associated with the determination of BC_e at low concentrations (i.e., LBA-EUSTACH 1). The LBA-EUSTACH 2 values of BC_e were obtained from the measurement of highly loaded filters and there is better agreement between the refractive indices determined by the iteration and mass closure approaches.

Table V-2 Comparison of aerosol refractive indices obtained from the iteration method with those derived from the volume-averaged chemical composition.

Table V-2a Comparison of aerosol refractive indices obtained from the iteration method with those derived from the volume-averaged chemical composition using the EC_a content measured for quartz filter samples. Average values and standard deviation of the measurements are presented.

	Aerosol composition volume average (%)					Refractive index ($m = n - ik$)			
	POM	EC_a quartz (HVDS)	hematite (Fe_2O_3)	INAM	Density (kg m^{-3})	n composition quartz	k composition quartz	n iteration	k iteration
LBA-EUSTACH 1 (6–12 May 99)	52.1 ± 4.3	2.1 ± 0.2	0.3 ± 0.1	45.6 ± 4.0	1558 ± 25	1.45 ± 0.01	0.011 ± 0.001	1.42 ± 0.04	0.006 ± 0.003
LBA-EUSTACH 1 (13–21 May .99)	64.7 ± 4.1	3.1 ± 0.3	0.4 ± 0.1	31.8 ± 3.5	1488 ± 27	1.44 ± 0.01	0.017 ± 0.004	1.46 ± 0.06	0.016 ± 0.003
LBA-EUSTACH 2 (12 Sep–31 Oct 99)	58.6 ± 4.0	1.4 ± 1.0	0	40.0 ± 3.8	1502 ± 24	1.44 ± 0.01	0.007 ± 0.001	1.41 ± 0.05	0.013 ± 0.005

Table V-2b Comparison of aerosol refractive indices obtained from the iteration method with those derived from the volume-averaged chemical composition using the BC_e content measured for Nuclepore filter samples.

	Aerosol composition volume average (%)					Refractive index ($m = n - ik$)			
	POM	BC_e Nuclepore (SFU)	hematite (Fe_2O_3)	INAM	Density (kg m^{-3})	n composition Nuclepore	k composition Nuclepore	n iteration	k iteration
LBA-EUSTACH 1 (6–12 May 99)	47.5 ± 4.1	10.6 ± 0.8	—	41.9 ± 3.3	1533 ± 21	1.46 ± 0.01	0.050 ± 0.004	1.42 ± 0.04	0.006 ± 0.003
LBA-EUSTACH 1 (13–21 May .99)	60.6 ± 3.9	9.3 ± 0.9	—	30.1 ± 3.0	1472 ± 24	1.45 ± 0.01	0.044 ± 0.004	1.46 ± 0.06	0.016 ± 0.003
LBA-EUSTACH 2 (12 Sep–31 Oct 99)	57.3 ± 4.0	3.6 ± 0.3	—	39.1 ± 3.1	1496 ± 24	1.44 ± 0.01	0.017 ± 0.002	1.41 ± 0.05	0.013 ± 0.005

V.4.3. Size distributions

The size distributions obtained from the PCASP instrument (after correction for the refractive index) were compared to those measured with a MOUDI. The PCASP has an output of spherical-equivalent physical diameters, whereas the MOUDI (and all impactors in general) provides size distributions in terms of aerodynamic-equivalent diameters, D_a. D_a is the diameter of a sphere with a density equal to that of water (ρ_w) having the same terminal velocity as the particle impacted. In order to compare the two size distributions, the aerodynamic diameters were converted into geometrical diameters, D. Assuming spherical particles of density ρ, the geometrical diameter can be calculated from the aerodynamic diameter using the following equation (Willeke and Baron, 1993):

$$D = D_a \sqrt{\frac{\rho_w C_a}{\rho C}} \qquad\qquad (V\text{-}1)$$

where C and C_a are the Cunningham slip correction factors for D and D_a, respectively.

The mass closure and densities established previously were used to determine an average aerosol density for each of the three periods defined above, and then these values were used to transform the size distribution measured by the MOUDI, with the aid of equation V-1. The calculated bulk densities of the fine aerosols obtained for the three periods are summarized in Table V-2a. The same densities were assumed for the coarse mode particles. The same respective average densities were also used to calculate mass/size distributions from the number/size distributions of the PCASP. Before comparing the calculated distributions, it should be cautioned that the calculation of average particle density from bulk analysis data has two major potential sources of error (Willeke and Baron, 1993). First, the presence of water in the particles is not accounted for. This would lower their average density, so that the geometric diameters would tend to be closer to the aerodynamic diameters. Second, such an approach does not take in account voids, which are present inside dry particles in particular. Therefore, the obtained geometric diameter falls into the definition of mass-equivalent diameter rather than envelope-equivalent diameter. The "true" spherical-equivalent geometric diameter of the

particles is probably somewhere in between the aerodynamic diameter and geometric diameter calculated as described above.

Figures V-5a–c show typical mass/size distributions obtained from the MOUDI and from the PCASP for the beginning and end of the LBA-EUSTACH 1 campaign, and for the LBA-EUSTACH 2 campaign. The original and the adjusted size distributions are shown in each case. For all three periods, bimodal distributions were found, with a fine mode centered at ca. 0.15–0.35 μm and a coarse mode at 2.3–4.2 μm. The fine-to-coarse mode ratio was found to increase on moving from the beginning to the end of the LBA-EUSTACH 1 campaign, and then to the LBA-EUSTACH 2 campaign, due to the increasing source contribution of biomass burning, which emits predominantly submicron accumulation-mode particles. It should be noted that the last two stages of the MOUDI were not available during the first campaign, and that the size distributions presented are for particle sizes between 10 μm and 0.18 μm in 8 stages only. Also, the smallest and the largest size bin of the PCASP are not presented, as the PCASP instrument does not have well-characterized upper and lower cutoff diameters; and the normalization over $\Delta\log_{10}(D)$ cannot be computed for these sizes. The observed shift in particle sizes (on the x-axis), between "PCASP not corrected" and "PCASP adjusted", and between "MOUDI aerodynamic" and "MOUDI geometric", is due to the correction of the particle size data of the PCASP (for the refractive index) and of the MOUDI (for the density), respectively. The shift in concentrations (on the y-axis) is due to the increase in the PCASP size bins from the adjustment in refractive index, and to the normalization over the difference of the logarithms of consecutive size bins.

It can be seen from Figures V-5a–c that adjusting the PCASP for the refractive index improves the agreement between the MOUDI and PCASP size distributions in the fine mode, but makes it worse for the coarse mode. The agreement in the fine aerosol mode between the two instruments is worse for the LBA-EUSTACH 2 data, with a large overestimation of the mass concentration from the PCASP. Note that assuming the commonly accepted specific density of 1000 kg m^{-3} for biomass burning aerosols (Radke et al., 1991), instead of the ca. 1500 kg m^{-3} estimated here, would lead to a more reasonable agreement.
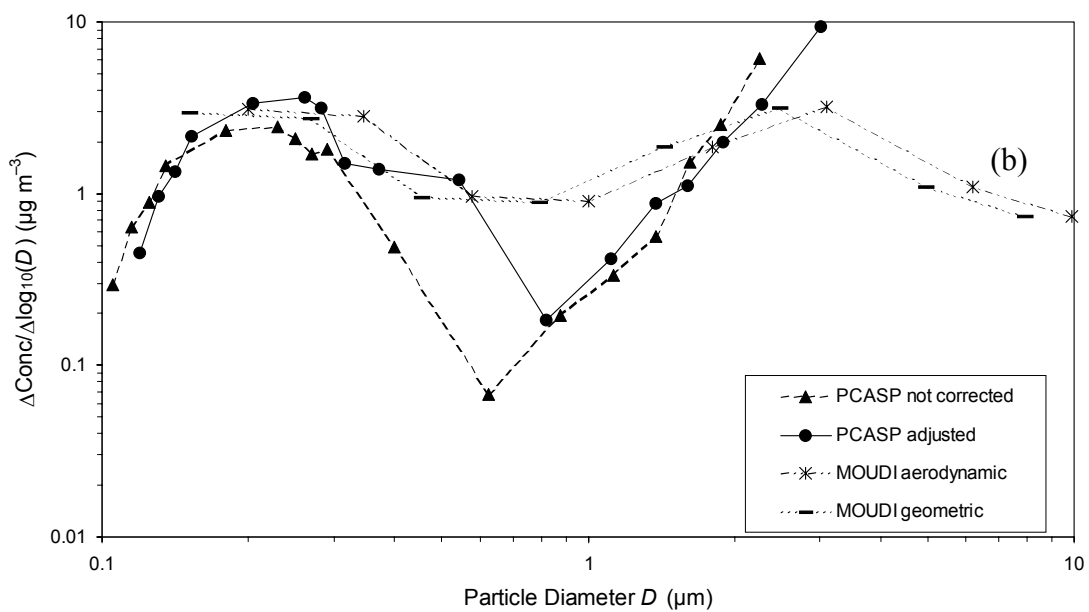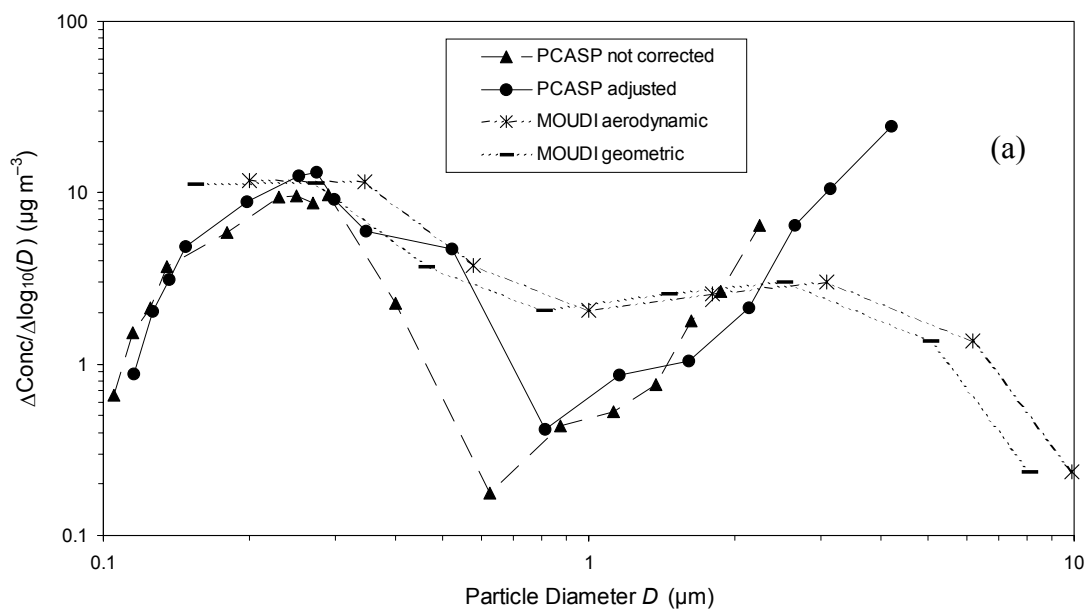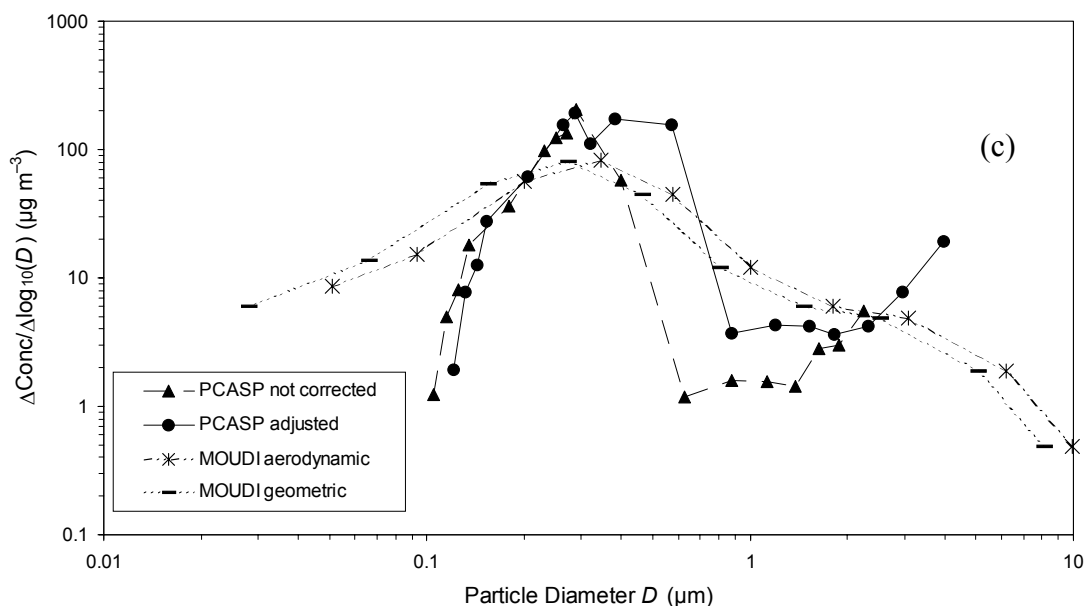
Figure V-5 Comparison of MOUDI and PCASP size distributions.
Typical mass/size distributions obtained from the MOUDI and from the PCASP for the beginning of the LBA-EUSTACH 1 campaign (a), the end of the LBA-EUSTACH 1 campaign (b), and the LBA-EUSTACH 2 campaign (c). The MOUDI samples were collected 8–11 May 1999, 17–20 May 1999, and 5 to 6 October 1999, for the three periods, respectively. The corrected and uncorrected size distributions are shown in each case.

In all three cases, coarse mode particle sizes obtained from the PCASP after adjustment for the refractive index are systematically larger than those obtained from the MOUDI. This effect is most likely due to the original assumption that the refractive index is the same over the whole size distribution. Such an assumption is the only option available with the PCASP size correction program distributed by the manufacturer, but it is also what is commonly assumed in aerosols optical properties modeling or in retrieving aerosol properties from radiometer data. Although fine and coarse mode aerosol probably have a similar real refractive index component, it is very likely that the coarse mode has a lower imaginary part, because black carbon is usually concentrated in fine aerosols. Since the size bins of the adjusted PCASP size distribution increase as the imaginary refractive index component increases, this may explain the overestimation of the coarse mode particle sizes by the iteration procedure. This overestimation is less pronounced in Figure V-5a, probably partly because the calculated imaginary part of the refractive index was relatively low for the first period of the LBA-EUSTACH 1 campaign (Figure V-3a).

Moreover, as discussed in Section V.3.2, the coarse mode was estimated to have contributed 30–60% of the absorption for this period, demonstrating that the imaginary part of the refractive index for the coarse mode could have been about as high as for the fine mode during this part of the campaign. The assumption of a unique refractive index over the whole size distribution is, therefore, a reasonable one in this case. However, as the importance of absorption by aerosols in the fine mode increases, due to increasing biomass burning activity, the offset between the adjusted PCASP and MOUDI distributions becomes more noticeable (Figures V-5b and 5c). This demonstrates that the imaginary part of the refractive index of the particles in the coarse mode was certainly overestimated for the biomass-burning-influenced periods.

However, it can be seen in Figures V-5a–c that the coarse mode mass concentration obtained from the nonadjusted PCASP data is already at least as large as that measured with the MOUDI. This means that any correction applied to the PCASP coarse mode, which increases the particle size, would result in an overestimation of the mass concentration derived from these data, as it can be observed in the "PCASP adjusted" curves. This points out to a fundamental problem in that no correction can actually be applied to the PCASP coarse particle sizes in order to improve the agreement between the two instruments. A potential explanation for this discrepancy could be the detection, by the PCASP, of large particles of low density, which would deposit on lower stages of the MOUDI. This could also be the reason why the two particle modes appear to be better defined in the PCASP-measured size distributions compared to the distributions measured by the MOUDI. It is not expected that this effect could be due to some particle bounce and/or re-entrainment of coarse mode particles to lower stages of the MOUDI, on the basis of what is explained in Section II.3.3. Also, the finest particles measured by the MOUDI are not apparent in the PCASP size distribution. This could be due partly to particle shrinkage inside the MOUDI instrument through evaporation of some components of the aerosols (e.g., water), particularly for the smallest sizes where the pressure drop is the largest, and/or to a low efficiency of the PCASP instrument in detecting these particles.

Comparing the adjusted PCASP size distributions to those given in the literature for Amazonian aerosols, the present data compare fairly well with the results of Remer et al. (1998) obtained from the inversion of radiometer sky radiance data. These results confirm the large coarse particle mode (peaking at ca. 11.5 μm on average) obtained from the adjusted PCASP data, in contrast to what was measured with the MOUDI. However, it should be noted that the method proposed by Remer et al. (1998) also requires the assumption of a unique refractive index representing the whole aerosol size distribution.

Given that the size of the particles in the coarse mode may have been systematically overestimated by overestimating the amount of absorption by this mode, it was decided to examine the impact of assuming the coarse mode to be completely nonabsorbing on the total particle volume, and on the calculation of the scattering and absorption coefficients via the Mie calculations used herein. This is the other extreme to what was assumed in the initial calculations (i.e., that the coarse mode is equally as absorbing as the fine), and it is likely that the "true" case lies somewhere between these two extremes. Table V-3 presents a summary of these calculations, performed on one representative data set from each of the three periods described above. The measured values of (truncated) scattering and absorption coefficients are displayed in the first row of the table. The second row gives values obtained by Mie calculations applied to the uncorrected PCASP size distributions, using the refractive index of latex ($1.59 - 0i$). The third row shows the results obtained from the iteration procedure, and row four shows those obtained using the same real refractive index as in row three, but without taking the absorption component into account (k set to zero for the whole size distribution). The last row presents values obtained assuming the fine particle mode ($D < 1.35$ μm) to be the sole absorbing component of the aerosol.

From Table V-3 it is clear that using a refractive index of $1.59 - 0i$ leads to large differences between calculated and measured parameters, highlighting the need for the PCASP size distribution to be corrected for the refractive index before being used to calculate optical properties.

Table V-3 Influence of absorption by coarse mode aerosols on the total particle volume, and scattering (truncated) and absorption coefficients calculated using the iteration method.

Refractive index ($m = n - ki$)	LBA-EUSTACH 1 (7–12 May)			LBA-EUSTACH 1 (13–21 May)			LBA-EUSTACH 2		
	Total volume ($\mu m^3\ cm^{-3}$)	Scattering coefficient (Mm^{-1})	Absorption coefficient (Mm^{-1})	Total volume ($\mu m^3\ cm^{-3}$)	Scattering coefficient (Mm^{-1})	Absorption coefficient (Mm^{-1})	Total volume ($\mu m^3\ cm^{-3}$)	Scattering coefficient (Mm^{-1})	Absorption coefficient (Mm^{-1})
Measured values	—	4.94	0.4	—	13.1	2.58	—	409	35
1.59 – 0i[1]	1.27	4.37	0	2.73	11.9	0	40.3	292	0
From iteration[1]	2.33	5.03	0.4	6.67	13.3	2.57	86.4	412	35.1
k = 0[1,2]	1.87	4.95	0	3.6	13	0	77.4	394	0
Coarse mode k = 0	1.91	5.01	0.22	3.78	13.3	1.57	83.8	412	34.1

[1] A unique refractive index was applied over the whole size distribution.
[2] Same real part of the refractive index as found from the iteration procedure, k set to zero.
[3] Real part of the refractive index applied over the whole size distribution. Coarse mode ($D > 1.35\ \mu m$) assumed to be nonabsorbing.

For LBA-EUSTACH 2, treating the coarse mode particles as nonabsorbing has negligible effect on the calculated scattering coefficient, and leads to values of the absorption coefficient and total volume only 3% lower than the corresponding values obtained when all particles are assumed to be equally absorbing over the whole size distribution. This means that in the case of a very dominant, absorbing fine mode, considering the coarse mode to have the same refractive index as the fine mode leads to only small errors in the determination of the optical properties from the PCASP size distribution, and, conversely, little error in the determination of the refractive index, while reproducing the optical properties from the iteration. Neglecting absorption for both the fine and coarse mode leads to an underestimation of the scattering coefficient by only 4.4%; however, the total volume is ca. 7.6% lower than that calculated assuming the fine mode to be the only absorbing fraction.

Considering next the LBA-EUSTACH 1 campaign, the scattering coefficient can be reproduced equally for the beginning and end of the campaign, by treating the coarse mode as nonabsorbing. The absorption coefficients for the two periods, however, are 45 and 39% lower than the values obtained when a constant refractive index is assumed, while the total volumes are 9 and 43% lower. This indicates that the coarse mode must have contributed substantially to the total absorption, in agreement with to other analyses reported in Section V.3.2. For the beginning of the campaign, it has been seen already that the corrected PCASP size distribution reproduces that measured by the MOUDI fairly well (Figure V-5a). This indicates that the use of a single refractive index to represent the whole size distribution is a reasonable approximation for this period, and moreover, that the real and imaginary part of the calculated effective refractive index are reasonable estimates for both the fine and the coarse modes.

For the end of the campaign, however, the discrepancy between the adjusted PCASP and MOUDI distributions for the coarse mode is more noticeable. This appears to be because the imaginary part of the effective refractive index calculated for this period (k = 0.016) is much higher (about as high as for LBA-EUSTACH 2). Evidently, it overrepresents the absorptive properties of the coarse mode particles, even though this mode was found to contribute significantly to total absorption throughout the campaign

(Section V.3.2). This serves to highlight the inherent problems associated with obtaining accurate size distribution data from OPC instruments, which use a single refractive index to represent the whole aerosol population.

V.4.4. Comparison with previous measurements

In this section, the refractive indices obtained from the iteration method are compared to values found in the literature. It should be emphasized that the notion of refractive index becomes somewhat ill-defined when applied to inhomogeneous particles. Indeed, the refractive index of a complex mixture of compounds can only be expressed as an "equivalent refractive index" specific for the given measurement conditions and set of assumptions made about the properties of the aerosol. In the present case, the calculated refractive indices can be defined as equivalent refractive indices for spherical, homogeneously internally mixed particles with the same bulk absorption and scattering properties as the actual particles. One should therefore remain cautious about drawing conclusions based on comparison of refractive indices of atmospheric aerosols obtained using different techniques. Table V-4 shows a summary of refractive indices obtained using various techniques for biomass burning aerosols and for aerosols from remote conditions.

The refractive index estimate for biomass burning aerosols obtained here is in the range of other values obtained recently, for the most part via sky radiance measurements (using a radiometer). The effective refractive index retrieved by this technique also requires the assumption that the aerosols are polydisperse, homogeneous, and spherical in shape. The imaginary part obtained in the present study is somewhat larger than that found by Dubovik et al. (2002) for burning of Amazonian forest, but closer to that found by the same authors for cerrado fires in Brazil. These authors also found biomass burning aerosols over boreal forest in the United States and Canada to have a refractive index similar to that of smoke aerosol from Amazonian forest. In contrast, values for Zambian savanna fires ($k = 0.021 \pm 0.01$), which typically release aerosols with a higher elemental carbon fraction, were closer to that for Brazilian cerrado.

157

Table V-4 Refractive indices of biomass burning and background aerosols.

Method	Wavelength (nm)	Relative humidity	Condition	Refractive index n; k	Reference
in situ size distribution, scattering, and absorption	545	Ambient, 48–80%	Biomass burning, Amazonian forest, Brazil (Sep–Oct 1999)	1.41 ± 0.05[1]; 0.013 ± 0.005[1]	This study
Sky radiance (AERONET radiometers)	440–1020[2]	Total column, not given	Biomass burning, Amazonian forest, Brazil (1993–1994) and Bolivia (1998–1999)	1.47 ± 0.03[1]; 0.0093 ± 0.003[1]	Dubovik et al. (2002)
Sky radiance (AERONET radiometers)	440–1020[2]	Total column, not given	South American cerrado, Brazil	1.52 ± 0.01[1]; 0.015 ± 0.004[1]	Dubovik et al. (2002)
Sky brightness (CIRATRA radiometers)	560–870[2]	"low" (ca. 50–80%) to "high" (> 80%)[3]	Southeast Asian forest fire haze (1997)	1.45 (1.37 – 1.55); k not given	von Hoyningen-Huene et al. (1999)
Sky radiance (AERONET radiometers)	440, 670, 870, and 1020	Total column, estimated "low"	Biomass burning, cerrado, Cuiabá, Brazil (1993–1994) and Bolivia (1998–1999)	1.53 ± 0.04[1], 1.55 ± 0.04[1], 1.59 ± 0.04[1], and 1.58 ± 0.04[1]; k not given[4]	Yamasoe et al. (1998)
Meteorology, aerosol, and radiative transfer model	500	Not given	Biomass burning, Canadian forest, July 1982	1.45–1.55; 0.01	Westphal and Toon (1991)

Table V-4 (continued)

Method	Wavelength (nm)	Relative humidity	Condition	Refractive index $n; k$	Reference
Remote sensing (Langley LASE) and in situ size distribution	815	"low" (30–50%) to "high" (80–100%)	Pollutant haze from United States over western Atlantic Ocean, July 1996 (TARFOX)	1.33–1.45; 0.001–0.008	Redemann et al. (2000)
in situ size distribution, scattering, and absorption	545	Ambient, 64–80%	Amazonian forest, background, Brazil (May 1999)	1.42 ± 0.04[1]; 0.006 ± 0.003[1]	This study
Transmittance	550	Not given	Rural	1.53; 0.006	Kent et al. (1983)
Transmittance	550	Not given	Maritime / rural	1.474; 0.004	Kent et al. (1983)
Various techniques	550	—	Dust-like	1.53; 0.008	Kent et al. (1983), Dubovik et al. (2002) and references therein

[1] Standard deviation of the measurements.
[2] Refractive index of biomass burning aerosols spectrally independent over the range given.
[3] At ground level.
[4] Values respective to the wavelength.

Westphal and Toon (1991) proposed an imaginary part of 0.01 for aerosols emitted during forest fires in Canada. They also mention, however, that laboratory studies of forest fire smoke yielded k values ranging between 0.01 and 0.1. Using Mie theory, they found that values of k between 0.01 and 0.02 gave the best fits to single-scattering albedo data obtained from Landsat imagery. They considered values as high as 0.1 as unrealistic for their case study. The value of 0.01 was then chosen over 0.02 for their subsequent calculations, because it gave better fit to global irradiance measurements, even though they later described these as "suspect".

To date, no measurements of the refractive index of Amazonian background aerosols have been reported. The lack of estimates from sky radiance measurements is due to the fact that this technique requires a relatively high aerosol loading (Dubovik et al., 2000). Reasonable measurements of the refractive index (with errors of ca. 30–50% for the imaginary part and ± 0.04 for the real part) can be obtained from this technique only for an aerosol optical thickness (at a wavelength of 440 nm) larger than 0.5 at a solar zenith angle >50°. Therefore, in the absence of data for background Amazonian aerosol, the well-accepted (Redemann et al., 2000) rural and maritime/rural values published by Kent et al. (1983) in a compilation of refractive indices were chosen as a reference. It is interesting to note that the estimate reported herein for the refractive index of Amazonian background aerosol is close to the value commonly accepted for dust particles ($m = 1.53 - 0.008i$), which was found to be a major component of the aerosols during the LBA-EUSTACH 1 campaign (see Section V.3.2).

Generally, the present estimates of the real refractive index component are lower than most previously reported values. As discussed in Section V.4.2, this is mainly attributable to the high relative humidity conditions encountered during both field campaigns (see also Section V.3.2). von Hoyningen-Huene et al. (1999) (Table V-4) also found values of n for forest fire haze in Malaysia as low as 1.37 (average of 1.45), and attributed these to the high RH conditions. Similarly, Redemann et al. (2000) observed that both the real and the imaginary parts of the refractive index of continental pollutant haze over the western Atlantic Ocean decreased with altitude, as the relative humidity increased and the aerosols became more aqueous in nature. The values published by

Yamasoe et al. (1998) (obtained with the same AERONET datasets as Dubovik et al. (2002), but with a different methodology) show the highest real parts for the refractive indices of cerrado biomass burning aerosols. In contrast to other investigators, Yamasoe et al. (1998) also found a slight wavelength dependence for the index of refraction (Table V-4).

V.4.5. Single-scattering albedo, asymmetry parameter, and backscattered fraction

Other climatically relevant parameters were also obtained from the iterative Mie calculations. Figures V-6a and 6b show the time series and Table V-5a the averaged values of the single-scattering albedo (ω_0), asymmetry parameter (g) (which describes the shape of the scattering function), and backscattered fraction (β) (fraction of radiation scattered at scattering angles in the range of 90 to 180 degrees) calculated at ambient RH <80%, for the LBA-EUSTACH 1 and 2 campaigns. The same sensitivity test was applied to these parameters as for the refractive index (Section V.3.3). A summary of the maximum errors associated with variation of measured aerosol parameters is given Table V-5b. The error associated with ω_0 and g was found to increase with decreasing values of ω_0 and g, whereas the error associated with β increased with increasing β.

The single-scattering albedo obtained from the Mie calculation differs from that calculated directly from the measured scattering and absorption coefficients, because the scattering coefficients were corrected for the truncation angle of the nephelometer. The relatively low average ω_0 value (0.85 ± 0.02) calculated for the end of the LBA-EUSTACH 1 campaign could be attributable to the aging process of the aerosols. Over the 2 to 3 days the aerosol particles traveled before being sampled (see Section V.4.1), a black carbon core could have become enveloped in a nonabsorbing shell due to cloud processing or uptake of gaseous species enhancing the absorption properties of the aerosols. Measurements under hazy conditions yielded average ω_0 values of 0.90 ± 0.03, which are higher than, e.g., the values of 0.85 ± 0.02 (Cuiabá, Mato Grosso) and 0.86 ± 0.05 (Porto Velho, Rondônia) reported by Reid et al. (1998a) for SCAR-B (measurements performed at the same wavelength of 550 nm, with a comparable set of instrumentation).

It is noted here that results similar to those presented by these authors were obtained when not correcting the PSAP data according to Bond et al. (1999) (ω_0 = of 0.86 ± 0.04).
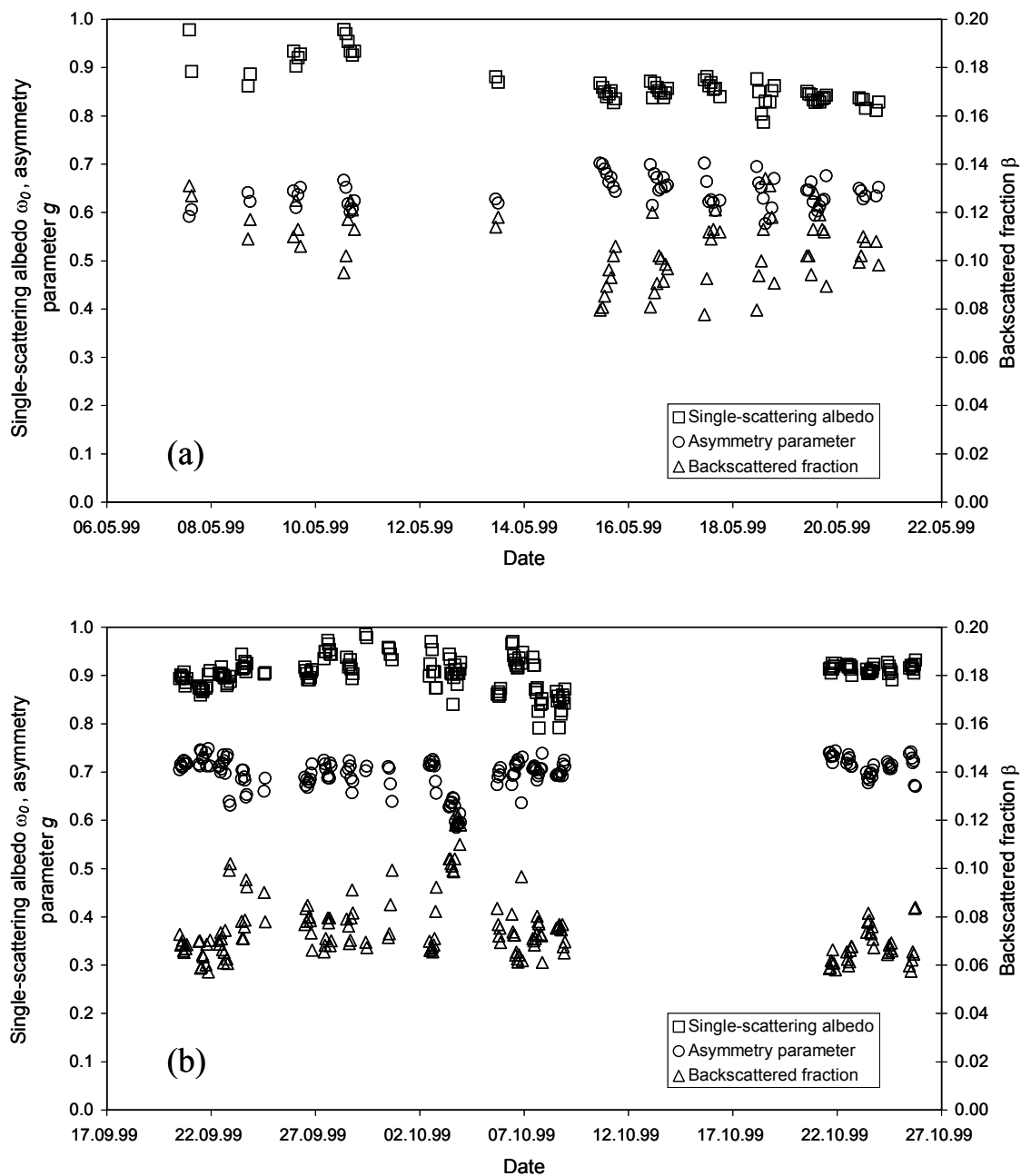
Figure V-6 Single-scattering albedo, asymmetry parameter, and backscattered fraction calculated for the LBA-EUSTACH 1 (a) and LBA-EUSTACH 2 (b) campaigns.
The data were obtained from Mie calculations iterative procedure, using the PCASP size distribution, PSAP absorption, and nephelometer scattering data measured when ambient RH was <80%.

The asymmetry parameter was found to decrease, and the backscatter ratio to increase, with increasing influence of fine particles, i.e., from the first part of LBA-EUSTACH 1 through to LBA-EUSTACH 2. Although this result may appear surprising since g usually increases (and β decreases) with increasing particle size for a given refractive index, it can be attributed to an increasing absorption efficiency of the aerosol (and imaginary refractive index component). This effect is particularly pronounced for very fine particles (smaller than 0.3 μm), as produced during biomass burning (Horvath, 1998). The values of g presented here for biomass burning haze compare well with those found by von Hoyningen-Huene et al. (1999) for Southeast Asian forest fire haze ($g = 0.69 \pm 0.02$). Dubovik et al. (2002) found g values of 0.69 ± 0.06 (at 440 nm) and 0.58 ± 0.06 (at 670 nm) for Amazonian forest biomass burning.

Reid et al. (1998a) reported β values of 0.11 to 0.12 ± 0.01 for Brazilian haze. These are larger than the average value found in the present study for the biomass burning season, but close to what was found on one particular day of the LBA-EUSTACH 2 campaign. The 3 October values could be significantly differentiated from averaged background haze by virtue of a higher real refractive index part (with $m = 1.50(\pm 0.04) - 0.015(\pm 0.004)i$), a lower asymmetry parameter, and a higher backscatter fraction. Interestingly, the single-scattering albedo was close to the average. The larger n value implies a smaller correction to the PCASP size bins (for a constant value of k), and thus a greater relative contribution of smaller particles to the total population than found on average. Moreover, of all MOUDI samples collected in parallel to the online measurements, the sample collected on 3 October was the only one over the whole campaign for which stage number 8 (D_{50} equal to 0.200 μm) was the dominant fraction; all other samples typically showed a maximum loading on stage number 7 (D_{50} equal to 0.346 μm). These data all suggest that the aerosol measured on this particular day was likely young smoke aerosol derived from nearby burning.

Table V-5a Single-scattering albedo (ω_0), asymmetry parameter (*g*), and backscattered fraction (β) (mean ± standard deviation) obtained from Mie calculation (for a wavelength of 550 nm) from measured size distribution, and scattering and absorption coefficients.

Parameter	LBA-EUSTACH 1 (7–12 May)	LBA-EUSTACH 1 (13–21 May)	LBA-EUSTACH 2 (20 Sep–25 Oct)	LBA-EUSTACH 2 (3 Oct)
ω_0	0.93 ± 0.03	0.85 ± 0.02	0.90 ± 0.03	0.91 ± 0.02
g	0.63 ± 0.02	0.65 ± 0.03	0.70 ± 0.03	0.62 ± 0.02
β	0.12 ± 0.01	0.10 ± 0.01	0.08 ± 0.01	0.11 ± 0.01

Table V-5b Maximum error associated with the variation of number size concentration, and scattering and absorption coefficients on the retrieval of single-scattering albedo (ω_0), asymmetry parameter (*g*), and backscattered fraction (β) obtained from the iteration method (for the range of values observed).

Parameter	LBA-EUSTACH 1			LBA-EUSTACH 2		
	PCASP number concentration ± 5%	Scattering coefficient ± 5%	Absorption coefficient ± uncertainty	PCASP number concentration ± 10%	Scattering coefficient ± 5%	Absorption coefficient ± uncertainty
ω_0	—	± 1%	± 2%	—	± 2%	± 2%
g	± 6%	± 5%	± 1%	± 8%	± 4%	± 1%
β	± 11%	± 11%	± 2%	± 20%	± 10%	± 1%

V.5. Summary and conclusion

In this chapter, an original, robust method both for retrieving the effective refractive index of aerosols, and for correcting the measured size distribution derived from an OPC (PCASP) was presented, using data obtained from commercially available instruments in combination with standard Mie calculations. The method was applied to data sets obtained at an Amazonian tropical rain forest site during both background and biomass burning conditions. For periods when ambient RH was <80%, average refractive indices of $1.42 - 0.006i$ and $1.41 - 0.013i$ were estimated for background and biomass burning aerosols, respectively. The latter value compares well with literature values; however, there is only limited information available about the refractive index of background aerosols, particularly in the tropics. This is largely due to the fact that the commonly employed sky radiance method for retrieving refractive indices requires relatively high aerosol loadings. The application of the method presented in this study may help to remedy this situation and facilitate the development of accurate radiation models.

A comparison of adjusted PCASP size distribution data with that obtained with a MOUDI indicates that reasonably accurate size distributions can be retrieved with an iterative method in cases when the fine mode dominates or the coarse mode has similar absorption properties to that of the fine. The use of a single effective refractive index to represent the aerosol population, however, prohibits reconciling these size distributions when the fine and coarse modes both contribute significantly to the total aerosol while having distinctly different optical properties. Future work will focus on extending the current iteration method to allow for the use of two refractive indices to represent the two separate modes of the aerosol.

CHAPTER VI.

SUMMARY, OVERALL CONCLUSIONS, AND OUTLOOK

In this work, the major chemical and physical properties of aerosol particles characteristic for the wet and the dry season in the Amazon basin were investigated. The results demonstrate the dramatic impact that biomass burning has on the naturally pristine conditions observable in this region. Non-polluted background conditions during the wet season were found to be comparable to those found for remote marine environments in terms of particle number concentration (ca. 400 cm^{-3}) and single-scattering albedo (close to unity). In sharp contrast, conditions observed during the biomass burning-influenced dry season were found to resemble those more commonly associated with urban smog, due to a massive injection of submicron smoke particles (CHAPTER III). Perhaps one of the most significant findings to emerge from this work is that even very small amounts of smoke aerosol can tremendously influence the overall characteristics of the aerosol population over the Amazon basin, overriding the effects of the background forest aerosol. This is likely to have important consequences for direct and indirect aerosol forcing, as well as the hydrological cycle, in this region (CHAPTER III and CHAPTER V).

This work also provides a new dataset describing the vertical spatial variation of aerosol through the Amazon rainforest canopy structure during both the wet and dry seasons, for which only limited data has previously been reported (Artaxo et al., 1990; Artaxo et al., 2002) (CHAPTER IV). These profile data indicate that the fine pyrogenic aerosol particles emitted during the dry season are generally fairly well mixed throughout the canopy. A net deposition of soil dust particles within the forest canopy was also observed, whilst clear evidence for the production of coarse mode biogenic particles underneath the canopy was found, with highest concentrations occurring during nighttime partly due to a shallow nocturnal inversion. It is suggested that turbulent mixing under the

canopy during nighttime may contribute to a natural redistribution of nutrients such as phosphorus within the Amazonian forest. This could be of major importance since phosphorus is known to be a limiting nutrient in the region, and is not present in significant amounts in rainwater falling on the forest.

The source and mass apportionment of the aerosols were retrieved through statistical analysis of the chemical composition data using multivariate techniques. Three components were found to contribute to the bulk of the aerosol mass for both the wet and dry seasons. These were identified as biomass burning smoke, biogenic particles and soil dust, and were often found to exist as a complex mixture in the aerosol. All three components, in both the fine and coarse aerosol fractions, were found to contribute significantly to the overall optical properties of the bulk aerosol, particularly light absorption. This appears to substantiate another (albeit indirect) finding of the current study, which is that compounds other than elemental carbon may significantly contribute to the light absorption from aerosols, in contrast to what has been traditionally assumed. It is suggested that these could be polymeric organic compounds, the presence of which has been noted in recent publications (Mukai and Ambe, 1986; Zappoli et al., 1999; Mayol-Bracero et al., 2002).

Whilst contributing important data pertaining to the aerosol particles of the Amazon basin, this work has also served to highlight the limitations of some of instrumentation commonly used in the aerosol community, and corrective measures have been suggested to address these. Most notably, in CHAPTER V a new iteration method was described for retrieving the refractive index of ambient aerosol particles (one of the least well characterized parameters of aerosols), which also allows for correction of the size distribution measured by an OPC, and calculation of the truncation angle of an integrating nephelometer.

It is of importance to note here that some aircraft measurements of aerosol number concentration, CCN concentration, and of scattering and absorption coefficients were performed during the LBA-EUSTACH 2 campaign. It would be interesting in the future to compare these data with those obtained on the measurement tower.

The precise effect that aerosol particles generated in the Amazon basin have on regional and global climate remain unclear from the results of this work, and this issue is certainly one that requires further attention. In-depth computer modeling studies are needed to account for all the various factors that contribute to climate change, of which aerosols are but one. The validity of the results of these calculations will always, however, depend on the quality of the input data provided by field and laboratory measurements. In this context, it is important to highlight the large uncertainty associated with some of the aerosol parameters (e.g., volume/size distribution, single-scattering albedo, state of mixing, etc.), which is evident not only from the errors associated with the measurements from individual instruments, but also from comparisons of data derived from different measurement techniques used to measure the same parameter. Given the potentially important role that aerosols may play in climate change, it is of major importance to reduce uncertainties in these measurements, most notably of volume distributions and optical absorption, the latter parameter being responsible for most of the uncertainty associated with current single-scattering albedo estimates.

To date, there is no perfect method for measuring aerosol volume/size distributions; all current methods require a series of assumptions about the shape, refractive index, and/or density of the particles, which, in turn, rank amongst the least well-characterized properties of aerosols. The obtained size distributions are also dependent on the specific aerosol physical property used to measure them, making it is difficult to compare them among each other (see Section V.4.3).

An accurate measurement of light absorption is hampered by the fact that no method currently exists that allows for the selective measurement of light-absorbing particles, as these particles may vary in size, composition, and state of mixing with other particles and therefore also scatter the light to a more or lesser degree. Most aerosol absorption measurements are made by measuring the transmission of light through a sample deposited on a filter medium, with compensation for losses of scattered light (e.g., PSAP and aethalometer). These methods suffer mainly from problems associated with interference by the filter medium, and the fact that light scattering by aerosol particles is usually much larger than absorption. This is also a major drawback of the "subtraction

method" for calculating absorption, which involves subtracting the scattering measured by a nephelometer from the extinction coefficient measured through an extinction cell. Because this usually requires the calculation of a fairly small difference between two large numbers, the resulting error may be large. Additionally, care must be taken to account for the effects of truncation by the nephelometer, which might be as large as the absorption itself.

An exciting recent development has been use of the photoacoustic spectrometer (PAS) to measure light absorption by aerosol particles. This instrument determines absorption by measuring pressure change due to the heat released by particles suspended in a measurement chamber, using a microphone. This instrument was developed to measure absorption by aerosol particles in their "true" airborne state, bypassing many of the problems inherent in the techniques described above. Thus far, the instrument has only been used in a few experimental studies, and preliminary results indicate the need for further extensive comparative measurements to be made. Differences between absorption estimates from the PAS and PSAP as large as a factor of three have been found (P. Guyon, M. O. Andreae, unpublished data).

As evident from the results of the current study, there is often large temporal and spatial variability in the properties of aerosols, and this adds an extra layer of complexity to any climate modeling studies that seek to include the effects of aerosols. This spatial and temporal variability can be monitored in some cases; the AERONET initiative, for example, allows worldwide monitoring of aerosol optical properties using a network of sun photometers (http://aeronet.gsfc.nasa.gov:8080/), in order to validate satellite retrievals of these properties. However, although the variability itself can be measured, the atmospheric transformations, which aerosols undergo, are still not fully understood. For example, whilst it is now clear that particle aging has a large influence on aerosol optical properties (especially light absorption), details of the process are uncertain, with the result that model studies usually "underpredict" absorption relative to that measured in situ. An understanding of the reasons for this discrepancy will hopefully emerge from laboratory experiments on particle aging.

One of the major effects, which, although systematically monitored, was not accounted for in this work, was that of relative humidity on the properties of the sampled aerosol. The use of Nafion dryers was found to be possibly suitable for monitoring aerosol properties under controlled RH, while minimizing particle losses; however, further tests are needed to determine which particles and constituents of the particles may undergo losses when using this technique. In future work, it would be interesting and worthwhile to measure the aerosol properties (e.g., size distribution, absorption, and scattering) both under dry conditions (RH < ca. 40%), and at varying humidities.

A final issue to emerge from this work, which requires further consideration by the aerosol community, is the need for a standard accepted understanding of what constitutes the light-absorbing component of aerosols. Traditionally, this component has been identified with what is known as "soot carbon", an impure form of near-elemental carbon that is formed in flaming combustion. The terms "elemental carbon" (EC) and "black carbon" (BC, the equivalent concentration of soot carbon that gives the same absorption response in the instrument as the absorbing substances contained in the sample) have come to be used interchangeably in the scientific literature, almost without regard to the measurement technique used (thermochemical or light absorption), despite the large discrepancies that exist between measurements. It is now becoming increasingly evident that light-absorbing matter in aerosols contains components other than elemental carbon, and that the standard nomenclature is inadequate. There is an urgent need for a standardized method for the determination of organic carbon, elemental carbon, and further absorbing carbonaceous matter, and their respective light absorbing properties.

LIST OF ABBREVIATIONS

ABLE	Amazon Boundary Layer Experiments
AOD	Aerosol optical depth
APCA	Absolute principal component analysis
APCS	Absolute principal component score
BC_e	Black carbon equivalent
CBL	Convective boundary layer
CCN	Cloud condensation nuclei
CPC	Condensation particle counter
CPM	Coarse particulate masses
EC_a	Apparent elemental carbon
EF	Enrichment factors
E_r	Enrichment ratios
EUSTACH	EUropean Studies on Trace gases and Atmospheric CHemistry
FNS	Fazenda Nossa Senhora Aparecida
FPM	Fine particulate masses
HVDS	High volume dichotomous sampler
INAM	inorganic nonabsorbing matter
IPCC	Intergovernmental panel on climate change
LBA	Large-Scale Biosphere-Atmosphere Experiment in Amazonia
MFR	Multifilter rotating shadowband radiometer
MOUDI	Microorifice uniform deposit impactor
MS	Mato Grosso do sul

MT	Mato Grosso
OC	Organic carbon
OPC	Optical particle counter
PAS	Photoacoustic spectrometer
PBL	Planetary boundary layer
PCA	Principal component analysis
PCASP	Passive cavity aerosol spectrometer probe
PIXE	Particle-induced X-ray emission analysis
PM	Particulate mass
POM	Particulate organic matter
PSAP	Particle soot absorption photometer
RBJ	Reserva Biologica Jarú
RH	Relative humidity
SCAR-B	Smoke, Cloud, Aerosol and Radiation-Brazil experiment
SFU	Stacked filter unit
TC	Total carbon
TOT	Thermo-optical transmission technique
VOC	Volatile organic compound

LIST OF SYMBOLS

α_0	Degree of nonsphericity of aerosol particles
α_a	Mass absorption efficiency
A_c	Fractional cloud cover
α_s	Mass scattering efficiency
β	Upscatter fraction (backscatter fraction at solar zenith angle $\theta_0 = 0$)
D	Particle diameter
D_{50}	Aerodynamic diameter cutoffs
D_{calib}	Deposition spot diameter assumed by the PSAP instrument
ΔF	Globally and annually top-of-atmosphere averaged forcing caused by an aerosol layer
D_{meas}	Diameter of the deposition spot measured for the PSAP instrument
$\Delta N/\Delta \log_{10}(D)$	Number/size distribution
D_p	Particle aerodynamic diameter
$\Delta V/\Delta \log_{10}(D)$	Volume/size distribution
$E(D)$	Collection efficiency of the MOUDI
F_0	Solar constant (~ 1360 W m^{-2})
F_{spot}	PSAP correction for the deposit spot area
F_{trunc}	Nephelometer truncation factor
g	asymmetry parameter
k	Imaginary part of the refractive index
λ	Wavelength of incident light
m	air mass (when indicated)

m	Refractive index
$m_{assumed}$	Assumed refractive index (model)
n	Real part of the refractive index
θ_0	Solar zenith angle
θ_1	Nephelometer forward scattering truncation angle
θ_2	Nephelometer backward scattering truncation angle
ρ	Particle density
R_s	Surface albedo
σ_a	Absorption coefficient
$\sigma_{a,calc}$	Calculated absorption coefficient (model)
$\sigma_{a,meas}$	Measured absorption coefficient
$\sigma_{a,prec}$	Precision uncertainty for the PSAP instrument
σ_{am}	PSAP absorption coefficient corrected for spot area and flow
$\sigma_{s,calc}$	Calculated scattering coefficient (model)
$\sigma_{s,trunc}$	Scattering coefficient not correction for the angular truncation
τ	Aerosol optical depth
T	Transmissivity of the atmosphere above the aerosol layer
ω_0	Single-scattering albedo
ω_{crit}	Critical single-scattering albedo
Z	Atomic number

BIBLIOGRAPHY

Ackerman, A. S., Toon, O. B., Stevens, D. E., Heymsfield, A. J., Ramanathan, V., and Welton, E. J.: Reduction of tropical cloudiness by soot, Science, 288, 1042-1047, 2000.

Albrecht, B. A.: Aerosols, cloud microphysics, and fractional cloudiness, Science, 245, 1227-1230, 1989.

Anderson, T. L., Covert, D. S., Marshall, S. F., Laucks, M. L., Charlson, R. J., Waggoner, A. P., Ogren, J. A., Caldow, R., Holm, R. L., Quant, F. R., Sem, G. J., Wiedensohler, A., Ahlquist, N. A., and Bates, T. S.: Performance characteristics of a high-sensitivity, three-wavelength, total scatter/backscatter nephelometer, J. Atmos. Ocean. Technol., 13, 967-986, 1996.

Anderson, T. L., Covert, D. S., Wheeler, J. D., Harris, J. M., Perry, K. D., Trost, B. E., Jaffe, D. J., and Ogren, J. A.: Aerosol backscatter fraction and single scattering albedo: Measured values and uncertainties at a coastal station in the Pacific Northwest, J. Geophys. Res.-Atmos., 104, 26793-26807, 1999.

Andreae, M. O.: Soot carbon and excess fine potassium - long-range transport of combustion-derived aerosols, Science, 220, 1148-1151, 1983.

Andreae, M. O.: Biomass burning: Its history, use, and distribution and its impacts on environmental quality and global climate, in Global biomass burning: Atmospheric, climatic, and biospheric implications, edited by J. S. Levine, pp. 3-21, MIT Press, Cambridge, Mass., 1991.

Andreae, M. O.: Raising dust in the greenhouse, Nature, 380, 389-390, 1996.

Andreae, M. O.: The dark side of aerosols, Nature, 409, 671-672, 2001.

Andreae, M. O., Andreae, T. W., Annegarn, H., Beer, J., Cachier, H., le Canut, P., Elbert, W., Maenhaut, W., Salma, I., Wienhold, F. G., and Zenker, T.: Airborne studies of aerosol emissions from savanna fires in Southern Africa: 2. Aerosol chemical composition, J. Geophys. Res.-Atmos., 103, 32119-32128, 1998.

Andreae, M. O., Artaxo, P., Brandao, C., Carswell, F. E., Ciccioli, P., Costa, A. L. d., Culf, A. D., Esteves, J. L., Gash, J. H. C., Grace, J., Kabat, P., Lelieveld, J., Malhi,

Y., Manzi, A. O., Meixner, F. X., Nobre, A. D., Nobre, C., Ruivo, M. d. L. P., Silva-Dias, M. A., Stefani, P., Valentini, R., Jouanne, J. v., and Waterloo, M. J.: Towards an understanding of the biogeochemical cycling of carbon, water, energy, trace gases and aerosols in Amazonia: The LBA-EUSTACH experiment, J. Geophys. Res.-Atmos., 107(D20), 8066, doi: 10.1029/2001JD000524, 2002.

Andreae, M. O., Artaxo, P., Fischer, H., Freitas, S. R., Gregoire, J. M., Hansel, A., Hoor, P., Kormann, R., Krejci, R., Lange, L., Lelieveld, J., Lindinger, W., Longo, K., Peters, W., de Reus, M., Scheeren, B., Dias, M., Ström, J., van Velthoven, P. F. J., and Williams, J.: Transport of biomass burning smoke to the upper troposphere by deep convection in the equatorial region, Geophys. Res. Lett., 28, 951-954, 2001.

Andreae, M. O., Browell, E. V., Garstang, M., Gregory, G. L., Harriss, R. C., Hill, G. F., Jacob, D. J., Pereira, M. C., Sachse, G. W., Setzer, A. W., Dias, P. L. S., Talbot, R. W., Torres, A. L., and Wofsy, S. C.: Biomass-burning emissions and associated haze layers over Amazonia, J. Geophys. Res.-Atmos., 93, 1509-1527, 1988.

Andreae, M. O., and Crutzen, P. J.: Atmospheric aerosols: Biogeochemical sources and role in atmospheric chemistry, Science, 276, 1052-1058, 1997.

Andreae, M. O., and Merlet, P.: Emission of trace gases and aerosols from biomass burning, Global Biogeochemical Cycles, 15, 955-966, 2001.

Artaxo, P., Andreae, M. O., Guenther, A., and Rosenfeld, D.: Lba atmospheric chemistry: Unveiling the lively interactions between the biosphere and the amazonian atmosphere, IGBP newsletter, 45, 12-15, 2001.

Artaxo, P., Fernandes, E. T., Martins, J. V., Yamasoe, M. A., Hobbs, P. V., Maenhaut, W., Longo, K. M., and Castanho, A.: Large-scale aerosol source apportionment in Amazonia, J. Geophys. Res.-Atmos., 103, 31837-31847, 1998.

Artaxo, P., Gerab, F., Yamasoe, M. A., and Martins, J. V.: Fine mode aerosol composition at 3 long-term atmospheric monitoring sites in the Amazon basin, J. Geophys. Res.-Atmos., 99, 22857-22868, 1994.

Artaxo, P., and Hansson, H. C.: Size distribution of biogenic aerosol-particles from the Amazon basin, Atmos. Environ., 29, 393-402, 1995.

Artaxo, P., Maenhaut, W., Storms, H., and van Grieken, R.: Aerosol characteristics and sources for the Amazon basin during the wet season, J. Geophys. Res.-Atmos., 95, 16971-16985, 1990.

Artaxo, P., Martins, J. V., Yamasoe, M. A., Procópio, A. S., Pauliquevis, T. M., Andreae, M. O., Guyon, P., Gatti, L. V., and Leal, A. M. G.: Physical and chemical properties of aerosols in the wet and dry season in Rondônia, Amazonia, J. Geophys. Res.-Atmos., 107, 8081, doi:8010.1029/2001JD000666, 2002.

Artaxo, P., Storms, H., Bruynseels, F., van Grieken, R., and Maenhaut, W.: Composition and sources of aerosols from the Amazon basin, J. Geophys. Res.-Atmos., 93, 1605-1615, 1988.

Beauford, W., Barber, J., and Barringer, A. R.: Release of particles containing metals from vegetation into the atmosphere, Science, 571-573, 1977.

Birch, M. E., and Cary, R. A.: Elemental carbon-based method for monitoring occupational exposures to particulate diesel exhaust, Aerosol Sci. Technol., 25, 221-241, 1996.

Bond, T. C., Anderson, T. L., and Campbell, D.: Calibration and intercomparison of filter-based measurements of visible light absorption by aerosols, Aerosol Sci. Technol., 30, 582-600, 1999.

Boucher, O., and Anderson, T. L.: General circulation model assessment of the sensitivity of direct climate forcing by anthropogenic sulfate aerosols to aerosol size and chemistry, J. Geophys. Res.-Atmos., 100, 26117-26134, 1995.

Boucher, O., and Haywood, J.: On summing the components of radiative forcing of climate change, Clim. Dyn., 18, 297-302, 2001.

Cachier, H., Liousse, C., Buat-Menard, P., and Gaudichet, A.: Particulate content of savanna fire emissions, J. Atmos. Chem., 22, 123-148, 1995.

Carrico, C. M., Rood, M. J., Ogren, J. A., Neususs, C., Wiedensohler, A., and Heintzenberg, J.: Aerosol optical properties at Sagres, Portugal during ACE-2, Tellus Ser. B-Chem. Phys. Meteorol., 52, 694-715, 2000.

Charlson, R. J., Schwartz, S. E., Hales, J. M., Cess, R. D., Coakley, J. A., Hansen, J. E., and Hofmann, D. J.: Climate forcing by anthropogenic aerosols, Science, 255, 423-430, 1992.

Chylek, P., and Wong, J.: Effect of absorbing aerosols on global radiation budget, Geophys. Res. Lett., 22, 929-931, 1995.

Collins, D. R., Jonsson, H. H., Seinfeld, J. H., Flagan, R. C., Gasso, S., Hegg, D. A., Russell, P. B., Schmid, B., Livingston, J. M., Ostrom, E., Noone, K. J., Russell, L. M., and Putaud, J. P.: In situ aerosol-size distributions and clear-column radiative closure during ACE-2, Tellus Ser. B-Chem. Phys. Meteorol., 52, 498-525, 2000.

Degroot, R. C.: Diurnal cycles of airborne spores produced by forest fungi, Phytopathology, 58, 1223-&, 1968.

Draxler, R. R., and Hess, G. D.: An overview of the HYSPLIT_4 modelling system for trajectories, dispersion, and deposition, Australian Meteorological Magazine, 47, 295-308, 1998.

Dubovik, O., Holben, B., Eck, T. F., Smirnov, A., Kaufman, Y. J., King, M. D., Tanré, D., and Slutsker, I.: Variability of absorption and optical properties of key aerosol types observed in worldwide locations, Journal of the Atmospheric Sciences, 59, 590–608, 2002.

Dubovik, O., Smirnov, A., Holben, B. N., King, M. D., Kaufman, Y. J., Eck, T. F., and Slutsker, I.: Accuracy assessments of aerosol optical properties retrieved from aerosol robotic network (AERONET) sun and sky radiance measurements, J. Geophys. Res.-Atmos., 105, 9791-9806, 2000.

Dzubay, T. G., Stevens, R. K., and Peterson, C. M.: Application of the dichotomous sampler to the characterization of ambient aerosols, in X-ray fluorescence analysis of environmental samples, edited by T. G. Dzubay, Ann Arbor Science Publishers Inc., Michigan, 1978.

Ebert, M., Weinbruch, S., Rausch, A., Gorzawski, G., Helas, G., Hoffmann, P., and Wex, H.: The complex refractive index of aerosols during LACE 98 as derived from the analysis of individual particles, J. Geophys. Res.-Atmos., 107(D21), 8121, doi: 10.1029/2000JD000195, 2002.

Echalar, F., Artaxo, P., Martins, J. V., Yamasoe, M., Gerab, F., Maenhaut, W., and Holben, B.: Long-term monitoring of atmospheric aerosols in the Amazon basin: Source identification and apportionment, J. Geophys. Res.-Atmos., 103, 31849-31864, 1998.

Eck, T. F., Holben, B. N., Slutsker, I., and Setzer, A.: Measurements of irradiance attenuation and estimation of aerosol single scattering albedo for biomass burning aerosols in Amazonia, J. Geophys. Res.-Atmos., 103, 31865-31878, 1998.

Ferek, R. J., Reid, J. S., Hobbs, P. V., Blake, D. R., and Liousse, C.: Emission factors of hydrocarbons, halocarbons, trace gases and particles from biomass burning in Brazil, J. Geophys. Res.-Atmos., 103, 32107-32118, 1998.

Ferrare, R. A., Fraser, R. S., and Kaufman, Y. J.: Satellite measurements of large-scale air-pollution - measurements of forest fire smoke, J. Geophys. Res.-Atmos., 95, 9911-9925, 1990.

Finlayson-Pitts, B. J., and Pitts, J. N.: Chemistry of the upper and lower atmosphere theory, experiments and applications, Academic Press, San Diego, 2000.

Fisch, G., Tota, J., Machado, L. A. T., Silva Dias, M. A. F., Lyra, R. F. d. F., Nobre, C. A., Dolman, A. J., Culf, A. D., Halveson, J., and Fuentes, J.: The convective boundary layer over pasture and forest in Amazonia, J. Geophys. Res.-Atmos., 2002, in press.

Fitzgerald, J. W.: Marine aerosols - a review, Atmospheric Environment Part a-General Topics, 25, 533-545, 1991.

Formenti, P., Andreae, M. O., Lange, L., Roberts, G., Cafmeyer, J., Rajta, I., Maenhaut, W., Holben, B. N., Artaxo, P., and Lelieveld, J.: Saharan dust in Brazil and Suriname during the large-scale biosphere-atmosphere experiment in Amazonia (LBA) - cooperative LBA regional experiment (CLAIRE) in march 1998, J. Geophys. Res.-Atmos., 106, 14919-14934, 2001.

Formenti, P., Andreae, M. O., and Lelieveld, J.: Measurements of aerosol optical depth above 3570 m asl in the north Atlantic free troposphere: Results from ACE-2, Tellus Ser. B-Chem. Phys. Meteorol., 52, 678-693, 2000.

Fuller, K. A., Malm, W. C., and Kreidenweis, S. M.: Effects of mixing on extinction by carbonaceous particles, J. Geophys. Res.-Atmos., 104, 15941-15954, 1999.

Gash, J. H. C., Nobre, C. A., Roberts, J. M., and Victoria, R. L.: Amazonian deforestation and climate, John Wiley & Sons Ltd, Chichester, England, 1996a.

Gash, J. H. C., Nobre, C. A., Roberts, J. M., and Victoria, R. L.: An overview of ABRACOS, in Amazonian deforestation and climate, edited by J. H. C. Gash, C.

A. Nobre, J. M. Roberts, and R. L. Victoria, pp. 1-14, John Wiley & Sons Ltd, Chichester, England, 1996b.

Hallett, J., Hudson, J. G., and Rogers, C. F.: Characterization of combustion aerosols for haze and cloud formation, Aerosol Sci. Technol., 10, 70-83, 1989.

Hao, W. M., and Liu, M. H.: Spatial and temporal distribution of tropical biomass burning, Global Biogeochemical Cycles, 8, 495-503, 1994.

Harrison, L., and Michalsky, J.: Objective algorithms for the retrieval of optical depths from ground-based measurements, Appl. Optics, 33, 5126-5132, 1994.

Harrison, L., Michalsky, J., and Berndt, J.: Automated multifilter rotating shadow-band radiometer - an instrument for optical depth and radiation measurements, Appl. Optics, 33, 5118-5125, 1994.

Harriss, R. C., Garstang, M., Wofsy, S. C., Beck, S. M., Bendura, R. J., Coelho, J. R. B., Drewry, J. W., Hoell, J. M., Matson, P. A., McNeal, R. J., Molion, L. C. B., Navarro, R. L., Rabine, V., and Snell, R. L.: The Amazon boundary-layer experiment - wet season 1987, J. Geophys. Res.-Atmos., 95, 16721-16736, 1990.

Harriss, R. C., Wofsy, S. C., Garstang, M., Browell, E. V., Molion, L. C. B., McNeal, R. J., Hoell, J. M., Bendura, R. J., Beck, S. M., Navarro, R. L., Riley, J. T., and Snell, R. L.: The Amazon boundary-layer experiment (ABLE-2A) - dry season 1985, J. Geophys. Res.-Atmos., 93, 1351-1360, 1988.

Haywood, J., and Boucher, O.: Estimates of the direct and indirect radiative forcing due to tropospheric aerosols: A review, Rev. Geophys., 38, 513-543, 2000.

Haywood, J. M., and Shine, K. P.: The effect of anthropogenic sulfate and soot aerosol on the clear-sky planetary radiation budget, Geophys. Res. Lett., 22, 603-606, 1995.

Hegg, D. A., Hobbs, P. V., Gasso, S., Nance, J. D., and Rangno, A. L.: Aerosol measurements in the arctic relevant to direct and indirect radiative forcing, J. Geophys. Res.-Atmos., 101, 23349-23363, 1996.

Heidam, N. Z.: Atmospheric aerosol factor models, mass and missing data, Atmos. Environ., 1923-1931, 1982.

Henry, R. C.: Multivariate receptor models, in Receptor modeling for air quality management, edited by P. K. Hopke, pp. 117-147, Elsevier, New York, 1991.

Hinds, W. C.: Aerosol technology: Properties, behavior, and measurement of airborne particles, Wiley-Interscience, New York, 1999.

Hoppel, W. A., Fitzgerald, J. W., Frick, G. M., Larson, R. E., and Mack, E. J.: Aerosol size distributions and optical-properties found in the marine boundary-layer over the Atlantic-Ocean, J. Geophys. Res.-Atmos., 95, 3659-3686, 1990.

Horvath, H.: Atmospheric light-absorption - a review, Atmospheric Environment Part a-General Topics, 27, 293-317, 1993.

Horvath, H.: Influence of atmospheric aerosols upon the global radiation balance, in Atmospheric particles, edited by R. M. Harrison, and R. Van Grieken, pp. 543-596, John Wiley & Sons Ltd., 1998.

IPCC: Climate change 2001: The third assessment report to the intergovernmental panel on climate change., Cambridge University Press, Cambridge, United kingdom, and New York, NY, USA, 2001.

Ito, K., Kneip, T. J., and Lioy, P. J.: The effects of number of samples and random error on the factor-analysis multiple-regression (Fa Mr) receptor modeling technique, Atmos. Environ., 20, 1433-1440, 1986.

Jacob, D. J., and Wofsy, S. C.: Photochemistry of biogenic emissions over the Amazon forest, J. Geophys. Res.-Atmos., 93, 1477-1486, 1988.

Jacob, D. J., and Wofsy, S. C.: Budgets of reactive nitrogen, hydrocarbons, and ozone over the Amazon-forest during the wet season, J. Geophys. Res.-Atmos., 95, 16737-16754, 1990.

Jacobson, M. C.: Strong radiative heating due to the mixing state of black carbon in atmospheric aerosols, Nature, 409, 695-697, 2001.

Johansson, S. A. E., and Campbell, J. L.: PIXE - a novel technique for elemental analysis, John Wiley, New York, 1988.

Kaufman, Y. J., Hobbs, P. V., Kirchhoff, V., Artaxo, P., Remer, L. A., Holben, B. N., King, M. D., Ward, D. E., Prins, E. M., Longo, K. M., Mattos, L. F., Nobre, C. A., Spinhirne, J. D., Ji, Q., Thompson, A. M., Gleason, J. F., Christopher, S. A., and Tsay, S. C.: Smoke, clouds, and radiation - Brazil (SCAR-B) experiment, J. Geophys. Res.-Atmos., 103, 31783-31808, 1998.

Kaufman, Y. J., Tucker, C. J., and Fung, I.: Remote-sensing of biomass burning in the tropics, J. Geophys. Res.-Atmos., 95, 9927-9939, 1990.

Keiding, K., Jensen, F. P., and Heidam, N. Z.: Absolute modeling of urban aerosol elemental composition by factor-analysis, Anal. Chim. Acta, 181, 79-85, 1986.

Kent, G. S., Yue, G. K., Farrukh, U. O., and Deepak, A.: Modeling atmospheric aerosol backscatter at CO_2-laser wavelengths .1. Aerosol properties, modeling techniques, and associated problems, Appl. Optics, 22, 1655-1665, 1983.

Kleeman, M. J., Schauer, J. J., and Cass, G. R.: Size and composition distribution of fine particulate matter emitted from wood burning, meat charbroiling, and cigarettes, Environ. Sci. Technol., 33, 3516-3523, 1999.

Kubátová, A., Vermeylen, R., Claeys, M., Cafmeyer, J., and Maenhaut, W.: Carbonaceous aerosols and particulate organic compounds in Gent, Belgium, during winter and summer of 1998, J. Aerosol. Sci., 30, suppl. 1, S905-S906, 1999.

Kuhlbusch, T. A. J., and Crutzen, P. J.: Black carbon, the global carbon cycle, and atmospheric carbon dioxide, in Biomass burning and global change, 1, edited by J. S. Levine, pp. 160-169, MIT press, Cambridge, Mass., 1996.

Le Canut, P., Andreae, M. O., Harris, G. W., Wienhold, F. G., and Zenker, T.: Airborne studies of emissions from savanna fires in Southern Africa .1. Aerosol emissions measured with a laser optical particle counter, J. Geophys. Res.-Atmos., 101, 23615-23630, 1996.

Li, X., Christopher, S. A., Chou, J., and Welch, R. M.: Estimation of shortwave direct radiative forcing of biomass-burning aerosols using new angular models, J. Appl. Meteorol., 39, 2278-2291, 2000.

Liousse, C., Devaux, C., Dulac, F., and Cachier, H.: Aging of savanna biomass burning aerosols - consequences on their optical-properties, J. Atmos. Chem., 22, 1-17, 1995.

Liousse, C., Penner, J. E., Walton, J. J., Eddleman, H., Chuang, C., and Cachier, H.: Modeling biomass burning aerosols, in Biomass burning and global change, 1, edited by J. S. Levine, pp. 492-508, MIT press, Cambridge, Mass., 1996.

Liu, Y. G., and Daum, P. H.: The effect of refractive index on size distributions and light scattering coefficients derived from optical particle counters, J. Aerosol. Sci., 31, 945-957, 2000.

Maenhaut, W., Fernandez-Jimenez, M. T., Rajta, I., and Artaxo, P.: Two-year study of atmospheric aerosols in Alta Floresta, Brazil: Multielemental composition and source apportionment, Nucl. Instrum. Methods Phys. Res. Sect. B-Beam Interact. Mater. Atoms, 189, 243-248, 2002.

Maenhaut, W., Francois, F., and Cafmeyer, J.: The "Gent" stacked filter unit (SFU) sampler for the collection of atmospheric aerosols in two size fractions: Description and instructions for installation and use, Applied research on air pollution using nuclear-related analytical techniques, Report on the first research co-ordination meeting, Vienna, Austria, 1994.

Maenhaut, W., Koppen, G., and Artaxo, P.: Long-term atmospheric aerosol study in Cuiabá, Brazil: Multielemental composition, sources, and impact of biomass burning, in Biomass burning and global change, 2, edited by J. S. Levine, pp. 637-652, MIT press, Cambridge, Mass., 1996.

Marley, N. A., Gaffney, J. S., Baird, C., Blazer, C. A., Drayton, P. J., and Frederick, J. E.: An empirical method for the determination of the complex refractive index of size-fractionated atmospheric aerosols for radiative transfer calculations, Aerosol Sci. Technol., 34, 535-549, 2001.

Marple, V. A., Rubow, K. L., and Behm, S. M.: A microorifice uniform deposit impactor (MOUDI) - description, calibration, and use, Aerosol Sci. Technol., 14, 434-446, 1991.

Martins, J. V., Artaxo, P., Liousse, C., Reid, J. S., Hobbs, P. V., and Kaufman, Y. J.: Effects of black carbon content, particle size, and mixing on light absorption by aerosols from biomass burning in Brazil, J. Geophys. Res.-Atmos., 103, 32041-32050, 1998a.

Martins, J. V., Hobbs, P. V., Weiss, R. E., and Artaxo, P.: Sphericity and morphology of smoke particles from biomass burning in Brazil, J. Geophys. Res.-Atmos., 103, 32051-32057, 1998b.

Mason, B., and Moore, C. B.: Principles of geochemistry, John Wiley, New York, 1982.

Mayol-Bracero, O. L., Guyon, P., Graham, B., Roberts, G., Andreae, M. O., Decesari, S., Facchini, M. C., Fuzzi, S., and Artaxo, P.: Water-soluble organic compounds in biomass burning aerosols over Amazonia: 2. Apportionment of the chemical composition and importance of the polyacidic fraction, J. Geophys. Res.-Atmos., 107, 8091, doi:8010.1029/2001JD000522, 2002.

Miller, J. M., Whelpdale, D. M., Barrie, L. A., Isaksen, I. S. A., Rodhe, H., and Smith, F. B.: The transport of sulfur and nitrogen through the remote atmosphere, in The biogeochemical cycling of sulfur and nitrogen in the remote atmosphere, 95, edited by J. N. Galloway, R. J. Charlson, M. O. Andreae, H. Rodhe, and D. Reidel, pp. 127-139, Hingham, Mass., 1985.

Mishchenko, M. I., Travis, L. D., Kahn, R. A., and West, R. A.: Modeling phase functions for dustlike tropospheric aerosols using a shape mixture of randomly oriented polydisperse spheroids, J. Geophys. Res.-Atmos., 102, 16831-16847, 1997.

Mukai, H., and Ambe, Y.: Characterization of a humic acid-like brown substance in airborne particulate matter and tentative identification of its origin, Atmos. Environ., 20, 813-819, 1986.

Novakov, T., and Corrigan, C. E.: Influence of sample composition on aerosol organic and black carbon determinations, in Biomass burning and global change, 1, edited by J. S. Levine, pp. 531-539, MIT press, Cambridge, Mass., 1996.

Parker, R. D., and Buzzard, G. H.: A two stage respirable aerosol sampler using Nuclepore filters in series, Atmos. Environ., 11, 617-621, 1977.

Penner, J. E., Chuang, C. C., and Grant, K.: Climate forcing by carbonaceous and sulfate aerosols, Clim. Dyn., 14, 839-851, 1998.

Pesava, P., Horvath, H., and Kasahara, M.: A local optical closure experiment in Vienna, J. Aerosol. Sci., 32, 1249-1267, 2001.

Pickering, K. E., Thompson, A. M., Wang, Y. S., Tao, W. K., McNamara, D. P., Kirchhoff, V., Heikes, B. G., Sachse, G. W., Bradshaw, J. D., Gregory, G. L., and Blake, D. R.: Convective transport of biomass burning emissions over Brazil during TRACE A, J. Geophys. Res.-Atmos., 101, 23993-24012, 1996.

Pilinis, C., and Li, X.: Particle shape and internal inhomogeneity effects on the optical properties of tropospheric aerosols of relevance to climate forcing, J. Geophys. Res.-Atmos., 103, 3789-3800, 1998.

Radke, L. F., Hegg, A. S., Hobbs, P. V., and Penner, J. E.: Effects of aging on the smoke from a large forest-fire, Atmos. Res., 38, 315-332, 1995.

Radke, L. F., Hegg, D. A., Hobbs, P. V., Nance, J. D., Lyons, J. H., Laursen, K. K., Weiss, R. E., Riggan, P. J., and Ward, D. E.: Particulates and trace gas emissions from large biomass fires in North America, in Global biomass burning: Atmospheric, climatic, and biospheric implications, edited by J. S. Levine, pp. 209-224, MIT Press, Cambridge, Mass., 1991.

Raes, F., Van Dingenen, R., Vignati, E., Wilson, J., Putaud, J. P., Seinfeld, J. H., and Adams, P.: Formation and cycling of aerosols in the global troposphere, Atmos. Environ., 34, 4215-4240, 2000.

Rahn, K. A.: Silicon and aluminum in atmospheric aerosols: Crust-air fractionation?, Atmos. Environ., 10, 597-601, 1976.

Ramanathan, V., Crutzen, P. J., Lelieveld, J., Mitra, A. P., Althausen, D., Anderson, J., Andreae, M. O., Cantrell, W., Cass, G. R., Chung, C. E., Clarke, A. D., Coakley, J. A., Collins, W. D., Conant, W. C., Dulac, F., Heintzenberg, J., Heymsfield, A. J., Holben, B., Howell, S., Hudson, J., Jayaraman, A., Kiehl, J. T., Krishnamurti, T. N., Lubin, D., McFarquhar, G., Novakov, T., Ogren, J. A., Podgorny, I. A., Prather, K., Priestley, K., Prospero, J. M., Quinn, P. K., Rajeev, K., Rasch, P., Rupert, S., Sadourny, R., Satheesh, S. K., Shaw, G. E., Sheridan, P., and Valero, F. P. J.: Indian Ocean experiment: An integrated analysis of the climate forcing and effects of the great Indo-Asian haze, J. Geophys. Res.-Atmos., 106, 28371-28398, 2001.

Ramaswamy, V., Boucher, O., Haigh, J., Hauglustaine, D., Haywood, J., Myhre, G., Nakajima, T., Shi, G. Y., and Solomon, S.: Radiative forcing of climate change, in Climate change 2001: The third assessment report to the intergovernmental panel on climate change., I, edited by J. T. Houghton et al. (eds), Cambridge University Press, Cambridge, United kingdom, and New York, NY, USA, 2001.

Redemann, J., Turco, R. P., Liou, K. N., Russell, P. B., Bergstrom, R. W., Schmid, B., Livingston, J. M., Hobbs, P. V., Hartley, W. S., Ismail, S., Ferrare, R. A., and Browell, E. V.: Retrieving the vertical structure of the effective aerosol complex index of refraction from a combination of aerosol in situ and remote sensing measurements during TARFOX, J. Geophys. Res.-Atmos., 105, 9949-9970, 2000.

Reid, J. S.: Emission, evolution, and radiative properties of particles from biomass burning in Brazil, PhD thesis Thesis, University of Washington, Washington, 1998.

Reid, J. S., and Hobbs, P. V.: Physical and optical properties of young smoke from individual biomass fires in Brazil, J. Geophys. Res.-Atmos., 103, 32013-32030, 1998.

Reid, J. S., Hobbs, P. V., Ferek, R. J., Blake, D. R., Martins, J. V., Dunlap, M. R., and Liousse, C.: Physical, chemical, and optical properties of regional hazes dominated by smoke in Brazil, J. Geophys. Res.-Atmos., 103, 32059-32080, 1998a.

Reid, J. S., Hobbs, P. V., Liousse, C., Martins, J. V., Weiss, R. E., and Eck, T. F.: Comparisons of techniques for measuring shortwave absorption and black carbon content of aerosols from biomass burning in Brazil, J. Geophys. Res.-Atmos., 103, 32031-32040, 1998b.

Remer, L. A., Kaufman, Y. J., Holben, B. N., Thompson, A. M., and McNamara, D.: Biomass burning aerosol size distribution and modeled optical properties, J. Geophys. Res.-Atmos., 103, 31879-31891, 1998.

Roberts, G. C., Artaxo, P., Zhou, J., Swietlicki, E., and Andreae, M. O.: Sensitivity of CCN spectra on chemical and physical properties of aerosols: A case study from the Amazon basin, J. Geophys. Res.-Atmos., 107(D20), 8070, doi: 10.1029/2001JD000583, 2002.

Roberts, M. C., Andreae, M. O., Zhou, J. C., and Artaxo, P.: Cloud condensation nuclei in the Amazon basin: "marine" conditions over a continent?, Geophys. Res. Lett., 28, 2807-2810, 2001.

Ross, J. L., Hobbs, P. V., and Holben, B.: Radiative characteristics of regional hazes dominated by smoke from biomass burning in Brazil: Closure tests and direct radiative forcing, J. Geophys. Res.-Atmos., 103, 31925-31941, 1998.

Rummel, U., Ammann, C., Gut, A., Meixner, F. X., and Andreae, M. O.: Eddy covariance measurements of nitric oxide flux within an Amazonian rain forest, J. Geophys. Res.-Atmos., 2002a.

Rummel, U., Ammann, C., and Meixner, F. X.: Characterizing turbulent trace gas exchange above a dense tropical rain forest using wavelet and surface renewal analysis, 15th AMS Symposium on Boundary Layers and Turbulence, Wageningen, pp. 602-605, 2002b.

Russell, P. B., Kinne, S. A., and Bergstrom, R. W.: Aerosol climate effects: Local radiative forcing and column closure experiments, J. Geophys. Res.-Atmos., 102, 9397-9407, 1997.

Salmon, L. G., Hildemann, L. M., Mazurek, M. A., Chrisforou, C., Frei, N. A., Solomon, P. A., Schauer, J. J., Hughes, L., and Johnson, R.: Procedures manual, Environmental quality laboratory, California Institute of Technology, Pasadena, California, August, 1998.

Savoie, D. L., Prospero, J. M., and Nees, R. T.: Nitrate, non-sea-salt sulfate, and mineral aerosol over the Northwestern Indian-Ocean, J. Geophys. Res.-Atmos., 92, 933-942, 1987.

Schachtman, D. P., Reid, R. J., and Ayling, S. M.: Phosphorus uptake by plants: From soil to cell, Plant Physiol., 116, 447-453, 1998.

Schmid, H., Laskus, L., Abraham, H. J., Baltensperger, U., Lavanchy, V., Bizjak, M., Burba, P., Cachier, H., Crow, D., Chow, J., Gnauk, T., Even, A., ten Brink, H. M., Giesen, K. P., Hitzenberger, R., Hueglin, E., Maenhaut, W., Pio, C., Carvalho, A., Putaud, J. P., Toom-Sauntry, D., and Puxbaum, H.: Results of the "carbon conference" international aerosol carbon round robin test stage I, Atmos. Environ., 35, 2111-2121, 2001.

Seinfeld, J. H., and Pandis, S. N.: Atmospheric chemistry and physics, Wiley-Interscience, New York, 1998.

Shine, K. P., and Forster, P. M. D.: The effect of human activity on radiative forcing of climate change: A review of recent developments, Glob. Planet. Change, 20, 205-225, 1999.

Silva Dias, M. A. F., Rutledge, S., Kabat, P., Silva Dias, P. L., Nobre, C., Fisch, G., Dolman, A. J., Zipser, E., Garstang, M., Manzi, A. O., Fuentes, J. D., Rocha, H., Ma-rengo, J., Plana-Fattori, A., Sá, L., Alvalá, R., Andreae, M. O., Artaxo, P., Gielow, R., and Gatti, L. V.: Clouds and rain processes in a biosphere-atmosphere interaction context in the Amazon Region, J. Geophys. Res.-Atmos., 107, 8072, doi:10.1029/2001JD000335, 2002.

Sokolik, I. N., and Toon, O. B.: Incorporation of mineralogical composition into models of the radiative properties of mineral aerosol from UV to IR wavelengths, J. Geophys. Res.-Atmos., 104, 9423-9444, 1999.

Solomon, P. A., Moyers, J. L., and Fletcher, R. A.: High-volume dichotomous virtual impactor for the fractionation and collection of particles according to aerodynamic size, Aerosol Sci. Technol., 2, 455-464, 1983.

Staudt, A. C., Jacob, D. J., Logan, J. A., Bachiochi, D., Krishnamurti, T. N., and Sachse, G. W.: Continental sources, transoceanic transport, and interhemispheric exchange of carbon monoxide over the pacific, J. Geophys. Res.-Atmos., 106, 32571-32589, 2001.

Stith, J. L., Radke, L. F., and Hobbs, P. V.: Particle emissions and the production of ozone and nitrogen oxides from the burning of forest slash, Atmos. Environ., 15, 73-82, 1981.

Stolzenburg, M., Kreisberg, N., and Hering, S.: Atmospheric size distributions measured by differential mobility optical particle size spectrometry, Aerosol Sci. Technol., 29, 402-418, 1998.

Swap, R., Garstang, M., Macko, S. A., Tyson, P. D., Maenhaut, W., Artaxo, P., Kallberg, P., and Talbot, R.: The long-range transport of Southern African aerosols the tropical south Atlantic, J. Geophys. Res.-Atmos., 101, 23777-23791, 1996.

Tegen, I., Lacis, A. A., and Fung, I.: The influence on climate forcing of mineral aerosols from disturbed soils, Nature, 380, 419-422, 1996.

Thurston, G. D., and Spengler, J. D.: A quantitative assessment of source contributions to inhalable particulate matter pollution in metropolitan boston, Atmos. Environ., 19, 9-25, 1985.

Turpin, B. J., and Lim, H. J.: Species contributions to pm2.5 mass concentrations: Revisiting common assumptions for estimating organic mass, Aerosol Sci. Technol., 35, 602-610, 2001.

Twomey, S.: Aerosols, clouds and radiation, Atmospheric Environment Part a-General Topics, 25, 2435-2442, 1991.

von Hoyningen-Huene, W., Schmidt, T., Schienbein, S., Kee, C. A., and Tick, L. J.: Climate-relevant aerosol parameters of south-east-asian forest fire haze, Atmos. Environ., 33, 3183-3190, 1999.

Ward, D. E., Susott, R. A., Kauffman, J. B., Babbitt, R. E., Cummings, D. L., Dias, B., Holben, B. N., Kaufman, Y. J., Rasmussen, R. A., and Setzer, A. W.: Smoke and fire characteristics for cerrado and deforestation burns in brazil - BASE-B experiment, J. Geophys. Res.-Atmos., 97, 14601-14619, 1992.

Wesely, M. L., and Hicks, B. B.: A review of the current status of knowledge on dry deposition, Atmos. Environ., 34, 2261-2282, 2000.

Westphal, D. L., and Toon, O. B.: Simulations of microphysical, radiative, and dynamic processes in a continental-scale forest-fire smoke plume, J. Geophys. Res.-Atmos., 96, 22379-22400, 1991.

Willeke, K., and Baron, P. A.: Aerosol measurements: Principles, techniques, and applications, Van Nostrand Reinhold, New York, 1993.

Winklmayr, W., Wang, H. C., and John, W.: Adaptation of the twomey algorithm to the inversion of cascade impactor data, Aerosol Sci. Technol., 13, 322-331, 1990.

Wong, J., and Li, Z. Q.: Retrieval of optical depth for heavy smoke aerosol plumes: Uncertainties and sensitivities to the optical properties, Journal of the Atmospheric Sciences, 59, 250-261, 2002.

Yamasoe, M. A., Kaufman, Y. J., Dubovik, O., Remer, L. A., Holben, B. N., and Artaxo, P.: Retrieval of the real part of the refractive index of smoke particles from sun/sky measurements during SCAR-B, J. Geophys. Res.-Atmos., 103, 31893-31902, 1998.

Yu, J. Z., Xu, J. H., and Yang, H.: Charring characteristics of atmospheric organic particulate matter in thermal analysis, Environ. Sci. Technol., 36, 754-761, 2002.

Zappoli, S., Andracchio, A., Fuzzi, S., Facchini, M. C., Gelencser, A., Kiss, G., Krivacsy, Z., Molnar, A., Meszaros, E., Hansson, H. C., Rosman, K., and Zebuhr, Y.: Inorganic, organic and macromolecular components of fine aerosol in different areas of europe in relation to their water solubility, Atmos. Environ., 33, 2733-2743, 1999.

Zhou, J., Swietlicki, E., Hansson, H. C., and Artaxo, P.: Submicrometer aerosol particle size distribution and hygroscopic growth measured in the amazon rain forest during the wet season, J. Geophys. Res.-Atmos., 107(D20), 8055, doi: 10.1029/2000JD000203, 2002.

CURRICULUM VITAE

Personal data:

Name: Pascal Guyon

Birth: 29.07.72, Amberieu-en-Bugey (01), France

Citizenship: French

Languages:

French: Mother Language

English: Fluent

German: Proficient

Portuguese: Proficient

Education:

06/96   Maîtrise Chemistry, University Joseph Fourier, Grenoble, France, by equivalence of BSc School of Chemistry, University of Bristol, England (2:1 Class Degree).

06/98   DESS Industrial Environment, Institute of Sciences and Technologies, Grenoble, France (1st Class Degree).

Employment/Career:

10/95-06/96   Research project for SmithKline Beecham Pharmaceuticals. Synthesis and studies of a model compound of the antibiotic Pseudomonic Acid C. Under the supervision of: Dr. C. Willis and Pr. T.J. Simpson, School of Chemistry, University of Bristol, England, and N. Broom and P.J. O'Haulon, SmithKline Beecham Pharmaceuticals.

1997	Compulsory Army as a secretary in the signal corps, Corsica.
05/98-10/98	Development of an automatic sampler for VOCs. Biogeochemistry department (Prof. Dr. J.Kesselmeier), Max Planck Institute for Chemistry (MPIC), Mainz, Germany.
10/98-01/99	Improvement and final development of a cloud condensation nuclei (CCN) counter Biogeochemistry department (Prof. Dr. M.O. Andreae), MPIC, Mainz, Germany.
01/99-04/99	Logistic organization of the EUSTACH-LBA measurement campaign for MPIC, Jí-Paraná, Rondônia, Brazil.
05/99-date	PhD thesis. entitled "Chemical and Physical Properties of Amazonian Aerosols" within the French-German cooperation (Cotutelle de thèse) under the supervision of: Prof. Dr. M.O. Andreae, MPIC, Mainz, Germany, Prof. Dr. K. G. Heumann, Mainz, Johannes Gutenberg-Universität Mainz, Mainz, Germany, and Prof. Dr. P. Carlier, Université de Paris VII – Denis Diderot, Paris, France.
03/01	Pre-organization of the CLAIRE 2001 LBA measurement campaign for MPIC, Manaus, Amazonia, Brazil.

Publications:

Z. Zdráhal, R. Vermeylen, M. Claeys, W. Maenhaut, **P. Guyon**, and P. Artaxo. 2001. Characterization of Novel Di- and Tricarboxylic acids in Fine Tropical Aerosols. Journal of Mass Spectrometry.

R. Lang, S van Dijk, **P. Guyon**, and F. Raes. Physical and Chemical Characteristics of Aerosols: Observations and Modeling. A contribution to the COACh book volume 2.

P. Guyon, A. Rausch, H. de Coninck, and P. Mirabel. Aerosol Formation in the Atmosphere. A contribution to the COACh book volume 2.

O. L. Mayol-Bracero, **P. Guyon**, B. Graham, G. Roberts, M. O. Andreae, S. Decesari, M. C. Facchini, S. Fuzzi, and P. Artaxo. 2002. Water-Soluble Organic Compounds in Biomass Burning Aerosols over Amazonia: 2. Apportionnement of the Chemical Composition and Importance of the Polyacidic fraction. Journal of Geophysical Research.

B. Graham, O. L. Mayol-Bracero, **P. Guyon**, G. C. Roberts, S. Decesari, M. C. Facchini, P. Artaxo, W. Maenhaut, P. Köll, and M. O. Andreae. 2002. Water-Soluble Organic Compounds in Biomass Burning Aerosols over Amazonia: 1. Characterization by NMR and GC/MS. Journal of Geophysical Research.

P. Artaxo, J. V. Martins, M. A. Yamasoe, A. S. Procópio, T. M. Pauliquevis, M. O. Andreae, **P. Guyon**, L. V. Gatti, and A. M. Cordova Leal. 2002.Physical and Chemical Properties of Aerosols in the Wet and Dry Season in Rondônia, Amazonia. Journal of Geophysical Research.

P. Guyon, O. Boucher, B. Graham, J. Beck, O. L. Mayol-Bracero, G. C. Roberts, W. Maenhaut, P. Artaxo, and M. O. Andreae. 2003. Refractive index of aerosol particles over the Amazon tropical forest during LBA-EUSTACH 1999. Journal of Aerosol Science. In Press.

P. Guyon, B. Graham, J. Beck, O. Boucher, E. Gerasopoulos, O. L. Mayol-Bracero, G. C. Roberts, P. Artaxo, and M. O. Andreae. 2003. Physical properties and concentration of aerosol particles over the Amazon tropical forest during background and biomass burning conditions. Atmospheric Chemistry and Physics. In Press.

P. Guyon, B. Graham, G. C. Roberts, O. L. Mayol-Bracero, W. Maenhaut, P. Artaxo, and M. O. Andreae. 2003. In-canopy gradients, composition, sources, and optical properties of aerosol over the Amazon forest. Submitted to Journal of Geophysical Research.